540
BOR

T329

GRAPHENE/GRAPHENE OXIDE BASED POLYMER NANOCOMPOSITES AND THEIR APPLICATIONS
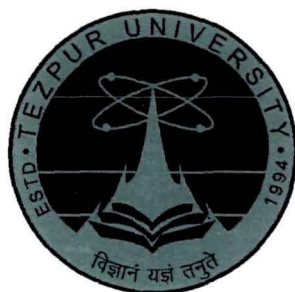
**A Thesis submitted
in partial fulfilment of the requirements for the degree of**

Doctor of Philosophy

By

Chandramika Bora

Registration no. TZ121400 of 2012

**School of Science
Department of Chemical Sciences
Tezpur University**
Napaam, Tezpur - 784028
Assam, India

November, 2014

Dedicated To
My Beloved Parents

DECLARATAION BY THE CANDIDATE

The thesis entitled *"Graphene/graphene oxide based polymer nanocomposites and their applications"* is being submitted to the Tezpur University in partial fulfillment for the award of the degree of *Doctor of Philosophy* in Chemical Sciences is a record of bonafide research work accomplished by me under the supervision of Prof. S.K. Dolui.

All helps received from various sources have been duly acknowledged.

No part of this thesis has been submitted elsewhere for award of any other degree.

Chandramika Bora

Date: 1-/2-/14

Place: Tezpur

Chandramika Bora

Department of Chemical sciences

Tezpur University

Tezpur University

(A Central University established by an Act of Parliament)
Napaam, Tezpur-784028
DISTRICT: SONITPUR:: Assam:: India

Ph: 03712-267004 (O) 9957198489 (M) Fax: 03712-267006 *Email: dolui@tezu.ernet.in*

CERTIFICATE OF THE PRINCIPAL SUPERVISOR

This is to certify that the thesis entitled *"Graphene/graphene oxide based polymer nanocomposites and their applications"* submitted to the School of Science, Tezpur University in partial fulfillment for the award of degree of *Doctor in Philosophy* in Chemical Sciences is a record of research work carried out by **Ms. Chandramika Bora** under my supervision and guidance.

All help received by her from various sources have been duly acknowledged.

No part of this thesis has been submitted elsewhere for award of any other degree.

Date: 1·12·14
Place: Tezpur

S. K. Dolui
Professor
Department of Chemical Sciences
School of Science

Tezpur University

(A Central University established by an Act of Parliament)
Napaam, Tezpur-784028
DISTRICT: SONITPUR:: Assam:: India

Ph: 03712-267004 (O) 9957198489 (M) Fax: 03712-267006 *Email: dolui@tezu.ernet.in*

CERTIFICATE OF THE EXTERNAL EXAMINER AND ODEC

This is to certify that the thesis entitled "***Graphene/graphene oxide based polymer nanocomposites and their applications***" submitted to the School of Science, Tezpur University in partial fulfillment for the award of degree of *Doctor in Philosophy* in Chemical Sciences has been examined by us on ………………………….. and found to be satisfactory.

Signature of:

Principal supervisor   External Examiner

Date:

Acknowledgement

First and foremost, I would like to offer my deep sense of gratitude and regards to my supervisor and mentor, *Prof. Swapan K. Dolui* for giving me an opportunity to carry out this research work and introducing me to the world of graphene. I am thankful to him for his inspiring guidance, constant support, time and patience which have helped me to complete this thesis without any hurdle. His enthusiasm, simplicity, constructive criticism, fatherly care and joyful nature will influence me for the rest of my life. I feel privileged and lucky to get him as a guide.

I am grateful to Prof. M.K. Chaudhuri, Vice-Chancellor, Tezpur University and authorities of Tezpur University for allowing me and providing necessary laboratory facilities to carry out this work.

I express my sincere thanks to the D.C. members, Prof. R.K. Dutta and Dr. D. Mohanta for their valuable suggestions and help during my research tenure.

I would like thank Dr. R. C. Deka, HOD, and all the faculty members of Department of Chemical Sciences, Tezpur University for their help and suggestions. I sincerely acknowledge all the members of technical staffs and official staff of Chemical Sciences department for their help.

I sincerely acknowledge Prof. S.K. Samdarshi, Department of Energy, for electrochemical test, Dr. P. Deb, Department of Physics, for AFM analysis and Prof. Prof. B. K. Konwar, Department of MBBT of Tezpur University for Antibacterial test. I am also thankful to Dr. R. Khan of CSIR-NEIST, Jorhat for helping me in charge-discharge test.

The financial supports received from Council of Scientific and Industrial Research (CSIR), india and Defence Research and Development Organisation (DRDO) is gratefully acknowledged.

I wish my heartiest thanks to all my past and present lab colleagues Surajitda, Amarda, Binodda, Ishada, Chandrama, Dhaneswar, Bhaskar, Pranab, Bikash, Kiron, Monalisha, Shyamalima, Momina for their help and for transforming the lab to a lively place of work.

My special thanks goes to my seniors and friends from Tezpur University, Jayashriba, Minakshiba, Shreemoyeeba, Anishaba, Nibedita, Sweety, Rekha, Himadri and many others for their love, help and moral support in many situations.

I am grateful to Mrs. Sutapa Dolui and Swapnil Dolui for their care, affection and hospitality.

Acknowledgement

My heartiest regards goes to all my teachers from primary school onwards who inspired me to pursue higher studies.

Finally, I take this opportunity to convey my profound gratitude and regards to my parents for their continuous encouragement, countless sacrifices, endless support and aspirations for me and my carrier ever since I started school. I am indebted to my younger brother who helps me and stands by me in every aspects of my life. I am also thankful to bordeuta, borma and all other relatives for their blessings and well wishes.

Last but not the least, I would like to thank God for giving me strength, health and opportunity to complete this study.

Chandramika Bora

Contents

Chapter 4:
Applications of graphene based polymer nanocomposites

4.1 Highly sensitive glucose biosensor based on polypyrrole/graphene composite synthesized by interfacial polymerization

4.2 Polypyrrole/sulfonated graphene composite as electrode material for supercapacitor

4.3 Polythiophene/graphene composite as a highly efficient platinum-free counter electrode in dye-sensitized solar cells

Abbreviations used:

AFM	atomic force microscopy
BET	Brunauer–Emmett–Teller
CNT	carbon nanotube
CV	cyclic voltammetry
CVD	chemical vapor deposition
DMF	dimethyl formamide
DMSO	dimethyl sulfoxide
DNA	deoxyribonucleic acid
DSC	differential scanning calorimetriy
DSSC	dye-sensitized solar cells
DI	deionized
EDLC	electrochemical double-layer capacitors
EDX	energy-dispersive X-ray
EMI	electromagnetic interference
ESD	electrostatic discharge
FGS	functionalized graphene sheets
FTIR	fourier transform infrared spectroscopy
FTO	fluorine tin oxide
GCE	glassy carbon electrode
GO	graphene oxide
GOD	glucose oxidase
GNS	graphene nanosheets
GR	graphene
HOMO	highest occupied molecular orbital
ITO	indium tin oxide
LUMO	lowest unoccupied molecular orbital
MEKP	methyl ethyl ketone peroxide
NADH	nicotinamide adenine dinucleotide
NMP	N-methyl pyrrolidone
PAN	poly(acrylonitrile)

Abbreviations used:

PANI	Polyaniline
PC	polycarbonate
PE	polyester
PET	poly(ethylene terepthalate)
PEDOT	poly (3,4 ethylenedioxythiophene)
PMMA	poly (methylmethacrylate)
PP	polypropylene
PPy	polypyrrole
PS	polystyrene
PSS	polystyreneslufonate
PTh	polythiophene
PVA	poly(vinyl alcohol)
PVC	poly(vinyl chloride)
PVDF	poly(vinylidene fluoride)
P3HT	poly (3-hexylthiophene)
QHE	quantum hall effect
SEM	scanning electron microscopy
SG	sulphonated graphene.
STM	scanning tunneling microscopy
SWCNT	single-walled carbon nanotube
TEM	transmission electron microscopy
THF	tetrahydrofuran
TGA	thermogravimetric analysis
TRG	thermally reduced graphene
T_g	glass-transition temperature
TPU	thermoplastic polyurethane
UV-visible	ultraviolet-visible
WPU	waterborne polyurethane
XRD	X-ray diffraction
XPS	X-ray photoelectron spectroscopy

CHAPTER 1

General Introduction
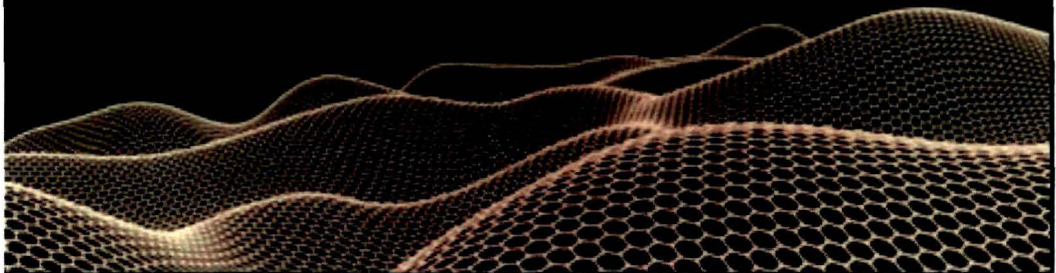
"*When carbon fibers just won't do, but nanotubes are too expensive, where a cost-conscious materials scientist can go to find a practical conductive composite? The answer could lie with graphene sheets*"- Nicholas A. Kotov.[1]

1.1 Motivation and Background

This thesis represents my research efforts focused on developing new ideas on the preparation and characterization of some graphene/graphene oxide based polymer nanocomposites. The motivation for this study was to synthesize polymer nanocomposites based on graphene and graphene oxide by using novel technique like interfacial polymerization and to explore the properties of these new nanocomposite materials. The synthesis and properties of graphene and graphene oxide filled polymer nanocomposites with polymers such as polypyrrole, polythiophene and polyester resin are demonstrated in the thesis. Also I have tried to investigate some of their applications. The composites exhibit good potential for use in diverse fields like sensors, supercapacitors and solar cells. The ideas presented in this thesis are an outcome of my years of studies in the area of graphene inspired by previous works.

Polymer nanocomposite has become a crucial area in modern science and technology.[2] They are commonly defined as the combination of a polymer matrix and fillers having dimension in the nanometer scale. They have a diverse range of applications in many areas such as structural materials, energy storage, sensors, biomedical and computing, etc.[3,4] Addition of minute quantity of nanofiller can enhance the properties of a polymer in a greater way than the polymer composites with conventional micron-scale fillers such as clay, ceramics, glass and carbon fibers.[5] Such enhancement in properties of nanocomposites can be attributed to the high aspect ratio and large surface area of the nanofillers. Good dispersion of nanofillers in the composite can develop novel structural and functional properties and thereby changing the nature of the pure polymer. However scientists are exploring polymer composites with an innovation in structure, property and application.

Polymer nanocomposites based on inorganic nanofillers have attracted considerable interest for their improved properties. They have shown application potential in many fields like construction, automotive, electronics and aerospace etc.[6-8]

The use of montmorillonite as filler in a Nylon-6 matrix by Toyota Motor Corporation has opened a new era in polymeric nanomaterials.[9] After that, several researchers have investigated nanocomposites based on layered silicate compounds or synthetic clay. But clay minerals show poor electrical and thermal conductivity. Therefore to overcome this drawback, carbon based nanofillers, such as carbon black, graphite, expanded graphite and carbon nanotube (CNT) have been employed to the preparation of polymer composites.[10-13] In particular, CNTs are found to be very effective as conductive fillers with combined properties, such as mechanical strength and thermal stability. But large scale production of CNT is a difficult task due to its high cost as well as its tendency to agglomerate during processing. Use of graphene has removed such difficulties associated with CNT.

Graphene, the latest sensation in modern science has brought a great revolution in the field of nanoscience and technology. Since its first discovery in 2004, this "thinnest material" has attracted huge scientific attention owing to its wonderful chemical and physical properties.[14] Graphene and graphene based materials have shown tremendous application potential in various fields such as electronic devices, super capacitors, rechargeable batteries, functional electrodes, sensors, biomedical and many others.[15]

1.2 Graphene (GR)

GR is a two-dimensional (2D) one atom thick planar sheet of sp^2-bonded carbon atoms that are arranged in a honeycomb crystal lattice. It is the mother of other carbon allotropes like graphite, CNT and fullerenes (Fig. 1.1).[16] Single-layer GR sheet was first isolated by Geim and Novoselov at Manchester University (2010 Nobel Prize in Physics).[17] They obtained it from naturally occurring graphite, which is a well known mineral for years and had been used to mark instruments in the Middle Ages. Since their discovery, studies on GR for various applications and opportunities for future are going in full swing. Due to its unique physical, electrical, thermal and mechanical properties GR is also termed as "super carbon."

2
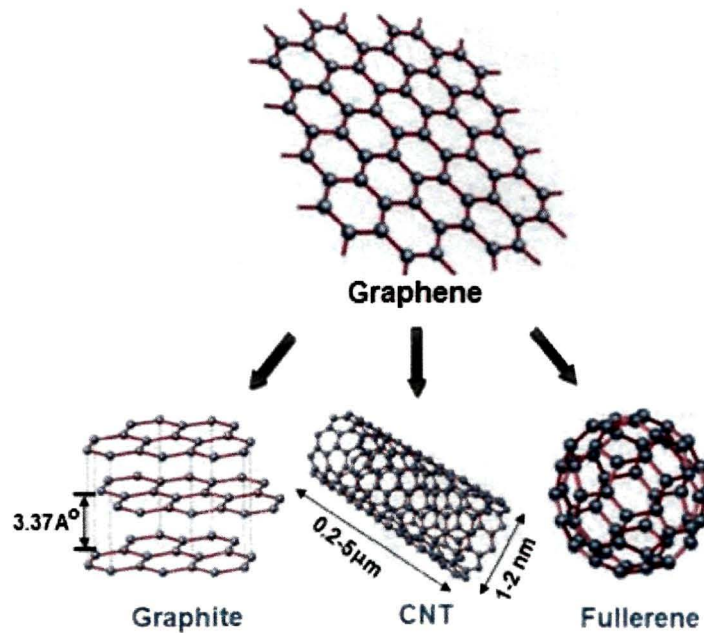
Fig. 1.1 Honeycomb lattice structure in GR (top). Different carbon allotropes (bottom).

The advantages of GR in constructing nanocomposites are as follows:

(1) *2D planar structure and high surface area.* GR has a planar structure for which it is easy for decoration of microspheres with a dimension of several hundred nanometers. But it is not possible with other carbon materials like CNT. Also synthesis of GR based nanocomposites by some new synthesis methods like thermal decomposition is possible because of its 2D structure.[18]

Surface area of GR is higher than any other carbon fillers. Therefore uniform dispersion of GR in polymer matrix can be achieved which leads to the great improvement in properties of GR based materials. As GR has individual sheet like structure, so secondary components can enter in between the sheets and prevent agglomeration of GR sheets. Single-layer GR has a large surface area close to 2600 $m^2 g^{-1}$.[19] Few layer GR samples have shown a surface area in the range of 270-1550 $m^2 g^{-1}$ as measured by the Brunauer–Emmett–Teller (BET) method. Fig. 1.2 shows the atomic and electronic structure of GR.[4,20]
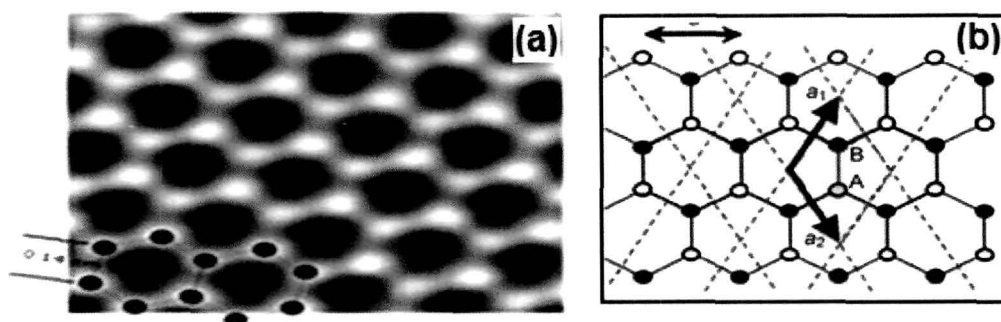
Fig. 1.2 (a) An atomic resolution image of GR sheet synthesized by the substrate-free gas-phase method (adopted from Ref. 19) and (b) electronic structure of GR (adopted from Ref. 14).

(2) *Simple and low cost production*. GR can be obtained from graphite which is a low cost and abundant material. So production cost of GR based composites is much lower compared to other nanomaterials. Moreover GR can be readily dispersed in various solvents. As a result, processing of GR based materials is easy compared to CNT as it doesn't require any chemical functionalization before processing.[21]

(3) *Electrical and electronic property*: GR is termed as a zero band gap semiconductor. The conductivity of GR decreases below 50 K and increases if it is heated to high temperatures. It shows high electron mobility (15 000 cm^2 V^{-1} s^{-1}) under ambient conditions.[22] High electron mobility of GR is important in applications involving charge transfer processes, such as supercapacitors, photovoltaic devices and sensors etc. GR also exhibits well-behaved field-effect transistor properties.[23] It shows a high charge capacity in the electrochemical study for which GR based materials are widely used as electrode materials for electrochemical supercapacitors. It exhibits a high lithium-storage capacity (540 mAhg^{-1}) which is applicable in lithium secondary batteries.[14] Additionally, an unusual half-integer quantum hall effect (QHE) for both electron and hole carriers in GR has been observed by adjusting the chemical potential with the use of the electric field effect.[14] Such QHE can be observed at room temperature and the fractional QHE was obtained when suspended GR devices were probed, which allows for the isolation of the sample from substrate-induced perturbations.

(4) *Optical property:* Optical transparency of GR is very high. Therefore, GR based nanocomposites are very popular for making transparent conductive films for application in transparent conducting electrodes and solar cells etc.[24] Single layer GR shows 2.3% white light absorption with a little reflectance (0.1%).[25] The absorbance increases as number of layers increases.

(5) *Mechanical properties.* GR is regarded as the stiffest material among other carbon based fillers like cabon black, expanded graphite and SWCNT. GR exhibits a high Young's modulus value of 1.0 TPa, elastic modulus of 0.25 TPa and a fracture strength of 130 GPa.[26] GR based polymer nanocomposite shows a remarkable improvement in mechanical properties even at a lower GR loading. Although GR is so robust, it is also very stretchable. It can be stretched up to 20% of its initial length. Therefore GR has proven to have promising application potential in making strong composite materials and flexible displays.[5]

(6) *Thermal properties.* Suspended single-layer GR exhibits a thermal conductivity value of about 5000 W m^{-1} K^{-1} at room temperature.[4,27] The value is around 50 times higher compared to metals like copper and silicon. Due to its 2D platelet-like structure, GR shows higher thermal conductivity than 1D CNT. This high thermal conductivity and excellent thermal stability of GR make it an excellent material for applications in electronic devices such as fuel cells and lithium-ion batteries.[28,29] However, enhancement in thermal conductivity of carbon based fillers is not as high as electrical conductivity. Table 1.1 shows superior properties of GR compared to other materials.[3]

Table 1.1 Properties of GR compared to other materials (adopted from Ref. 3)

Materials	Tensile strength	Thermal conductivity (W/mk) at room temperature	Electrical conductivity (S m^{-1})
Graphene	130±10 GPa	4.84×10^3-5.3×10^3	7200
CNT	60-150 GPa	3500	3000-4000
Nano-sized steel	1769 GPa	5-6	1.35×10^6
Plastic (HDPE)	18-20 MPa	0.46-0.52	Insulator
Natural rubber	20-30 MPa	0.13-0.142	Insulator
Fiber (kevler)	3620 MPa	0.04	Insulator

1.2.1 GR Synthesis

Till now, various approaches have been developed for the synthesis of GR. Some of the methods are given below:

Bottom -up method

GR can be synthesized by several *Bottom-up processes* such as chemical vapor deposition (CVD), epitaxial growth on electrically insulating surfaces (SiC), arc discharge, unzipping of CNT etc.[4] In CVD, GR can be synthesized by dissolving carbon atoms into a metal catalyst substrate, such as Ni, Cu, Co, Pt, Ir and then forcing them to precipitate out after cooling, to form large-scale GR films.[30] In epitaxial growth method, single crystal SiC substrates are heated in vacuum at high temperatures. Evaporation of silicon atoms from the crystal surface results in the formation of GR layers.[31] Both CVD and epitaxial growth are suitable for preparing defect-free uniform GR sheets for electronic applications but they are not applicable for mass scale production. The advantages and disadvantages of bottom-up methods are summarized in Table 1.2 as adopted from Ref. 4.

Table 1.2 Bottom-up methods for GR synthesis[4]

Method	Thickness	Advantage	Disadvantage
CVD	Few layers	Large size, high quality	Small production scale
Arc discharge	Single, bi- and few layers	Can produce 10 g/h of GR	Low yield of GR
Epitaxial growth on SiC	Few layers	Very large area of GR	Very small scale
Unzipping of CNT	Multiple layers	Size can be controlled	Expensive starting material

Top-Down method

Top down methods are used for large scale production of GR. Here, GR sheets are prepared by exfoliation or separation of graphite.

Exfoliation of Graphite

Single layer GR has been prepared by micromechanical cleavage of graphite. In 2004, Novoselov et al.[32] isolated GR by putting a small amount of graphite between two layers of cellophane tape and peeled the tape apart; and thus single layered GR was

obtained. Single or few layered GR can also be obtained by direct exfoliation of graphite by sonication in the presence of polyvinylpyrrolidone.[33] Large quantitity of GR can be obtained by this method which is helpful in composite preparation. GR sheets can also be produced by electrochemical exfoliation method by dispersing in aprotic solvents.[34]

Chemical reduction of GO

     In this method first graphite oxide is prepared using Brodie[35] or Hummers[36] methods where graphite is first oxidized using strong oxidizing agents such as $KMnO_4$, $NaNO_3$ in the presence of nitric acid or sulfuric acid. Then it is exfoliated to graphene oxide (GO) by ultrasonication in the protic solvents like dimethyl formamide (DMF), tetrahydrofuran (THF) and N-methyl pyrrolidone (NMP) etc. Chemical reduction of the exfoliated graphite oxide sheets produces GR with one to three layers. Generally used reducing agents in these methods are hydrazine, dimethylhydrazine and sodiumborohydride etc.[37,38] Although chemical reduction method is an efficient one, but use of hazardous and costly reducing agents limits its applications. Fig. 1.3 shows the images of GO dispersion (brown in colour) and GR suspension (black) after reduction by hydrazine.
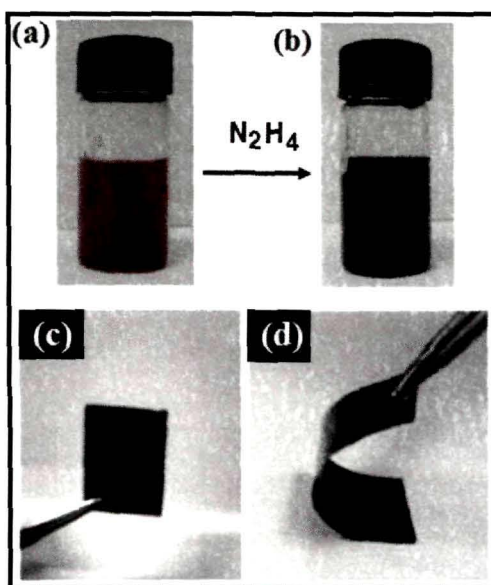
Fig. 1.3 Photographs of (a) GO dispersion, (b) chemically reduced GR suspension after addition of hydrazine, (c) freestanding and (d) a flexible GR paper.

Thermal reduction method

In this method GO is heated rapidly under inert gas and high temperature which leads to the exfoliation of GO and reduction producing reduced GO sheets[39] During heating, CO_2 gas evolves due to the decomposition of epoxy and hydroxyl groups of GO, which generates pressure leading to the exfoliation GO sheets This method produces GR which has high structural defects, however, this method is useful for producing chemically modified GR without the use of a solvent Several top-down methods for synthesis of GR are listed in Table 1 3

**Table 1.3** Different top-down approaches for synthesis of GR (adopted from Ref 4)

Method	Thickness	Advantage	Disadvantage
Micromechanical exfoliation	Few layers	Large size and unmodified GR sheets	Very small scale production
Direct sonication of graphite	Single and multiple layers	Unmodified GR, low cost	Low yield
Electrochemical exfoliation	Single and few layers	Single scale functionalization and exfoliation, high conductivity	Expensive
Superacid dissolution of graphite	Mostly single layer	Unmodified GR, scalable	Use of hazardous acid
Chemical reduction of GO	Single and multiple layer	Large sheet size, Water is used as a solvent	Use of hazardous reducing agents
Thermal reduction	Single and few layer	One step exfoliation, short heating time	High heating temperature, small sheet size

All these methods have their own merits and demerits However, in the preparation of polymer composites, mostly GR is synthesized from GO using chemical reduction method

1.2.2 Characterization of GR

A variety of spectroscopic and analytical techniques are used to characterize GR such as X-ray diffraction (XRD), Raman spectroscopy, atomic force microscopy (AFM), transmission electron microscopy (TEM) and scanning electron microscopy (SEM) etc XRD is used to study whether graphite has been intercalated or exfoliated Graphite shows a diffraction peak at $2\theta = 26\ 3°$, which shifts to around $11\text{-}14°$ in

graphite oxide.[14] XRD peak disappears in case of full exfoliation of GO into single sheets.[40] AFM gives the information regarding the size of GR sheets, number of layers, topology and defects etc (Fig. 1.4(b)).[41] The structure and morphology of GR can be obtained from SEM and TEM analyses. Apart from size determination, using High-Resolution TEM (HR-TEM), atomic bonds on functionalized sheets and atomistic defect can also be identified.[42] Raman spectroscopy is also an important technique used for quantitative and qualitative analyses of GR.[43] Conversion of sp^3-hybridized carbons to sp^2 carbons can also be analyzed with the help of Raman spectroscopy (Fig. 1.4(c)).[44]
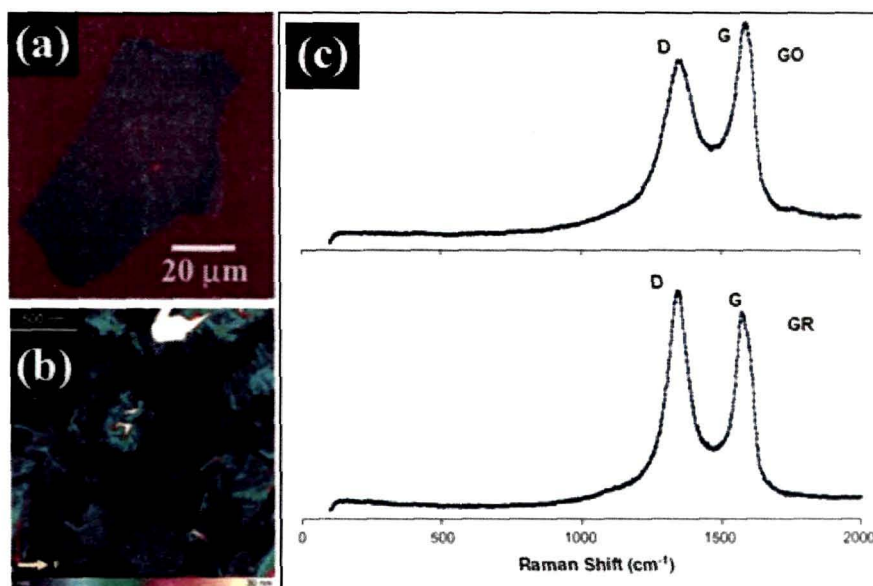
Fig. 1.4 (a) Single layer GR, first observed by Geim[32], (b) AFM images of a chemically converted GR sheet on Si/SiO₂ substrate (adopted from Ref. 41) and (c) Raman spectra of GO and GR (adopted from Ref. 43).

1.3 Graphene oxide (GO)

GO is the single-layer of graphite oxide which is generally produced by chemical oxidation of graphite. It has sp^3 hybridized carbon atoms that are covalently bonded with variety of oxygen containing functional groups such as hydroxyl, epoxy and carbonyl groups on its basal plane and edges (Fig. 1.5(b)).[45] To investigate the oxygen functionality and chemical composition of GO various spectroscopic techniques like Fourier Transform Infrared Spectroscopy (FTIR), Nuclear Magnetic

Resonance Spectroscopy (NMR), Raman spectroscopy, X-ray photoelectron spectroscopy (XPS) have been used.[46] SEM (Fig. 1.5(b)),[5] are TEM are used to investigate the morphology and structure of GO sheets. AFM analysis is also used to measure the thickness as well as the number of layers of GO (Fig. 1.5(c)).[16] However complete structural features of GO is yet not clear due to the presence of high defects and irregular packing of layers.
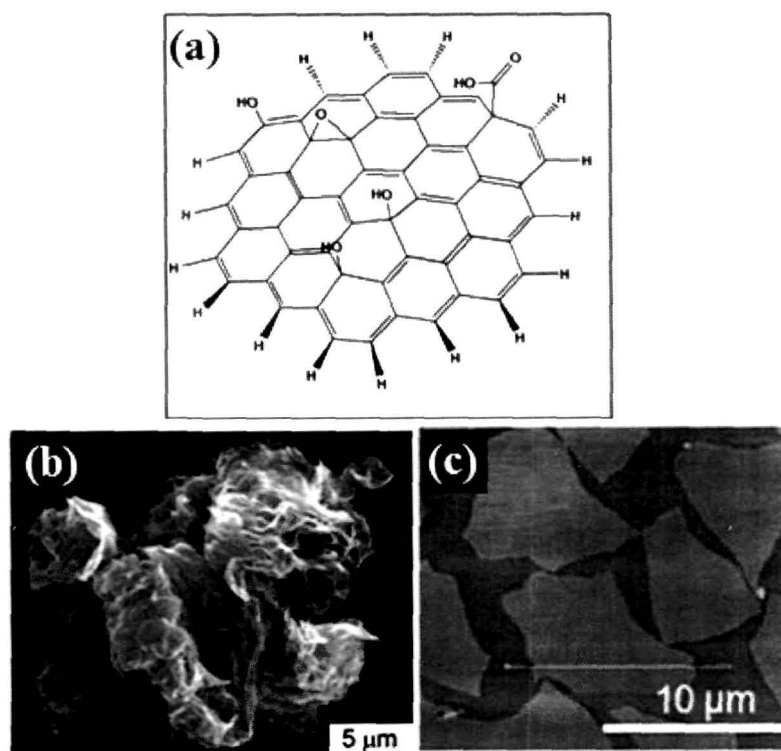
Fig. 1.5 (a) Structure of GO, (b) SEM (adopted from Ref. 5) and (c) AFM images of a graphite oxide film (adopted from Ref. 16).

Due to its 2D structure and the presence of oxygenated functional groups, GO exhibit excellent thermal, mechanical, electronic, optical and electrochemical properties. Pristine GR is not compatible with organic polymers and does not form homogeneous composites. In contrast, tunable oxygen-containing groups of GO impart strong interaction with polar molecules or polymers to form GO intercalated or exfoliated composites.[46,47] Therefore, GO has attracted remarkable interest as a nanofiller for polymer nanocomposites. Several GO based polymer composites have

been developed till date and great improvement in thermal, mechanical, electrical properties of these composites were observed.[48-51]

The functional groups in GO facilitates its chemical functionalization. GO can be covalently functionalized either by adding small molecules or polymers through esterification, amidation or by non-covalent functionalization like π-π stacking, hydrogen bonding and van der Waals interaction. GO shows unique photoluminescence properties which occurs from the near-UV-visible to near-infrared wavelength range. For which it is used in various optoelectronics applications.[52] Moreover, GO exhibits specific ultrafast optical dynamics and nonlinear optical properties. The electrochemical properties of GO has also become popular recently. Due to the high specific surface area, GO can accommodate electroactive species on its surface and facilitates the electron transfer at the surface of the electrode.[53,54] GO stable dispersion can be used to deposit on various substrates to make thin films in electrode materials. Thus an inexpensive electrode with large surface area can be obtained with the use of GO based conductive film.[55] However, direct application of GO in electrically active material is limited by the presence of electrical resistant groups like carboxyl, hydroxyl and epoxy in GO sheets. So the reduction of GO through various chemical and thermal methods can facilitates the transport of charge carriers and thereby improving its electrical behavior.[56,57] Use of GO as a catalyst for various oxidation and hydration reactions has also been reported so far.

1.4 GR/GO based polymer nanocomposites

GR/GO based polymer composites show superior mechanical, thermal, gas barrier, electrical and electrochemical properties than that of the composites with conventional fillers like lay and other carbon based fillers.[3-5] The interesting features of these nanocomposites is that these enhancements in properties are achieved at very low filler loadings in the polymer matrix. The improvement in properties strongly depends upon the degree of dispersion of the nanofillers in the polymer matrix. Polymer nanocomposites based on GR and GO with multifunctional property enhancements has shown great potential in a wide variety of applications and has opened a vast interesting research area.[58]

1.4.1 Preparation methods of GR/GO based polymer nanocomposites

A variety of methods have been reported for the preparation of GR/GO based polymer composites recently. The interaction of GR/GO with polymer matrix depends upon several factors like polarity, molecular weight, hydrophobicity and reactive groups etc. of each component as well as the solvent.[59] Also homogeneous dispersion of the nanofillers in the polymer matrix plays a crucial role in the improvement of properties in a nanocomposite system. There are three main methods for incorporating polymer chains inside the GO and GR layers which are described below:

i. In-situ intercalative polymerization:

In this method, GR or GO is first dispersed in the liquid monomer. Then initiator is added and polymerization reaction proceeds in presence of heat or radiation.[60] The in-situ polymerization has been used to prepare non-covalent composites of a large number of polymers like polymers, such as polystyrene (PS),[61] poly(ethylene terepthalate) (PET),[59] poly (methylmethacrylate) (PMMA)[62] etc. Here, the neat monomer is intercalated in between the layers of GR or GO and then polymerization separates the layers.

ii. Solution intercalation:

In this method GR or GO is first dispersed in a suitable solvent by ultrasonication, then the polymer is solubilized in that solvent followed by removal of the solvent by evaporation or distillation.[2] Here polymer is first adsorbed on the exfoliated nanosheets and on removal of the solvent, the sheets restack forming the nanocomposites with polymer chains sandwiched in between them. GR and GO can be dispersed in a variety of solvents such as water, THF, acetone, chloroform and DMF etc. Synthesis of intercalated nanocomposites with polymers having low polarity is possible in this method. Several composites with polymers such as epoxy,[63] polypropylene (PP),[64] poly(vinyl alcohol) (PVA),[65] poly(vinyl chloride) (PVC)[66] based composites have been prepared using this method. One limitation of this method is that traces amount of solvents remained on the composite material even after the careful removal of the solvent.

iii. *Melt intercalation*:

In the melt intercalation method, GR or GO is mixed with the molten polymer matrix under high shear conditions. This method is considered as more economical and environment friendly method compared to other two methods as no solvent is used here. Here the polymer is mixed with the nanofillers at elevated temperatures using extrusion and injection molding process and then polymer chains are intercalated or exfoliated to form the nanocomposites. This method is mostly used in industrial applications for preparing nanocomposites based on thermoplastic polymers such as PP,[67] polyamide[68] and HDPE[69] etc. However, this method provides the lower dispersion level than the solution mixing or in situ polymerization methods which results in poorer mechanical and physical properties of the nanocomposite. Also the low bulk density of exfoliated GR causes difficulty in processing such as feeding to the melt extruder.

iv. *Interfacial polymerization method:*

In this work we have synthesized the composites mostly by interfacial polymerization. In interfacial polymerization method, the nanofiller, initiator and the monomer are dispersed in two immiscible liquids.[70] The nanofillers are exfoliated through ultrasonication prior to the mixing. Then both the liquids with different phases (organic and aqueous phase) are mixed together. As the reaction proceeds, the reactants diffuse to the interface and the monomer gets adsorbed on the nanofiller. The polymerization takes place at the interface of two immiscible liquids and polymer chains are intercalated or exfoliated in between the layers of nanofillers. The process of interfacial polymerization is shown schematically in Fig. 1.6.
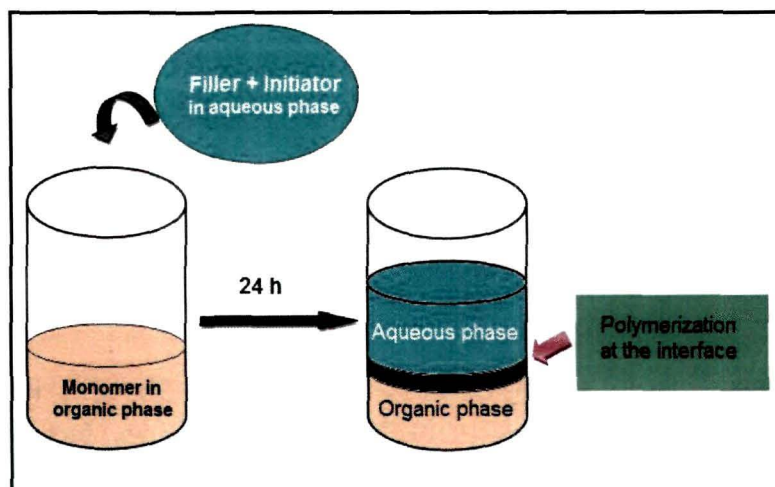
Fig. 1.6 Schematic diagram of interfacial polymerization method

The interfacial polymerization has several advantages over other polymerization technique which are given below:

a) This process is simple and requires ordinary equipment.

b) Unlike bulk condensation polymerization, high molecular weights are obtained rapidly in interfacial polymerization because the monomer meets the growing polymer chain than the opposing monomer that leads to termination of the polymerization.

c) Polymers which are unstable at the high temperatures can be easily synthesized by this method as it requires low temperature for synthesis.

d) This polymerization process is effective in controlling the structure and composition of the resulting polymer chain as well as the copolymer, without the need for a conventional catalyst.

e) It is a direct method of forming polymer solutions, dispersions, polymer coatings encapsulants, fibrous particulates and films.

Due to the above advantages we have chosen the interfacial polymerization technique to prepare few GO/GR based nanocomposites such as GR/GO based polypyrrole and polythiophene composites. For the first time we have applied this method to prepare polymer nanocomposites. The composites showed good

enhancement in various properties like mechanical, thermal, electrical and electrochemical properties with remarkable application potential.

1.4.2 Property enhancement in GR/GO based polymer composites

GR based polymer nanocomposites have shown significant improvement in electrical conductivity. Eda et al.[71] synthesized PS/GR composite films using solution blending method. The composite thin films exhibited an electrical conductivity ranging from 1 to 24 Sm[-1], which is in good agreement with the values reported by Stankovich et al.[2] (Fig. 1.7). The conductivity decreased with decreasing temperature upto 50 K and then slightly increased with further decreases in temperature.
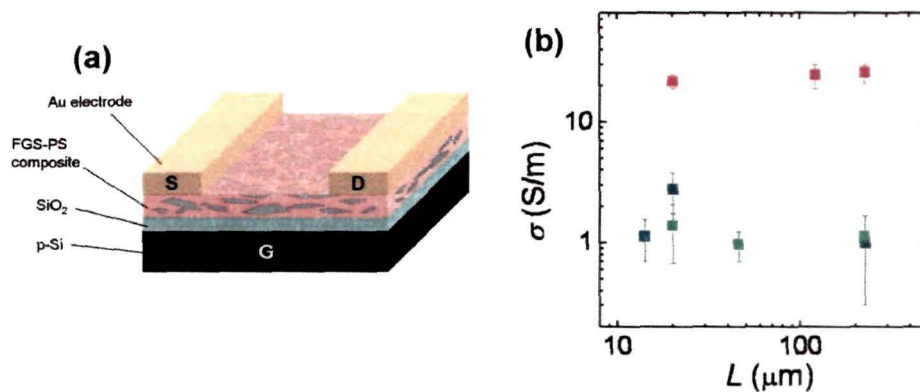
Fig. 1.7 (a) Schematic diagram of FGS-PS composite thin film field effect devices, (b) Device conductivities measured in ambient conditions as a function of channel length (adopted from Ref. 71)

Patole et al.[73] reported a large scale production route for PS functionalized GR sheets using water based in-situ microemulsion polymerization which showed good improvement in electrical properties compared to pure PS. As reported by Zhang et al.[59] PET/GR composite showed a high electrical conductivity value of 2.11 S m^{-1} at 3 vol.% of GR. Kim et al.[73] prepared polycarbonate (PC) composites reinforced with functionalized GR sheets (FGS) by melt compounding. A higher electrical conductivity was achieved at lower FGS loading than with the graphite filler. Lee et al.[74] prepared waterborne polyurethane (WPU)/FGS nanocomposites using an in-situ method. The composite exhibited remarkable improvement in the electrical conductivity compared

to pristine WPU which is due to the homogeneous dispersion of FGS particles in the WPU matrix. Electrical conductivities of some GR/GO based polymer composites are shown in Table 1.4.

Table 1.4 Electrical properties of GR/GO based polymer nanocomposites

[a]Polymer matrix	[b]Filler	Filler wt.%	loading vol. %	σ (S m^{-1}) of matrix	σ (S m^{-1}) of composite	References
PS	GR	2.0	0.10	10^{-10}	10^{-2}	75
	GR			10^{-16}	10^{-5}	2
PANI	GO	-	-	2	1000	76
	GR	-	-	-	9030	77
PMMA	GNS	1		1.3×10^{-11}	-	78
PP	GO	4.90		-	3.12×10^{-1}	79
PVDF	FGS	2.0		10^{-11}	10^{-2}	80
PC	FGS	2.0		10^{-14}	10^{-9}	73
PET	GR		0.47	10^{-14}	7.4×10^{-2}	59
Epoxy	GR		0.52	10^{-10}	10^{-2}	60
Nylon 6	FGS		0.75	10^{-15}	10^{-5}	81

[a]PS: polystyrene; PMMA: poly(methyl methacrylate); PP: polypropylene;; PVDF: poly(vinylidene fluoride); PC: polycarbonate; PET: poly(ethylene terephthalate); [b]GR: graphene; GO: graphene oxide; GNS: graphene nanosheets; FGS: functionalized graphene sheets.

GR is one of the strongest materials with a high Young's modulus value of 1.0 TPa and a fracture strength of 130 GPa.[26] Incorporation of GR and GO in polymer matrix can improve its mechanical strength in a dramatic way. GR based PVA was successfully prepared by Zhao et al.[82] incorporating GO into PVA matrix and reducing GO into GR. The composite films showed uniform dispersion and exhibited a significant improvement in mechanical properties. Around 150% improvement of

tensile strength and around 10 times increase of Young's modulus are obtained at a 1.8 vol.% of GR loading (Fig. 1.8).
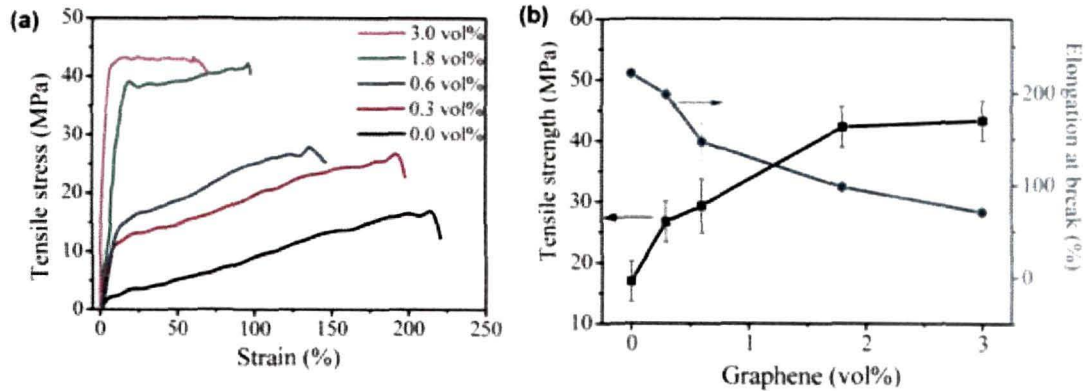
Fig. 1.8 (a) Typical stress-strain plots of GR/PVA nanocomposites with various GR loadings, (b) Mechanical properties of the nanocomposites with various GR loadings: tensile strength (left) and elongation at break (right) versus GR loadings (adopted from Ref. 82).

Xu et al.[83] prepared mechanically strong PVA/GO composite film by vacuum filtration which showed a high Young's modulus and tensile strength value of 4.8 GPa and 110 ± MPa, respectively at 3 wt.% GO loading. GR and PVC thin composite film was synthesized by a simple solution blending, drop casting method as reported by Vadukumpully et al.[84] The film showed around 58% increase in Young's modulus and 130% improvement of tensile strength at 2 wt.% of GR loading. Liu et al.[85] reported a new method to synthesize polyester/reduced GO composites via simultaneous dispersion and thermo-reduction of GO during in situ melt polycondensation. The composite showed significant improvement in tensile strength and elongation at break. Rafiee et al.[86] prepared epoxy nanocomposites with GR platelets which showed significantly superior mechanical properties than that of CNT. The nanocomposite showed around 31% increase in Young's modulus and 40% increase in tensile strength compared to the pristine epoxy. These strong and ductile composites can be used as high strength and flaw tolerance structural materials. Table 1.5 summarizes the enhancement in the mechanical properties of some GR/GO based polymer nanocomposites with respect to the polymer matrix.

Table 1.5: Mechanical properties of GR/GO based polymer nanocomposites

[a]Polymer matrix	[b]Filler type	Filler loading		Modulus increase (%)	Tensile strength increase ((%)	Reference
		wt.%	vol%			
PVA	GO	0.7		-	76	65
	GR	-	1.8	-	150	82
PMMA	GO	-	1.7	54	-	87
	TRG	-	0.5	80	-	48
PP	TRG	-	1.9	43	-	88
PS	GR	-	0.4	57	-	47
PC	TRG	-	2.5	52	-	88
Epoxy	TRG	-	0.05	31	40	86
	GO	-	2.4	900	19	89
TPU	TRG	-	1.6	250	-	90
	SG	1.0		-	75	91

[a]PVA: poly(vinyl alcohol); TPU: thermoplastic polyurethane. [b]TRG: thermally reduced graphene; SG: sulphonated graphene.
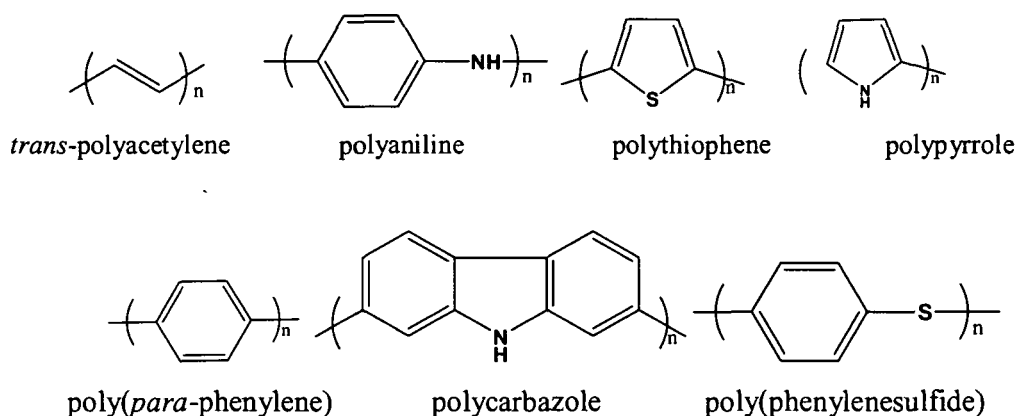
Besides mechanical and electrical property, thermal stability of polymers can also be improved by incorporating fillers like GR and GO which have superior thermal properties. For example, in poly(acrylonitrile)(PAN)/FGS composite, the T_g (glass transition temperature) value increased more than 40 °C at 1 wt.% FGS loading.[48] Similarly, PMMA/FGS composite showed an increase of 30 °C in T_g at a low loading of FGS (0.05 wt.%).[48] The enhancement in various properties in these reports is attributed to the large surface area of highly conducting GR sheets, good interaction between filler and matrix induced by the surface functional groups present in GO as well as their homogeneous dispersion in the polymer matrix.

1.5. Conducting polymers

Conducting polymers are getting huge interest in scientific research in last few decades because it shows a combination of properties i.e. semiconductor or metal like electrical properties as well as the advantages of conventional polymers such as easy

and low cost synthesis. In 1974, MacDiarmid and co-workers discovered the conducting nature of polyacetylene when it is doped with I_2, Br_2 or AsF_5.[92] Since then many aromatic conducting polymers have been studied for their conductivity.[93]

Among the conducting polymers, polyaniline (PANI),[94] polypyrrole (PPy),[95] polythiophene (PTh)[96] and poly (3,4 ethylenedioxythiophene) (PEDOT)[97] are getting more importance among the researchers as they show high conductivity values and good stabilities. Conducting polymers have of sp^2 hybridized carbon atoms with a valence electron in a p_z orbital. These electrons exhibit high mobility on doping, removing some delocalized electron and thus an electronic band structure is formed by the conjugated p-orbitals. However, conventional polymers possess sp^3 hybridized covalent bonds with the valence electrons residing in it. Due to these less mobile sigma-bonding electrons, the electrical conductivity of such polymers is poor. Fig. 1.9 shows the structures of some commonly used conducting polymers.

trans-polyacetylene   polyaniline   polythiophene   polypyrrole

poly(para-phenylene)   polycarbazole   poly(phenylenesulfide)

Fig. 1.9 Structures of some conducting polymers.

The conductivity value of conducting polymers is found to be around 10^5 S cm^{-1} which is much higher than that of conventional polymers (10^{-12} S cm^{-1}). The chemical and electrical properties of conducting polymers can be manipulated to get different properties for diverse range of applications. Conductive polymers are synthesized using variety of methods such as chemical, electrochemical, photochemical, metathesis, solid-state, plasma, pyrolysis, concentrated emulsion and inclusion polymerization etc.[95] Among all these, chemical and electrochemical polymerization are the most widely

used methods for preparing conductive polymers.[98,99] Chemical polymerization is mostly used for preparing large amount of conductive polymers without the use of an electrode. Chemical polymerization (oxidative coupling) is done in presence of oxidizing agents like ferric chloride, ammonium persulphate etc. which oxidizes the monomers to a cation radical followed by the coupling of the radicals to form dications (Fig. 1.10). This process repeats generating a polymer.
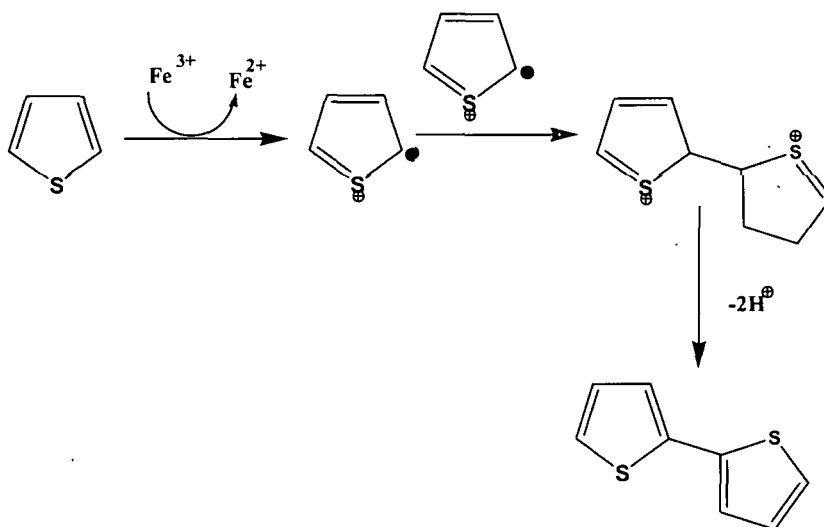

Fig. 1.10 Mechanism of chemical polymerization of thiophene.

Electrochemical polymerization is done in a standard three-electrode cell in a supporting electrolyte with an appropriate power supply (potentiostat to obtain thin films, galvanostat to obtain thick films).[100] This is a simple technique to obtain a simultaneously doped polymer with high conductivity value. Also using electrochemical polymerization, free-standing conductive polymer films of required thickness can be prepared. A variety of conductive polymers like PANI, PPy, PTh etc. have been synthesized by this method.

1.6. GR and GO based conducting polymer composites

The combination of GR and GO with conducting polymers offers an attractive route not only to reinforce polymer films but also to introduce new electronic properties based on morphological modifications or electronic interactions between the two

components.[101] Several works have been reported on GR/GO based conducting polymer composites which showed great improvements in various properties. Some of them are described briefly as follows.

Zhang *et al.*[102] successfully prepared GR and PANI nanofiber composites by in situ polymerization. The composites showed high electrical conductivities. They exhibited good application potential in supercapacitors with high specific capacitance (480 F/g at a current density of 0.1 A/g) and good cycling stability during charging-discharging process (Fig. 1.11). Wu *et al.*[103] synthesized PANI/GR nanocomposite simply by ultrasonication and studied their application as supercapacitor. The conducting composite film showed a high capacitance value of 210 F/g and great electrochemical stability.
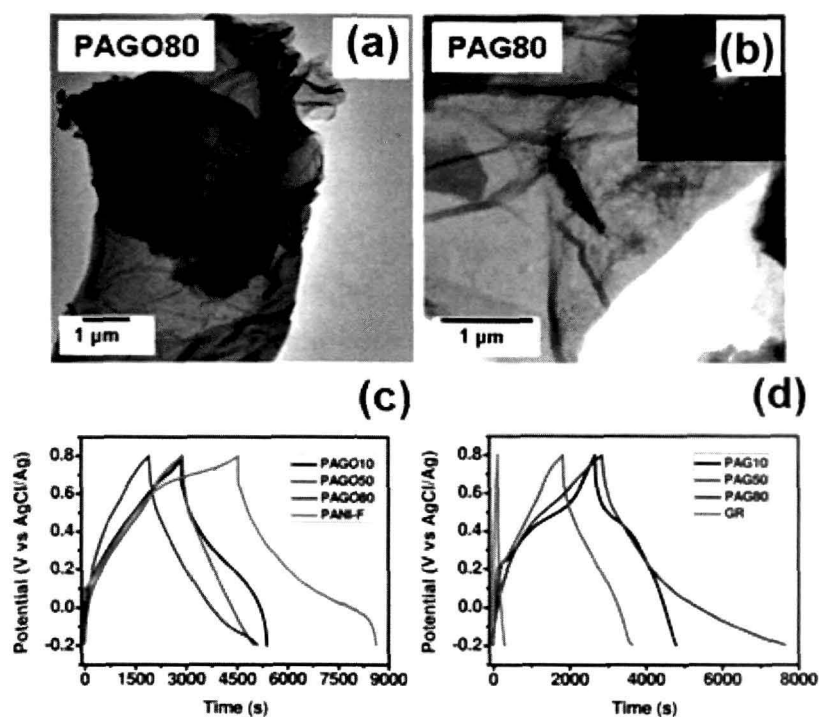
Fig. 1.11 TEM images of (a) PAGO80, (b) PAG80 composite, (c) and (d) Charge/discharge cycling curves of different composite electrodes at a current density of 0.1 A/g (adopted from Ref. 102).

Hao *et al.*[104] prepared PANI/sulfonated GR (SGEP) nanocomposite by liquid/liquid interfacial polymerization method. The morphology of the composites was

21

controlled by adding additional acidic dopant or changing the ratio of filler and PANI. Nanocomposite showed excellent electrochemical capacitance of 763 F/g, and good cycling stability upto 1000 electrochemical cycles. Thus the composite exhibited great potential for application in energy storage devices. Wang et al.[105] prepared GO/ PANI composite by in-situ polymerization which showed good electrochemical performance as supercapacitor electrode. The composite exhibited fibrillar morphology in the SEM analysis. An excellent electrochemical capacitance and capacitance retention value (73% and 64% after 500 cycles) of the composite was observed in the cyclic voltammetry study. Polymer nanocomposites based on PANI and GNS modified with poly(sodium-4-styrensulfonate) (PSS-GNS) was synthesized by Tung et al.[106] The composite showed higher electrical conductivity and improved thermal stability than that of pure PANI.

Gu et al.[107] prepared PPy/GO composites by in-situ polymerization without doping material. SEM and HRTEM showed that the GO surface is coated with a uniform PPy layer. The electrical conductivity of the composite increased four times higher than that of pristine GO. TGA analysis showed that PPy/GO composites are thermally more stable in comparison to pure PPy. These highly conductive PPy/GO composites can be used in high temperature electronics. A single-step preparation of a PPy sensor on a disposable screen-printed electrode was done by Scott et al.[108] The SGNF/PPy composite shows a high selectivity when used in the oxidation of guanine and hydrogen peroxide, both of which are important biomarkers used for biosensing. This single step method of formation of a SGNF/PPy composite produces a high output of sensitive, portable and disposable electrodes, with least contamination and allows for further applications in the detection of biomedically important compounds and DNA sensing. Zhang et al.[109] synthesized PPy/GNS composite via in situ polymerization of pyrrole monomer under acid conditions. The composite showed higher specific capacitance, better rate capability and cycling stability than that of pure PPy and thus it allows its applications in supercapacitors. PPy/GR nanocomposites were successfully prepared by Bose et al.[110] via in-situ polymerization of GO and pyrrole monomer followed by chemical reduction using hydrazine monohydrate. The XPS data indicated the removal of oxygen functionality of GO upon reduction. XRD and FTIR analysis

confirmed the formation a structure similar to GR. In the Raman spectroscopy, intensity ratio was found to be 1.17 for PPy/GR, suggesting the increased number of sp^2 domains which were formed during the reduction process. TGA analysis showed a reasonable improvement in thermal stability of the reduced composite (Fig. 1.12). The composites exhibit a high value of conductivity which may be due to the high aspect ratio and large specific surface area of the in-situ formed GR nanosheets in PPy matrix.
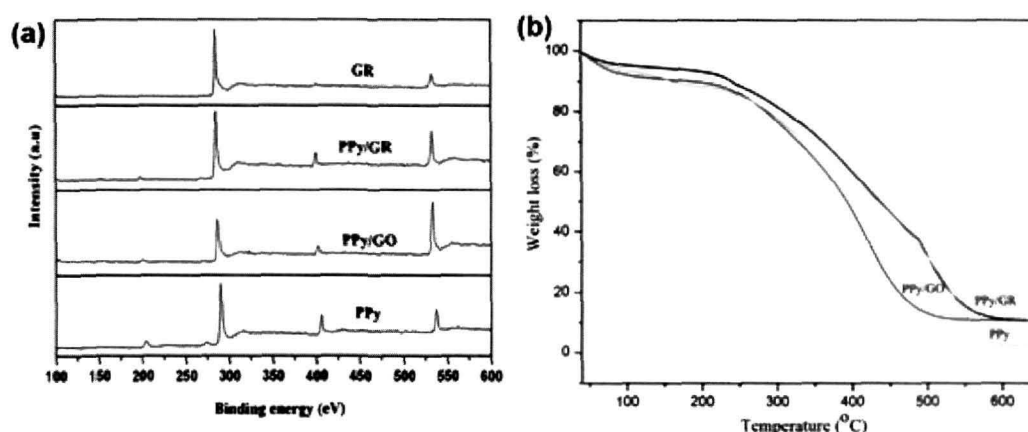
Fig. 1.12 (a) Wide region XPS study of pure PPy, GR, PPy/GO, and PPy/GR composites, (b) TGA of pure PPy, GR, PPy/GO, and PPy/GR composites (adopted from Ref. 110).

1.7. Applications of GR/GO based polymer composites

GR based polymer composites have been explored for a wide range of applications in many areas such as energy storage device,[111] sensors,[112] ESD and EMI shielding,[113] solar cells,[114] liquid crystal devices,[115] organic light emitting diodes,[116] field emission devices[117] and biomedical applications[118] etc. GO based polymer composites exhibit a moderate conductivity, high chemical stability and excellent electrochemical properties. GO based composites are also found to be attractive for electrochemical applications due to its high surface area and good interaction with water and organic solvents. It is reported that GO facilitates the electron transfer of enzymes and proteins.[119] GO based electrodes are widely used in various electrochemical applications such as electrochemical sensors,[120] electrochemiluminescence[121] and electrocatalysis[122] etc.
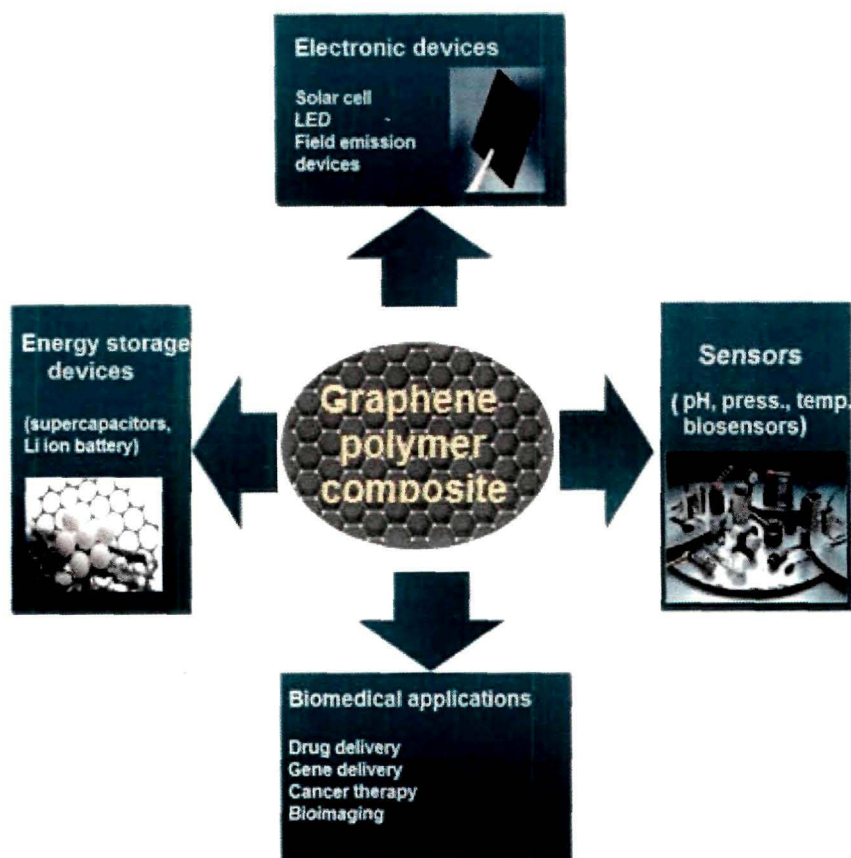
23

Fig. 1.13 Applications of GR based polymer composites.

Some of the applications of GR and GO based polymer nanocomposites are summarized below.

1.7.1 Electrochemical sensors

A sensor is a device that is used to detect a variable quantity and transforms the measurement into corresponding signals which can be recorded. Sensors are widely used in diverse fields such as medical diagnostics, food, pharmaceutical laboratories, occupational safety and environmental analysis.[123] Sensors may be of different types such as electrochemical, electromagnetic, thermal and mechanical sensor. Among them, the electrochemical sensors are getting more attention due to their high selectivity and sensitivity. They have many benefits like low detection limits, a wide linear response range, good stability and reproducibility.

GR based electrochemical sensors have been widely used to detect a variety of gas and biomolecules in recent years.[124] GR has shown superior performance compared to CNT for applications in electrochemical sensors. GR possesses good electrocatalytic activity towards hydrogen peroxide, NADH etc. which make it an effective candidate for biosensor applications. Hydrogen peroxide is a product of oxidase enzymes which is essential in making of biosensors as well as in pharmaceutical and environmental analyses.[125] Zhou *et al.*[126] constructed a glucose biosensor based on reduced GO which shows a superior electrocatalytic activity towards H_2O_2. The biosensor showed high sensitivity with a low detection limit (2.00 mM at -0.20 V) for sensing glucose. They also reported a highly sensitive electrochemical DNA sensor based on which can detect selected DNA sequences or mutated genes that are responsible for human disease. Liu *et al.*[127] reported a novel, highly efficient enzyme electrode using covalent attachment between carboxyl acid groups of GO sheets and amines of glucose oxidase (GOD). The amperometric response curve of the biosensor electrode is shown in Fig. 1.14(d). The resultant biosensor showed a good sensitivity of 8.045 $mA.cm^{-2}$ M^{-1} as well as good reproducibility and storage stability. The biosensor electrode also showed good biocompatibility indicating a good potential for use in medical field.
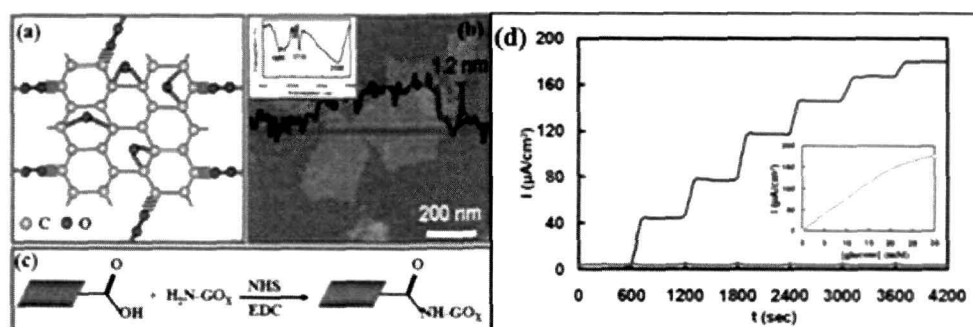
Fig. 1.14 (a) Schematic representation of the molecular structure of a GO sheet, (b) AFM micrograph of the GO sheets, (c) schematic immobilization of GOD into GO sheets via peptide bonds between the amine groups of GOD and the carboxylic acid of GO and (d) Amperometric responses at the GOD covalently immobilized GO electrode (blue line) and the pristine GO electrode (pink line) in 0.4MPBS (pH 7.4) with the successive injection of glucose. (Inset) Calibration curve obtained for glucose determination at 0.4 V vs Ag/AgCl in 0.4MPBS (pH 7.4) (adopted from Ref. 127).

Shan *et al.*[128] reported the first GR-based glucose biosensor using poly(vinylpyrrolidone)-protected/polyethylenimine-functionalized ionic liquid/GOD electrochemical biosensor, which showed the direct electron transfer of GOD, with linear glucose response up to 14 mM. Lian et al. fabricated a highly sensitive uric acid sensor by using GR doped chitosan composite which showed higher sensitivity compared to undoped sensor.[129] A GR-nafion matrix modified glassy carbon electrode was developed by Xue *et al.*[130] for the determination of organophosphorus pesticides. The sensor has been used successfully to determine methyl parathion present in vegetable samples. Kang *et al.*[131] studied the electrochemical behavior of GOD at a GR-chitosan modified electrode. This electrode showed excellent sensitivity $(37.93 AmM^{-1} cm^{-2})$ and long-term stability for measuring glucose due to the large surface-to-volume ratio and high conductivity of GR. A novel bionanocomposite film consisting of GOD/Pt/FGS/chitosan for glucose sensing was prepared by Wu *et al.*[132] The biosensor showed good sensitivity with a detection limit of 0.6 M glucose. The biosensor also has good reproducibility, long-term stability and negligible interfering signals from ascorbic acid and uric acid. Such sensitivity is attributed to the good electrocatalytic activity of FGS and Pt nanoparticles towards H_2O_2 and the large surface area and rapid electron transfer of both the component (Fig. 1.15). Alwarappan *et al.*[133] reported PPy/GOD based enzymatic biosensors used for in-vitro electrochemical glucose detection. The biosensor exhibited an excellent sensitivity of 3 µM (applied potential +200 mV) for glucose detection which is better than the previously reported biosensors based on other carbon material.

1.7.2 Energy Storage

Super capacitors, the energy storage devices, have attracted considerable attention over the past decades owing to higher power density, longer cycle life, short charge-discharge time, low cost, safe operation and better environmental friendliness compared to secondary battery.[134] A supercapacitor consists of two porous electrodes that are isolated from electrical contact by a separator (Fig. 1.15 (a)). The electrodes and separators are immersed in an electrolyte. The electrolyte allows the ionic current to flow between the electrodes, preventing electronic current from discharging the cell.

When the voltage is supplied, accumulation of opposite charges at the two electrodes would result and these charges would generate an electric field that would allow the supercapacitor to store energy.[135]

For a supercapacitor, capacitance is measured by the following equation[136]

$$C = \varepsilon_o \varepsilon_r \frac{A}{D} \qquad (1)$$

where A is the surface area of each electrode, D is the distance between the electrodes, ε_o is the dielectric constant of free space and ε_r is the dielectric constant of the insulating material between the electrodes. The surface area of electrodes in a supercapacitor is much higher compared to the conventional capacitors.

Energy density and power density are the two primary characteristics of a supercapacitor. Energy density is the ability to store energy and it determines how long the supercapacitor can act as a power source. The energy storage capability of a supercapacitor is represented by the equation below.[137]

$$E = \frac{1}{2} CV^2, \text{ where C is the capacitance.} \qquad (2)$$

In the Ragone plot (Fig. 1.15 (b)), power densities of various energy storage devices are presented along the vertical axis, while their energy densities are presented along the horizontal axis. It is observed that supercapacitors occupy a position between conventional capacitors and batteries in the plot.[138]
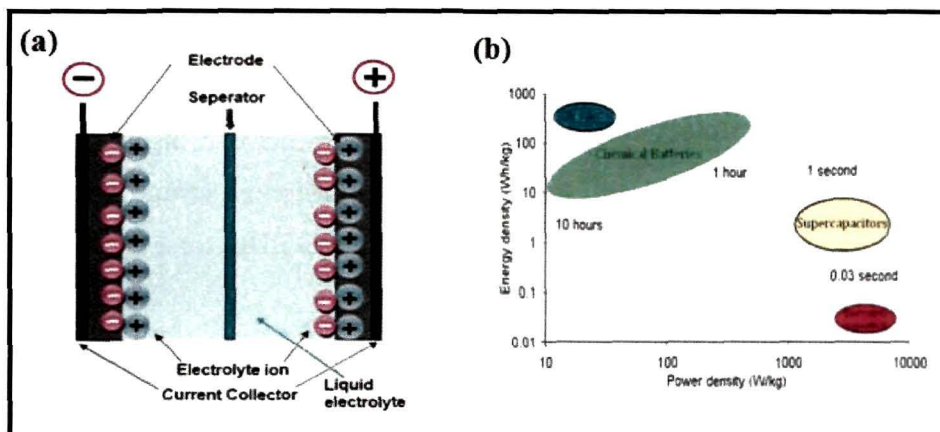

Fig. 1.15 Schematic representation of a EDLC supercapacitor.

Both batteries and supercapacitors depends on electrochemical processes, however batteries take more time to recharge compared to supercapacitors.[139] Table 1.6 represents some basic differences between batteries and supercapacitors.

Table 1.6 Differences between rechargeable batteries and supercapacitors

Supercapacitors	Batteries
Higher power density	Have higher energy density
Much faster charge and discharge rate	Typically 200–1000 charge-discharge cycles
Environmentally friendly	
Extremely low internal resistance or ESR	Contain highly reactive and hazardous chemicals
High efficiency (97-98%)	
Over a million charge-discharge cycle	Negatively affected by low temperatures

Supercapacitors can be divided into three catagories on the basis of energy storage mechanism: electrochemical double-layer capacitors (non-Faradaic), pseudocapacitors (Faradaic) and hybrid capacitors (combination of Faradic and non-Faradic).[137] Electrochemical double-layer capacitors (EDLCs) are constructed from two carbon-based electrodes, an electrolyte and a separator. EDLCs do not use a chemical mechanism and they store charge electrostatically (non faradically) by utilizing an electrochemical double-layer.[140] As voltage is applied, charge accumulates on the electrode surfaces and ions in the electrolyte solution diffuse across the separator into the pores of the electrode of opposite charge. Thus, a double-layer of charge is produced at each electrode which increases the surface area and decreases the distance between electrodes. Thus it allows EDLCs to achieve higher energy densities than conventional capacitors. As there is no transfer of charge between electrode and electrolyte, charge storage is highly reversible in EDLC and high cycling stabilities are obtained.

In pseudocapacitors, energy storage takes place via reversible faradaic redox reactions with transfer of charges between electrode and electrolyte.[141] Due to these Faradaic processes pseudocapacitors achieve greater capacitances and energy densities than EDLCs. There are two electrode materials that are used to store charge in

pseudocapacitors i.e. conducting polymers and metal oxides. Conducting polymers have a relatively high capacitance, conductivity and are low cost compared to carbon-based electrode materials. Because of their high conductivity, metal oxides have also been explored as a possible electrode material for pseudocapacitors. The mostly used metal oxide is ruthenium oxide which possesses high capacitance than that of carbon-based and conducting polymer materials.

Hybrid Capacitors uses combination of Faradaic and non-Faradaic processes to store charge, and has advantages of both EDLCs and pseodocapacitors. On the basis of electrode configuration, hybrid capacitors can be divided into three types: *composite, asymmetric and battery-type*. A composite electrode uses carbon based materials with conducting polymer or metal oxide materials in a single electrode.[142] The carbon-based materials provide a double-layer capacitance with high surface area and the pseudocapacitive materials increase the capacitance of the composite electrode through Faradaic reactions. Asymmetric hybrids capacitors couple an EDLC electrode with a pseudocapacitor electrode.[143] For example, combination of an activated carbon negative electrode with conducting polymer positive electrode has shown high energy, power density and cycling stability compared to their individual component. Battery-type hybrids couple a supercapacitor electrode with a battery electrode,[144] for example, nickel hydroxide, lead dioxide as one electrode and activated carbon as the other. Thus it combines energy characteristics of batteries with the power, cycle life and low recharging times of supercapacitors.

GR has proven to be a promising candidate for energy storage applications due to its high surface area, high conductivity, excellent optical transparency, good stability and good mechanical performance. GR shows the specific capacitances of around 135 F g^{-1} in aqueous electrolytes.[136] Although pseudocapacitive materials have higher charge storing capacity than carbon materials, their direct application in supercapacitors are limited due to their lower cycle life in a charge-discharge process than carbon based electrodes. Also they have poor stability and high resistance during cycling. Therefore combination of GR and metal oxides or conducting polymers are used as the hybrid type of supercapacitor and are found to be effective for improvement of the electrochemical performance of supercapacitors.[145] Ku et al.[46] reported the coating of

the GR on Au or Pd using a drop-dry method for the preparation of working electrodes for supercapacitor application. A reasonably high value of capacitance of 50 F g^{-1} was achieved at 300 mV s^{-1}. Almost 82% retention of capacitance was obtained after 1500 cycles. Liu et al.[147] reported GR based supercapacitor using an ionic liquid as electrolyte which showed high specific energy density of 85.6 Wh kg^{-1} at room temperature. Yu et al.[148] prepared ultrathin, transparent GR films to be used as supercapacitor. The capacitance was obtained as 135 F g^{-1} and almost 75-80% of initial capacitance value was retained at the higher scan rate of 200 mV s^{-1}.

GR-metal oxide composites have been widely studied in recent years as they show excellent electrode performance in supercapacitors. Hydrous ruthenium dioxide (RuO$_2$) was used to fabricate RuO$_2$/GR sheet composite via sol-gel and low-temperature annealing processes. The composite showed a high capacitance value of 570 F g^{-1} at 38.3 wt.% Ru loading, compared to 148 F g^{-1} for pure GR.[149] Zhang et al.[150] reported fabrication of GR-ZnO composite film for supercapacitor application, where ZnO was deposited on GR by ultrasonic spray pyrolysis. The composite exhibited a capacitance of 11.3 F g^{-1} and excellent charge-discharge stability. Li et al.[151] examined GR/SnO$_2$ nanocomposites as electrochemical supercapacitor which exhibited a capacitance value of 43.7 F g^{-1}. Fabrication of MnO$_2$/graphene composite and its use for supercapacitor was investigated by Qian et al.[152] The composite exhibited excellent electrochemical property with a high capacitance value of 324 F g^{-1} and good cyclic stability.

GR based conducting polymer composites have proven to be attractive materials for applications as supercapacitors. Among them, PANI is the mostly used polymer with GO or reduced GO sheets for supercapacitors. Wang et al.[153] synthesized flexible GR/PANI composite paper (GPCP) via in-situ anodic electropolymerization. These GPCP exhibited good potential for application as an electrode material in supercapacitor. A high capacitance value of 233 F g^{-1} was achieved for the composite which was much larger than GR paper (147 F g^{-1}). The cyclic voltammetry curves and Nyquist plots of GPCPs are shown in Fig. 1.16 which indicated good cycling stability of the composite.
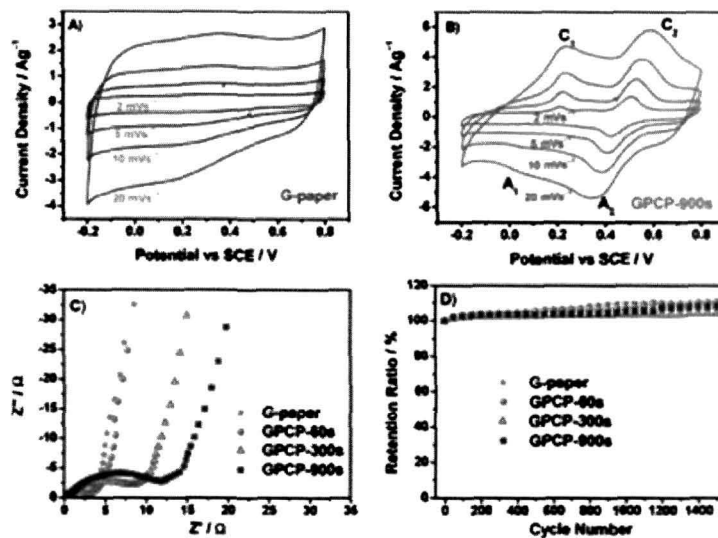
Fig. 1.16 Cyclic voltammograms of (A) G-paper and (B) GPCP, recorded from 2 to 20 mV s^{-1} in 1M H$_2$SO$_4$. (C) Nyquist plots of the G-paper and GPCP 60 s/300 s/900 s. (D) Cycling stability measured at 50 mV s^{-1} (adopted from Ref. 153).

Qi et al.[154] synthesized PPy/GO composite using pulse electro-polymerization method for application in supercapacitor in absence of additional dopants. The composite showed a high specific capacitance of 660 F g^{-1} at a current density of 0.5 mA cm^{-2}. Biswas et al.[155] reported preparation of a multilayered nanocomposite based on PPy and GNS for supercapacitor electrode applications. The composite electrode exhibited a high capacitance of 165 Fg^{-1} which is due to the strong van der Waals interaction between nanostructured PPy and GR sheets. Bose et al.[156] reported preparation of GNS/PPy nanocomposites which revealed the specific capacitance values of 417 and 267 F g^{-1} at scan rates of 10 and 100 mV s^{-1} respectively. The composite also exhibited excellent electrochemical cyclic stability with a capacity retention value of 90% after 500 cycles. Apart from GR, GO has also showed improved capacitance value when combined with conducting polymers. Xu et al.[157] synthesized hierarchical PANI nanowire/GO composite which showed a high specific capacitance value of 555 F g^{-1} at a discharge current density of 0.2 A g^{-1}. The composite exhibited better cycle life compared to PANI nanowires. Zhang et al.[158] reported a general method for the preparation of layered GO structures with sandwiched PPy of different morphologies based on the electrostatic interactions between negatively charged GO

31

and positively charged surfactant micelles. The composite exhibited a high specific capacitance of 500 F g^{-1} as well as good cycle stability.

1.7.3 Photovoltaic devices

A photovoltaic device generates electrical power by converting solar energy into electricity using semiconductors. GR based solar cells are receiving great interest in these days. There are different types of solar cells like dye-sensitized solar cell, organic solar cell, quantum dot based and silicon based solar cell.[159] Among these, dye-sensitized solar cells (DSSCs) are considered as one of the most attractive low cost photovoltaic (PV) devices since their discovery by O'Regan and Grätzel in 1991.[160] DSSC consists of semiconducting materials which are deposited on the anode dipped in photosensitive dyes and are connected to a platinum cathode by an electrolyte. GR based materials for application in DSSC is widely investigated recently due to its excellent physical and chemical properties.[161] Large surface area of GR facilitates the loading of the dye molecules. Wang et al.[162] used thin and transparent GR films, as an alternative to the metal oxides electrodes for solid-state DSSCs (Fig. 1.17). The GR films showed a conductivity value of 550 S cm^{-1} and a 70% transparency over 1000-3000 nm. This highly stable, transparent GR electrode can replace traditional indium tin oxide (ITO) and fluorine tin oxide (FTO) glass electrode for application in DSSC.
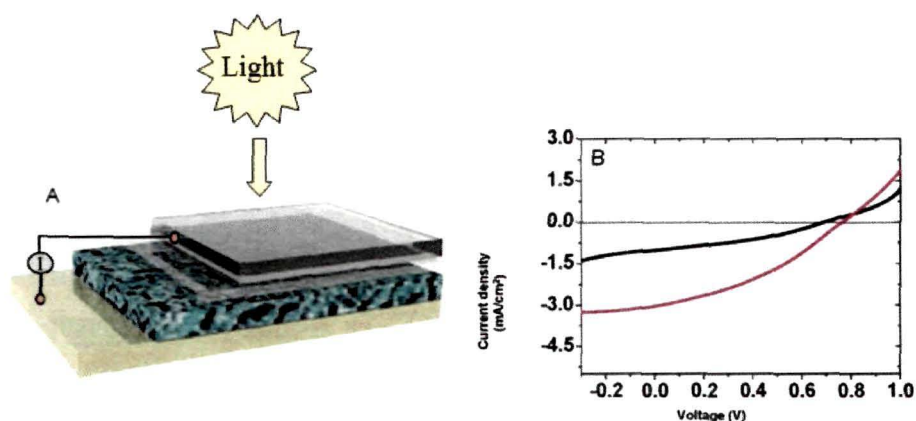
Fig. 1.17 (A) Illustration of dye-sensitized solar cell using GR film as electrode, the four layers from bottom to top are Au, dye-sensitized heterojunction, compact TiO$_2$, and GR film. (B) I-V curve of GR based cell (black) and the FTO-based cell (red), under illumination (adopted from Ref. 162).

GR based composites with conducting polymers such poly (3-hexylthiophene) (P3HT), PEDOT have shown good power consumption efficiency in DSSC applications.[163] Hong et al.[164] reported the preparation of electrode based on GR and polystyreneslufonate (PSS) doped PEDOT composite with 4.5% energy conversion efficiency of the cell. Yue et al.[165] prepared low-cost and platinum-free DSSC using GR based PEDOT:PSS composite film. The film was electrodeposited on FTO conductive substrate by one-step electrochemical polymerization method. The composite showed high power conversion efficiency of 7.86% under a simulated sunlight illumination of 100 mW cm^{-2}. Wang et al.[166] reported the preparation of PANI/GR hybrids by in situ polymerization. The resulting hybrid material was used as a counter electrode in DSSCs which showed a conversion efficiency of 6.09%. The value was comparable to that of Pt CE. Gong et al.[167] reported fabrication of reduced GO/PPy composite and used it as a counter electrode for DSSCs. The incorporation of reduced GO sheets improved short-circuit current density from 14.27 to 15.81 mA.cm^{-2} and conversion efficiency from 7.11% to 8.14%.

2. Objective of the present investigation:

From the literature survey it has been found that the work on graphene and graphene oxide based polymer nanocomposites is an upcoming subject of interest and can provide a wide variety of applications in future. So there is enough scope to do work in this field. The aim of the work is to develop graphene/graphene oxide based polymer nanocomposites and to investigate their properties for future industrial applications in diverse fields. With all these background and possibilities in view, the present work has been taken.

The objective of the work is

i. To synthesize graphene and graphene oxide filled polymer nanocomposites.

ii. To characterize the polymer composites using various spectroscopic and analytical techniques.

iii. To study the electrochemical, electrical, thermal and mechanical properties of the synthesized composites.

iv. To explore applications of some graphene based polymer composites in biosensor, supercapacitor and solar cells etc.

3. Plan of the present work

The plan for the work can be summarized as follows:

i) Synthesis of graphene and graphene oxide from natural graphite by Hummer's method.

ii) Preparation of composites of graphene and graphene oxide with polymers like polypyrrole, polythiophene and polyester resin.

iii) Characterizations of the composite films by Fourier Transform Infrared (FTIR) spectroscopy, UV-visible spectroscopy, scanning electron microscopy (SEM), thermo gravimetrical analysis (TGA), X-ray diffractions (XRD) and tensile strength measurement.

iv) Study the electrochemical and electrical properties of the composites by cyclic voltametry, charging-diacharging and four probe method.

v) Applications of the composites as electrode materials in glucose biosensor, supercapacitor and dye-sensitized solar cell.

4. Outline of the thesis

This thesis addresses the preparation and properties of a series of GR and GO based polymer nanocomposites. The work in the thesis is organized in five chapters as follows:

Chapter 1 deals with the general introduction on GR and GO based polymer nanocomposites. The preparation methods and properties of GR, GO and their composites are briefly described in the chapter with the literature review till 2014. Applications of the GR/GO based composites in various fields like sensors, supercapacitors and solar cells are also described concisely in this chapter with latest literature survey. The objectives and the plan of the present investigation are stated at the end of this chapter.

Chapter 2 describes the synthesis and characterization of GR and GO based composites with conducting polymers, polypyrrole (PPy) and polythiophene (PTh). The composites were prepared by liquid/liquid interfacial polymerization. The synthesized composites were characterized using various spectroscopic and analytical techniques such as FTIR, UV, XRD, TGA, SEM and TEM etc. The thermal, electrical and electrochemical properties of the composites are thoroughly studied in the chapter. The incorporation of small amount of GO and GR in the PPy and PTh matrix greatly improved the properties of the composites.

Chapter 3 discusses the preparation and properties of GR/GO based polyester (PE) resin composites. The samples were characterized using several spectroscopic and analytical methods. The enhancement in mechanical and thermal properties of the

composites with different GR and GO loading is described in this chapter. The antibacterial activity of the PE/GR composite is also investigated. The GR based PE resin composite showed proficient antibacterial activity towards the five different kinds of bacterial strains and the antibacterial activity was found to be increased with increasing GR content.

Chapter 4 includes the study of applications of the synthesized composites in biosensor, supercapacitor and solar cells. This chapter is divided into three sections.

Section A describes the application of PPy/GR composite in glucose sensor. The sensitivity, selectivity and the reproducibility of the PPy/GR based biosensor is elaborately investigated in this section. This PPy/GR based biosensor showed a high value of sensitivity (29.6 μM/cm^2.mM) and lower limit of detection (0.1 μM) compared to other GR and carbon nanotube based biosensor. The biosensor also showed reasonable stability which is crucial for practical application of biosensors.

Section B deals with the preparation of PPy/sulphonated graphene (SG) composite and its application as an electrode material in super capacitors. The electrochemical properties of the prepared electrode is analysed by cyclic voltammetry, charging-discharging and electrochemical impedence spectroscopy techniques. Charging-discharging study revealed a high specific capacitance value (360 F g^{-1}) of PPy/SG composite at a current density of 1 A g^{-1}. Furthermore, the composite exhibited a good electrochemical stability, around 90% capacitance retained after 500 charging/discharging cycles at a current density of 1 A g^{-1}.

· *Section C* deals with the application of PTh/GR composite as a counter electrode in dye-sensitized solar cell. The energy conversion efficiency of the catalytic activity of the composite electrode is evaluated in this section and the results were compared with the conventional Pt electrode. The photovoltaic performance of DSSCs was investigated which revealed a higher value of conversion efficiency 4.8% which was comparable to that of the device based on the Pt counter electrode.

Chapter 5 is the concluding chapter of the thesis which includes the overall summary, major findings and future aspect of the present work. GR/GO based conducting polymer composites showed superior electrical and electrochemical properties compared to that of pure polymer. Similarly, GR/GO based PE resin composites revealed great improvement in mechanical and thermal properties than that of pristine polymer. GR based polymer composites exhibited good application potential in various field such as biosensor, supercapacitor and solar cells. These exciting materials could open a new dimension for further development of high performance composite materials for a range of applications in coming years.

REFERENCES

1. Kotov, N.A. Carbon sheet solutions, *Nature* **442**, 254-255, 2006.

2. Stankovich, S., et al. Graphene-based composite materials, *Nature* **442**, 282-286, 2006.

3. Kuilla, T., et al. Recent advances in graphene based polymer composites, *Prog. Polym. Sci.* **35**, 1350-1375, 2010.

4. Kim, H., et al. Graphene/Polymer nanocomposites, *Macromolecules* **43**, 6515-6530, 2010.

5. Potts, J.R., et al. Graphene based polymer nanocomposites, *Polymer* **52**, 5-25, 2011.

6. Godovsky, D.Y. Device applications of polymer-nanocomposites, *Adv. Polym. Sci.* **153**, 163-205, 2000.

7. Ray, S.S., & Okamoto, M. Polymer/layered silicate nanocomposites: a review from preparation to processing, *Prog. Polym. Sci.* **28**, 1539-1641, 2003.

8. Zhiaho, Z., et al. Partial delamination of the organo-monmorillonite with surfactant containing hydroxyl groups in maleated poly(propylene carbonate), *Polymer* **47**, 8548-8555, 2006.

9. Usuki, A., et al. Synthesis of nylon 6-clay hybrid, *J. Mater. Res.* **8**, 1179-1184, 1993.

10. Li, Q., et al. Positive temperature coefficient behavior of HDPE/EVA blends filled with carbon black, *Adv. Mater. Res.* **79**, 2267-2270, 2009.

11. Li, Q., et al. Positive temperature coefficient behavior of the graphite nanofibre and carbon black filled high-density polyethylene hybrid composites, *Adv. Mater. Res.* **47**, 226-229, 2008.

12. Su, L., et al. Symmetric self-hybrid supercapacitor consisting of multiwall carbon nanotubes and Co-Al layered double hydroxides, *J. Electrochem. Soc.* **155**, 110-114, 2008.

13. Lee, C.Y., et al. Characteristics and electrochemical performance of supercapacitors with manganese oxide-carbon nanotube nanocomposite electrodes, *J. Electrochem. Soc.* **152**, 716-720, 2005.

14. Rao, C.N.R., et al. Graphene: the new two-dimensional nanomaterial, *Angew. Chem. Eng.* **48**, 7752-7777, 2009.

15. C.N.R. Rao. Some novel attributes of graphene, J. Phys. Chem. Lett. **1**, 572-580, 2010.

16. Matthew, J., et al. Honeycomb carbon: a review of graphene, *Chem. Rev.* **110**, 132-145, 2010.

17. Geim, A.K., & Novoselov, K.S. The rise of graphene, *Nat. Mater.* **6**, 183-191, 2007.

18. Zhou, K., et al. One-pot preparation of graphene/Fe_3O_4 composites by a solvothermal reaction, *New J. Chem.* **34**, 2950-2955, 2010.

19. Jin, Z., et al. Decoration, migration and aggregation of palladium nanoparticles on graphene sheets, *Chem. Mater.* **22**, 5695-5699, 2010.

20. Dato, A., et al. Substrate-free gas-phase synthesis of graphene sheets, *Nano Lett.*, **8**, 2012-16, 2008.

21. Hernandez, Y., et al. High-yield production of graphene by liquid-phase exfoliation of graphite, *Nat. Nanotechnol.* **3**, 563-568, 2008.

22. Novoselov, K.S. Two-dimensional gas of massless Dirac fermions in graphene, *Nature* **438**, 197-200, 2005.

23. Tung, V.C., et al. High-throughput solution processing of large-scale graphene, *Nat. Nanotechnol.* **4**, 25-29, 2009.

24. Hong, T.K., et al. Transparent, flexible, conducting hybrid multilayer thin films of multiwalled carbon nanotubes with graphene nanosheets, *ACS Nano*, **4**, 3861-3868, 2010.

25. Nair, R.R., et al. Fine structure constant defines visual transparency of graphene, *Science* **320**, 1308-1308, 2008.

26. Lee, C., et al. Measurement of the elastic properties and intrinsic strength of monolayer graphene, *Science* **321**, 385-388, 2008.

27. Bai, S., & Shen, X. Graphene-inorganic nanocomposites, *RSC Advances* **2**, 64-98, 2012.

28. Zhou, Y.G., et al. A facile approach to the synthesis of highly electroactive Pt nanoparticles on graphene as an anode catalyst for direct methanol fuel cells, *Chem. Commun.* **46**, 5951-5953, 2010.

29. Wang, G., et al. Graphene nanosheets for enhanced lithium storage in lithium ion batteries, *Carbon* **47**, 2049-2053, 2009.

30. Wang, X., et al. Large-scale synthesis of few-layered graphene using CVD, *J. Chem. Vap. Deposition* **15**, 53-56, 2009.

31. Rollings, E., et al. Synthesis and characterization of atomically thin graphite films on a silicon carbide substrate, *J. Phys. Chem. Solids* **67**, 2172-2177, 2006.

32. Novoselov, K.S., et al. Electric field effect in atomically thin carbon films, *Science* **306**, 666-669, 2004.

33. Bourlinos, A.B., et al. Liquid-phase exfoliation of graphite towards solubilized graphenes, *Small* **5**, 1841-1845, 2009.

34. Liu, N., et al. One-step ionic-liquid-assisted electrochemical synthesis of ionic-liquid-functionalized graphene sheets directly from graphite, *J. Adv. Funct. Mater.* **18**, 1518-1525, 2008.

35. Brodie, B.C., et al. On the atomic weight of graphite, *Philos. Trans. R. Soc. London* **149**, 249-259, 1859.

36. Hummers, W.S., & Jr. Offeman, R.E. Preparation of graphitic oxide, *J. Am. Chem. Soc.* **80**, 1339-1939, 1958.

37. Lomeda, J.R., et al. Diazonium functionalization of surfactant-wrapped chemically converted graphene sheets, *J. Am. Chem. Soc.* **130**, 16201-16206, 2008.

38. Si, Y., & Samulski, E.T. Synthesis of water soluble graphene, *Nano Lett.* **8**, 1679-1682, 2008.

39. McAllister, M.J., et al. Single sheet functionalized graphene by oxidation and thermal expansion of graphite, *Chem. Mater.* **19**, 4396-4404, 2007.

40. Schniepp, H.C., et al. Functionalized single graphene sheets derived from splitting graphite oxide, *J. Phys. Chem. B* **110**, 8535-8539, 2006.

41. Schniepp, H.C., et al. Bending properties of single functionalized graphene sheets probed by atomic force microscopy, *ACS Nano* **2**, 2577-2584, 2008.

42. Mkhoyan, K.A., et al. Atomic and electronic structure of graphene-oxide, *Nano Lett.* **9**, 1058-1063, 2009.

43. Stankovich, S., et al. Synthesis of graphene-based nanosheets via chemical reduction of exfoliated graphite oxide, *Carbon* **45**, 1558-1565, 2007.

44. Eswaraiah, V., et al. Top down method for synthesis of highly conducting graphene by exfoliation of graphite oxide using focused solar radiation, *J. Mater. Chem.* **21**, 6800-6803, 2011.

45. Lerf, A., et al. Structure of graphite oxide revisited, *J. Phys. Chem. B* **102**, 4477-4482, 1998.

46. Chen, D., et al. Graphene oxide: preparation, functionalization, and electrochemical applications, *Chem. Rev.* **112**, 6027-6053, 2012.

47. Fang, M., et al. Covalent polymer functionalization of graphene nanosheets and mechanical properties of composites, *J. Mater. Chem.* **19**, 7098-7105, 2009.

48. Ramanathan, T., et al. Functionalized graphene sheets for polymer nanocomposites, *Nat. Nanotechnol.* **3**, 327-331, 2008.

49. Li, G.L., et al. Organo- and water-dispersible graphene oxide-polymer nanosheets for organic electronic memory and gold nanocomposites, *J. Phys. Chem. C* **114**, 12742-12748, 2010.

50. Stankovich, S., et al. Stable aqueous dispersions of graphitic nanoplatelates via the reduction of exfoliated graphite oxide in the presence of poly(sodium 4-styrenesulfonate), *J. Mater. Chem.* **16**, 155-158, 2006.

51. Zu, S.Z., & Han, B.H. Aqueous dispersion of graphene sheets stabilized by pluronic copolymers: formation of supramolecular hydrogels, *J. Phys. Chem. C* **113**, 13651-13657, 2009.

52. Eda, G., et al. Blue photoluminescence from chemically derived graphene oxide, *Adv. Mater.* **22**, 505-509, 2010.

53. Liu, H., et al. Processing of graphene for electrochemical application: noncovalently functionalized graphene sheets with water-soluble electroactive methylene green, *Langmuir* **25**, 12006-12010, 2009.

54. Wang, Z.J., et al. Direct electrochemical reduction of single-layer graphene oxide and subsequent functionalization with glucose oxidase, *J. Phys. Chem. C* **113**, 14071-14075, 2009.

55. Liu, F., et al. Graphene oxide arrays for detecting specific DNA hybridization by fluorescence resonance energy transfer, *Biosens. Bioelectron.* **25**, 2361-2365, 2010.

56. Tang, L., et al. Preperation, structure, and electrochemical properties of reduced graphene sheet films, *Adv. Funct. Mater.* **19**, 2782-2789, 2009.

57. Tang, Y.M., et al. Preparation and electrochemical performance for methanol oxidation of pt/graphene nanocomposites, *Electrochem. Commun.* **11**, 846-849, 2009.

58. Verdejo, R., et al. Graphene filled polymer nanocomposites, *J. Mater. Chem.* **21**, 3301-3310, 2011.

59. Zhang, H.B., et al. Electrically conductive polyethylene terephthalate/graphene nanocomposites prepared by melt compounding, *Polymer* **51**, 1191-1196, 2010.

60. Lianga, J., et al. Electromagnetic interference shielding of graphene/epoxy composites, *Carbon* **47**, 922-925, 2009.

61. Ye, L., et al. Synthesis and characterization of expandable graphite-poly(methyl methacrylate) composite particles and their application to flame retardation of rigid polyurethane foams, *Polym. Degrad. Stab.* **94**, 971-979, 2009.

62. Mohamadi, S., et al. Functionalization of graphene sheets via chemically grafting of PMMA chains through in situ polymerization, *J. Macromol. Sci. Pt. A* **48**, 577-582, 2011.

63. Hsueh, H.B., & Chen, C.Y. Preparation and properties of LDHs/epoxy nanocomposites, *Polymer* **44**, 5275-5283, 2003.

64. Kalaitzidou, K., et al. A new compounding method for exfoliated graphite-polypropylene nanocomposites with enhanced flexural properties and lower percolation threshold, *Compos. Sci. Technol.* **67**, 2045-2051, 2007.

65. Liang, J., et al. Molecular-level dispersion of graphene into poly(vinyl alcohol) and effective reinforcement of their nanocomposites, *Adv. Funct. Mater.* **19**, 2297-2302, 2009.

66. Broza, G., et al. Nanocomposites of poly(vinyl chloride) with carbon nanotubes (CNT), *Compos. Sci. Technol.* **67**, 890-894, 2007.

67. Kalaitzidou, K., et al. Multifunctional polypropylene composites produced by incorporation of exfoliated graphite nanoplatelets, *Carbon* **45**, 1446-1452, 2007.

68. Weng, W., et al. Transport properties of electrically conducting nylon 6/exfoliated graphite nanocomposites, *Polymer* **46**, 6250-6257, 2005.

69. Kim, S., et al. Thermal stability and dynamic mechanical behavior of exfoliated graphite nanoplatelets-LLDPE nanocomposites, *Polym. Compos.* **31**, 755-761, 2009.

70. Dallas, P., et al. Interfacial polymerization of pyrrole and in situ synthesis of polypyrrole/silver nanocomposites, *Polymer* **48**, 2007-2013, 2007.

71. Eda, G., & Chhowalla, M. Graphene-based composite thin films for electronics, *Nano Lett.* **9**, 814-818, 2009.

72. Patole, A.S., et al. A facile approach to the fabrication of graphene/polystyrene nanocomposite by in situ microemulsion polymerization, *J. Colloid Interf. Sci.* **350**, 530-537, 2010.

73. Kim, H., & Macosko, C.W. Processing-property relationships of polycarbonate/graphene nanocomposites, *Polymer* **50**, 3797-3809, 2009.

74. Lee, Y.R., et al. Properties of waterborne polyurethane/functionalized graphene sheet nanocomposites prepared by an in situ method, *Macromol. Chem.* **210**, 1247-1254, 2009.

75. Hu, H., et al. Preparation and properties of graphene nanosheets-polystyrene nanocomposites via in situ emulsion polymerization, *Chem. Phys. Lett.* **484**, 247-753, 2010.

76. Wang, H., et al. Graphene oxide doped polyaniline for supercapacitors, *Electrochem. Commun.* **11**, 1158-1161, 2009.

77. Lin, Y.C. Enhanced conductivity and thermal stability of conductive polyaniline/graphene composite synthesized by in-situ chemical oxidation polymerization with sodium dodecyl sulfate, *Synth. Met.* **184**, 29-34, 2013.

78. Wang, J., et al. Preparation and mechanical and electrical properties of graphene nanosheets-poly(methyl methacrylate) nanocomposites via in-situ suspension polymerization, *J. Appl. Polym. Sci.* **122**, 1866-1871, 2011.

79. Huang, Y. Polypropylene/graphene oxide nanocomposites prepared by in situ Ziegler-Natta polymerization, *Chem. Mater.* **22**, 4096-4102, 2010.

80. Ansari, S., & Giannelis, E.P. Functionalized graphene sheet poly(vinylidene fluoride) conductive nanocomposites, *J. Polym. Sci. Part B Polym. Phys.* **47**, 888-897, 2009.

81. Weng, W., et al. Fabrication and characterization of nylon 6/foliated graphite electrically conducting nanocomposite, *J. Polym. Sci. Part B Polym. Phys.* **42**, 2842-2856, 2004.

82. Zhao, X., et al. Enhanced mechanical properties of graphene-based poly(vinyl alcohol) composites, *Macromolecules* **43**, 2357-2363, 2010.

83. Xu, Y., et al. Strong and ductile poly (vinyl alcohol)/graphene oxide composite films with a layered structure, *Carbon* **47**, 3538-3543, 2009.

84. Vadukumpully, S., et al. Flexible conductive graphene/poly (vinyl chloride) composite thin films with high mechanical strength and thermal stability, *Carbon* **49**, 198-205, 2011.

85. Liu, K., et al. Preparation of polyester/reduced graphene oxide composites via in situ melt polycondensation and simultaneous thermo-reduction of graphene oxide, *J. Mater. Chem.* **21**, 8612-8617, 2011.

86. Rafiee, M.A., et al. Enhanced mechanical properties of nanocomposites at low graphene content, *ACS Nano* **3**, 3884-3890, 2009.

87. Jang, J.Y., et al. Graphite oxide/poly (methyl methacrylate) nanocomposites prepared by a novel method utilizing macroazoinitiator, *Compos. Sci.Technol.* **69**, 186-191, 2009.

88. Steurer, P., et al. Functionalized graphenes and thermoplastic nanocomposites based upon expanded graphite oxide, *Macromol. Rapid Commun.* **30**, 316-327. 2009.

89. Cai, D., et al. The mechanical properties and morphology of a graphite oxide nanoplatelet/polyurethane composite, *Nanotechnology* **20**, 085712-085717, 2009.

90. Kim, H., et al. Graphene/polyurethane nanocomposites for improved gas barrier and electrical conductivity, *Chem. Mater.* **22**, 3441-3450, 2010.

91. Liang, J., et al. Infrared triggered actuators from graphene-based nanocomposites, *J. Phys. Chem. C* **113**, 9921-9927, 2009.

92. Chiang, C.K., et al. Electrical conductivity in doped polyacetylene, *Phys. Rev. Lett.* **39**, 1098-1101, 1977.

93. Kumar, D., & Sharma, R.C. Advances in conductive polymers, *Eur. Polym. J.* **34**, 1053-1060, 1998.

94. Gospodinova, N., & Terlemezyan, L. Conducting polymers prepared by oxidative polymerization: polyaniline, *Prog. Polym. Sci.* **3**, 1443-1484, 1998.

95. Hsueh, C., & Brajter-Toth, A. Electrochemical preparation and analytical applications of ultrathin overoxidized polypyrrole films, *Anal. Chem.* **66**, 2458-2464, 1994.

96. Huang, W.S. Synthesizing and processing conducting polythiophene derivatives for charge dissipation in electron-beam lithography, *Polymer* **35**, 4057-4064, 1994.

97. Heywang, G., & Jonas, F. Poly(alkylenedioxythiophene)s-new, very stable conducting polymers, *Adv. Mater.* **4**, 116-118, 1992.

98. Chen, S.A., & Tsai, C.C. Structure/properties of conjugated conductive polymers 2.3-ether-substituted polythiophene and poly(4-methyltiophene)s, *Macromolecules* **26**, 2234-2239, 1993.

99. Beadle, P., et al. Electrically conductive polyaniline-copolymer latex composites, *Macromolecules* **25**, 2526-2530, 1992.

100. West, K., et al. Electrochemical synthesis of polypyrrole: Influence of current density on structure, *Synth. Met.* **55**, 1412-1417, 1993.

101. Guoab, S., & Dong, S. Graphene nanosheet: synthesis, molecular engineering, thin film, hybrids, and energy and analytical applications, *Chem. Soc. Rev.* **40**, 2644-2672, 2011.

102. Zhang, K., et al. Graphene/polyaniline nanofiber composites as supercapacitor electrodes, *Chem. Mater.* **22**, 1392-1401, 2010.

103. Wu, Q., et al. Supercapacitors based on flexible graphene/polyaniline nanofiber composite films, *ACS Nano* **4**, 1963-1970, 2010.

104. Hao, Q., et al. Morphology-controlled fabrication of sulfonated graphene/polyaniline nanocomposites by liquid/liquid interfacial polymerization and investigation of their electrochemical properties, *Nano Res.* **4**, 323-333, 2011.

105. Wang, H., et al. Effect of graphene oxide on the properties of its composite with polyaniline, *Appl. Mater. Interfaces* **2**, 821-828, 2010.

106. Tung, N.T., et al. Preparation and characterization of nanocomposite based on polyaniline and graphene nanosheets, *Macromol. Res.* **19**, 203-208, 2011.

107. Gu, Z., et al. Preparation of highly conductive polypyrrole/graphite oxide composites via in situ polymerization, *J. Macromol. Sci. B* **48**, 1093-1102, 2009.

108. Scott, C.L., et al. Stacked graphene nanofibers doped polypyrrole nanocomposites for electrochemical sensing, *Electrochem. Commu.* **12**, 1788-1791, 2010.

109. Zhang, D., et al. Enhanced capacitance and rate capability of graphene/polypyrrole composite as electrode material for supercapacitors, *J. Power Sources* **196**, 5990-5996, 2011.

110. Bose, S., et al. In-situ synthesis and characterization of electrically conductive polypyrrole/graphene nanocomposites, *Polymer* **51**, 5921-5928, 2010.

111. Murugan, A.V., et al. Rapid, facile microwave-solvothermal synthesis of graphene nanosheets and their polyaniline nanocomposites for energy strorage, *Chem. Mater.* **21**, 5004-5006, 2009.

112. Xu, C., et al. Synthesis and photoelectrical properties of β-cyclodextrin functionalized graphene materials with high bio-recognition capability, *Chem. Phys. Lett.* **498**, 162-167, 2010.

113. Liang, J.J., et al. Electromagnetic interference shielding of graphene/epoxy composites, *Carbon* **47**, 922-925, 2009.

114. Hong, W., et al. Transparent graphene/PEDOT-PSS composite films as counter electrodes of dye sensitized solar cells, *Electrochem. Commun.* **10**, 1555-1558, 2008.

115. Blake, P., et al. Graphene-based liquid crystal devices, *Nano Lett.* **8**, 1704-1708, 2008.

116. Eda, G., et al. Field emission from graphene based composite thin films, *Appl. Phys. Lett.* **93**, 233502-233503, 2008.

117. Verma, V.P., et al. Large-area graphene on polymer film for flexible and transparent anode in field emission device, *Appl. Phys. Lett.* **96**, 2031081-2031083, 2010.

118. Sun, X., et al. Nano-graphene oxide for cellular imaging and drug delivery, *Nano Res.* **1**, 203-212, 2008.

119. Zuo, X.L., et al. Graphene oxide-facilitated electron transfer of metalloproteins at electrode surfaces, *Langmuir* **26**, 1936-1939, 2010.

120. Baby, T.T. Metal decorated graphene nanosheets as immobilization matrix for amperometric glucose biosensor, *Sens. Actuators B* **145**, 71-77, 2010.

121. Richter, M.M. Electrochemiluminescence (ECL), *Chem. Rev.* **104**, 3003-3036, 2004.

122. Seger, B., & Kamat, P.V. Electrocatalytically active graphene-platinum nanocomposites. Role of 2-D carbon support in PEM fuel cells, *J. Phys. Chem. C* **113**, 7990-7995, 2009.

123. Ahammad, A.J.S., et al. Electrochemical Sensors Based on Carbon Nanotube, *Sensors* **9**, 2289-2319, 2009.

124. Wang, Y., et al. Nitrogen-doped Graphene and its application in electrochemical biosensing, *ACS Nano* **4**, 1790-1798, 2010.

125. Liu, Y., et al. Biological and chemical sensors based on graphene materials, *Chem. Soc. Rev.* **41**, 2283-2307, 2012.

126. Zhou, M., et al. Electrochemical sensing and biosensing platform based on chemically reduced graphene oxide, *Anal. Chem.* **81**, 5603-5608, 2009.

127. Liu, Y., et al. Biocompatible graphene oxide-based glucose biosensors, *Langmuir* **26**, 6158-6160, 2010.

128. Shan, C., et al. Direct electrochemistry of glucose oxidase and biosensing for glucose based on graphene, *Anal. Chem.* **81**, 2378-2382, 2009.

129. Lian, H., et al. Graphene doped molecularly imprinted electrochemical sensor for uric acid, *Anal. Lett.* **45**, 2717-2727, 2012.

130. Xuea, R., et al. Electrochemical sensor based on the graphene-nafion matrix for sensitive determination of organophosphorus pesticides, *Anal. Lett.* **46**, 131-141, 2013.

131. Kang, X., et al. Glucose oxidase–graphene–chitosan modified electrode for direct electrochemistry and glucose sensing, *Biosens. Bioelectron.* **25**, 901-905, 2009.

132. Wu, H., et al. Glucose biosensor based on immobilization of glucose oxidase in platinum nanoparticles/graphene/chitosan nanocomposite film, *Talanta* **80**, 403-406, 2009.

133. Alwarappan, S., et al. Enzyme-doped graphene nanosheets for enhanced glucose biosensing, *J. Phys. Chem. C* **114**, 12920-12924, 2010.

134. Winter, M., & Brodd, R.J. What are batteries, fuel cells and supercapacitors, *Chem. Rev.* **104**, 4245-4268, 2004.

135. Bose, S., et al. Carbon-based nanostructured materials and their composites as supercapacitor electrodes, *J. Mater. Chem.* **22**, 767-784, 2012.

136. Zhang, L.L., et al. Graphene-based materials as supercapacitor electrodes, *J. Mater. Chem.* **20**, 5983-5992, 2010.

137. Tan, Y.B., & Lee, J.M. Graphene for supercapacitor applications, *J. Mater. Chem. A* **1**, 14814-14843, 2013.

138. Kotz, R., & Carlen, M. Principles and applications of electrochemical capacitors, *Electrochim. Acta* **45**, 2483-2498, 2000.

139. Simon, P., et al. Where do batteries end and supercapacitors begin, *Science* **343**, 1210-1211, 2014.

140. Pan, H., et al. Carbon nanotubes for supercapacitor, *Nanoscale Res. Lett* **5**, 654-668, 2010.

141. Zhang, K., et al. Graphene/polyaniline nanofiber composites as supercapacitor electrodes, *Chem. Mater.* **22**, 1392-1401, 2010.

142. Frackowiak, E., et al. Supercapacitors based on conducting polymers/nanotubes composites, *J. Power Sources* **153**, 413-418, 2006.

143. Laforgue, A., et al. Activated carbon/conducting polymer hybrid supercapacitors, *J. Electrochem. Soc.* **150**, 645-651, 2003.

144. Pasquier, A.D., et al. A comparative study of Li-ion battery, supercapacitor and nonaqueous asymmetric hybrid devices for automotive applications, *J. Power Sources* **115**, 171-178, 2003.

145. Wang, D.W., et al. Fabrication of graphene/polyaniline composite paper via *in situ* anodic electropolymerization for high-performance flexible electrode, *ACS Nano* **3**, 1745-1752, 2009.

146. Ku, K., et al. Characterization of graphene-based supercapacitors fabricated on Al foils using Au or Pd thin films as interlayers, *Synth. Met.* **160**, 2613-2617, 2010.

147. Liu, C., et al. Graphene-based supercapacitor with an ultrahigh energy density, *Nano Lett.* **10**, 4863-4868, 2010.

148. Yu, A., et al. Ultrathin, transparent, and flexible graphene films for supercapacitor application, *Appl. Phys. Lett.* **96**, 253105-253107, 2010.

149. Wu, Z.S., et al. Anchoring hydrous RuO_2 on graphene sheets for high-performance electrochemical capacitors, *Adv. Funct. Mater.* **20**, 3595-3602, 2010.

150. Zhang, Y., et al. Capacitive behavior of graphene-ZnO composite film for supercapacitors, *J. Electroanal. Chem.* **634**, 68-71, 2009.

151. Li, F. One-step synthesis of graphene/SnO_2 nanocomposites and its application in electrochemical supercapacitors, *Nanotechnology* **20**, 455602-455608, 2009.

152. Qian, Y., et al. Preparation of MnO_2/graphene composite as electrode material for supercapacitors, *J. Mater. Sci.* **46**, 3517-3522, 2011.

153. Wang, D.W., et al. Fabrication of graphene/polyaniline composite paper via in situ anodic electropolymerization for high-performance flexible electrode, *ACS Nano* **3**, 1745-1752, 2009.

154. Qi, K., et al. Pulse electrochemical incorporation of graphene oxide into polypyrrole films for supercapacitor electrode materials, *Electrochim. Acta* **137**, 685-692, 2014.

155. Biswas, S., & Drzal, L.T. Multilayered nanoarchitecture of graphene nanosheets and polypyrrole nanowires for high performance supercapacitor electrodes, *Chem. Mater.* **22**, 5667-5671, 2010.

156. Bose, S., et al. Electrochemical performance of a graphene-polypyrrole nanocomposite as a supercapacitor electrode, *Nanotechnology* **22**, 295202-295211, 2011.

157. Xu, J. Hierarchical nanocomposites of polyaniline nanowire arrays on graphene oxide sheets with synergistic effect for energy storage, *ACS Nano* **4**, 5019-5026, 2010.

158. Zhang, L.L., et al. Layered graphene oxide nanostructures with sandwiched conducting polymers as supercapacitor electrodes, *Langmuir* **22**, 17624-17628, 2010.

159. Huang, X., et al. Graphene-based composites, *Chem. Soc. Rev.* **41**, 666-686, 2012.

160. O'Regan, B., & Grätzel, M. A low-cost, high-efficiency solar cell based on dye-sensitized colloidal TiO_2 films, *Nature* **353**, 737-740, 1991.

161. Kavan, L., et al. Optically transparent cathode for dye-sensitized solar cells based on graphene nanoplatelets, *ACS Nano* **5**, 165-172, 2010.

162. Wang, X., et al. Transparent, conductive graphene electrodes for dye-sensitized solar cells, *Nano lett.* **8**, 323-327, 2008.

163. Lee, K.M., et al. A high-performance counter electrode based on poly(3,4-alkylenedioxythiophene) for dye-sensitized solar cells, *J. Power Sources* **188**, 313-318, 2009.

164. Hong. W., et al. Transparent graphene/PEDOT–PSS composite films as counter electrodes of dye-sensitized solar cells, *Electrochem. Commun.* **10**, 1555-1558, 2008.

165. Yue, G., et al. Functionalized graphene/poly (3,4-ethylenedioxythiophene): polystyrenesulfonate as counter electrode catalyst for dye-sensitized solar cells, *Energy* **54**, 315-321, 2013.

166. Wang, G., et al. The production of polyaniline/graphene hybrids for use as a counter electrodein dye-sensitized solar cells, *Electrochim. Acta* **66**, 151-157, 2012.

167. Gong, F., et al. Enhanced charge transportation in a polypyrrole counter electrode via incorporation of reduced graphene oxide sheets for dye-sensitized solar cells, *Phys. Chem. Chem. Phys.* **15**, 546-552, 2013.
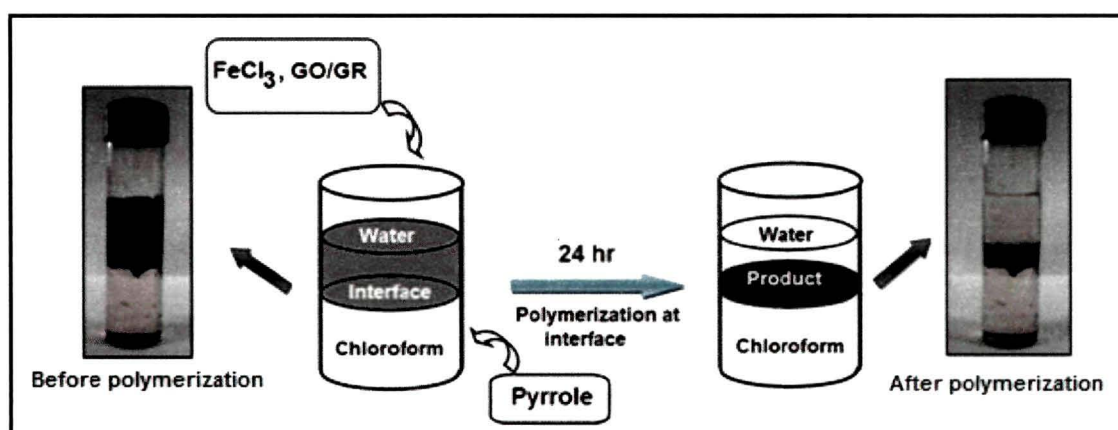
CHAPTER 2

Synthesis of graphene (GR)/graphene oxide (GO) based polypyrrole (PPy) and polythiophene (PTh) composites by liquid/liquid interfacial polymerization and their optical, electrical and electrochemical properties

GRAPHICAL ABSTRACT
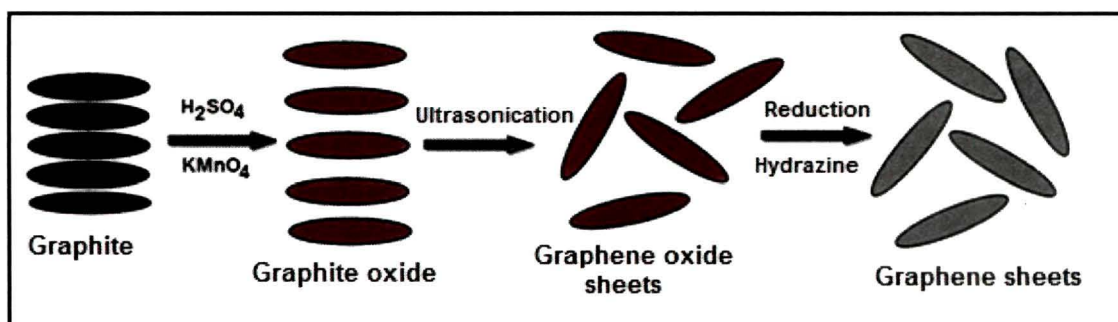
Synthesis of graphene oxide and graphene by Hummer's method

Fabrication process of GO and GR based PPy composite

Synthesis of graphene (GR)/graphene oxide (GO) based polypyrrole (PPy) and polythiophene (PTh) nanocomposites by liquid/liquid interfacial polymerization and their optical, electrical and electrochemical properties

2.1 Introduction

Polymer nanocomposite has become a key area in nanoscience and nanotechnology offering significant potential in the development of advanced materials in numerous and diverse application areas such as electronic devices, super capacitors, rechargeable batteries, functional electrodes, sensors and many other fields.[1] Polymer nanocomposites have attracted a lot of scientific interest due to their dramatic improvement in properties resulting from the incorporation of a small quantity of nanofiller.[2] Nanocomposites based on layered materials of a natural origin like montmorillonite type of layered silicate compounds or synthetic clay has been investigated for decades. But the electrical and thermal conductivity of clay minerals are quite poor. To overcome these drawbacks, carbon-based nanofillers, such as carbon black, expanded graphite, carbon nanotube (CNT) have been introduced to the preparation of polymer nanocomposites.[3] Recently, graphene oxide (GO), a single sheet of graphite oxide bearing oxygen functional groups on their basal planes and edges has become more effective as a nanofiller due to its superior mechanical, structural and thermal properties compared to other conventional nanofillers.[4,5] It can be prepared in large scales from natural graphite which is an easily available low cost material and therefore it is preferred over other expensive fillers like CNT. Owing to its hydrophilic nature GO can be readily dispersed in water and the tunable oxygen containing groups of GO impart strong interaction with polar molecules or polymers to form GO intercalated or exfoliated composites. Several GO based polymer composites have been developed till date and the thermal, mechanical, electrical properties of these composites were found to be improved as reported.[6-9]

Xu et al.[10] prepared mechanically strong poly (vinyl alcohol) (PVA)/GO composite film by vacuum filtration. These strong and ductile composites can be used as high strength, flaw tolerance structural materials. Composites have also been produced in aprotic solvents with hydrophobic polymers such as polystyrene, polyurethane or poly (methyl methacrylate) etc. using GO after chemical modification with isocyanate or amine. Liu et al.[11] reported a novel route to fabricate polyester/reduced GO composites via simultaneous dispersion and thermo-reduction of GO during in-situ melt polycondensation. A significant improvement in tensile strength and elongation at break of PET has been achieved. However, electrical conductivity of GO is very poor. The direct application of GO in electrically active material is limited by the presence of highly electrical resistant groups like carboxyl, hydroxyl, or epoxy in GO sheets. Incorporation of GO in a conducting polymer matrix leads to the formation of nanocomposites which have advantages of both the component such as good mechanical strength.[12-15] Wang et al.[16] prepared GO based polyaniline (PANI) composite with improved electrochemical performance as supercapacitor electrode by in-situ polymerization. The GO/PANI nanocomposites have shown good application potential in super capacitors.[17]

Graphene (GR), a one-atom-thick sp^2-bonded carbon sheet, with unique properties has become like a rising star on the horizon of materials science since its discovery in 2004.[1,18] The special physical and chemical properties of GR make it promising for many applications such as supercapacitors, sensors, solar cells, batteries, fuel cells and many others.[18-22] Owing to its high surface area, excellent conductivity, good mechanical strength, easy availability and cost efficiency, GR can be used as an effective nanofiller in polymers compared with other carbon materials like CNTs, carbon fibers and fullerenes.[3] Hence GR based composites have attracted tremendous scientific interest recently. The incorporation of a small quantity of GR nanofiller into polymer matrices remarkably improves the properties of the composite material.[2,23,24] Such improvement in the properties of GR-based composites results from the homogeneous dispersion of nanofillers in the polymer matrix due to the high aspect and surface-to-volume ratios of GR. Several GR-based polymer composites show good enhancement in thermal, mechanical and electrical properties.[25,26]

On the other hand, conducting polymers such as PANI, polypyrrole (PPy) and polythiophene (PTh) have been studied extensively in the last few decades because of their good electrical properties, high specific capacity, easy processability and light weight. Amongst these, PPy is particularly attractive because of its low cost, easy synthesis and relatively high conductivity.[27] However, PPy is usually mechanically weak and insulating in its neutral state which hinders some of its applications. It also exhibits poor stability during the charge-discharge process. Incorporation of GO and GR in a conducting polymer matrix leads to the formation of composites with synergistic properties. Hence, both GO and GR can be considered as effective nanofillers for PPy because of its high surface area, good mechanical strength and excellent conductivity. Until recently, some efforts have been made to achieve improved properties of GR/GO based PPy composites. Zhang et al.[28] synthesized GR-based PPy composite by in-situ polymerization of pyrrole monomer in the presence of GR under acidic conditions. The composite showed higher specific capacitance and better cycling stability than pure PPy which allows its applications in supercapacitors. Bose et al.[29] successfully prepared PPy/GR composites by in-situ polymerization of pyrrole monomer in presence of GO followed by chemical reduction using hydrazine monohydrate. The composite exhibited good improvement in thermal stability as well as electrical conductivity. Liu et al.[30] synthesized composite films of sulfonated GR and PPy by electrochemical deposition from aqueous solutions containing pyrrole monomer, sulfonated GR sheets and dodecylbenzene sulfonic acid. The composite exhibited improved conductivity, electrochemical stability and rate performance. However, in most cases the preparation of polymer composites is done by in-situ polymerization. But GR and GO sheets stack together especially by in-situ polymerization and may become the barrier of electron transportation.[31]

PTh is also considered as one of the most promising materials due to its low cost, high environmental stability, good electrical conductivity and other specific properties. It has large areas of applications in electronics, photovoltaic cells, electrocatalysis, corrosion protection, sensors and actuators.[32,33] A variety of nanofillers such as metals, metal oxides and carbon-based fillers has been introduced into the PTh matrix for various improvements in properties including electrical conductivity and

thermomechanical properties.[34-36] Karim *et al.*[37] synthesized PTh/SWCNT composites using the in-situ polymerization method. The composites showed good improvement in thermal as well as electrical conductivity (0.41 S cm^{-1}) compared to pure PTh. Wang *et al.*[38] synthesized ordered PTh/fullerene composite core–shell nanorod arrays using melt-assisted wetting of porous alumina templates. The composites showed good application potential in solar cells. Zhao *et al.*[39] synthesized an electromagnetic material of GNS/PTh composites prepared using the in-situ chemical polymerization method. The composites exhibited clear hysteretic behaviour as well as having the characteristics of a semiconductor. However, few studies have been reported of GR/GO based PTh nanocomposites so far, and mostly they are prepared using the solution polymerization method.[40]

In the present investigation both GR and GO filled composites based on conducting polymers like PPy and PTh were prepared by liquid/liquid interfacial polymerization, in which GO/GR was dispersed in water phase and the monomer was dispersed in organic phase. For comparison, pure polymer was prepared via the same route. Interfacial polymerization is regarded as a simple and easy approach to make bulk quantities of PPy and PTh.[41] The main advantage of the interfacial polymerization is that it is more controllable than conventional polymerization techniques and requires ordinary equipment. Moreover, it allows synthesis of polymers that may be unstable at high temperatures. This polymerization process has the ability to control the structure of the resulting polymer chain. To the best of our knowledge no previous work has been reported for preparing GO/GR based PPy and PTh composites by this route. This work aims at obtaining a good dispersion of GR and GO sheets within the polymer matrix as well as achieving good improvement in thermal, electrical, optical and electrochemical properties. The introduction of fewer amounts of fillers into the conducting polymer matrix is found to greatly enhance the properties of the polymer.

2.2 Experimental

2.2.1 Materials

Graphite flakes was obtained from Carbon India Ltd., Guwahati and was used as purchased. Pyrrole and thiophene monomers were purchased from Sigma Aldrich

and were used as received. Sodium nitrate (Merck), sulfuric acid (Merck), potassium permanganate ($KMnO_4$) (Merck), hydrogen peroxide (H_2O_2) (Qualigens Fine Chemicals), ferric chloride ($FeCl_3 \cdot 6H_2O$) (Aldrich), hydrazine monohydrate (Aldrich), and Lithium perchlorate (Fluka) are commercial products and were used as received. Chloroform ($CHCl_3$), n-hexane ($n-C_6H_{14}$) and nitromethane (CH_3NO_2) were obtained from Merck and was distilled and kept with molecular sieves before use. The solvent methanol (CH_3OH) was distilled before used. Acetonitrile (CH_3CN) was purchased from Merck and was dried by passing over neutral alumina followed by storage over 3 A^o molecular sieves. For all purposes double-distilled water was used.

2.2.2 Preparation of GO

GO dispersion was prepared from natural graphite using a modified Hummers method[42] using $KMnO_4$ and H_2SO_4 as oxidizing agent. For purification, the product was washed with 5% of HCl and then deionized (DI) H_2O for several times. Finally the product was exfoliated by ultrasonication for 1 h and GO dispersion was obtained. The powdered GO was obtained by filtration, drying the product under vacuum at 65 °C.

2.2.3 Preparation of GR by reduction of GO

To prepare GR, 0.1 g of GO was dispersed in 50 mL of doubly ionized water. Then 1 mL of hydrazine monohydrate was added to the mixture and heated at 95 °C for 12 h. After that the mixture was filtered and the reduced GO was obtained as a black powder. The product thus obtained was washed with DI H_2O several times.

2.2.4 Preparation of PPy/GO and PPy/GR nanocomposites

Composites were prepared by liquid/liquid interfacial polymerization as follows. Firstly, required amount of GO and 300 mg of $FeCl_3 \cdot 6H_2O$ were dispersed in 15 mL of H_2O. The organic phase was obtained by dissolving 0.8 ml of pyrrole in 15 mL $CHCl_3$ in beaker. The water phase was added to the organic phase dropwise and the beaker was kept undisturbed for 24 h. During this time, a black film slowly grew in the interface between the two phases. Finally, the product was filtered and washed several times with water and alcohol and air dried. The weight percentages of GO to pyrrole

were varied as 1%, 2% and 3% and the resulting composites were designated as PPyGO1, PPyGO2 and PPyGO3. By following the same procedure, composites of different weight percentages of GR to pyrrole (1%, 2% and 3%) were prepared and designated PPyGR1, PPyGR2 and PPyGR3.

2.2.5 Preparation of PTh/GO and PTh/GR composites

PTh/GO composites were prepared by liquid/liquid interfacial polymerization as follows. The required amount of GO was dispersed in 20 mL of CH_3NO_2 (solvent) using an ultrasonicator. Then $FeCl_3$ (2.44 g) was added to the dispersion and mixed thoroughly. The solution as obtained was added dropwise into a thiophene (0.4 mL) solution in 10 mL of $n\text{-}C_6H_{14}$ and the mixture was continuously stirred for 24 h. The product was obtained from the reaction mixture by centrifugation and then washed with ethanol for purification. Finally, the powdery composite was dried at 60 °C for 24 h. PTh/GO composites of various weight percentages of GO to thiophene (1, 2 and 3%) were labeled as PTGO1, PTGO2 and PTGO3. PTh/GR composites were prepared in a similar way with that of PTh/GO composites.

2.3 Characterization

2.3.1 Fourier transformed infrared spectroscopy (FTIR)

FTIR study of the prepared samples were carried out using a using a Nicolet Impact 410 spectrophotometer at room temperature (298 K) over a frequency range of 4000-500 cm^{-1}. The samples were crushed well and then examined in KBr pellets.

2.3.2 Ultraviolet (UV)-visible spectroscopy

UV-visible spectra of the samples in dispersion state were recorded on Shimadzu UV-2550 UV-visible spectrophotometer. The samples were well dispersed in dimethyl formamide with a concentration of 1mg/mL

2.3.3   Raman spectroscopy

Raman spectra were recorded using a Nanofinder 30 confocal Raman with He-Ne laser beam having a wave length of 532 nm with a CCD detector.

2.3.4   X-ray diffraction (XRD) study

XRD study was done to determine the crystallographic structures of the materials. The XRD study of the prepared samples was carried out using a Rigaku X-ray diffractometer at room temperature (ca. 298 K) with Cu-Ka radiation (λ= 0.15418 nm) at 30 kV and 15 mA using a scanning rate of 0.05°/s in the range of 2θ = 10°-70°. The samples were in powder form and the XRD patterns were recorded on a glass slide.

2.3.5   Scanning electron microscopy (SEM)

SEM studies were performed to investigate the surface morphology of the samples. All SEM measurements were carried out in a JSM-6390LV (JEOL, Japan) at an accelerating voltage of 5-15 kV. The powder samples were placed on an aluminum holder and then coated with a thin layer of platinum.

2.3.6   Transmission electron microscopy (TEM)

TEM analysis was performed with a PHILIPS CM 200 TEM microscope at 200 kV. A small amount of powdery sample was dispersed in ethanol for TEM analysis. Then, the suspension was dropped on 300 mesh copper TEM grids covered with thin carbon films.

2.3.7 Thermogravimetric analysis (TGA)

TGA analysis of each sample of 2 mg weight was conducted by using Shimadzu TG 50 thermogravimetric analyzer in the temperature range of 25-700 °C, with a heating rate of 10°C/min under nitrogen atmosphere. Thermogravimetric analysis gives information about the thermal characteristics of polymers including degradation temperature, absorbed moisture content the level of oligomer in polymer etc.

2.3.8 Electrical conductivity measurements

Current-voltage (I-V) characteristics of prepared samples were recorded by Keithley 2400 source meter at the room temperature with the scan rate 0.1 V s^{-1}. Measurements of electrical conductivities of the samples were performed using a four probe technique. For this round shaped pellets (1.5 cm diameter, 3 mm thickness) of the samples were made using a compression-molding machine at room temperature (298 K). The resistivity of the pressed samples was measured in a four-point probe unit using the following equation.[29]

Resistivity (ρ, ohm-cm) = (V/I) 2πd   (1)

Conductivity (σ, S/cm) = 1/ρ (2)

where V is the applied voltage, I is the measured current through the sample and d is the distance between the probes.

2.3.9 Electrochemical measurement

2.3.9.1 Cyclic voltammetry study:

The electrochemical behavior of the prepared samples was studied using Sycopel AEW2-10 cyclic voltammeter. Measurements were performed with a standard one compartment three electrode configuration cell where platinum and an Ag/AgCl electrode were used as counter and reference electrodes respectively, in 0.1 M lithium perchlorate (LiClO$_4$) - acetonitrile solution at the scan rate of 50 mV s^{-1}. Pellet shaped samples of 1.5 cm diameter and 3 mm width were prepared by pressing the composite materials using a compression-molding machine at a high pressure (1.5-2 ton). The capacitances were calculated by the following equation.[43]

C$_{sp}$= (I_+ $-$ I_-) / ($\upsilon \times$m)   (3)

where I_+ and I_- are maximum currents in positive and negative voltage scan respectively, υ is the scan rate and m is the mass of the composite material (10 mg).

2.3.9.2. Galvanostatic Charge-Discharge Study

The capacitor performance was characterized by means of galvanostatic charge–discharge tests using on an Autolab PGSTAT302N with a three electrode system at room temperature (25 °C). The specific capacitance (C_s) was measured by a charge-discharge method using the following equation[30]

$$C_s = (I \times \Delta t) / (m \times \Delta V) \tag{4}$$

where I is the discharge current, ΔV is the potential drop during discharging, Δt is the discharge time and m is the mass of active material in a single electrode.

2.4 Results and discussion

Section A:

2.4.1 Synthesis of GO and GR based PPy composites by interfacial polymerization

The synthetic process of preparation of PPy/GO and PPy/GR composite by the liquid/liquid interfacial polymerization is illustrated in Fig. 2.1. Polymerization is performed in an aqueous/organic biphasic system where pyrrole is dissolved in an organic solvent and GO/GR along with the oxidant ferric chloride is dissolved in an aqueous solution. As the reaction proceeds, the reactants diffuse to the water/chloroform interface and the pyrrole gets adsorbed on the GO/GR sheets. Then polymerization of pyrrole occurs at the interface of the two immiscible liquids. As a result a black film appears at the interface slowly. The reaction is controllable, slow and completed in 24 h. The by-products of the reaction can be easily removed due to their solubility in the aqueous or organic media. Also here the separation of product is easy as the product is insoluble in both aqueous and organic phase. During the progress of reaction, pyrrole oligomers were detected in the aqueous phase which may be due to the limited bulk polymerization of the monomer as a result of migration of small amount of pyrrole to the aqueous phase.
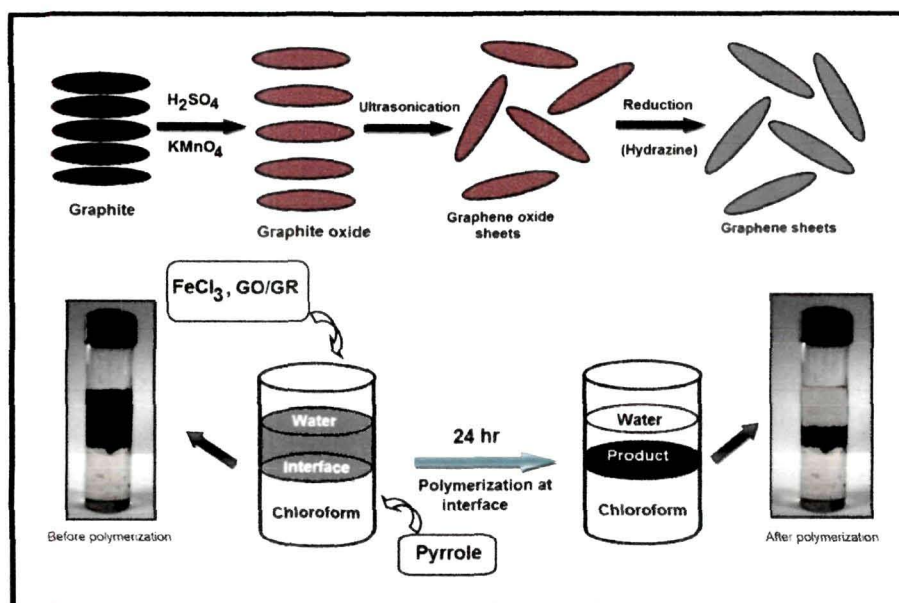
Fig. 2.1 Fabrication process of GO and GR based PPy composite.

2.4.1.1 FTIR analysis

FTIR spectra of pure PPy, GO, GR and their composites are represented in Fig. 2.2. In the FTIR spectra of PPy (Fig.2.2 (a)), peaks at 1549, 1465, and 3460 cm^{-1} are associated with the C-C, C-N, and N-H stretching vibration in the pyrrole ring. The peaks located at 2920 and 2831 cm^{-1} are designated as the asymmetric stretching and symmetric vibrations of CH$_2$.[43] In the FTIR spectrum of GO (Fig. 2.2 (b)), the broad peak at 3409 cm^{-1} and a peak at 1719 cm^{-1} can be assigned to O-H stretching vibration and the carbonyl (C=O) stretching respectively. The peaks at 1409 cm^{-1} and 1234 cm^{-1} represent the O-H deformation and C-OH stretching vibration.[17] The peak near 1065 cm^{-1} represents C-O stretching vibrations which confirms the presence of the epoxide group in the GO layers. Upon reduction of GO, the peaks at 1370, 1250 and 1060 cm^{-1} disappear which indicates that the epoxide and the hydroxyl groups have been removed from the basal GR layer (Fig. 2.2, curve (c)). Also the characteristic peak at 1719 cm^{-1} for the carbonyl group becomes weaker in the FTIR spectrum of GR, indicating successful reduction of GO into GR.

In the FTIR spectra of PPy/GO composites (Fig. 2.2 (d)), the peak due to the –C=O group has been downshifted to 1706 cm^{-1} which is probably due to the π-π interaction between the GO layers and aromatic PPy rings.[44] The characteristic peaks of

PPy appear at 1545 and 1438 cm^{-1} in the PPy/GO spectra which confirm the presence of PPy in the composite. Moreover, the peak due to the epoxide group at 1065 cm^{-1} in the GO spectra is shifted to 1080 cm^{-1} in the FTIR spectra of PPy/GO composite. Also it has also been observed that the peak at 1041 cm^{-1} which is obtained due to the C-H in-plane vibration of PPy ring, is shifted to 1038 cm^{-1}. The shifting of the peaks indicates the change in chemical environment during the formation of the composite. In the FTIR spectrum of PPy/GR composite we observed peaks for both PPy and GR (Fig. 2.2, curve (e)). The appearance of characteristic peaks of PPy at 1545 and 1450 cm^{-1} confirms the presence of PPy in the composite. However, the peaks have been downshifted compared with pure PPy. Also the peak intensity decreases in the composite. This indicates that GR has been successfully incorporated in the polymer matrix in the composite. Thus the FTIR results reveal the presence of the filler and polymer in the composites as well as the successful combination of both the component.
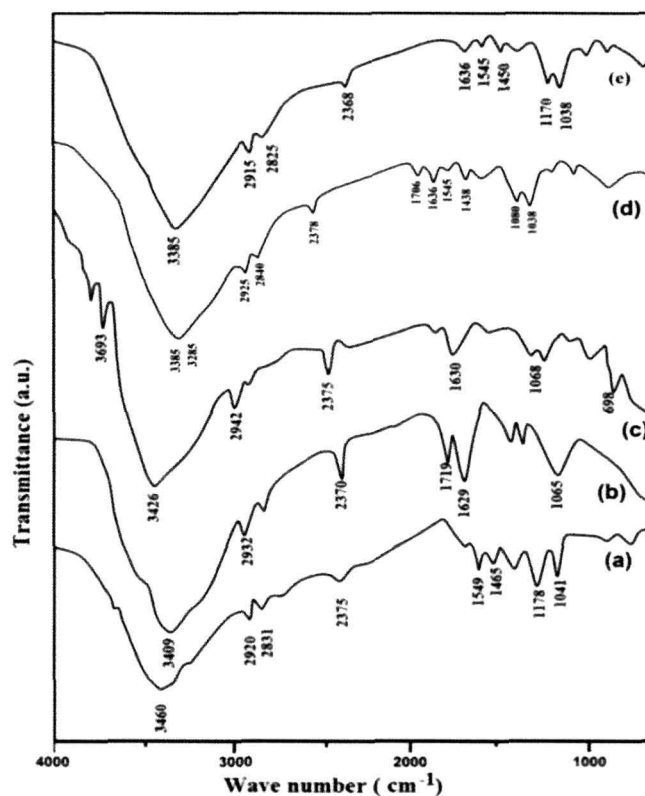
Fig. 2.2 FTIR spectra of (a) pure PPy, (b) GO, (c) GR, (d) PPy/GO and (d) PPy/GR composite.

60

2.4.1.2 UV-visible analysis

Fig. 2.3 demonstrates the UV-vis spectra of GO, PPy, PPy/GO and PPy/GR composites recorded in dimethylformamide. GO shows a characteristic absorption peak at 235 nm.[17] In PPy, the spectrum shows a weaker absorption peak at around 300 nm and stronger absorption at around 510 nm. The first peak is associated with the molecular conjugation and the second is related to the bipolaron state of PPy respectively.[45,46] Similar peaks are observed for the PPy/GO as shown in Fig. 2.3. The peaks related to molecular conjugation are observed at 310-320 nm which indicate the π-π interaction between PPy and GO of the composite. Significantly, a strong band at around 580-670 nm (2.13-1.85 eV) is also observed which confirms that PPy is also in the bipolaron state in the composite. The characteristic red shift of PPy/GO nanocomposites spectra was observed in the ranges for π-π* transition and for polaron, bipolaron band transition on increasing GO percentage. This is due to the extended conjugation length of PPy chains. This extend of conjugation length of the polymer composite may be attributed to the π-π stacking between the polymer backbone and the GO sheets and there may be some coupling in between the conjugation length of the PPy and GO.
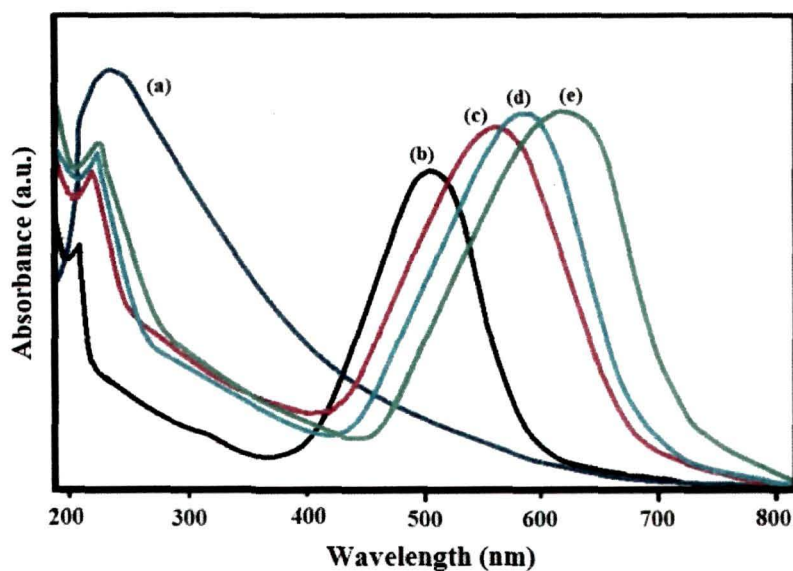
Fig. 2.3   UV-vis spectra of (a) GO, (b) PPy, (c) PPyGO1, (d) PPyGO2 and (e) PPyGO3 composite.

UV-visible spectra of GR, PPy and PPy/GR composites are shown in Fig. 2.4. GR shows a characteristic absorption peak at 255nm (Fig. 2.4, curve (a)) which is attributed to π-π* transitions of aromatic C−C bonds. In the PPy/GR composite, the peaks related to molecular conjugation are observed at 270–300 nm and are attributed to π-π* interaction between PPy and GR of the composite. Also a strong band is observed at around 500–590 nm which confirms that PPy is also in the bipolaron state in the composite. Significantly, the absorption peaks have been red shifted in the composite spectra with increasing GR percentage. This is ascribed to the extended conjugation length of PPy chains resulting from the π-π* stacking between the polymer backbone and GR sheets.
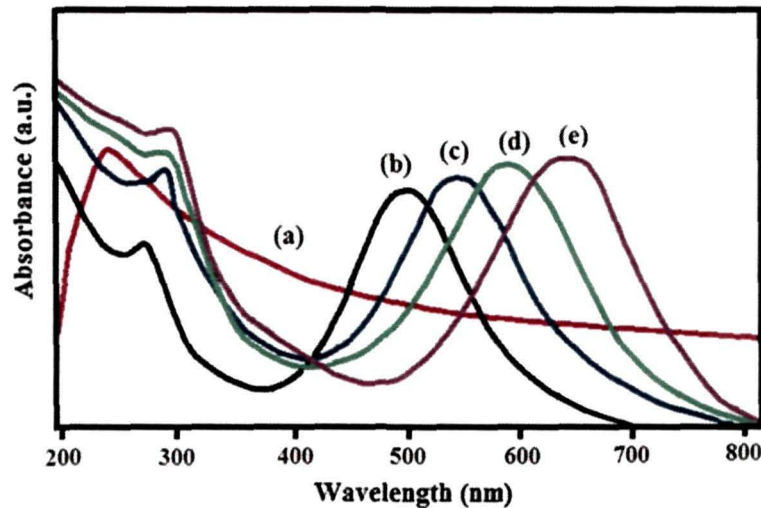
Fig. 2.4 UV-visible spectra of (a) GR, (b) PPy, (c) PPyGR1, (d) PPyGR2 and (e) PPyGR3 composite.

The optical absorption in conjugated polymers which are mostly amorphous or semicrystalline may be due to the transition of charge carriers, through a forbidden energy gap. The optical band gaps of PPy, PPy/GO and PPy/GR composites is calculated by using the following equation[48]

$$E^{opt}_{g} (eV) = 1240/\lambda_{edge} (nm) \qquad (4)$$

where E^{opt}_g is the optical band gap and ledge is the absorption edge. The absorption edge and optical band gap of the polymer and composites are listed in Table 2.1. The band gap of PPy is found to be 2.43 eV, whereas in PPy/GO and PPy/GR composites the band gaps are decreased from 2.13 eV to 1.85 eV and 2.10 eV to 1.82 eV respectively.

Table 2.1 Electrochemical data of PPy, PPy/GO and PPy/GR composite

[a]Sample particulars	$\varphi_{onset}{}^{ox}/ E_{HOMO}$	$\varphi_{onset}{}^{red}/E_{LUMO}$	E^{ec} (eV)	E^{opt}(eV)
PPy	1.40/-6.11	-1.2/-3.51	2.60	2.43
PPyGO1	0.97/-5.68	-1.2/-3.92	2.17	2.13
PPyGO2	0.93/-5.64	-1.0/-3.71	2.06	2.01
PPyGO3	0.80/-5.51	-1.1/-3.61	1.90	1.85
PPyGR1	0.85/-5.56	-0.5/-4.21	1.35	2.10
PPyGR2	0.60/-5.31	-0.4/-4.31	1.00	1.90
PPyGR3	0.40/-5.11	-0.25/-4.46	0.65	1.82

[a]PPy: polypyrrole; GO: graphene oxide; PPyGO1: 1 wt. % of GO w.r.t. pyrrole; PPyGO2: 2 wt.% of GO w.r.t pyrrole and so on; GR: graphene; PPyGR1: 1 wt. % of GR w.r.t. pyrrole.

2.4.1.3 Raman spectroscopy

Raman spectroscopy is a powerful nondestructive tool used for the qualitative and quantitative analyses of carbon products. The conjugated and carbon-carbon double bonds lead to high Raman intensities. The Raman spectra for GO, GR, PPy/GO and PPy/GR composite are shown in Figure 2.5. The Raman spectrum of GO displays two characteristic peaks at 1335 and 1565 cm^{-1} that correspond to the D and G bands, respectively.[17,49] The D band is ascribed to edges, other defects, and disordered carbon and the G band arises from the zone center E_{2g} mode, corresponding to ordered sp^2-bonded carbon atoms. The intensity ratio between the D band and G band is a measure of the extent of disorderness in graphite. If these two bands have similar intensity this indicates a high quantity of structural defects. The intensity ratio (I_D/I_G) is found to be

0.80 for pure GO which indicates a high level of disorder of the GO layers due to the oxidation of graphite. In the Raman spectra of pure GR (Figure 2.5. (b)), the D and G band appears at 1340 and 1585 cm^{-1} respectively. However, the I_D/I_G value increased upto 1.17 which may be attributed to the presence of unrepaired defects that remained after the removal of large amounts of oxygen-containing functional.[30,49]
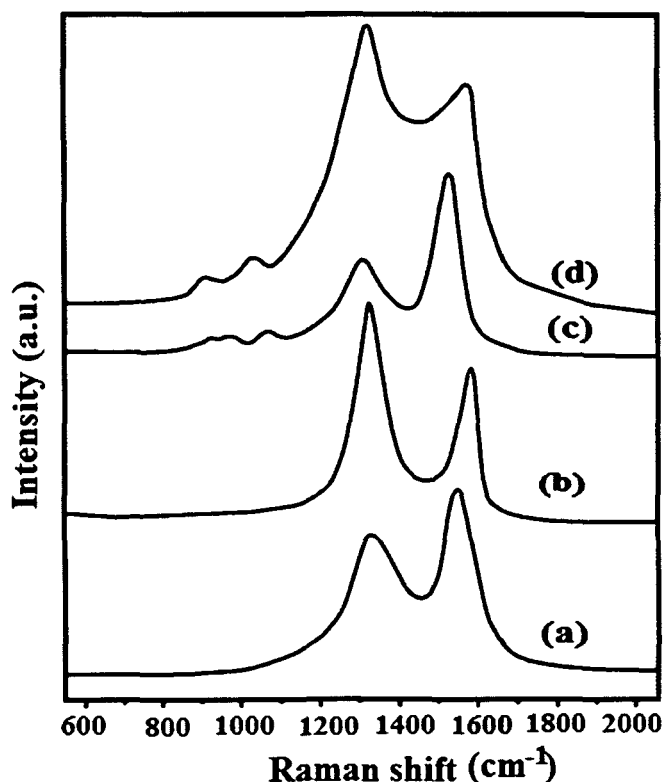

Fig. 2.5 Raman spectra of (a) GO, (b) GR, (c) PPy/GO and (d) PPy/GR composite.

In the Raman spectra of PPy/GO composite, both these D and G band shift to 1332 and 1560 cm^{-1} which reveals π–π interaction between the PPy and the GO sheets. Additionally, a broad peak at 1050 cm^{-1} and two small peaks at 930 and 980 cm^{-1} appear in case of PPy/GO composite, which are the characteristic peaks of PPy. The bands at 930 cm^{-1} and 980 cm^{-1} are associated with the bipolaron and polaron structure of PPy. In the Raman spectra of PPy/GR composite (Figure 2.5 (d)), a broad peak at 1050 cm^{-1} and two small peaks at 930 and 980 cm^{-1} reveals the presence of PPy in the composite. The bands at 930 cm^{-1} and 980 cm^{-1} are associated with the bipolaron and

polaron structure of PPy. Moreover, the D and G band shift to 1332 and 1560 cm^{-1} which indicates π-π interaction between the PPy and the GR sheets. The peak intensity ratio, I_D/I_G of the composites was 1.14. This indicates the presence of defects within the sp^2 carbon network which may favor the chemical grafting of polymers to the GR surface.[28] Thus Raman spectra of the composites show the bands related to both of their polymer and filler components. This is in good agreement with FTIR results.

2.4.1.4 XRD analysis

The structure of the composites was investigated by X-ray diffraction (XRD) measurements. The XRD patterns of GO, GR, PPy, PPy/GO and PPy/GR composite are given in Fig. 2.6. The X-ray diffraction pattern of GO displays the presence of a strong peak at 2θ=11.45° corresponds to (001) reflection peak.[33] GR shows a broad reflection peak centered at 2θ= 24.5° and 43° (Fig. 2.6(b)) corresponding to d spacing of 0.35 nm which indicates the loosely stacked GR sheets and is different from the crystalline graphite. Pure PPy exhibit a weak and broad diffraction peak at 2θ= 24.65°,[30] which indicates that the PPy is amorphous in nature. For the PPy/GO composite, the peak at 11.45° has shifted to 11.65 with significant decrease in peak intensity. This decrease in the peak intensity may be due to exfoliation of GO layers upon ultrasonication.[29] In addition, one broad peak appears at around 2θ= 25.6° which is the characteristic peak of PPy, indicating the presence PPy in the composite. Appearance of peak at 2θ= 11.65°(for GO) and 2θ= 25.6° (for PPy) in the XRD pattern of the PPy/GO composite indicates the successful development of the composite. The XRD data of PPy/GR composite is almost similar to that of pure PPy, however, the peak at 26° has been shifted to 25.2° with a slight increase in peak intensity. The disappearance of diffraction peaks at 43° reveals the full interaction between PPy and GR sheets (Figure 2.6 (d)). Thus the XRD results reveal that the GO/GR sheets were well exfoliated and uniformly dispersed in the PPy matrix and the semicrystalline structure of PPy is slightly affected by the incorporation of these nanofillers.
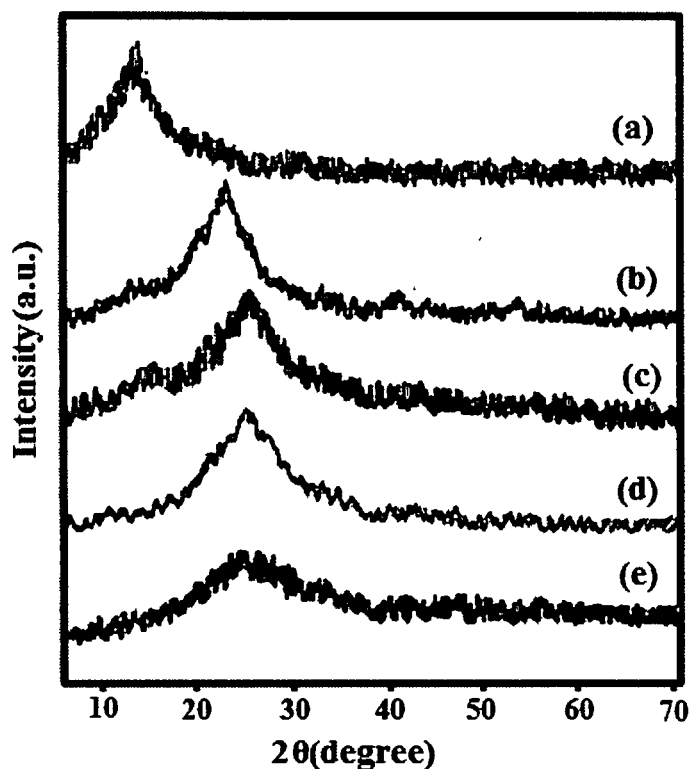
**Fig. 2.6** XRD patterns of (a) GO, (b) GR, (c) PPy/GO, (d) PPy/GR composite and (e) Pure PPy.

2.4.1.5 Morphology and Structure

The structure of the PPy, GR and PPy/GR composites were investigated using scanning electron microscope (SEM) and transmission electron microscope (TEM). Fig. 2.7 shows the SEM images of GO, GR, PPy, PPy/GO and PPy/GR composites. In the SEM image of GO (Fig. 2.7 (a)) a flat; multilayered structure with stacked GO sheets is observed which is consistent with the report given by Zhang et al.[50] In the SEM image of GR, a layered, wrinkle-like structure is observed (Fig. 2.7(b)). The pure PPy shows an irregular sphere-like structure (Fig. 2.7 (c), 2.7 (d)). Sphere-like PPy is obtained as the polymerization is initiated at the interface between the two immiscible liquids. These PPy spheres disappear and a flaky, rough morphology is observed in case of both PPy/GO and PPy/GR composites (Fig. 2.7(e), 2.7(f)). The change in morphology of the composite from the individual components can be attributed to the polymerization of PPy on the surface of GO and GR sheets.

The TEM images for GO, GR, PPy/GO and PPy/GR composites are shown in Fig. 2.8. A layered structure of individual GO sheets with a lateral dimension of few micrometers is observed in the TEM image of Fig. 2.8 (a). TEM image of GR (Fig. 2.8 (b)) shows a crumpled and agglomerated sheet like structure with hundreds of nanometers. The wrinkled structure observed in the TEM image of GR sheets is due to the rapid removal of intercalated functional groups in graphitic oxide during exfoliation.[28] The TEM image of the PPy/GO composite (Fig. 2.8 (c)) shows some fiber like structures of PPy which are decorated at the surface of the GO sheets. It confirms the formation ordered PPy chain on the surface of the GO sheets. From the TEM image of PPy/GR composite, (Fig. 2.8 (d)) it is observed that the exfoliated GR sheets are decorated by PPy nanoparticles, leading to the formation of well-dispersed composite sheets. Also it is clear that PPy/GO and PPy/GR composite sheets are folded with dark edges which indicate the flexible character of the composites. Both GO and GR acts as a template in the liquid/liquid interfacial polymerization, which results in the formation of such well dispersed flexible composite sheets.[51] These changes in structure of the composite from the individual components may introduce superior electrochemical properties. The structure of the composites obtained by liquid/liquid interfacial polymerization is quite different from the earlier reported methods.[29,30]
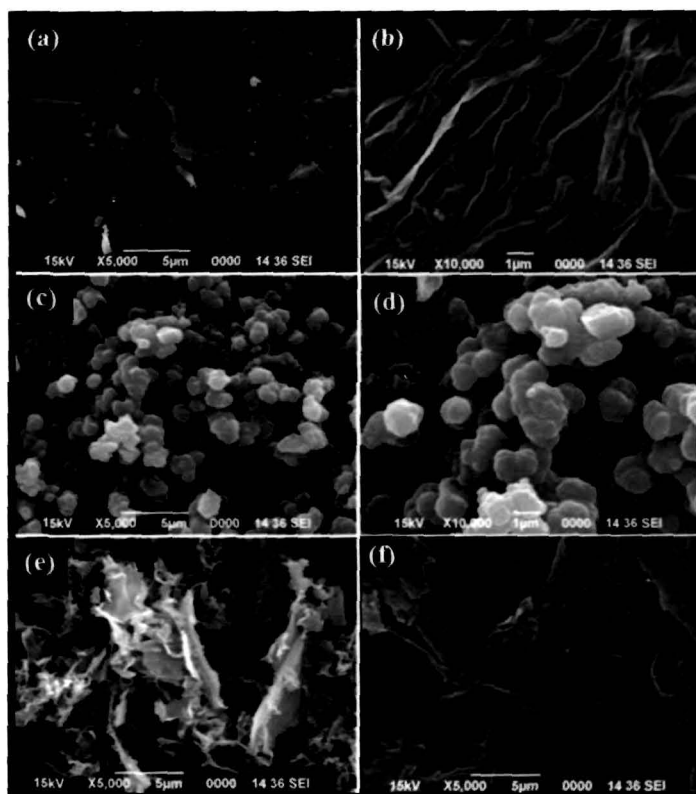
Fig. 2.7 SEM images of (a) GO, (b) GR, (c) PPy at lower magnification, (d) PPy at higher magnification, (e) PPy/GO and (f) PPy/GR composite.
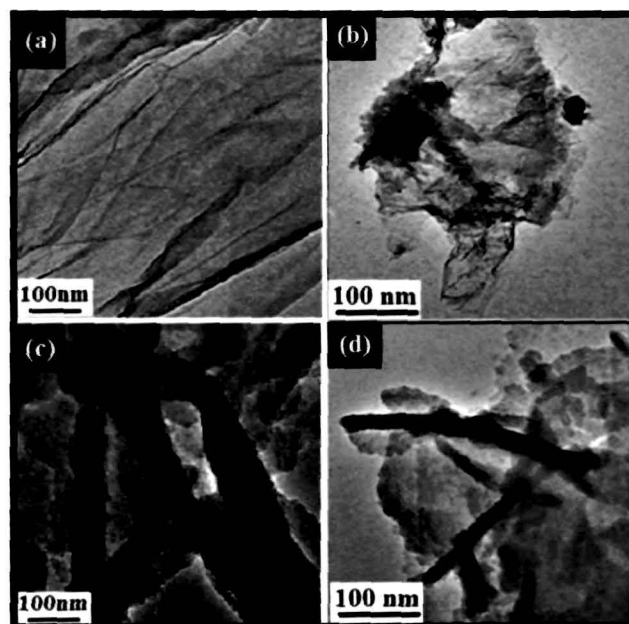
Fig. 2.8 TEM images (a) GO, (b) GR, (c) PPy/GO and (d) PPy/GR composite.

2.4.1.6 Thermal Gravimetric Analysis (TGA)

The thermal stability of PPy, PPy/GO composites and pure GO were studied by TGA. The TGA curves of pure PPy, GO and PPy/GO composites are shown in Fig. 2.9, with respective data are being summarized in Table 2.2. From the TGA curve of pure PPy (Fig. 2.9 (a)), it is observed that PPy is stable upto 200 °C and only about 10% weight loss occurs due to the removal of moisture. The weight loss after 300 °C corresponds to the complete degradation of the polymer. In case of GO, major weight loss at the temperature range of 200-320 °C is attributed to the removal of most of the oxygen-containing functional groups. The 58% residual weight of GO indicates that some functional groups existed on GO surface before the thermal treatment.

Incorporation of GO in the PPy matrix increases' the thermal stability of the composites. Although the thermal degradation process is almost the same, but the major degradation in the composites start at higher temperatures compared to pure PPy as shown in the Table 2.2. In the TGA curve of PPy/GO composites, the weight loss near 200 °C can be attributed to pyrolysis of the labile oxygen-containing functional groups. After 200 °C, major weight loss has occurred which may be due to the decomposition of the PPy from the composite. Also, the residual weight value of the composites was found to be increased compared to pure PPy. PPy/GO composites show almost 15-32% weight retention value at 600 °C which is probably due to the existence of a carbon net structure in the composite.[29,52]

Table 2.2 TGA data of PPy and PPy /GO composites

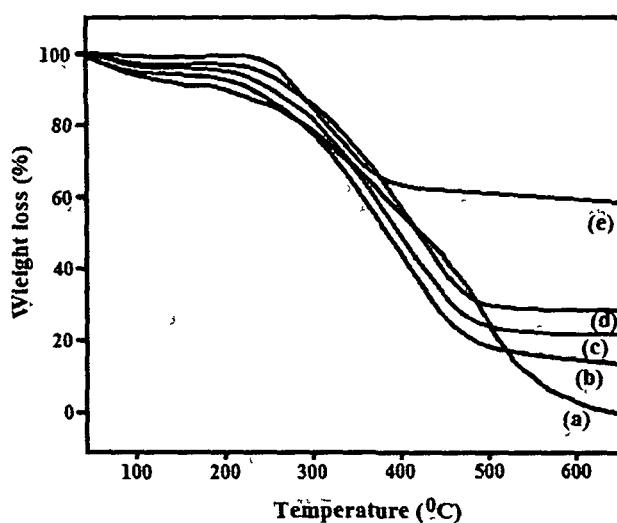| Samples	Weight loss % at temperature				Major degradation temperature (Td) °C	Weight retention (%) at 600 °C
	200 °C	300 °C	400 °C	500 °C		
PPy	10	19	40	70	230	3
PPy/GO1	8	20	55	80	249	15
PPy/GO2	5	18	51	70	250	22
PPy/GO3	2	12	39	65	252	32
GO	1	25	30	35	256	58

Fig. 2.9 TGA curves of (a) PPy, (b) PPyGO1, (c) PPyGO2, (d) PPyGO3 composite and (e) GO.

The TGA curves of pure PPy, GR and PPy/GR composites are shown in Fig. 2.10. GR exhibited around 20% weight loss at the temperature range of 250 to 500 °C, which is attributed to the removal of most of the oxygen-containing functional groups during the chemical reduction process. About 70% residual weight at 600 °C indicates the excellent thermal stability of GR (Figure 2.10 (a), Table 2.3). Pure PPy displays a major weight loss in the temperature scale of 250 to 500 °C and only 10% weight retention at 600 °C corresponds to the complete degradation of the polymer (Fig. 2.10 (e)). PPy/GR composites exhibit a considerable enhancement in thermal stability on incorporation of GR (Fig. 2.10 (b-d)). In case of the composites, the major decomposition starts at higher temperatures compared to pure PPy. The major weight loss in the temperature range of 250 to 500 °C can be attributed to the decomposition of the PPy and functional groups of GR from the composite. The PPy/GR composites showed improved thermal stability compared to PPy/GO composites. Around 65% weight loss was observed for PPy/GO (3 wt.%) composite at 500 °C, compared to the 58% weight loss for PPy/GR (3 wt.%) composite at this temperature. Also, the major degradation started at relatively higher temperature (290 °C) for PPy/GR composite compared to PPy/GO composite (252 °C). Thus the TGA results indicate the superior thermal stability of GR-based PPy composite than GO-based PPy composite.

Table 2.3 TGA data of PPy, GR and PPy/GR composites

Samples	weight loss % at temperature (°C)				major degradation temperature (Td) °C	weight retention (%) at 600 °C
	200	300	400	500		
PPy	10	20	44	75	240	10
PPyGR1	6	15	40	72	250	18
PPyGR2	4	10	36	65	265	24
PPyGR3	2	8	25	58	290	35
GR	1	10	15	25	310	70
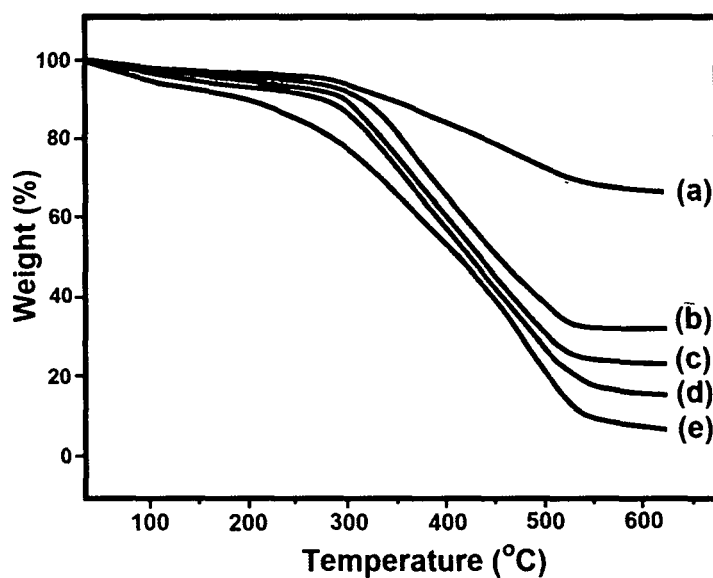
Fig. 2.10 TGA curves of (a) GR, (b) PPyGR1, (c) PPyGR2, (d) PPyGR3 composite and (e) PPy.

2.4.1.7 Electrical behavior:

(a) Current–voltage relationship

Fig. 2.11 shows the current–voltage relationship of PPy and PPy/GO composites at room temperature. For both PPy and PPy/GO composite, the current (in mA) increases with increase in the applied voltage (in volt) in a nonlinear way. Thus the

samples exhibit a non ohmic behavior as V/I is not constant. This nonlinearity of I–V curves indicates the semi conducting behavior of the composites and their ability to be used in electronic devices. However, with increasing GO content in the polymer matrix, the nonlinearity decreases. This may be due to the increase in charge mobility of the composite on incorporation of GO.
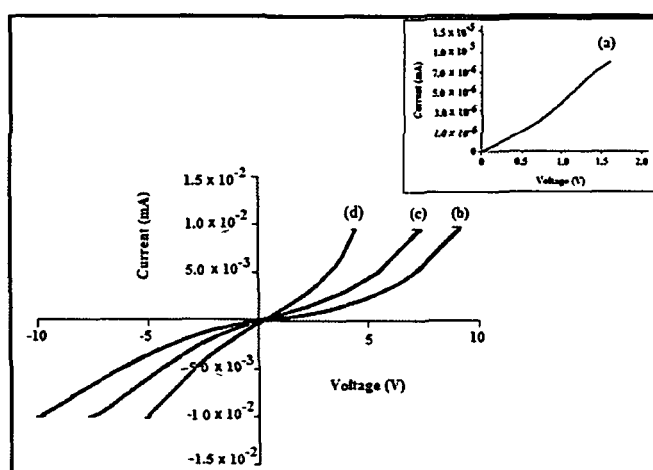

Fig. 2.11 I-V plot of (a) PPy, (b) PPyGO1, (c) PPyGO2 and (d) PPyGO3 composite.

(b) Measurements of electrical conductivity

The electrical conductivities of pure PPy, GR, PPy/GO and PPy/GR composites are determined using a fourpoint probe resistivity measurement system. The average conductivities are summarized in Table 2.4. Pure PPy shows a conductivity of 0.210 S cm^{-1} which is lower than that of PPy synthesized by the electrochemical method (10-50 S cm^{-1})[53] but higher than that of PPy synthesized by the chemical method using FeCl$_3$ as the oxidant (0.07 S/cm) and prepared by the in-situ polymerization, with HCl as medium (0.939 S cm^{-1}).

Table 2.4 Conductivity measurements

Sample particulars	Thickness (d, cm)	Resistivity (ρ, ohm-cm)	Conductivity (σ, S cm^{-1})
PPy	0.3	4.9	0.210
PPyGO1	0.3	2.80	0.360
PPyGO2	0.3	2.36	0.423
PPyGO3	0.3	1.97	0.507
PPyGR1	0.3	0.340	2.510
PPyGR2	0.3	0.210	4.520
PPyGR3	0.3	0.126	8.450
GR	0.3	0.021	50.400

The DC electrical conductivity of the PPy/GO composites is found to be increased in comparison to the pure PPy. The composites showed an increase in magnitude of conductivity even at a low GO content. For PPyGO1, PPyGO2 and PPyGO3, the conductivities are 0.360, 0.423 and 0.507 S cm^{-1} respectively at room temperature (298 K). Due to the large aspect ratio and surface area of the GO sheets, they may serve as effective percolative conducting bridges and thereby increase the conductivity of PPy/GO composite at low GO content.[55] At higher concentration of GO, increase in conductivity may be due to the π-π stacking between the GO layers and PPy for which electron mobility inside the composite system increases. It is observed that incorporation of these highly conductive GR (50.4 S cm^{-1}) sheets into PPy matrix greatly improved the conductivity of the PPy/GR composite. For PPyGR1, PPyGR2 and PPyGR3, the conductivities are 2.51, 4.52 and 8.45 S cm^{-1} respectively at room temperature (298 K). The significant increment in conductivities of the reduced composites is due to the high aspect ratio and large specific surface area of the highly conducting GR sheets which act as conducting bridges inside the composite system.

## 2.4.1.8 Electrochemical behavior

(a) Cyclic voltammetry (CV)

The cyclic voltammogram of PPy/GO and PPy/GR composites are shown in Fig. 2.12 and 2.13 respectively. Ag/AgCl and Pt wire were used as reference electrode and counter electrode, respectively. All potentials are reported with respect to reference electrode. Acetonitrile containing $LiClO_4$ (0.1M) was used as the electrolytic medium. The measurements were calibrated using ferrocene as the standard and the scan rate was 50 mV s^{-1}. The CV curve of a pure PPy in Fig. 2.12 (d) shows a couple of redox waves with a nearly rectangular shape which indicates the electrochemical double-layer capacitor character (EDLC). CV curves of PPy/GO composites have larger rectangular areas, indicating higher double-layer capacitances and better charge propagation within the electrode compared to PPy (Fig. 2.12 (a)-(c)).
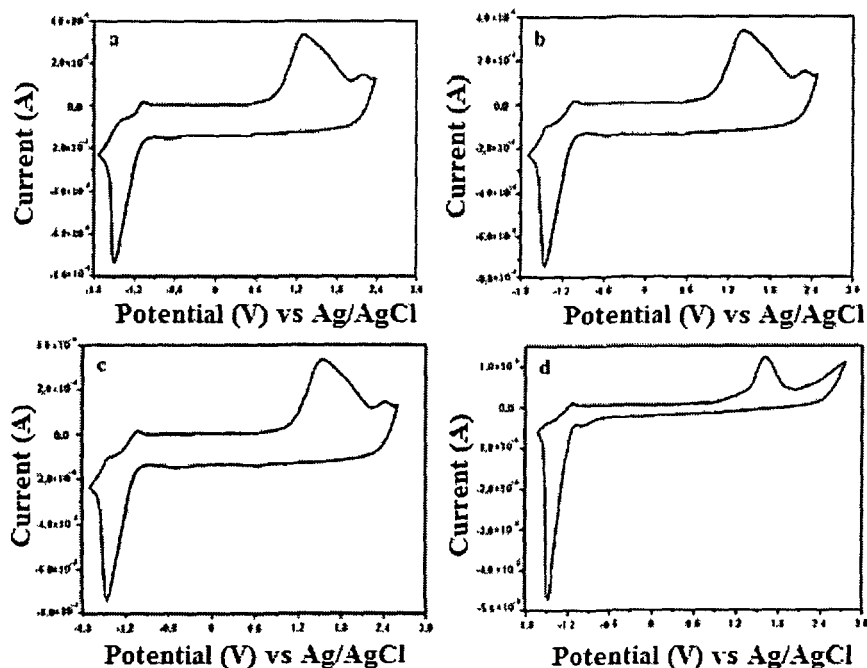
Fig. 2.12 Cyclic voltammogram of (a) PPyGO3, (b) PPyGO2, (c) PPyGO1 composites and (d) PPy at a scan rate of 50 mV s^{-1}.

In Fig. 2.13 (a), CV curve of GR exhibits a much smaller rectangular area, perhaps due to its compact structure. For PPy/GR composites, the redox waves became wider and shifted to more positive potentials compared to PPy. Also the areas

of CV curves in PPy/GR composites are much larger compared to that of PPy/GO composite which indicates higher capacitances of the PPy/GR composites. This is possibly due to the introduction of highly conducting GR sheets which increases the conductivity and surface area of the PPy/GR composites, thereby increasing the capacitances.
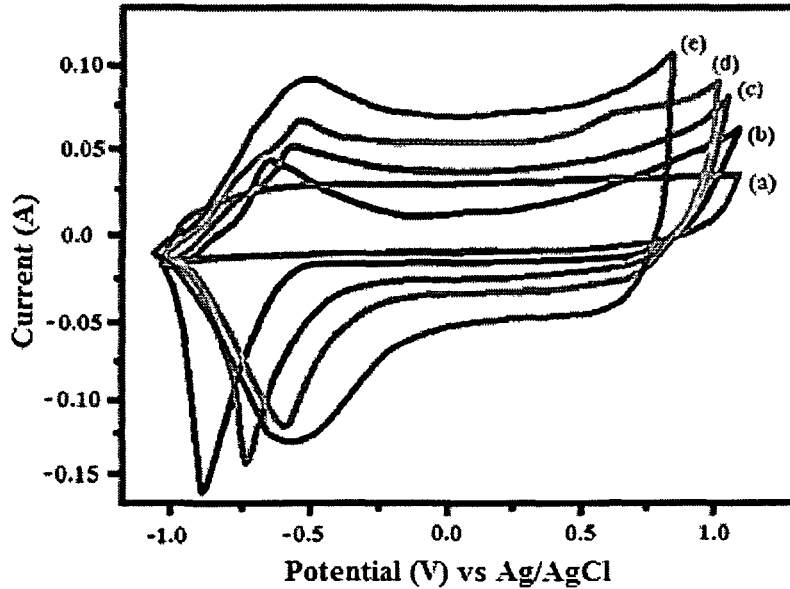
Fig. 2.13 Cyclic voltammogram of (a) GR, (b) PPy, (c) PPyGR1, (d) PPyGR2 and (e) PPyGR3 composites at a scan rate of 50 mV s^{-1}.

The electrochemical band gap of the samples was calculated by using the following formulae[56]

$$HOMO = -[\varphi_{onset}^{ox} + 4.71] \tag{4}$$

$$LUMO = -[\varphi_{onset}^{red} + 4.71] \tag{5}$$

$$E_{ec}^{g} = (\varphi_{onset}^{ox} - \varphi_{onset}^{red}) \tag{6}$$

where the units φ_{onset}^{ox} and are φ_{onset}^{red} oxidation onset potential and reduction onset potential, respectively and E_{ec}^{g} is the electrochemical band gap.

The electrochemical band-gaps of the PPy, PPy/GO and PPy/GR composites were calculated from the CVs (Fig. 2.12 and 2.13) and are listed in Table 2.1. The

band gap of pure PPy was found to be 2.60 eV which decreases to 1.93 eV for PPy/GO composites. The band gaps of the composites decreases with increase in the amount of incorporated GO into the PPy matrix. The incorporation of GO changes the electronic band structure of PPy/GO composites which manifest a new mid-gap state and thereby results in a decreasing of band gap. The PPy/GR composites showed much lower band gap values (1.35-0.65 eV) compared to pure PPy and PPy/GO composites. With the increase in the amount of GR in the PPy matrix the band gap decreases (Table 2.1). This may be due to the changes of electronic band structure of PPy/GR composites on incorporation of highly conducting GR which manifest a new mid-gap state and thereby results in a decreasing of band gap.

The intrinsic electronic, optical properties and electrical conductivity of conjugated polymers are influenced by the band gap parameter. We have compared the optical band gap data with electrochemical band gap of the composites. The electrochemical determination of band gap actually leads to the formation of charge carriers, while optical transition does not reveal the formation of free charge carriers as the excited state in conjugated polymers may be viewed as a bound exciton. Therefore, the optical band gap cannot be directly compared to the electrochemical band gap. The band gaps of PPy/GO composites are found to be 2.13-1.85 eV (optically) and 2.17-1.90 eV (electrochemically). The electrochemical band gaps give higher values than the optical band gaps. Similarly the band gaps of PPy/GR composites are calculated and found to be 2.10–1.82 eV (optically) and 1.35–0.65 eV (electrochemically). The PPy/GR composites showed lower electrochemical band gap values than that of the optical band gaps. However, in both the methods, same trend of band gap is observed. Moreover, the band gaps of PPy/GR composites are lower compared to PPy/GO composites which indicates the better electrochemical properties of GR based composites than that of GO based composites.

(b) Cyclic stability

Cyclic voltammetry study also provides information regarding the stability of the composite during multiple redox cycles. The PPy/GO and PPy/GR composites were exposed to cyclic oxidation and reduction upto 100th cycles (Fig. 2.14). It was

observed that there was no significant change in redox potentials and the composites were quite stable even upto 100th repeated cycles indicating a good cycling performance of the composite. Introduction of GO/GR sheets can significantly improve the cycling stability of the composites due to their homogeneous dispersion in PPy matrix and the synergic effect of GO/GR and PPy in the composites. The results indicate that the composites bear a good application potential in rechargeable batteries.[57]
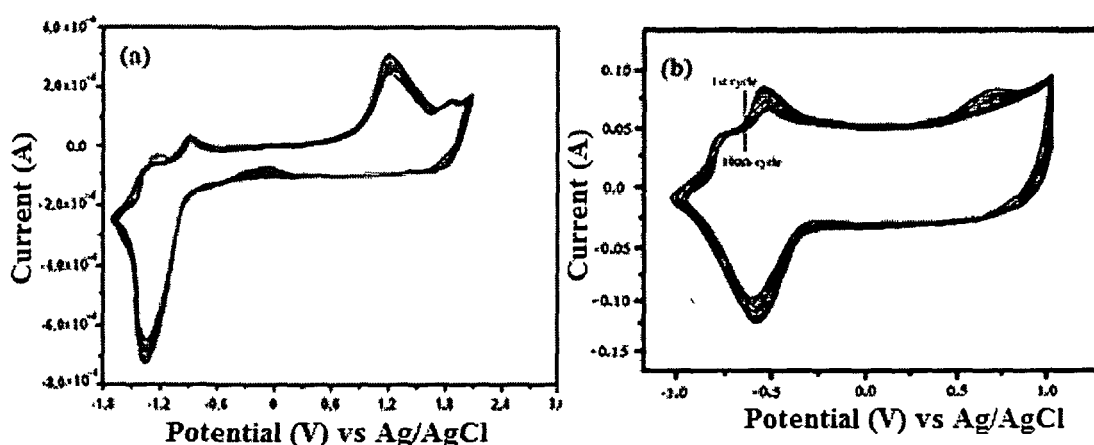

Fig. 2.14 Successive electrochemical cycles of (a) PPyGO3 composite and (b) PPyGR3 composite up to 100th cycles.

(c) Charge capacity

The specific capacitance of pure PPy and PPy/GO composites were calculated from the CV curves (Fig. 2.12) and summarized in Table 2.5. The composites showed higher specific capacitance than that of pure PPy. PPGO3 shows maximum capacitance of 92.2 F g^{-1}. The specific capacitance of the composites increases with increase in GO content. GO acts as a template for the growth of the polymer chain. Thereby, the composite provides more active surfaces allowing facile redox reaction.

Table 2.5 Specific capacitance of PPy and composites

Sample	Specific capacitance $(F\ g^{-1})$ at scan rate 50 mV s^{-1}
PPy	52
PPGO1	56.4
PPGO2	82.5
PPGO3	92.2

(d) Galvanostatic charge-discharge study

Galvanostatic charge-discharge behaviour was investigated to study capacity of the PPy/GR composites. Figure 2.15 demonstrates the galvanostatic charge/discharge curves of PPy and PPy/GR composite with a potential window from 0.0 to 1.0 V at a current density of 100 mA g^{-1}. The charge/discharge curves of PPy and PPy/GR composite electrodes are nearly triangular in shape, implying its capacitance is mainly attributed to pure EDL capacitance.[30,50] Compared with PPy, PPy/GR composite exhibited longer discharge times at the same current density.
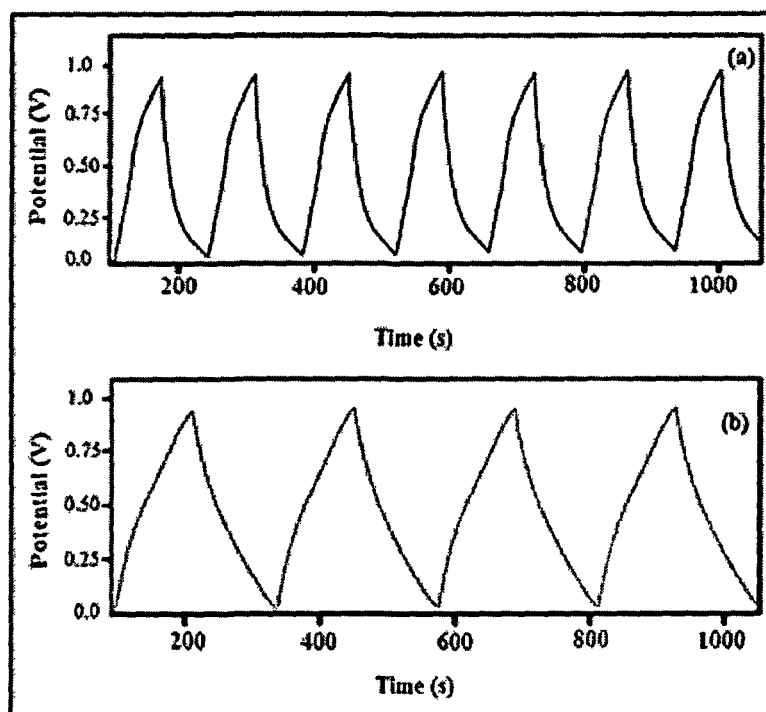
Fig. 2.15 Galvanostatic charge/discharge curves of (a) PPy and (b) PPy/GR (3 wt.%) composite with at a current density of 100 mA g^{-1}.

78

The specific capacitances of pure PPy and PPy/GR composites were calculated from the galvanostatic charge/discharge curves. The PPy/GR (3 wt.%) composite shows much higher specific capacitance value of 260 F g^{-1} compared to pure PPy (65 F g^{-1}). This increase in the specific capacitance of the composite is possibly due to the following factors. Firstly, the incorporation of highly conductive GR favors the redox reaction of PPy component, thereby increasing the pseudo-capacitance of PPy. Secondly, presence of GR sheets within PPy matrix greatly improves the double layer capacitance of the composite by forming a porous structure which has high specific surface area. We have compared the specific capacitances of PPy/GR composites with some previous reports. Biswas et al.[58] synthesized nanocomposites based on GR nanosheets and PPy nanowire and obtained a specific capacitance value of 165 F g^{-1}. Bose et al.[59] developed PPy/GR composite which exhibited a specific capacitance value of 267 F g^{-1}. Davies et al.[60] prepared a flexible, uniform PPy/GR composite by a pulsed electropolymerization technique which exhibited a specific capacitance value of 237 F g^{-1}. Thus it can be concluded that the specific capacitance value of the composite synthesized by interfacial polymerization is higher than various previously reported PPy/GR composite synthesized by other methods.

Section B:

2.4.2 Synthesis of GO and GR based PTh composites by interfacial polymerization

The method of preparation of PTh/GO composite by interfacial polymerization is shown in Fig. 2.16. In this method, monomer thiophene is dissolved in n-C_6H_{14} forming the organic phase and GO/GR along with the oxidant $FeCl_3$ is dissolved in CH_3NO_2 which formed the aqueous phase. The polymerization occurs at the interface between these two immiscible phases. After 24 h of constant stirring black colored PTh microparticles were obtained as a suspension in CH_3NO_2 which was further washed and dried. The process is controllable, slow and the separation of the product is easy due to its insolubility in both aqueous and organic phases.
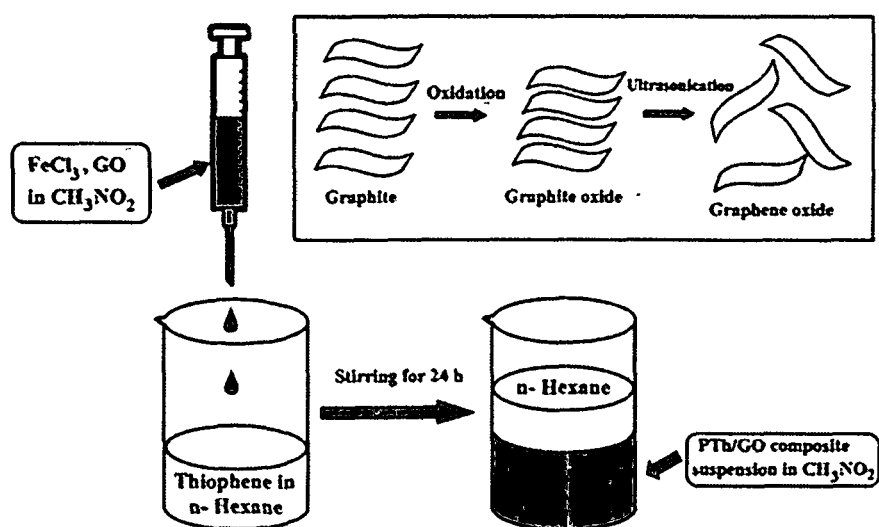

Fig. 2.16 Illustration of the fabrication process for PTh/GO composites.

2.4.2.1 FTIR analysis

FTIR spectra of PTh, GO and PTh/GO composite are shown in Fig. 2.17. In PTh, a broad band appears at around 3423 cm^{-1} which is due to the O-H stretching vibration (Fig. 2.17 (a)). The bands at 2923 cm^{-1}, 1640 and 1426 cm^{-1} is ascribed to C-H stretching vibration, C=C asymmetric and symmetric stretching vibrations of

thiophene units respectively.[61] The band at 1167 cm^{-1} is assigned to C-H (in-plane) bending vibration of thiophene. A band at 790 cm^{-1} appears due to C-H (out-of-plane) bending vibration of thiophene unit indicating the α-position linkage between the thiophene rings. Moreover, the bands at 830 and 692 cm^{-1} may be assigned to C-S stretching and C-S-C bending vibrations indicating the presence of thiophene rings.[62] The FTIR spectrum of GO (Fig. 2.17 (c)) shows a broad peak at 3409 cm^{-1} for O-H stretching and a peak at 1719 cm^{-1} which can be assigned to the carbonyl (C=O) stretching vibration. The peak at 1066 cm^{-1} for C-O stretching vibrations appears due to the presence of the epoxide group in the GO layers. The peaks at 1236 and 1411 cm^{-1} can be ascribed to the C-OH stretching vibration and O-H deformation respectively.[63] The FTIR spectra of PTh/ GO composite (Fig. 2.17 (b)) shows almost similar bands to that of PTh, however, the bands have been shifted to longer wavelength. Also peak at nearly 1720 cm^{-1} for the carbonyl (C=O) stretching vibration appears in the composite which is absent in the pure polymer. Thus the FTIR results show characteristic peaks of both the components and thereby reveal the successful incorporation of GO in the PTh matrix.

In the spectrum of GR, the peaks at 3426 cm^{-1} and 1630 cm^{-1} represent the O-H stretching vibration and benzene ring stretching vibration, respectively. The characteristic peak at 1719 cm^{-1} for carbonyl group in the FTIR spectrum of GO (Fig. 2.17 (d)) disappears in the spectrum of GR. This indicates successful reduction of GO into GR. The peak at 2912 cm^{-1} represents the C-H stretching vibration. In the FTIR spectrum of PTh/GR composite we have observed peaks for both PTh and GR (Fig. 2.17 (e)). Comparing to the spectrum of pure PTh, we have seen that shifting of peaks occurs. Also peak intensity decreases in the composite. This indicates that GR was successfully incorporated in the polymer matrix in the composite.
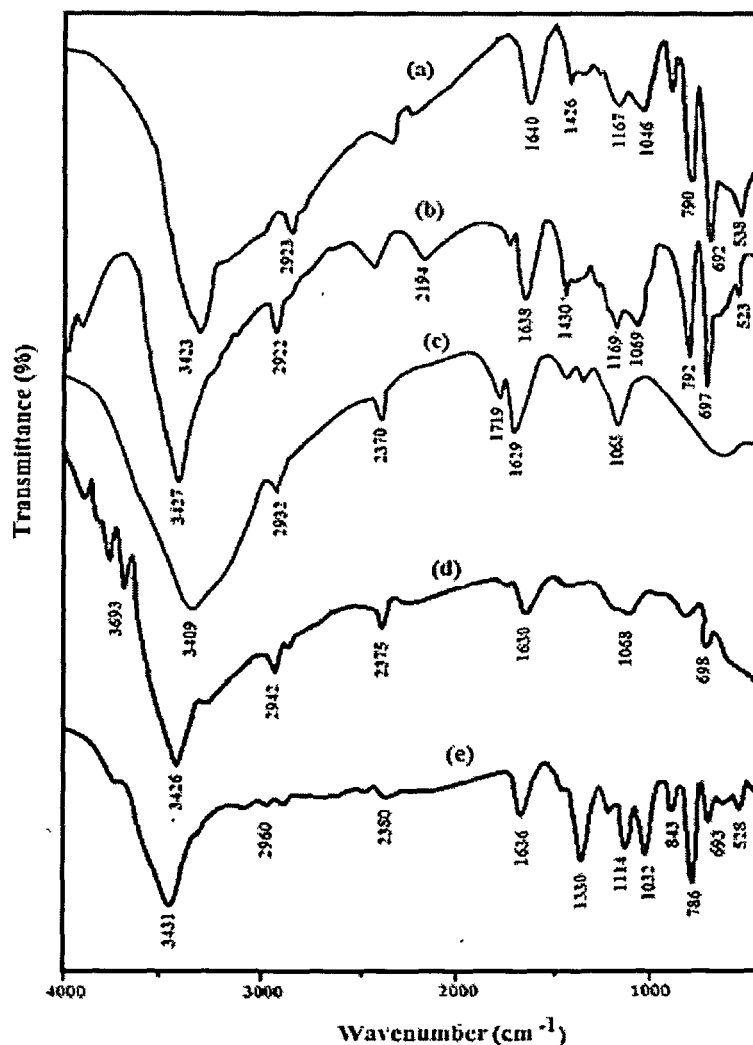
Fig. 2.17 FTIR spectra of (a) PTh, (b) PTh/GO composite and (c) GO, (d) GR and (e) PTh/GR composite.

2.4.2.2 UV-visible analysis

UV-vis spectra of the samples are shown in Fig. 2.18. A characteristic absorption peak of GO was observed at 236 nm.[17] PTh shows a strong band at 260 nm which is attributed to π-π* transition of 2,5-thiophenylene unit.[64] An additional broad band appears at around 435 nm which is related to bipolaron state of PTh. Similar peaks are observed for the PTh/GO composites (Fig. 2.18 (c)-(e)). The peaks at 264-270 nm indicate the π-π interaction between PTh and GO of the composite. Band at around 441-460 nm (2.15-2.01 eV) is also observed which confirms bipolaron state of PTh in the composite. The absorption bands of PTh/GO nanocomposites showed a red

shift in the ranges for π-π* transition and for polaron-bipolaron band transition on increasing GO percentage. This shifting results from the π-π stacking between the polymer chain and the GO sheets. Incorporation of GO extends the conjugation length of PTh chain.
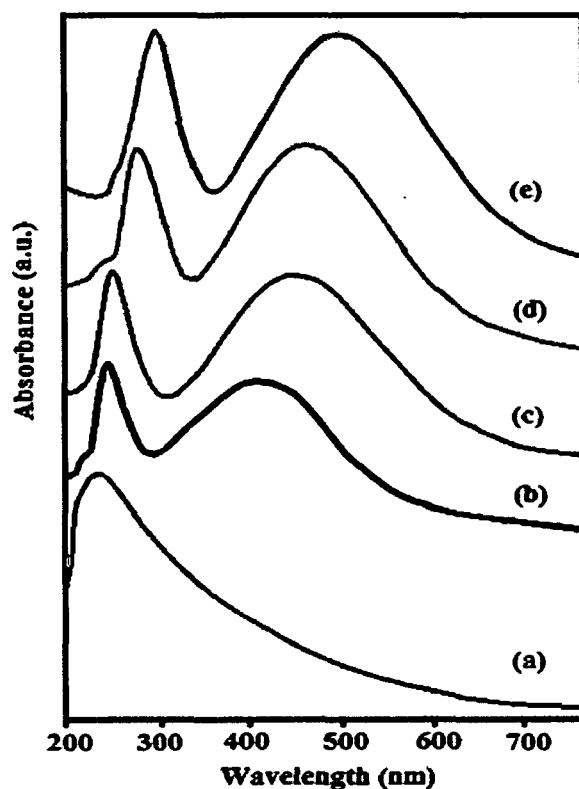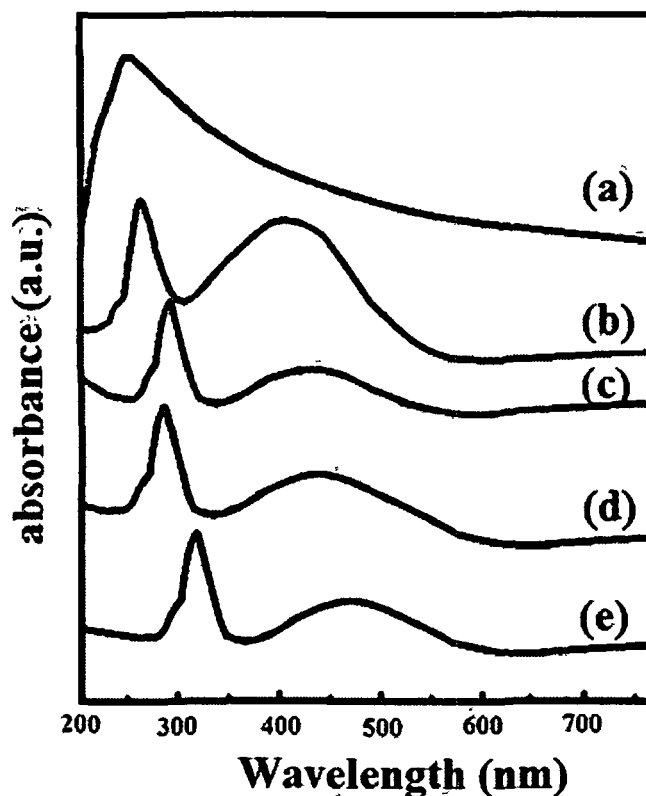

Fig.. 2.18 UV-visible spectra of (a) GO, (b) PTh, (c) PTGO1, (d) PTGO2 and (e) PTGO3 composite.

In the UV spectra of GR, the absorption peak of GO (236 nm) shifts to ~270 nm (Fig. 2.19 (a)). These effects suggest that the electronic conjugation within the carbon framework of the graphene nanocomposites has been restored upon hydrazine reduction. The results are in agreement with the reports presented by Zhao et al.[65] The characteristic red shift of the peaks of PTh/GR composite spectra was observed in the ranges for π-π* transition and n-π* transition which is due to the extended conjugation length of PTh chain on incorporation of GR. This extend of conjugation length of the polymer composite may be attributed to the π-π stacking between the polymer backbone and the GR sheets.

Fig. 2.19 UV-visible spectra of (a) GR, (b) PTh, (c) PTGR1, (d) PTGR2 and (e) PTGR3 composite.

In conjugated polymers, the optical absorption may be attributed to the transition of charge carriers, through a forbidden energy gap. The optical band gaps of the nanocomposites are calculated from the following equation[48] and are listed in Table 2.6.

$$E^{opt}{}_g \text{ (eV)} = 1240/\, \lambda_{edge} \text{ (nm)}\,. \tag{3}$$

where $E^{opt}{}_g$ is the optical band gap and λ_{edge} is the absorption edge. Pure PTh shows a band gap of 2.23 eV. In PTh/GO composites, the band gap is decreased from 2.15 eV to 2.01 eV on increasing GO content. Similarly in PTh/GR composite a decrease in band gaps is observed from 2.13 to 1.96 on increasing GR loading.

**Table 2.6** Electrochemical and optical data of PTh and PTh/GO composite.

aSample	E^{cc} (eV)	λ_{edge} (nm)	E^{opt}(eV)
PTh	2.40	556	2.23
PTGO1	2.23	575	2.15
PTGO2	2.16	593	2.09
PTGO3	2.07	615	2.01
PTGR1	2.06	582	2.13
PTGR2	1.90	610	2.03
PTGR3	0.90	630	1.96

aPTh: polythiophene; PTGO1: 1 wt.% of GO w.r.t. thiophene monomer; PTGR1: 1 wt.% of GR w.r.t thiophene and so on.

2.4.2.3 XRD analysis

The XRD patterns of GO, PTh/GO composite and pure PTh are presented in Fig. 2.20. The X-ray pattern of GO (Fig. 2.20 (c)) shows a strong peak at $2\theta= 11.46°$ corresponding to (001) reflection peak.[29] Pure PTh exhibits a broad diffraction peak at $2\theta= 22°$ indicating the amorphous nature of the polymer (Fig. 2.20 (a)). For the PTh/GO composites, the characteristic broad peak of PTh appeared at $23.5°$ indicating the presence PTh in the composite (Fig. 2.20 (b)). Also a peak appears at $2\theta= 11.6°$ which indicates the presence of GO in the composite. Thus the XRD study exhibits the interactions between GO and PTh. After reduction of GO into GR, one broad reflection peak centered at $2\theta= 24°$ was observed in the XRD pattern of GR. In the PTh/GR composite (Fig. 2.20 (e)), the broad peak of the PTh and the characteristic peak of GR is observed indicating presence of GR in the PTh matrix. However, the peak for GR has been shifted. Thus from the results we can say that GR is well exfoliated in the PTh matrix.
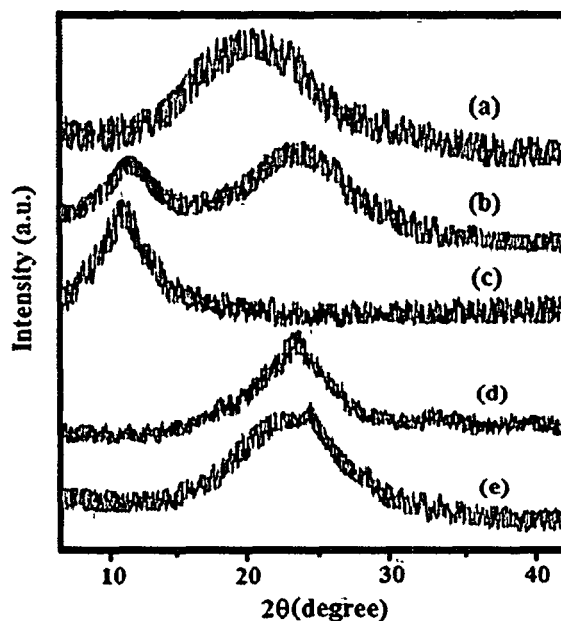
Fig. 2.20 XRD patterns of (a) Pure PTh, (b) PTh/GO composite, (c) GO,
(d) GR and (e) PTh/GR composite.

2.4.2.4 Morphological analysis

The surface morphology of GO, PTh and PTh/GO composite were
investigated using SEM. In the SEM image of GO (Fig. 2.21 (a)) a multilayered sheet
structure is observed which is in accordance with the earlier report.[50] SEM image of
GR shows a layered, wrinkle-like structure (Fig. 2.21 (b)). Pure PTh shows an
granular structure of a few micrometers (Fig. 2.21 (c) and (d)). This granular
morphology vanished and an uneven, flaky morphology is observed in case of
PTh/GO and PTh/GR composites (Fig. 2.21 (e), (f)). The changes in morphology of
the composites from the individual components can be attributed to the successful
polymerization of PTh on the surface of GO and GR sheets. Fig. 2.22 shows the TEM
images of GO, GR, PTh/GO and PTh/GR composite. In the TEM image of GO, a
layered structure with a few micrometers in dimension is observed (Fig. 2.22 (a)).
TEM image of GR shows a 2D layered nanostructure (Fig. 2.22 (b)). In the TEM
images of the PTh/GO and PTh/GR composite (Fig. 2.22 (c), (d)) some spherical
structures of PTh decorated at the surface of the GO and GR sheets are observed
which indicated the formation of the PTh chain on the surface of the GO/GR sheets.
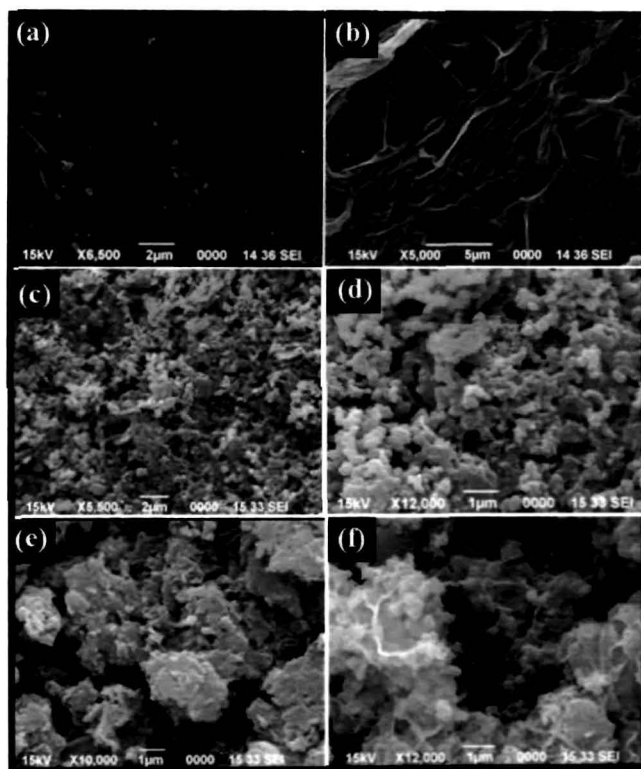
Fig. 2.21 SEM images of (a) GO, (b) GR, (c) PTh at higher magnification, (d) PTh at lower magnification, (e) PTh/GO and (f) PTh/GR composite.
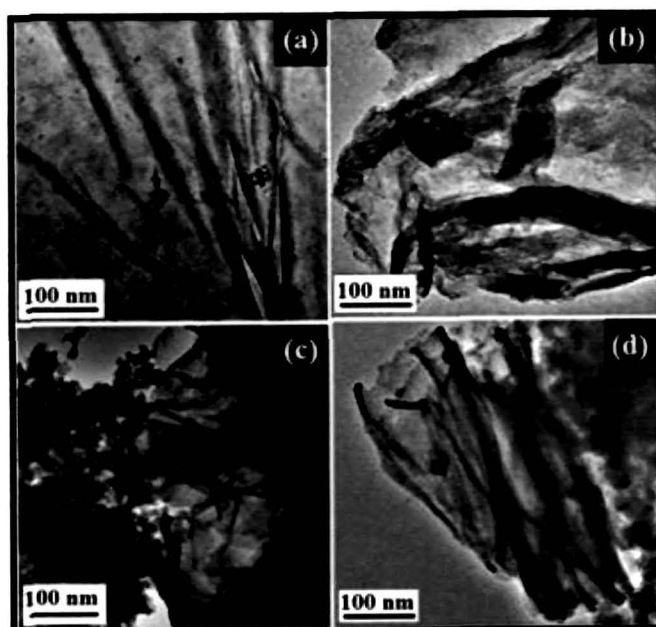
Fig. 2.22 TEM image of (a) GO, (b) GR, (c) PTh/GO and (d) PTh/GR composite.

2.4.2.5 Thermogravimetric analysis

The thermal stability of the samples was investigated by TGA. The TGA curves of GO, PTh and PTh/GO composites are shown in Fig. 2.23 and respective data are summarized in Table 2.7. The TGA curve of pure PTh (Fig. 2.23(a)) shows that PTh is stable upto 200 °C and then major degradation starts at 240 °C which is due to the thermal decomposition of PTh. In the TGA curve of GO major weight loss occurs in the temperature range of 200-300 °C, which is due to the removal of most of the oxygen functionalities (Fig 2.23(e)). In the composites major degradation starts at higher temperatures (248-260 °C) compared to pure PTh. Further it is observed that the weight retention value of the PTh/GO (3 wt.%) composite increases upto 19% on incorporation of GO compared to pure PTh which shows only 4% weight retention value at 600 °C. Thus from the above data, it has been seen that both the decomposition temperature and the residual weight increases on incorporating GO. Hence we can say that by incorporating GO in PTh matrix the thermal stability of the polymer can be increased. The results are in consistent with the earlier reports given by Karim *et al.*[37]
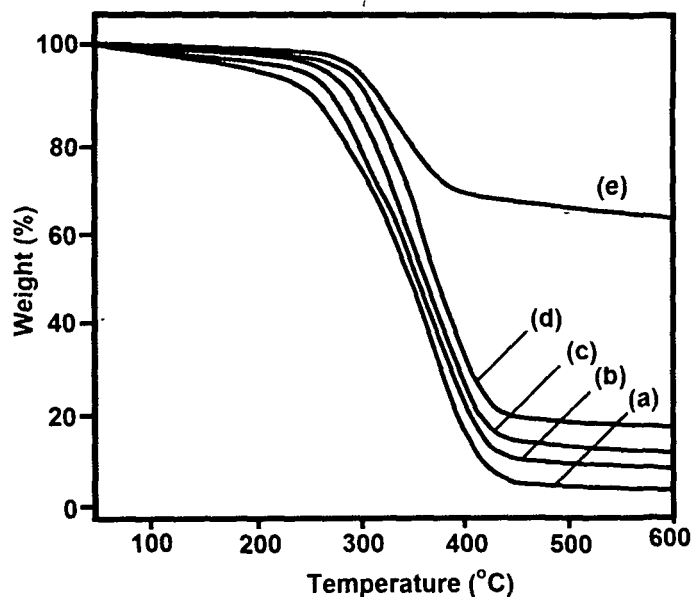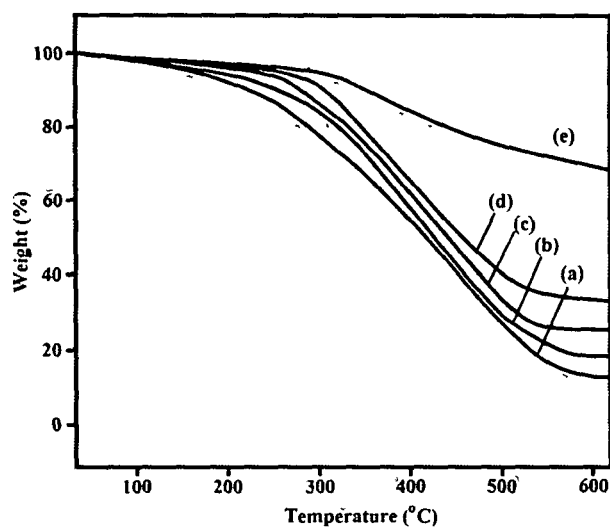

Fig. 2.23 TGA curves of (a) PTh, (b) PThGO1, (c) PThGO2, (d) PThGO3 composite and (e) GO.

Table 2.7 TGA data of PTh, GO and PTh/GO composites

Samples	Major degradation temperature (Td) °C	Weight loss % at temperature				Weight retention (%) at 600°C
		200 °C	300 °C	400 °C	500 °C	
PTh	240	10	15	40	80	4
PThGO1	248	8	13	36	77	11
PThGO2	256	7	12	34	73	17
PThGO3	260	6	10	30	70	19
GO	266	1	25	30	35	60

The TGA curves of pure PTh, GR and PTh/GR composites are shown in Fig. 2.24. Pure PTh shows a major weight loss in the temperature range of 250-500 °C. Only 12% weight retention value of PTh at 600 °C corresponds to the complete degradation of the polymer (Fig. 2.24 (a)). The major degradation starts at higher temperatures in the PTh/GR composites (Fig. 2.24 (b-d)), compared to pure PTh which can be attributed to the decomposition of the PTh and functional groups of GR from the composite. The thermal stability of PTh/GR composite was found to be higher compared to PTh/GO composite. The major degradation started at relatively higher temperature (295 °C) for PTh/GR composite compared to PTh/GO composite (252 °C). Also the weight retention value of the PTh/GR composite was more compared to PTh/GO composite. Thus the TGA results indicate the superior thermal stability of GR-based PTh composite than GO-based PTh composite.

Fig. 2.24   TGA curves of (a) PTh, (b) PThGR1, (c) PThGR2, (d) PThGR3
composite and (e) GR.

Table 2.8 TGA data of PTh, GR and PTh/GR composites

Samples	weight loss % at temperature (°C)				major degradation temperature (Td) °C	weight retention (%) at 600 °C
	200	300	400	500		
PTh	10	20	44	75	250	12
PThGR1	6	15	40	72	255	20
PThGR2	4	10	36	65	268	27
PThGR3	2	8	25	58	295	34
GR	1	10	15	25	310	70

2.4.2.6 Electrical conductivity measurements

The DC electrical conductivities of the samples are measured using a four point probe resistivity measurement system. The conductivity measurements were carried out on pellet shaped samples pressed from powders. The average conductivity values are shown in Table 2.9. Pure PTh shows a conductivity of 5.8×10^{-5} S cm^{-1}. The conductivity of the resulting PTh/GO (3 wt.%) composite, is 2.7×10^{-4} S cm^{-1} at room temperature (25 °C), which is higher than that of the pure PTh. The DC conductivity values of the PTh/GO composites are found to be increased with increasing GO content. The

increase in conductivity may be attributed to the increased electron mobility arising from the π-π stacking between the GO layers and PTh within the composite system. The PTh/GR composites show higher value of conductivity (7.35×10^{-3} S cm^{-1} for 3 wt.% GR composite) compared to PTh/GO composites. This may be due to the incorporation of highly conducting GR sheets (conductivity, 50 S cm^{-1}) which forms an effective percolative conducting bridge inside the composite system.[55] The conductivity values are found to be increased with increasing GR content.

Table 2.9 Electrical conductivity and specific capacitance of PTh, PTh/GO and PTh/GR composites

Sample	Thickness (d, cm)	Conductivity (σ, S cm^{-1})	Specific capacitance (F g^{-1})
PTh	0.3	5.8×10^{-5}	71
PThGO1	0.3	0.8×10^{-4}	84
PThGO2	0.3	1.2×10^{-4}	92
PThGO3	0.3	2.7×10^{-4}	99
PThGR1	0.3	5.3×10^{-4}	156
PThGR2	0.3	4.6×10^{-3}	178
PThGR3	0.3	7.4×10^{-3}	210

2.4.2.7 Electrochemical behavior

(a) Cyclic voltammetry (CV)

CV was performed to study the electrochemical properties of the composites. Fig. 2.25 (a)-(d) shows the CV curves of PTh and PTh/GO composites in 0.1M LiClO$_4$ - acetonitrile solution at the scan rate of 50 mV s^{-1}. Pt wire and Ag/AgCl were used as counter and reference electrode, respectively. It is seen that the CV curves are almost rectangular in shape within the measured potential indicating good redox behavior of the samples. CV curves of PTh/GO composites have large rectangular areas, indicating good electrochemical double-layer capacitances. Also the redox waves shifted to more positive potentials compared to PTh. This is possibly due to the increased conductivity and surface area of the composite on introduction of GO.
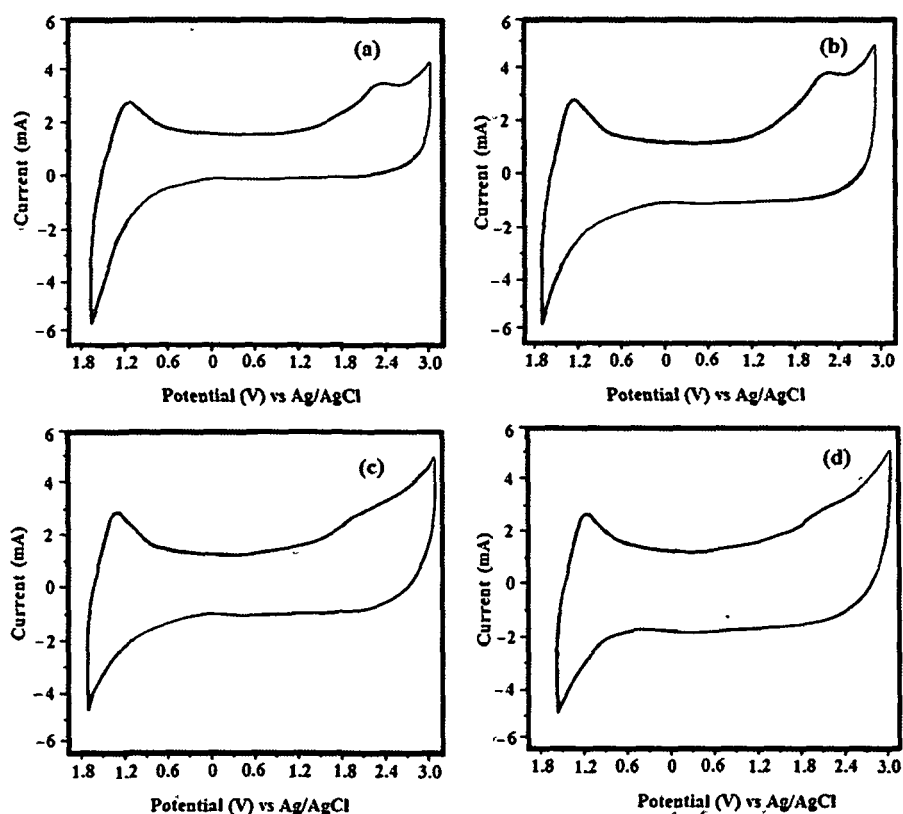
Fig. 2.25 Cyclic voltammogram of (a) PTh, (b) PThGO1, (c) PThGO2 and
(d) PThGO3 composite at a scan rate of 50 mV s^{-1}.

The CV plots of PTh/GR composites are shown in Fig. 2.26. The composites exhibit rectangular CV curves indicating good reversibility and ideal capacitive behaviour of the electrode. Also, the redox waves have shifted to more positive potentials compared to PTh. The area under the CV curves of PTh/GR composites is larger compared to PTh and PTh/GO composites, suggesting the higher capacitance of the PTh/GR composites. Incorporation of highly conducting GR sheets facilitates the charge transfer mechanism and increases the surface area of the PPy/GR composites, resulting in an increase in the capacitances.
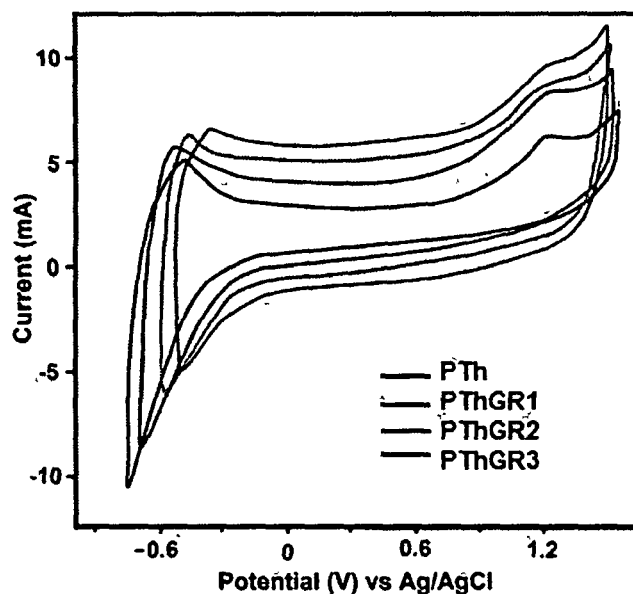
Fig. 2.26 Cyclic voltammogram of (a) PTh, (b) PThGR1, (c) PThGR2 and (d) PThGR3 composite at a scan rate of 50 mV s^{-1}.

We have also determined the electrochemical band gap energies of the samples from CV. The band gap of the samples was calculated by using the following formulae[56]

$$HOMO = - [\varphi_{onset}{}^{ox} + 4.71] \qquad (5)$$

$$LUMO = - [\varphi_{onset}{}^{red} + 4.71] \qquad (6)$$

$$E_{ec}{}^{g} = - (\varphi_{onset}{}^{ox} \quad \varphi_{onset}{}^{red}) \qquad (7)$$

where the units $\varphi_{onset}{}^{ox}$ and $\varphi_{onset}{}^{red}$ are oxidation onset potential and reduction onset potential, respectively and $E_{ec}{}^{g}$ is the electrochemical band gap.

The obtained electrochemical data are summarized in Table 2.6. The electrochemical band-gap for PTh was found to be 2.40 eV. The PTh/GO composites showed lower band gap values (2.33-2.07 eV) compared to pure PTh. The band gap decreases with increased GO content in the composites. A much lower band gap values were obtained for PTh/GR composites (2.06-0.90 eV) than that of PTh/GO composites. Similar to PTh/GO composites, the band gap values decreased with increasing GR loading. The

decrease in band gaps in the composites may be due to the changes in the electronic band structure of PTh/GO and PTh/GR composites which demonstrates a new mid-gap state. The electrochemical band gap actually reveals the formation of charge carriers, while in optical transition no such charge carriers form as the excited state in conjugated polymers may be viewed as a bound exciton. We have compared the optical band gap data with electrochemical band gaps of PTh/GO and PTh/GR composites. In PTh/GO composites, the electrochemical band gaps were found to be higher than that of optical band gaps, whereas in PTh/GR composites the optical band gaps were found to be higher than the electrochemical band gaps. Although optical band gap cannot be directly compared to the electrochemical band gap, we have noticed the same trend of band gaps in both the method.

(b) Cycling stability

The cycling performances of the PTh/GO and PTh/GR composites were estimated by repeating the CV tests for 100th oxidation and reduction cycles at a scan rate of 50 mV s^{-1} (Fig. 2.27). In both the composites, the curves show clear redox peaks for the first cycle and as the cycling increases, the peak shape becomes weaker and broader. However, the redox potentials remained same even upto 100th repeated cycles. This improved cycling stability of the composites is mainly due to the interaction of GO and GR with PTh which restricts the change of network structure during cycling. Thus the composites exhibit a good application potential in capacitors and rechargeable batteries.[28]
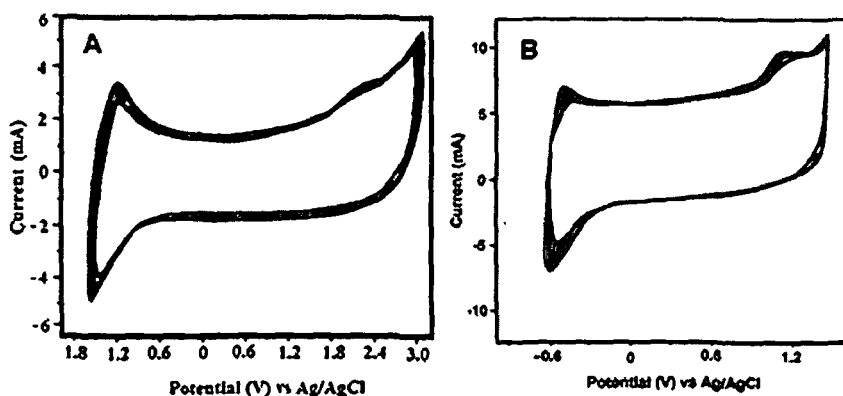
Fig. 2.27 Successive electrochemical cycles of the (A) PThGO3 and (B) PThGR3 composites up to 100th cycles.

(c) Charge capacity

The specific capacitance of PTh and the composites were measured from the cyclic voltammograms (Fig. 2.25 and 2.26) and shown in Table 2.9. Pure PTh showed a specific capacitance value of 71 Fg^{-1}. PTh/GO composite containing 3 wt.% of GO exhibited a higher capacitance value of 99 $F\ g^{-1}$ compared to pure PTh. The specific capacitance of the PTh/GO composites increases with increase in GO content. This is because sheet like structure of GO provides more active surfaces for facile oxidation-reduction reaction. Also, due to the increase in conjugation length (as observed from FTIR and UV-vis results) and conductivity of PTh on incorporation of GO, specific capacitance value in the composites increases. PTh/GR composites showed much higher specific capacitance values (210 $F\ g^{-1}$ for PTGR3 composite) than that of PTh/GO composites. This enhancement in the capacitance values of PTh/GR composites can be attributed to the incorporation of highly conducting GR sheets in the PTh matrix which facilitates the charge transfer within the composite system and increases the surface area of the composite thereby increasing the capacitances.

95

2.5 Conclusions

- This report presents the successful preparation of GR/GO based PPy and PTh composites by liquid/liquid interfacial polymerization. Interfacial polymerization has been found to be an effective method to fabricate GO and GR based polymer composites which have vast application potential in supercapacitors, biosensors and many other fields.

- Both Raman and XRD results indicate the incorporation of GO and GR in the polymer matrix. TEM and SEM study showed uniform distribution of the nanofillers throughout the polymer matrix.

- Both the composites exhibited an improved thermal stability compared to pure polymer.

- Both optical and electrochemical band gaps of the composites were calculated and found to be decreased dramatically on incorporation of GO and GR into the polymer matrix.

- The PPy/GR composites exhibited a higher value of conductivity (2.51-8.45 S cm^{-1}) compared to PPy (0.210 S cm^{-1}) and PPy/GO composites (0.360-0.507 S cm^{-1}), which may be attributed to the high aspect ratio and large specific surface area of GR nanosheets present within the polymer matrix.

- Electrical conductivity of PTh/GR composites was found to be higher (7.4×10^{-3} Scm^{-1} for PTGR3 composite) than that of PPy/GO composite (2.7×10^{-4} S cm^{-1} for PTGO3) and pure PTh (5.8×10^{-5} S cm^{-1}).

- Both the composites showed reversible electrochemical response and a good cycling stability even up to 100th cycles.

- A charging-discharging study also reveals a consistent high capacitance value (260 F g^{-1}) for the PPy/GR composite (3 wt.% of GR loading) at 100 mA g^{-1}. This value is much higher than that of PPy/GO composites which showed maximum capacitance value of only 92.2 F g^{-1} at 100 mV s^{-1} (for 3 wt.% GO loading).

- The specific capacitance of PTh/GR (3 wt.% of GR) composite electrode was evaluated as 210 F g^{-1}, whereas the specific capacitances of PTh/GO composite (3

wt.% of GO) and pure PTh were 99 F g^{-1} and 71 F g^{-1} respectively (at scan rate of 50mV s^{-1}).

- The present work shows that the GR/GO based PPy and PTh composites prepared using the interfacial polymerization method possess great promise for a range of potential applications in batteries and optoelectronic devices. Also this work suggests that the GR based PPy composites have superior thermal stability, electrical and electrochemical properties than that of GO based composites.

REFERENCES

1. Kim, H., et al. Graphene/polymer nanocomposites, *Macromolecules* **43**, 6515-6530, 2010.

2. Potts, J.R., et al. Graphene-based polymer nanocomposites, *Polymer* **52**, 5-25, 2011.

3. Kuilla, T., et al. Recent advances in graphene based polymer composites, *Prog. Polym. Sci.* **35**, 1350-1375, 2010.

4. Liu, N., et al. One-step ionic-liquid-assisted electrochemical synthesis of ionic-liquid-functionalized graphene sheets directly from graphite, *J. Adv. Funct. Mater.* **18**, 1518-1525, 2008.

5. Cassagneau, T., et al. Preparation and characterization of ultrathin films layer-by-layer self-assembled from graphite oxide nanoplatelets and polymers, *Langmuir* **16**, 7318-7324, 2000.

6. Matsuo, Y., et al. Structure and thermal properties of poly(ethylene oxide)-intercalated graphite oxide, *Carbon* **35**, 113-120, 1997.

7. Liu, P., et al. Preparation and characterization of poly(vinyl acetate)-intercalated graphite oxide nanocomposite, *J. Mater. Chem.* **10**, 933-935, 2000.

8. Kotov, N.A., et al. Ultrathin graphite oxide–polyelectrolyte composites prepared by self-assembly: Transition between conductive and non-conductive states, *Adv. Mater.* **8**, 637-641, 1996.

9. Cassagneau, T., & Fendler, J.H., High density rechargeable lithium-ion batteries self-assembled from graphite oxide nanoplatelets and polyelectrolytes, *Adv. Mater.* **10**, 877-881, 1998.

10. Xu, Y., et al. Strong and ductile poly(vinyl alcohol)/graphene oxide composite films with a layered structure, *Carbon* **47**, 3538-3543, 2009.

11. Liu, K., et al. Preparation of polyester/reduced graphene oxide composites via in situ melt polycondensation and simultaneous thermo-reduction of graphene oxide, *J. Mater. Chem.* **21**, 8612-8617, 2011.

12. Zhou, M., et al. Electrochemical sensing and biosensing platform based on chemically reduced graphene oxide, *Anal. Chem.* **81**, 5603-5613, 2009.

13. Yang, W., et al. Carbon nanomaterials in biosensors: should you use nanotubes or graphene, *Angew. Chem. Eng.* **49**, 2114-2138, 2010.

14. Wang, D.W., et al. Fabrication of graphene/polyaniline composite paper via *in situ* anodic electropolymerization for high-performance flexible electrode, *ACS Nano* **3**, 1745-1752, 2009.

15. Wei, T., et al. Mechanical properties of graphite flakes and spherulites measured by nanoindentation, *Carbon* **47**, 2290-2299, 2009.

16. Wang, H., et al. Graphene oxide doped polyaniline for supercapacitors, *Electrochem. Commun.* **11**, 1158-1161, 2009.

17. Wang, H., et al. Effect of graphene oxide on the properties of its composite with polyaniline, *Appl. Mater. Interfaces* **2**, 821-828, 2010.

18. Novoselov, K.S., et al. Electric field effect in atomically thin carbon films, *Science* **306**, 666-669, 2004.

19. Allen, M.J., et al. Honeycomb carbon: a review of graphene, *Chem. Rev.* **110**, 132-145, 2010.

20. Zhu, Y., et al. Graphene and graphene oxide: synthesis, properties and applications, *Adv. Mater.* **22**, 3906-3924, 2010.

21. Mishra, A.K., & Ramaprabhu, S., Functionalized graphene-based nanocomposites for supercapacitor application, *J. Phys. Chem. C* **115**, 14006-14013, 2011.

22. Gomez, H., et al. Graphene-conducting polymer nanocomposite as novel electrode for supercapacitors, *J. Power Sources* **196**, 4102-4108, 2011.

23. Rao, C.N.R., et al. Graphene: the new two-dimensional nanomaterial, *Angew. Chem. Eng.* **48**, 7752-7777, 2009.

24. Wang, S., et al. Thermal expansion of graphene composites, *Macromolecules* **42**, 5251-5255, 2009.

25. Fang, M., et al. Covalent polymer functionalization of graphene nanosheets and mechanical properties of composites, *J. Mater. Chem.* **19**, 7098-7105, 2009.

26. Stankovich, S., et al. Graphene-based composite materials, *Nature* **442**, 282-286, 2006.

27. Wu, T.M., & Lin, S.H., Synthesis, characterization, and electrical properties of polypyrrole/multiwalled carbon nanotube composites, *J. Polym. Sci. Part A: Polym Chem* **44**, 6449-6457, 2006.

28. Zhang, D., et al. Enhanced capacitance and rate capability of graphene/polypyrrole composite as electrode material for supercapacitors, *J. Power Sources* **196**, 5990-5996, 2011.

29. Bose, S., et al. In-situ synthesis and characterization of electrically conductive polypyrrole/graphene nanocomposites, *Polymer* **51**, 5921-5928, 2010.

30. Liu, A., Electrochemical deposition of polypyrrole/sulfonated graphene composite films, *J. Phys. Chem. C* **114**, 22783-22789, 2010.

31. Gu, Z., et al. Synthesis and characterization of polypyrrole/graphite oxide composite by *in situ* emulsion polymerization, *J. Polym. Sci. Part B Polym. Phys.* **48**, 1329-1335, 2010.

32. Sakurai, Y., et al. Novel array-type gas sensors using conducting polymers, and their performance for gas identification, *Sens. Actuators B* **83**, 270-274, 2002.

33. Otsuka, Y., et al. Photoinduced formation of polythiophene/TiO_2 nanohybrid heterojunction films for solar cell applications, *J. Phys. Chem. C* **112**, 4767-4772, 2008.

34. Lu, Q., & Zhou, Y., Synthesis of mesoporous polythiophene/MnO_2 nanocomposite and its enhanced pseudocapacitive, *J. Power Sources* **196**, 4088-4094, 2011.

35. Uygun, A., et al. Polythiophene/SiO_2 nanocomposites prepared in the presence of surfactants and their application to glucose biosensing, *Synth. Met.* **159**, 2022-2028, 2009.

36. Wang, S.H., et al. Inverted heterojunction solar cells incorporating fullerene/polythiophene composite core/shell nanorod arrays, *Nanotechnology* **21**, 145203-145211, 2010.

37. Karim, M.R., et al. Synthesis and characterization of conducting polythiophene/carbon nanotubes composites, *J. Polym. Sci. Part A: Polym. Chem.* **44**, 5283-5290, 2006.

38. Wang, H.S., et al. Ordered polythiophene/fullerene composite core–shell nanorod arrays for solar cell applications, *Nanotechnology* **20**, 75201-75206, 2009.

39. Zhao, J., et al. Preparation and characterization of an electromagnetic material: The graphene nanosheet/polythiophene composite, *Synth. Met.* **181**, 110-116, 2013.

40. Wang, S., et al. Graphene oxide-polythiophene hybrid with broad-band absorption and photocatalytic properties, *J. Phys. Chem. Lett.* **3**, 2332-2336, 2012.

41. Dallas, P., et al. Interfacial polymerization of pyrrole and in situ synthesis of polypyrrole/silver nanocomposites, *Polymer* **48**, 2007-2013, 2007.

42. Hummers, W.S., & Jr. Offeman, R.E. Preparation of graphitic oxide, *J. Am. Chem. Soc.* **80**, 1339-1939, 1958.

43. Sahoo, S., et al. Electrochemical characterization of in situ polypyrrole coated graphene nanocomposites, *Synth. Met.* **161**, 1713-1719, 2011.

44. Konwer, S., et al. Studies on conducting polypyrrole/graphene oxide composites as supercapacitor electrode, *J. Electron. Mater.* **40**, 2248-2255, 2011.

45. Bissessur, R., et al. Intercalation of polypyrrole into graphite oxide, *Synth. Met.* **156**, 1023-1027, 2006.

46. Konwer, S., et al. Preparation and optical/electrical/electrochemical properties of expanded graphite-filled polypyrrole nanocomposite, *Mater. Chem. Phys.* **128**, 283-290, 2011.

47. Deng, J., et al. Magnetic and conducting Fe_3O_4-polypyrrole nanoparticles with core-shell structure, *Polym. Int.* **52**, 1182-1187, 2003.

48. Tsai, F.C., et al. New thiophene-linked conjugated poly(azomethine)s: theoretical electronic structure, synthesis and properties, *Macromolecules* **38**, 1958-1966, 2005.

49. Kudin, K.N., et al. Raman spectra of graphite oxide and functionalized graphene sheets, *Nano Lett.* **8**, 36-41, 2008.

50. Zhang, L.L., et al. Layered graphene oxide nanostructures with sandwiched conducting polymers as supercapacitor electrodes, *Langmuir* **26**, 17624-17628, 2010.

51. Hao, Q., et al. Morphology-controlled fabrication of sulfonate graphene/polyaniline nanocomposites by liquid/liquid interfacial polymerization and investigation of their electrochemical properties, *Nano Res.* **4**, 323-333, 2011.

52. Konwer, S., et al. Studies on conducting polypyrrole/graphene oxide composites as supercapacitor electrode, *J. Electron. Mater.* **40**, 2248-2255, 2011.

53. Deepa, M., & Ahmad, S. Polypyrrole films electropolymerized from ionic liquids and in a traditional liquid electrolyte: A comparison of morphology and electro-optical properties, *Eur. Polym. J.* **44**, 3288-3299, 2008.

54. Tsang, S.C., et al. Simple chemical method of opening and filling carbon nanotubes, *Nature* **372**, 159-162, 1994.

55. Zengin, H., et al. Carbon nanotube doped polyaniline, *J. Adv. Mater.* **14**, 1480-1484, 2002.

56. Pokhrel, B., & Dolui, S.K. Synthesis and characterization of 1, 1'-bis-2-naphthol chromophore containing polyurethanes and their electrochemical and photoluminescence, *J. Polym. Mater.* **26**, 417-501, 2009.

57. Ghanbari, K., et al. Synthesis of polyaniline/graphite composite as a cathode of Zn-polyaniline rechargeable battery, *J. Power Sources* **170**, 513-517, 2007.

58. Biswas, S. & Drzal, L.T. Multilayered nanoarchitecture of graphene nanosheets and polypyrrole nanowires for high performance supercapacitor electrodes. *Chem. Mater.* **22**, 5667-5671, 2010.

59. Bose, S., et al. Electrochemical performance of a graphene–polypyrrole nanocomposite as a supercapacitor electrode, *Nanotechnology* **22**, 295202, 2011.

60. Davies, A., et al. Graphene-based flexible supercapacitors: pulse-electropolymerization of polypyrrole on free-standing graphene films, *J. Phys. Chem. C* **15**, 17612-17620, 2011.

61. Gok, A., et al. Synthesis and characterization polythiophenes prepared in the presence of surfactants, *Synth. Met.* **157**, 23-29, 2007.

62. Gao, H.X., et al. Aqueous/ionic liquid interfacial polymerization for preparing polyaniline nanoparticles, *Polymer* **45**, 3017-3024, 2004.

63. Jeong, H.K., et al. X-ray absorption spectroscopy of graphite oxide, *Europhys. Lett.* **82**, 67004-6708, 2008.

64. Li, X.G., et al. Interfacial synthesis and widely controllable conductivity of polythiophene microparticles, *J. Phys. Chem. B* **113**, 9718-9727, 2009.

65. Zhao, X., et al. Enhanced mechanical properties of graphene-based poly (vinyl alcohol) composites, *Macromolecules* **43**, 2357-2363, 2010.

CHAPTER 3

Graphene oxide (GO) and graphene (GR) based polyester (PE) resin composites with improved mechanical strength
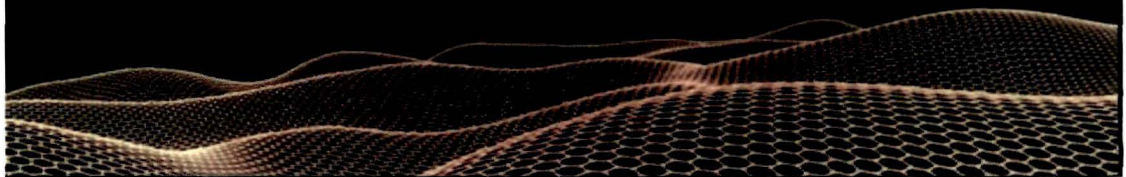
GRAPHICAL ABSTRACT
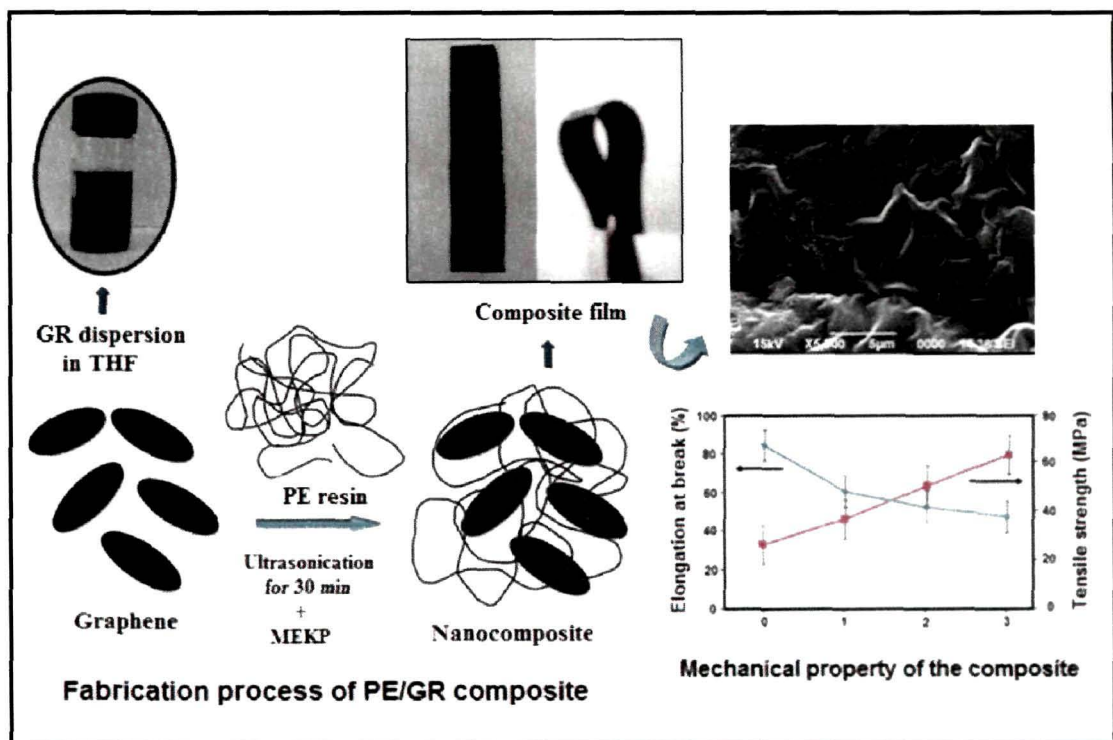
Graphene oxide (GO) and graphene (GR) based polyester (PE) resin composites with improved mechanical strength

3.1 Inroduction

Recently, most of the scientific researchers have focused on nanotechnology and nanomaterials. Nanomaterials exhibit superior properties, as compared to other conventional micro or macro sized analogues. To get improved properties in nanocomposites, layered materials of natural origin like montmorillonite type of layered silicate compounds or synthetic clay have been widely used for decades. But the electrical and thermal conductivity of clay minerals are quite poor. To overcome these drawbacks, carbon-based nanofillers such as carbon black, expanded graphite and carbon nanotube (CNT) have been introduced in the preparation of polymer nanocomposites.[1]

Graphene oxide (GO), a single sheet of graphite oxide bearing oxygen functional groups on their basal planes and edges is found to be a promising filler in polymer matrices.[2,3] GO sheets consisting of covalently attached oxygen-containing groups such as hydroxyl, epoxy, carbonyl and carboxyl groups can alter the van der Waals interactions significantly and facilitate its dispersion in solvent as well as in the polymeric matrix. GO can be prepared in large scales from low-cost natural graphite which is an easily available material. The oxygen-containing groups of GO impart strong interaction with polar molecules or polymers to form GO intercalated or exfoliated composites. Similarly, graphene (GR) is considered as promising versatile nanofiller due to its extraordinarily high electrical and thermal conductivities, great mechanical strength and low manufacturing cost. GO/GR based nanocomposites have attracted enormous interest due to its wide variety of applications in the areas of materials science and engineering.[4-6] Several GO and GR based polymer composites have been developed till date and the mechanical, thermal and electrical properties of these composites are found to be improved as reported.[7-10]

Polyester (PE) resin is a thermosetting polymer which is widely used in various industries such as coating, construction, transportation, storage tanks and piping. PE is also commonly used as matrix material, particularly with glass fiber reinforcement. It is an economic and chemically resistant material which has high dimensional stability and low moisture absorption. The disadvantages of these thermosetting resins are that they show significantly higher cure shrinkage, as compared to epoxy resins. Also tensile strength and stiffness of the polyester resin are lower than those of epoxy resin. To get improved properties in the PE resin composites, different fillers like clay, layered silicates, carbon fiber and CNTs have been used till date.[11-13] Bharadwaj et al.[14] prepared crosslinked polyester-clay nanocomposite by dispersing organically modified montmorillonite. The composite showed good thermal, mechanical and rheological behavior. Vilcakova et al.[15] investigated the electrical conductivity of composites of PE resin filled with short carbon fibers and the composites showed a very low percolation threshold (at 0.7-0.8 vol.% of the filler). Seyhan et al.[16] prepared CNT/unsaturated thermoset PE nanocomposites using 3-roll mill and sonication techniques. The CNT/PE blend exhibited a shear thinning behavior, while PE resin blends act as a Newtonian fluid. Nanotubes with amine functional groups showed superior tensile strength, as compared to those with untreated CNTs. Battisti et al.[17] developed electrically conductive nanocomposites based on MWCNT in an unsaturated PE matrix. The nanocomposite showed a higher value of conductivity, with percolation threshold at 0.026 wt.% loading of nanotubes.

GO and GR are preferred over other expensive fillers like CNT due to their higher aspect ratio, extraordinary mechanical and thermal properties. They have great potential to improve the properties of low cost resins at very low filler content. Wang et al.[18] studied the curing dynamics and network formation of cyanate ester resin/GO nanocomposites by means of differential scanning calorimetry (DSC). The incorporation of GO into the resin showed a strong catalytic effect on the cure of the resin and addition of 4 wt.% GO resulted in the decrease of curing temperature significantly at about 97°C. Yu et al.[19] prepared epoxy/GO composites and got improved thermal conductivity, elastic modulus and tensile strength. Liu et al.[20] reported a novel route to fabricate PE/GR composites via simultaneous dispersion and

thermo-reduction of GO during in-situ melt polycondensation. The composite showed a significant improvement in tensile strength and elongation at break.

However, to the best of our knowledge only few works have been reported in the literature based on GO and GR filled PE resin composite. Therefore in our present investigation we have used GO and GR as fillers in the PE resin matrix to improve mechanical strength, thermal stability, as well as to introduce new characteristic like electrical conductivity of the resin at very low filler content. In this work we have reported preparation of GO and GR based PE resin composite by dispersing GO/GR in PE resin and subsequently crosslinked using methyl ethyl ketone peroxide (MEKP) catalyst at different GO concentration. Our work aims at obtaining a good dispersion of GO/GR sheets within the polymer matrix as well as achieving good improvement in thermal and mechanical properties. GR has been found to have good antibacterial activity towards microorganisms. Hu et al.[21] reported the antibacterial activity of water dispersible GO and GR nanosheets. They found that such GR-based nanomaterials can effectively inhibit the growth of Escherichia coli bacteria while showing minimal cytotoxicity. The antibacterial activity of the PE/GR nanocomposite was also evaluated against a number of bacterial strains.

3.2 Experimental

3.2.1 Materials

PE resin and hardener MEKP were of commercial grade and used as received. Graphite powder, concentrated sulfuric acid (98%), sodium nitrate, potassium permanganate, 30% H_2O_2 solution, hydrochloric acid, acetone, N,N-dimethylformamide (DMF) and hydrazine monohydrate were of reagent grade and purchased from Merck. All the reagents were used without further purification. GO and GR is prepared from natural graphite using modified Hummers method as described in Chapter 2.

3.2.2 Preparation of PE/GO nanocomposites

The required amount of GO was dispersed in minimum amount of THF (solvent) by ultrasonication for 1 hr. Then required amount of PE resin was introduced into the above dispersion and mixed under vigorous mechanical stirring followed by ultrasonication for 30 min. The mixture was then degassed for about 20 min under vacuum until it was completely bubble free. Afterwards, 4% of the hardener (MEKP) with respect to PE resin was added into the mixture and the mixture was cast on teflon plates and dried under vacuum in desiccators for overnight at room temperature. Then they were allowed to cure at 120°C for further study.

3.2.3 Preparation of PE/GR nanocomposites

PE/GR composites of different weight percentage of GR to PE resin (1-3 wt.%) were prepared as follows: The required amount of GR was dispersed in a minimum amount of THF (solvent) by ultrasonication for 1 h. Then required amount of PE resin was introduced into the above dispersion and mixed under vigorous mechanical stirring followed by ultrasonication for 30 min. The mixture was then degassed for about 20 min under vacuum until it was completely bubble free. Afterwards, 4% of the hardener (MEKP) with respect to PE resin was added into the mixture and the mixture was cast on teflon plates and dried under vacuum in desiccators for overnight at room temperature. After that the composite films were cured at 120 °C. Compositions of nanocomposites are given in Table 3.1.

Table 3.1: Composition of PE resin/GO and PE resin/GR nanocomposites

[a]Sample particulars	PE resin (wt. in gm)	MEKP (wt.%)	GR (wt. %)
PE	3	4	0
PE/GO1	3	4	1
PE/GO2	3	4	2
PE/GO3	3	4	3
PE/GR1	3	4	1
PE/GR2	3	4	2
PE/GR3	3	4	3

[a]PE: polyester resin; PE/GO1:1 wt.% of GO w.r. to PE; PE/GO2: 2 wt.% of GO w.r.to PE; GR: graphene; PE/GR1: 1 wt.% of GR w.r.to PE resin and so on.

3.3 Characterization

Fourier transform infrared (FTIR) spectra were recorded using a Nicolet Impact 410 spectrophotometer at room temperature, over a frequency range of 500-4000 cm⁻

The samples were crushed well and then examined in KBr pellets. The X-ray diffraction (XRD) study was carried out at room temperature (25 °C) using a Rigaku X-ray diffractometer (Miniflex, UK) with Cu Ka radiation (k = 0.15418 nm) at 30 kV and 15 mA with a scanning rate of 0.05 h/s in the range of $2\theta = (10°-70°)$. The surface morphology of the composites was observed by scanning electron microscope (SEM) of model JSM-6390LV, JEOL, Japan at an accelerating voltage of 5-15 kV. The surface of the sample was coated with platinum before SEM analysis. Transmission electron microscope (TEM) measurement was carried out by a PHILIPS CM 200 microscope at 200 kV. The TEM sample was prepared by dispensing a small amount of dry powder in ethanol. Then, one drop of the suspension was dropped on 300 mesh copper TEM grids covered with thin amorphous carbon films. Atomic force microscopy (AFM) observation was performed on the DI Multimode V in tapping-mode. To study the thermal degradation of the samples, thermogravimetric analysis (TGA) was performed using Shimazdu TGA 50 thermal analyzer, Japan from temperature range 25-700 °C with a heating rate of 10 °C min⁻¹ under the nitrogen flow rate of 30 mL min⁻¹. Differential scanning calorimetric (DSC) analysis of the samples was done using Shimadzu DSC-60. The analysis was run in the presence of nitrogen gas at a scanning speed 10 °C/min in the temperature range of 0-300 °C. For measurement of the mechanical properties, the composite films were cut to a width of 10 mm and a thickness of 3 mm. The tensile strength measurements were conducted with a Zwick Z010 (Germany) universal testing machine (UTM) with a 10-kN load cell and at jaw separation speed of 50 mm/min at room temperature (25 °C). Measurements of electrical conductivities of the samples were performed using Keithley 2000 (Keithley Instruments Inc., USA) instrument. The resistivity of the samples was measured in a four-point probe unit using the following equation:[22]

$$\text{Resistivity } (\rho, \text{ ohm-cm}) = (V/I)\ 2\pi d \qquad (1)$$

$$\text{Conductivity } (\sigma, \text{ S cm}^{-1}) = 1/\rho \qquad (2)$$

where V is the applied voltage, I is the measured current through the sample and d is the distance between the probes.

3.4 Antimicrobial activity test

The well diffusion technique was used in the present investigation. 200μl of the log phase culture of the test microbes (10^{-7}-10^{-8}) cell as per McFarland standard) which includes *Staphylococcus aureus* (ATCC 11632), *Bacillus subtilis* (ATCC 11774), *Escherichia coli* (MTCC 40), *Pseudomonas aeruginosa* (MTCC 7812) and *Klebsilla pneumoniae* (ATCC10031) were seeded on the surface of the Muller Hinton agar medium, using a micropipette and spread over the medium uniformly using a sterile glass spreader. Further, with the help of a sterile cork borer three wells, each with a diameter of 6 mm were made on Muller Hinton agar (MHA) plate. Samples were dissolved in sterilized dimethyl sulfoxide (DMSO) (10%, v/v) and introduced into each of the wells. Streptomycin sulfate (1mg/mL) was taken as a positive control. The culture plates were incubated at 37±2 °C for 24 h. The observed zones of inhibition were measured using transparent metric ruler. The experiment was done thrice and the mean values were determined.

3.5 Results and discussion

GO and GR based PE resin composite films at different GO/GR concentration were prepared by dispersing the nanofillers in polyester resin and subsequently crosslinked using MEKP catalyst at different GO/GR concentration. A 3 mm-thick smooth, uniform and flexible composite film containing 3 wt.% GO is shown in Figure 3.1. The synthetic process of PE/GR composite is illustrated in Fig. 3.2.
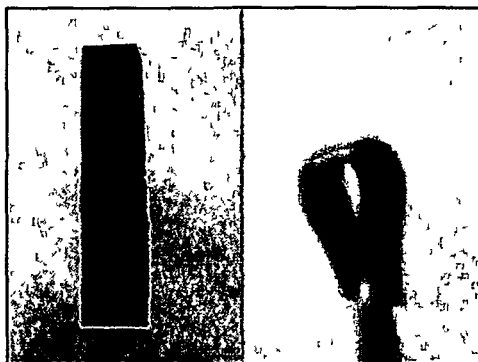
Fig. 3.1 Photograph of a PE/GO (3 wt.%) composite film.
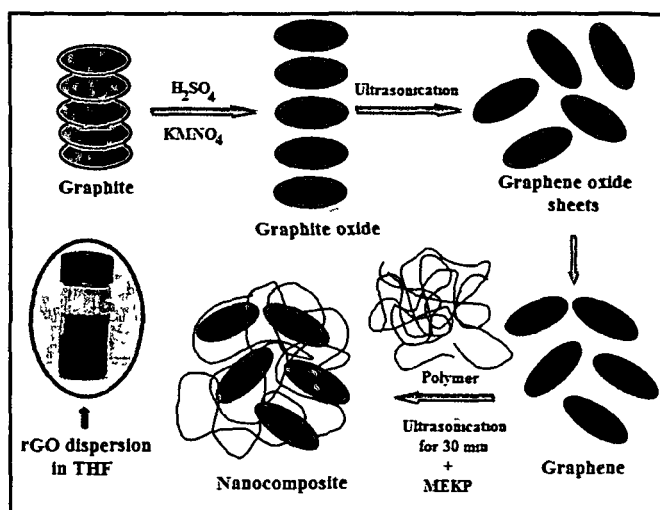

Fig. 3.2 Fabrication process of PE/GR composite.

3.5.1 FTIR study

FTIR spectra of pure PE resin, GO, GR and PE/GR composite are represented in Fig. 3.3 (a). In the FTIR spectrum of GO, the broad peak at 3409 cm^{-1} and a peak at 1719 cm^{-1} can be assigned to O-H stretching vibration and the carbonyl (C=O) stretching respectively. The peaks at 1370 and 1250 cm^{-1} represent the C-O-C and C-OH stretching vibration.[23] The peak near 1065 cm^{-1} represents C-O stretching vibrations which confirm the presence of the epoxide groups in the GO layers. In the FTIR spectrum of GR (3.3 (b)), a broad peak appears at 3426 cm^{-1} corresponding to O-H stretching vibration which is due to the absorption of moisture by the GR sheets. The peaks at 2850 and 2915 cm^{-1} corresponds to aromatic C-H stretching vibration.[24]

Upon reduction of GO, the absorption bands at 1719, 1370, 1250 and 1060 cm^{-1} decreased indicating successful reduction of GO into GR. The PE resin film shows important characteristic absorption bands at 1732 cm^{-1} for carbonyl group (C=O), 3428 cm^{-1} for O-H stretching and 1629 cm^{-1} for aromatic C=C stretching. The peaks at 1166 cm^{-1} and 1263 cm^{-1} band appears for C-O-C stretching vibrations attached with aliphatic and aromatic moiety. From the FTIR spectrum of PE/GO composite (Fig. 3.3 (c)), it is observed that the absorption peaks are almost similar to pure PE resin except that the carbonyl stretching vibration is shifted to lower frequencies (1720 cm^{-1}) than the pristine polyester. The shifting of the peaks indicates the interactions of the PE segments (−COOH and −OH) with GO through H-bonding or other polar-polar interactions. FTIR spectrum of PE/GR composite shows similar absorption peaks to pure PE resin. However some peaks have shifted to lower frequencies than the pristine PE. The shifting of the peaks indicates the interactions of the PE segments (−COOH and −OH) with the remaining oxygen functional groups of GR through H-bonding or other polar-polar interactions. Thus from the FTIR results we can say that both GO and GR have been successfully incorporated in the polymer matrix.
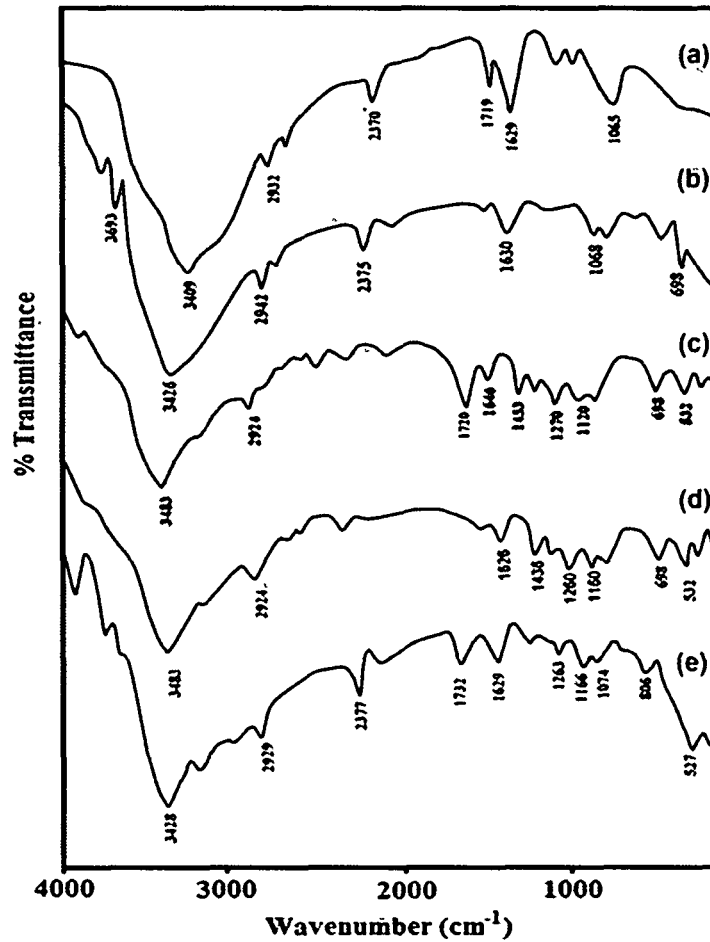
Fig. 3.3 FTIR spectra of (a) GO, (b) GR, (c) PE/GO, (d) PE/GR composite and
(e) PE resin.

3.5.2 XRD analysis

The X-ray analysis was used to determine the structure and crystallinity of polymer matrices. The XRD patterns of GO, GR, pristine PE resin and its composites are given in Figure 3.4. The X-ray pattern of GO (Fig. 3.4 (a)) displays the presence of a strong peak at $2\theta = 11.45°$ corresponds to (001) reflection peak.[3,22] In GR, the peak at $11.45°$ disappears and a broader diffraction peak at $2\theta = 24°$ is observed which can be correlated to an interlayer spacing of 0.36 nm in the graphene sample (Fig. 3.4 (b)). This indicates the successful reduction of GO to GR. From the Fig. 3.4 (e) it can be seen that polyester resin exhibits a weak and a broad diffraction peak at $25.5°$ which indicates that the resin is amorphous in nature. The XRD pattern of PE/GO

composite (3 wt.%) exhibits peak for both PE resin and GO in the angular range of the study (Fig. 3.4 (c)). However, the diffraction peak of GO becomes negligible in the nanocomposite which can be attributed to the exfoliation and homogeneous dispersion of GO in the polyester matrix. The PE/GR composite (3 wt.%) exhibits a weaker diffraction peak compared to the neat resin indicating strong interaction between the polymer chains and the filler (Fig. 3.4 (d)). The diffraction peak of GR disappears in the nanocomposite indicating exfoliation and homogeneous dispersion of GR in the PE matrix.[25]
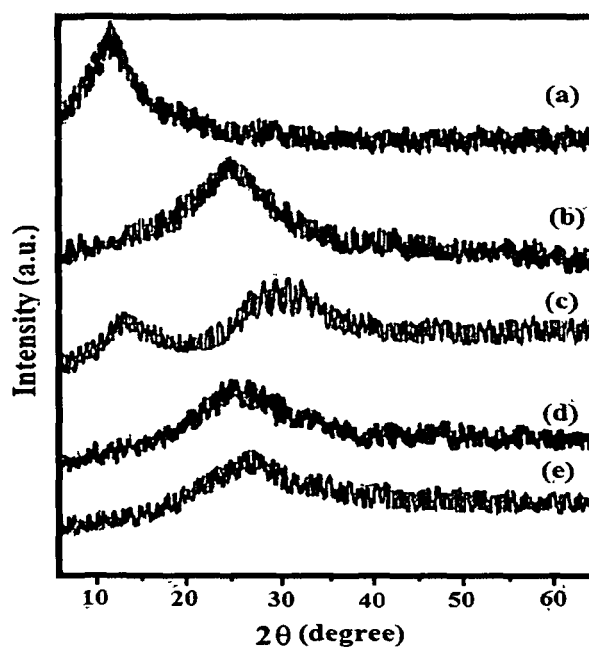
Fig. 3.4 XRD spectra of (a) GO, (b) GR, (c) PE/GO composite, (d) PE/GR composite and (e) PE resin.

3.5.3 Morphological studies

The surface characteristic of the composites was investigated using scanning electron microscope. A layered, wrinkled structure of individual GO sheets with a lateral dimension of few micrometers is observed in the SEM and TEM images of GO (Fig. 3.5 (a) and (b)). In the SEM image of PE resin a smooth surface appears. SEM image of the composite shows a rough, layered surface which is totally different from that of pure PE resin (Fig. 3.5 (d)). Appearance of this layered structure in the composites results from the uniform dispersion of expanding GO layers in the

polymer matrix. Figure 3.5 (e) shows a SEM image of the cross-section of the PE/GO with a loading of 3 wt.% GO. The image shows well dispersion of GO within the polymer matrix. It also demonstrates the random dispersion of GO in the polymer matrix with a few restacks which might affect the improvement in mechanical property. Thus from the morphological study of the surfaces it can be concluded that GO has been successfully incorporated in the PE resin matrix.

In the SEM of GR a layered, wrinkle-like structure is observed (Fig. 3.6 (a)). The TEM image of GR (Fig. 3.6 (e)) shows a crumpled and agglomerated sheet like structure with hundreds of nanometers. The wrinkled structure observed in the TEM image of GR sheets is due to the rapid removal of intercalated functional groups in graphitic oxide during exfoliation. SEM image of the composite (Fig. 3.6 (c)) displays a rough, layered structure compared to the smooth surface of the neat PE resin (Fig. 3.6 (b)). Appearance of this layered structure in the composites results from the uniform dispersion of GR sheets in the polymer matrix and the strong interaction between remaining oxygen functional groups. Fig. 3.6 (d) shows a fractured surface of the PE/GR (3 wt.%) composite film. The image reveals the random dispersion of GR sheets in the polymer matrix with a few restacking which may affect the mechanical and other properties of the composite. Fig. 3.7 shows the Energy-dispersive X-ray (EDX) spectra of GO and GR. GO exhibits oxygen content of 45 atom%. The atomic ratio of carbon to oxygen in GO was found to be 1.25. After reduction, the atomic ratio of carbon to oxygen was 9, as shown in the EDX spectra of GR. Only 15% oxygen content remained in the GR which indicates successful reduction of the GO.

The dispersion of GO sheets in the matrix was investigated by tapping mode AFM. Fig. 3.8 shows topology of surface of the pristine PE resin and PE/GO (3 wt.%) composite. The surface of neat resin appears very smooth which is similar to the SEM analysis. The average roughness of the surface was found to be around 0.01 μm. On the other hand, the composite shows a rough surface which is consistent with SEM observations. The average roughness of the composite surface was increased to 0.1 μm. Moreover, no significant thickness variations were observed in the PE/GO composite film which indicates the uniform distribution of GO in the polyester matrix.
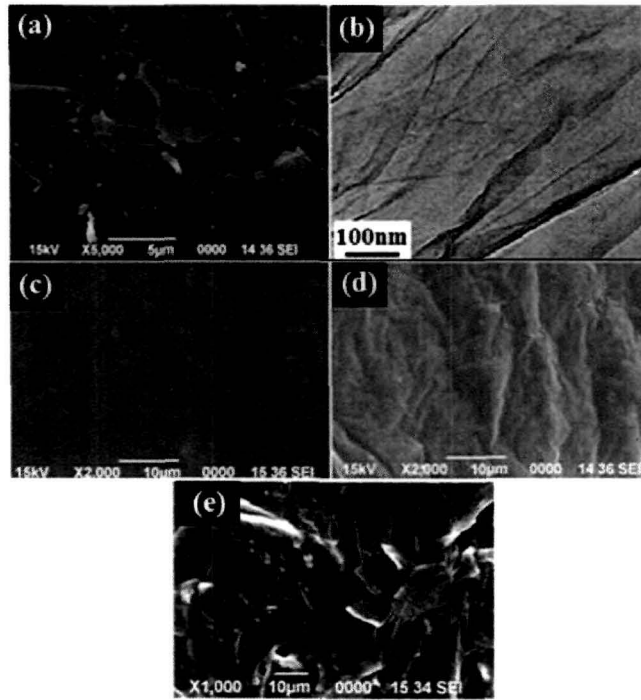
Fig. 3.5 (a) SEM image of GO, (b) TEM image of GO; SEM images of (c) PE resin, (d) PE/GO composite (3 wt.%) and (e) cross section of the composite.
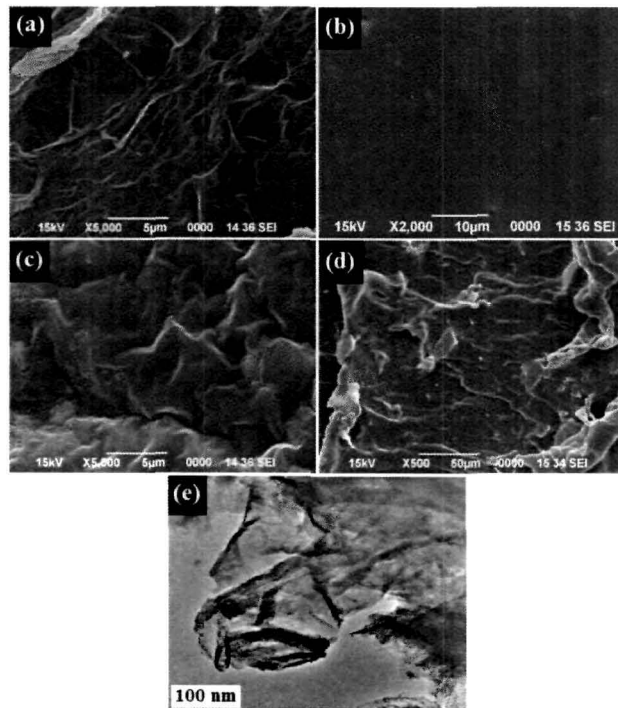
Fig. 3.6 SEM images of (a) GR, (b) PE resin and (c) PE/GR composite (3 wt.%), (d) SEM image of cross section of the composite, (e) TEM image of GR.
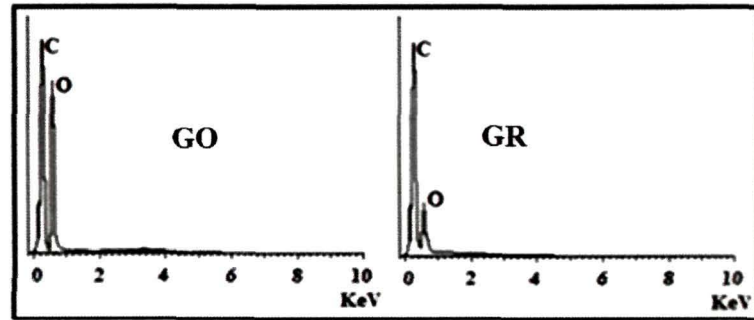
114

Fig. 3.7 EDX spectra of GO and GR

The dispersion of GO sheets in the matrix was investigated by tapping mode AFM. Fig. 3.8 shows topology of surface of the pristine PE resin and PE/GO (3 wt.%) composite. The surface of neat resin appears very smooth which is similar to the SEM analysis. The average roughness of the surface was found to be around 0.01 μm. On the other hand, the composite shows a rough surface which is consistent with SEM observations. The average roughness of the composite surface was increased to 0.1 μm. Moreover, no significant thickness variations were observed in the PE/GO composite film which indicates the uniform distribution of GO in the polyester matrix.
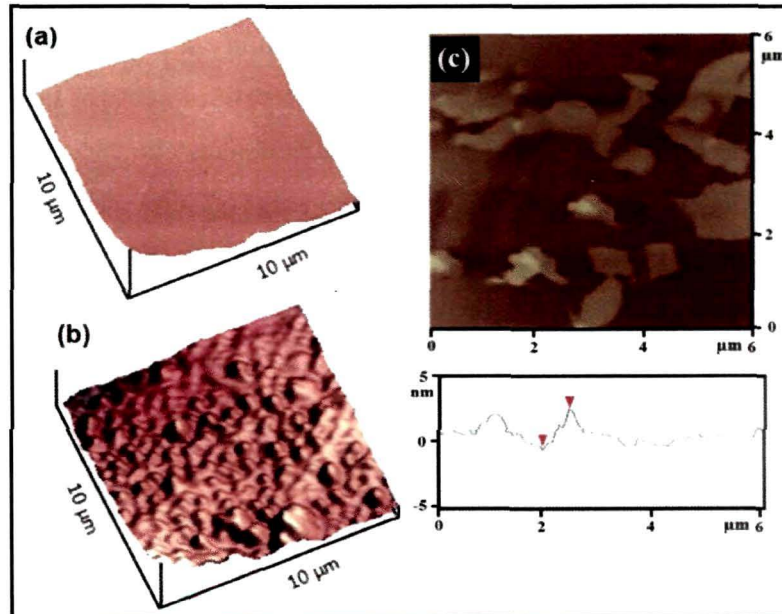

Fig. 3.8 Tapping mode AFM images of (a) PE resin (b) PE/GO (3 wt. %) composite and (c) GR.

AFM is also used to measure the thickness of the GR sheets. Fig. 3.8 (c) shows a typical tapping-mode AFM image of GR sheets deposited onto a mica substrate. It revealed that the average thickness of the GR sheets was around 4 nm, indicating well exfoliated nanosheets.

3.5.4 Thermal properties

The effect of GO on the thermal degradation of polyester resin and its composites were studied by TGA. TGA curve for PE resin, PE/GO composite and GO are shown in Fig. 3.9 with respective data are being summarized in Table 2. From the TGA curve of PE resin, it is seen that the initial weight loss occurs at temperature of 240 °C (Fig. 3.9 (a)). The weight loss after 300 °C corresponds to the complete degradation of the polymer. In case of GO major weight loss at the temperature range of 200 °C to 320 °C is attributed to the removal of most of the oxygen-containing functional groups such as hydroxyl, epoxy, carbonyl and carboxyl groups (Fig. 3.9 (e)). The 60% residual weight of GO indicates that some functional groups existed on GO surface before the thermal treatment.[26] GO plays an important role in the thermostability of the composites. On incorporation of GO, the major degradation temperature of PE resin was remarkably improved from 230 to 285 °C (Fig. 3.9 (b)-(d)). This improvement in thermal stability is attributed to the strong interaction between GO and PE resin which restricts the mobility of the polymer segments at the interfaces of PE and GO. The interaction is may be due to the formation of hydrogen bonding between oxygen functionality on GO and polymer or some dipolar interactions between the two component. Further it is seen that the weight retention value increases with the incorporation of GO with PE resin matrix. The PE/ GO composites show almost 15-25% weight retention values at 600 °C which is probably due to the existence of a carbon net structure in the composite.[27] Also, the incorporation of GO into the matrix acts as a mass transport barrier to the volatile products generated during decomposition which may enhance the overall thermal stability of the composite. The values obtained here are better than other PE resin composites[13,14] which showed only 30-40% improvement in major degradation temperature.
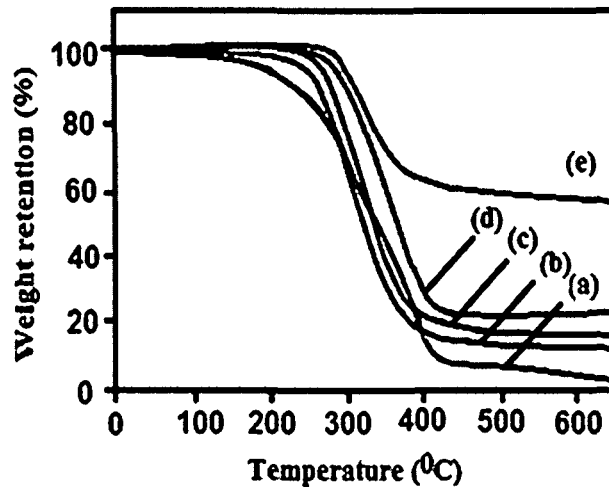
Fig. 3.9 TGA curves of (a) PE resin, (b) PEGO1, (c) PEGO2, (d) PEGO3 composite and (e) GO.

Table 3.2 TGA data of PE and PE/GO composites

[a]Sample particulars	Major degradation temperature (Td) °C	Weight loss % at temperature				Weight retention (%) at 600 °C
		200 °C	300 °C	400 °C	500 °C	
PE resin	245	8	30	80	90	5
PEGO1	260	6	35	80	82	15
PEGO2	270	5	25	75	80	20
PEGO3	285	3	15	65	70	25
GO	300	1	10	35	40	60

TGA curve for PE resin, PE/GR composite and GR are shown in Fig. 3.10 with respective data are being summarized in Table 3.3. GR showed around 20% weight loss at the temperature range of 250 to 500 °C, which is due to the removal of most of the oxygen-containing functional groups during the chemical reduction process. About 70% residual weight of GR at 600 °C indicated its higher thermal stability compared to GO. In the TGA curve of PE resin, initial weight loss occurs at a temperature of 240 °C. The weight loss after 300 °C is due to the complete degradation of the polymer. The major degradation temperature of polyester was found to be improved from 245 to 289 °C on incorporation of the GR. This

improvement in thermal stability is ascribed to the strong interaction between GR and PE resin which restricts the mobility of the polymer chains. The interaction is may be due to the formation of hydrogen bonding between residual oxygen functionality on GR and polymer or some dipolar interactions between the two components. Also the weight retention value increases with the incorporation of GR with PE resin matrix. Almost 25-30% weight retention values were observed in the TGA curves of the composites at 600 °C which is much higher than the 15-25% weight retention value of the PE/GO composite at the same temperature. Thus GR based PE resin composites have shown better thermal stability compared to GO and other nanofillers based PE resin composites.[15,16]
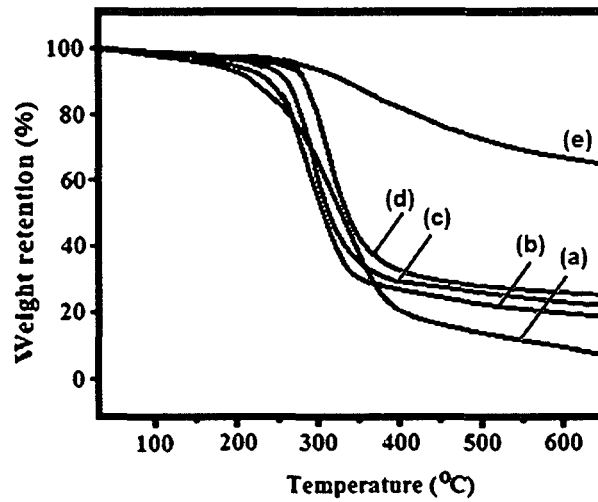

Fig. 3.10 TGA curves of (a) PE resin, (b) PE/GR1, (c) PE/GR2, (d) PE/GR3 composite and (e) GR.

Table 3.3 TGA data of PE resin and PE/GR composites

Sample particulars	Major degradation temperature (Td) °C	Weight loss % at temperature				Weight retention (%) at 600 °C
		200 °C	300 °C	400 °C	500 °C	
PE resin	245	8	30	80	90	5
PEGR1	265	7	32	75	80	25
PEGR2	274	5	25	72	75	27
PEGR3	289	3	15	60	65	30
GR	310	1	10	15	25	70

The glass transition behavior of PE/GO composites was also investigated by using DSC. PE resin exhibits glass-transition temperature (T_g) at around 54 °C as shown in Fig. 3.11. With increasing GO loading in the composites, the T_g of PE resin increases gradually from 54 °C to 62 °C. Similarly, in PE/GR composite (Fig. 3.12.), the T_g of PE resin increases from 55 °C to 63 °C with an increase in the GR content. The increase in T_g in both the composites can be attributed to the reinforcing effects of GO and GR which reduces the segmental motion of the polymer chain.
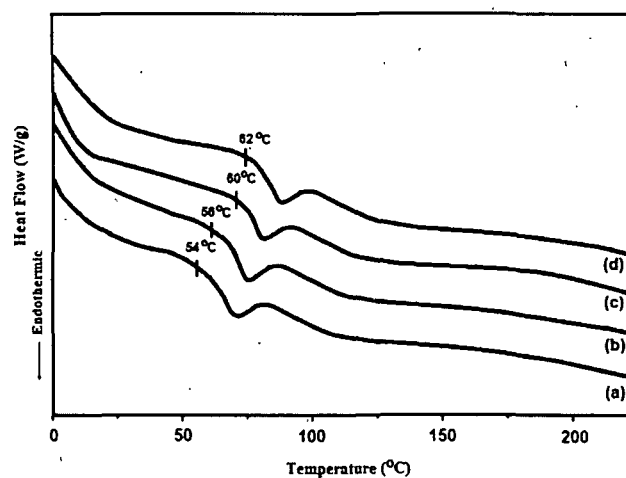
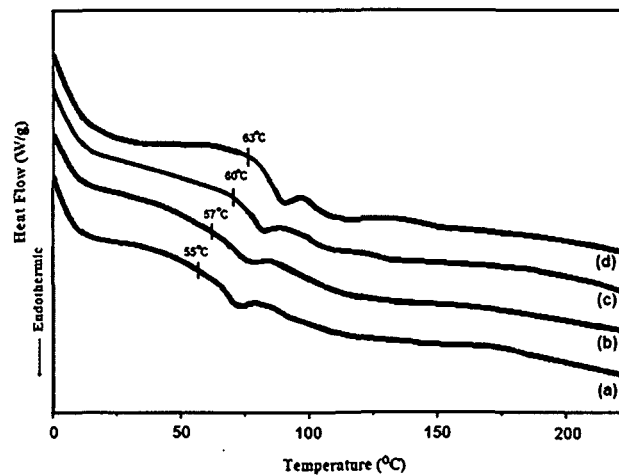Fig. 3.11 DSC curves of (a) PE resin, (b) PEGO1, (c) PEGO2 and (d) PEGO3 composite.

Fig. 3.12 DSC curves of (a) PE resin, (b) PEGR1, (c) PEGR2 and (d) PEGR3 composite.

3.5.5 Mechanical properties

The tensile strength of PE resin and PE/GO composite were measured with a UTM. GO is expected to have good reinforcement effect for tensile properties due to its large aspect ratio and excellent mechanical strength. The mechanical properties of the composite films were found to be increased significantly compared to pure PE resin. Fig. 3.13 represents the stress-strain curves of PE/GO composites with various GO loadings. The slope of the curves increases with increasing GO content. The corresponding Young's modulus values are shown in Table 4. For the composite film with 3 wt.% of GO loading, Young's modulus increased to 1.7 GPa, corresponding to an increase of 41% compared to pure PE resin.
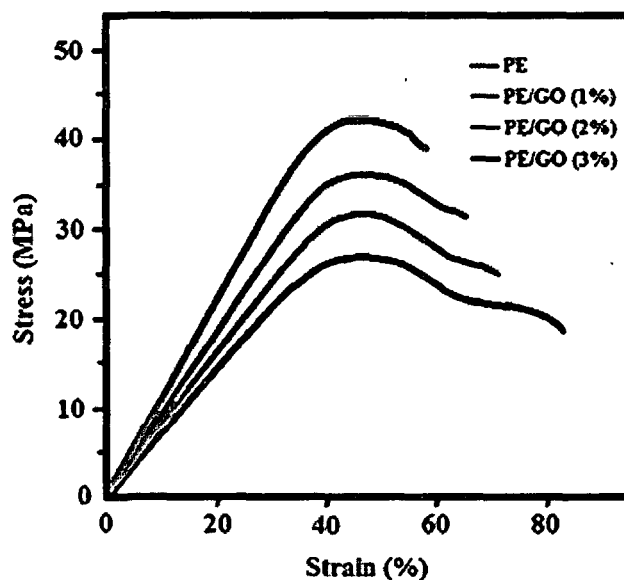

Fig. 3.13 Representative stress-strain curves of the composites with various
GO loadings.

The tensile properties of the PE/GO composite films are illustrated in Fig. 3.14 and Table 3.4. It is obvious that the addition of GO into the polymer matrix has a significant influence on the mechanical behavior of pure PE resin. The composites showed a maximum of 76% increase in tensile strength for 3 wt.% of GO loading i.e. 54 MPa compared to neat resin (25 MPa). The value is higher than that of carbon nanotube based PE resin composites which showed only 17% increase in tensile strength.[16] Also the tensile strength values are found to be increased with increasing

GO loading. The enhanced tensile properties can be ascribed to the homogeneous dispersion of GO in resin matrix and the stronger interfacial interactions such as hydrogen bonding or some possible ionic interactions between both the components.
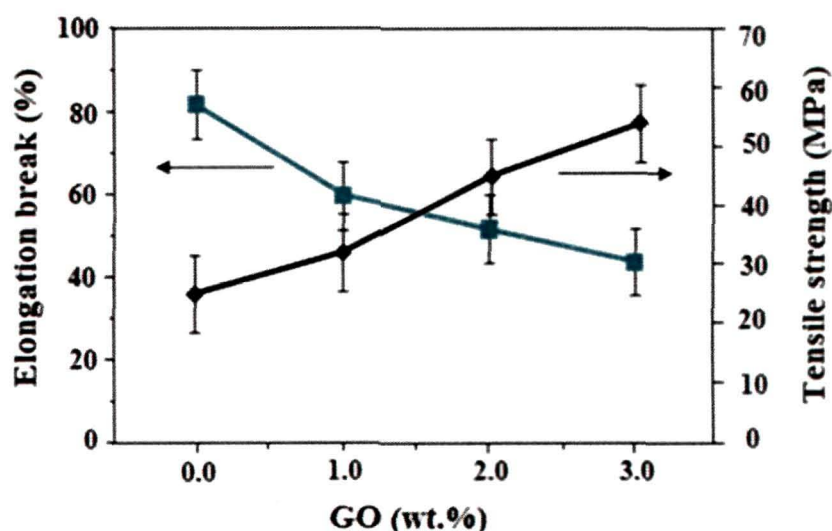

Fig. 3.14 Mechanical properties of PE/GO comoposites with various GO loadings: tensile strength (right) and elongation at break (left) versus GO loadings.

Table 3.4 Mechanical properties from the tensile test

| Sample	Tensile strength (MPa)	Elongation (%)	Young's modulus (GPa)
PE resin	25	80	1.2
PEGO1	32	60	1.4
PEGO2	46	52	1.5
PEGO3	54	47	1.7

On the other hand, the elongation at break of the composites gradually decreases with increasing GO content. The average value of elongation at break decreases to 47% for the 3 wt.% GO loading from 80% for the pure sample. The reason may be attributed to a large aspect ratio and the interaction between GO and the polymer matrix, which confines the movement of the polymer chains. Similar results were observed for other GO based polymer composites.[28,29] The incorporation of GR into

121

the polymer matrix has a significant influence on the mechanical behavior of the composite due to its large aspect ratio and excellent mechanical strength. The representative stress-strain curves of neat PE resin and its composites at various GR loadings are shown in Fig. 3.15. The mechanical properties of the composite films were found to be increased significantly compared to pure PE resin. The slope of the curves increases with the increasing GR content. Based on the slope of the elastic region, the Young's modulus values are calculated and are shown in Table 3.5. On introduction of GR sheets the Young's modulus values are found to be increased. For the composite film with 3 wt.% of GR loading, Young's modulus increased to 3 GPa, corresponding to an increase of 87% compared to pure PE resin.
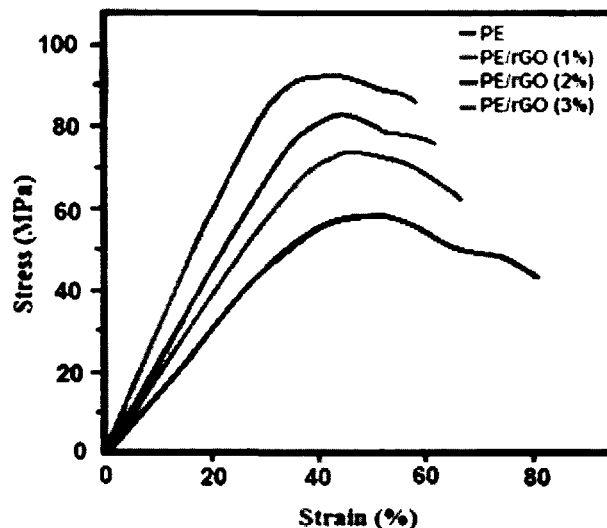
Fig. 3.15 Representative stress-strain curves of the composites with various GR loadings.

The tensile strength and the percentage elongation at break of the PE/GR films are represented in Fig. 3.16 and Table 3.5. The average tensile strength for pure PE resin is 26 MPa. The tensile strength values are found to be increased with increasing GR loading. PE/GR composite with 3 wt.% of GR loading showed the tensile strength value of 58 MPa, corresponding to an improvement of 123% compared to neat resin. The value is higher than the above mentioned PE/GO composite as well as other carbon nanofiber and carbon nanotube based PE resin composites.[16,30]

122
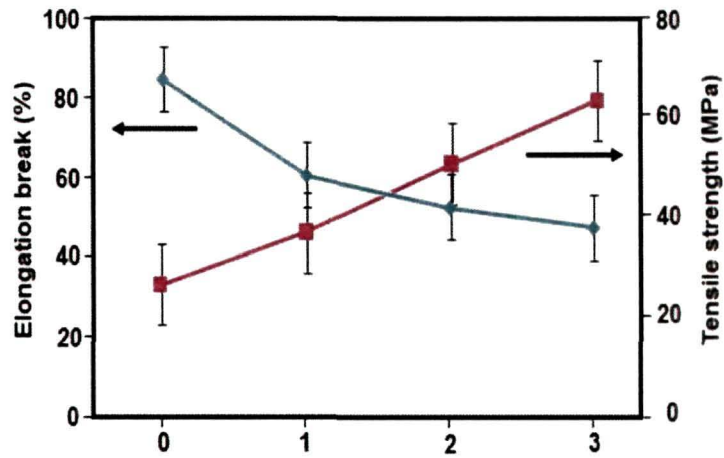
Fig. 3.16 Mechanical properties of PE/GR comoposites with various GR loadings: tensile strength (right) and elongation at break (left) versus GR loadings.

This enhanced tensile property can be attributed to the well dispersion of GR in the polymer matrix and strong interfacial interactions between both the components. On the other hand, a gradual decrease in the elongation at break of the composites was observed with increasing GR content. For the 3 wt.% GR loading, the elongation at break decreased to 45% from 81% for the pure polymer. It could be due to the large aspect ratio and the interaction between GR and the polymer matrix, which restricts the movement of the polymer chains. The results were similar to that of other GR based polymer composites.[31] These mechanically strong composite systems with improved thermal stability can be used in any high-tech structural applications, where high strength, stiffness are required.

Table 3.5 Properties of PE/GR composites

| Sample	Tensile strength/MPa	Elongation (%)	Young's modulus/GPa	Conductivity (σ, S cm^{-1})
PE resin	26	81	1.4	3.09×10^{-12}
PEGR1	35	58	1.9	1.10×10^{-5}
PEGR2	47	50	2.3	7.50×10^{-5}
PEGR3	58	45	3.07	3.70×10^{-4}

3.5.6 Electrical properties

The electrical conductivities of pure PE resin and PE/GR composites at different GR content were determined using a fourpoint probe resistivity measurement system (Table 3 5) The conductivity of pristine PE resin is around $3\,09\times10^{12}$ S cm^{1} On incorporation of GR the conductivity of the composites increases rapidly and the highest conductivity of $3\,7\times10^{4}$ S cm^{1} is achieved for composite containing 3 wt % GR Such an improvement in conductivity can be explained by the large specific surface area and excellent homogeneous dispersion of GR sheets which form a conducting network in the insulating resin matrix The conductivity obtained here is higher than that of carbon fiber and CNT based PE resin composite [15,17] However, PE/GO composites showed negligible value of conductivity which may be due to the insulating nature of GO

3.5.7 Antibacterial Activity

An organized glimpse of data for the antibacterial property of the synthesized composites is illustrated in Table 3 6, which shows a highly significant and pronounced antibacterial behavior of the tested samples against five different bacterial growths of *Staphylococcus aureus*, *Bacillus subtilis*, *Escherichia coli*, *Pseudomonas aeruginosa* and *Klebsilla pneumonia* Samples were dissolved and tested for corresponding antimicrobial activities in 10% DMSO (v/v) aqueous solution It was found from literature that 10% DMSO (v/v) has been used for antimicrobial and other biological activities as it is highly miscible with water, highly polar and stable [32,33] In the presence of 10% DMSO (v/v) both the gram positive and gram negative bacteria showed no detectable effect on bacterial growth Both gram positive and gram negative bacteria were found sensitive to the composites, predominantly the composites were appeared to be more effective towards the gram negative It is clear from the above set of tests that *Pseudomonas aeruginosa* bacteria is very sensitive toward the PE/GR composites and *Escherichia coli* shows the lowest degree of inhibition The antibacterial effect of composites increases with the GR content The composite containing 3 wt % of GR has showed the highest degree of inhibition

against all the five kinds of bacterial strains for which the diameter of the zone of inhibition is more (Fig. 3.17).
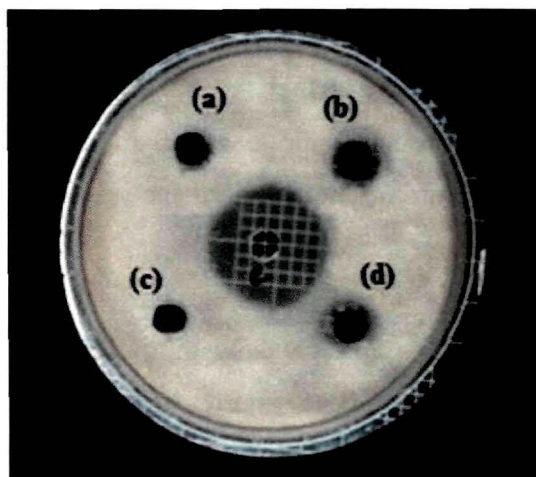
Fig. 3.17 Antibacterial test against *Escherichia coli*, (a) Pure PE resin, (b) PE/GR1, PE/GR2 and PE/GR3 composite.

The reason for the growth inhibitory property of the nanocomposites might be due to the cellular damages of the bacterial cells. Such cellular damages are caused due to the effect of either oxidative stress or physical disorder caused by GR. Similar observation was also reported in other carbon nanomaterials like CNTs and fullerene.[34,35]

Table 3.6 Antibacterial activities of synthesized compounds against different bacterial strains

Test sample	Zone of Inhibition (mm) against				
	Staphylococcus aureus (ATCC11632)	*Bacillus subtilis* (ATCC11774)	*Escherichia coli* (MTCC40)	*Pseudomonas aeruginosa* (MTCC7812)	*Klebsilla pneumoniae* (ATCC10031)
10% DMSO (v/v)	0	0	0	0	0
PE resin	10	10	10	11	10
PEGR1	11	11	10	12	12
PEGR2	12	11	11	13	13
PEGR3	13	12	12	15	14

3.6   Conclusion

- This work demonstrates the successful preparation of GO and GR based PE resin composite with high thermal stability and mechanical strength. The FTIR and XRD results indicate successful incorporation of GO and GR in the polymer matrix. Morphological analysis shows good dispersion of GO and GR within the resin matrix.

- The PE/GO composites show improved thermal stability compared to the pure PE resin. A significant improvement in major degradation temperature (260-285 °C) and weight retention value (15-25%) is obtained on incorporation of GO in the resin matrix. A much enhancement in thermal stability of the PE/GR composites was obtained compared to PE/GO composites. The major degradation temperature of the composite started at relatively higher temperature (260-285 °C) than that of PE/GO composites. Also, the PE/GR composites showed a higher weight retention value (25-30%) compared to PE/GO composites.

- The PE/GO composite films exhibited a significant improvement in the mechanical properties. A 76% increase of tensile strength and 41% increase in Young's modulus are obtained with 3 wt.% of GO loading, which reveals the efficient load transfer between GO and the polymer matrix. The PE/GR composite demonstrated superior mechanical properties compared to PE/GO composites at very low GR loading. Around 123% increase of tensile strength and 87% increase in Young's modulus are obtained with 3 wt.% of GR loading.

- The PE/GR composite film (with 3 wt.% GR loading) was found to possess a higher value of conductivity (3.7 10^{-4} S cm^{-1}) compared to pure resin due to

the incorporation of highly conducting GR sheets which forms a conducting network in the insulating resin matrix.

- The PE/GR composites imply proficient antibacterial activity towards the five different kinds of bacterial strains and the antibacterial activity was found to be increased with increasing GR content. Among all the bacterial strains, *Pseudomonas aeruginosa* was much more sensitive towards the PE/GR composites.

- These mechanically strong and ductile PE/GO and PE/GR composite films exhibit good potential in industrial applications. The GR based PE resin composites with improved antibacterial activity could offer new opportunities for the development of a new range of environmental friendly and high strength structural material.

REFRENCES

1. Potts, J.R., et al. Graphene-based polymer nanocomposites, *Polymer* **52**, 5-25, 2011.

2. Kim, H., et al. Graphene/polymer nanocomposites, *Macromolecules* **43**, 6515-6530, 2010.

3. Yang, X. Layer-structured poly (vinyl alcohol)/graphene oxide nanocomposites with improved thermal and mechanical properties, *J. Appl. Polym. Sci.* **120**, 1355-1360, 2011.

4. Rao, C.N.R., et al. Graphene: the new two-dimensional nanomaterial, *Angew. Chem. Eng.* **48**, 7752-7777, 2009.

5. Wang, S., et al. Thermal expansion of graphene composites, *Macromolecules* **42**, 5251-5255, 2009.

6. Fang, M., et al. Covalent polymer functionalization of graphene nanosheets and mechanical properties of composites, *J. Mater. Chem.* **19**, 7098-7105, 2009.

7. Chen, Y., et al. Preparation, mechanical properties and biocompatibility of graphene oxide/ultrahigh molecular weight polyethylene composites, *Eur. Polym. J.* **48**, 1026-1033, 2012.

8. Liu, P., et al. Preparation and characterization of poly (vinyl acetate)-intercalated graphite oxide nanocomposite, *J. Mater. Chem.* **10**, 933-935, 2000.

9. Kotov, N.A., et al. Ultrathin graphite oxide-polyelectrolyte composites prepared by self-assembly: Transition between conductive and non-conductive states, *Adv. Mater.* **8**, 637-641, 1996.

10. Cassagneau, T., & Fendler, J.H. High density rechargeable lithium-ion batteries self-assembled from graphite oxide nanoplatelets and polyelectrolytes, *Adv. Mater.* **10**, 877-881, 1998.

11. Aziz S.H. et al. Modified polyester resins for natural fibre composites, *Compos. Sci. Technol.* **65**, 525-535, 2005.

12. Battisti, A., et al. Monitoring dispersion of carbon nanotubes in a thermosetting polyester resin, *Compos. Sci. Technol.* **69**, 1516-1520, 2009.
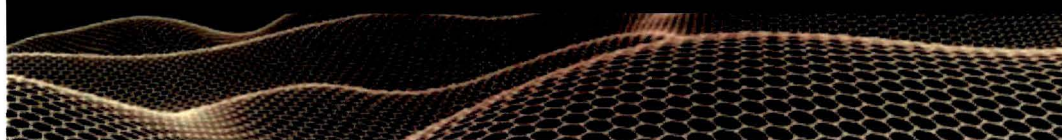
13. Tibiletti, L., et al. Thermal degradation and fire behaviour of unsaturated polyesters filled with metallic oxides, *Polym. Degrad. Stab.* **96**, 67-75, 2011.

14. Bharadwaj, R.K., et al. Structure-property · relationships in cross-linked polyester-clay nanocomposites, *Polymer* **43**, 3699-3705, 2002.

15. Vilcakova, J., et al. Electrical conductivity of carbon fibres/polyester resin composites in the percolation threshold region, *Eur. Polym. J.* **38**, 2343-23477, 2002.

16. Seyhan, T., et al. Critical aspects related to processing of carbon nanotube/unsaturated thermoset polyester nanocomposites, *Eur. Polym. J.* **43**, 374-379, 2007.

17. Battisti, A., et al. Percolation threshold of carbon nanotubes filled unsaturated polyesters, *Compos. Sci. Technol.* **70**, 633-637, 2010.

18. Wang, X., et al. Cyanate ester resin/graphene nanocomposite: Curing dynamics and network formation, *Eur. Polym. J.* **48**, 1034-1041, 2012.

19. Yu, A., et al. Graphite nanoplatelet-epoxy composite thermal interface materials, *J. Phys. Chem. C* **111**, 7565-7569, 2007.

20. Liu, K., et al. Preparation of polyester/reduced graphene oxide composites *via* *in situ* melt polycondensation and simultaneous thermo-reduction of graphene oxide, *J. Mater. Chem.* **21**, 8612-8617, 2011.

21. Hu, W., et al. Graphene-based antibacterial paper, *ACS Nano* **4**, 4317-4323, 2010.

22. Bose, S., et al. In-situ synthesis and characterization of electrically conductive polypyrrole/graphene nanocomposites, *Polymer* **51**, 5921-5928, 2010.

23. Patole, A.S., et al. A facile approach to the fabrication of graphene/polystyrene nanocomposite by in situ microemulsion polymerization, *J. Colloid Interf. Sci.* **350**, 530-537, 2010.

24. Pandey, R.K., et al. Electrooxidation of formic acid, methanol, and ethanol on electrodeposited Pd polyaniline nanofiber films in acidic and alkaline medium, *J. Phys. Chem. C* **113**, 21596-603, 2009.

25. Salavagione, H.J., et al. Synthesis of poly (vinyl alcohol)/reduced graphite oxide nanocomposites with improved thermal and electrical properties, *J. Mater. Chem.* **19**, 5027-32, 2009.

26. Bora, C., & Dolui, S.K. Fabrication of polypyrrole/graphene oxide nanocomposites by liquid/liquid interfacial polymerization and evaluation of their optical, electrical and electrochemical properties, *Polymer* **53**, 923-932. 2012.

27. Konwer, S., et al. Studies on conducting polypyrrole/graphene oxide composites as supercapacitor electrode, *J. Electron. Mater.* **40**, 2248-2256, 2011.

28. Kong, J., et al. Preparation and properties of polyimide/graphene oxide nanocomposite films with Mg ion crosslinker, *Euro. Polym. J.* **48**, 1394-1405. 2012.

29. Xu, Y., et al. Strong and ductile poly (vinyl alcohol)/graphene oxide composite films with a layered structure, *Carbon* **47**, 3538-3543, 2009.

30. Agullo J.V., et al. Comparative study of the dispersion and functional properties of multiwall carbon nanotubes and helical-ribbon carbon nanofibers in polyester nanocomposites, *Compos. Sci. Technol.* **69**, 1521-1532, 2009.

31. Zhao, X., et al. Enhanced mechanical properties of graphene-based Poly (vinyl alcohol) composites, *Macromolecules* **43**, 2357-2363, 2010.

32. Hussain, A.I., et al. Rosmarinus officinalis essential oil: antiproliferative, antioxidant and antibacterial activities, *Braz. J. Microbiol.* **41**, 1070-1078, 2010.

33. Das, S., et al. An efficient stereo-controlled synthesis of bis-pyrimido-[4,5-d]-pyrimidine derivatives via aza-Diels-Alder methodology and their preliminary bioactivity, *RSC Adv.* **3**, 3407-3413, 2013.

34. Tang, Y.J., et al. Charge associated effects of fullerene derivatives on microbial structural integrity and central metabolism, *Nano Lett.* **7**, 754-760, 2007.

35. Szabo, T., et al. Evolution of surface functional groups in a series of progressively oxidized graphite oxides, *Chem. Mater.* **18**, 2740-2749, 2006.
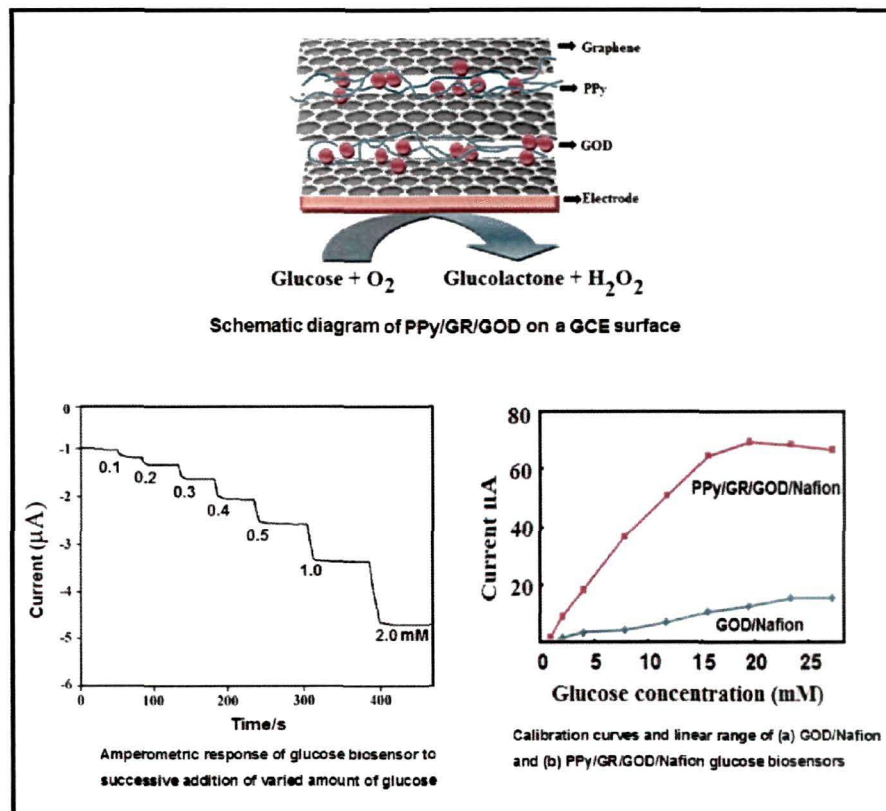
CHAPTER 4: Section A

Applications of graphene based polymer nanocomposites:

Highly sensitive glucose biosensor based on polypyrrole (PPy)/graphene (GR) composite synthesized by interfacial polymerization

GRAPHICAL ABSTRACT

Glucose + O_2 Glucolactone + H_2O_2

Schematic diagram of PPy/GR/GOD on a GCE surface

Amperometric response of glucose biosensor to successive addition of varied amount of glucose

Calibration curves and linear range of (a) GOD/Nafion and (b) PPy/GR/GOD/Nafion glucose biosensors

4.1 Highly sensitive glucose biosensor based on polypyrrole (PPy)/graphene (GR) composite synthesized by interfacial polymerization

4.1.1 Introduction

Biosensors are attracting increased attention due to their potential applications in clinical chemistry, food industry, and environmental fields.[1] They are becoming a crucial part of modern life from diagnosis of life-threatening diseases to detection of biological agents in warfare. Recently, conducting polymers have attracted much attention in the development of biosensors.[2] An electrochemical biosensor can be made by immobilizing biological component onto conducting polymer. Use of conducting polymers such as polypyrrole, polyaniline and poly-3, 4-ethylenedioxythiophene in the preparation of amperometric biosensors have been reported till date.[3-5] Amongst the conducting polymers, polypyrrole (PPy) plays a leading role because of its stability, facile synthesis, easy processability and environmental stability. However, the overall conductivity of conducting polymer is limited because of the use of insulating dopants.[6]

Graphene (GR), a single layer of carbon atoms in a closely packed honeycomb two-dimensional lattice, has attracted huge attention from scientific communities in recent years. Due to its high electrical conductivity, high surface area, strong mechanical strength and cost benefit, GR has been used as electrode material to prepared electrochemical sensors or biosensors.[7-9] Unlike carbon nanotube (CNT), GR is entirely free from catalytic impurities, which simplifies its intrinsic electrochemistry and potentially offers a more reproducible sensing response. Other excellent properties of GR include its low thermal noise, high flexibility and high transparency which are required for mechanically robust sensors. The first GR-based electrical biosensors were demonstrated by Mohanty and Berry, who produced sensors by treating graphite oxide with nitrogenous plasmas or ethylenediamine.[10] Single-stranded oligonucleotides were chemically grafted to the GR-derivatives. Then rhodamine-

green-tagged complementary oligonucleotides were hybridized with the tethered strands and monitored fluorescence.

On the basis of the high electrocatalytic activity of GR toward H_2O_2 and glucose oxidase (GOD), PPy/GR combining with GOD could be an excellent electrode material for oxidase biosensors. Worldwide, diabetes is a rapidly growing problem that can be handled by monitoring and controlling blood glucose levels. Glucose detection is clinically significant for diagnosis and management of diabetes. Its electrochemical detection can be realized by using GOD as the mediator. Several GR-based glucose biosensors have been reported till date.[11-13] Shan et al.[14] reported the GR-based glucose biosensor with GR/polyethylenimine-functionalized ionic liquid nanocomposites modified electrode which exhibited a wide linear glucose response (2 to 14 mM, R=0.994), good reproducibility and high stability (response current +4.9% after 1 week). Kang et al.[15] employed biocompatible chitosan to disperse GR for use as glucose biosensors. It was found that chitosan helped to form a well-dispersed GR suspension and immobilize the enzyme molecules. The biosensor showed excellent sensitivity and long-term stability for detection of glucose. Wang et al.[16] developed a sensor based on an N-doped GR/Chitosan/GOD hybrid. It has a detection limit as low as 10 mM. The reduction potential of the electrode was shifted by 400 mV towards the positive potential as compared with a bare glassy carbon electrode (GCE), indicating its fast electron transfer kinetics. However, the development of GR based materials is still in its infancy and relatively few reports have been made based on GR based biosensor.

Several reports have been made based on the preparation of conducting polymer and GR composites. These composites showed superior electrical conductivity, charge density and electrocatalytic activity compared with pure conducting polymers.[17-19] However, in most of cases, polymer composites were prepared by chemical or electrochemical methods. Herein, we report a new route to synthesize PPy/GR nanocomposite by liquid/liquid interfacial polymerization and demonstrate its application for sensitive glucose sensing.

132

4.1.2 Experimental

4.1.2.1 Materials and methods

Glucose oxidase (GOD) (Type X-S, Aspergillus niger (EC 1.1.3.4), 179 units/mg), d-glucose, phosphate buffer saline, Nafion (5 wt.% in lower aliphatic alcohol and water mixture), 2-propanol, sodium phosphate monobasic, sodium phosphate dibasic and H_2O_2 were obtained from Sigma-Aldrich and used as received. All solutions used in the experiments were prepared with ultra-pure water. Graphite flakes (Carbon India Ltd., Guwahati) were used as purchased. Pyrrole monomer was purchased from Sigma Aldrich and was used as received. Sodium nitrate (Merck), sulfuric acid (Merck), potassium permanganate (Merck), ferric chloride (Aldrich), hydrazine monohydrate (Aldrich) and lithium perchlorate (Fluka) are commercial products and were used as received. Chloroform ($CHCl_3$) was obtained from Merck and was distilled and kept with molecular sieves before use. GR was prepared by reduction of Graphene Oxide (GO) as described in the previous chapter (Chapter 2). PPy/GR composites were prepared by liquid/liquid interfacial polymerization involving pyrrole and GR as described in Chapter 2. Composites containing 1, 2 and 3 wt.% of GR were prepared and designated as PPyGR1, PPyGR2 and PPyGR3.

4.1.2.2 Preparation of PPy/GR/Nafion Composite Film

A 0.5 wt.% Nafion solution was prepared by diluting the 5 wt.% Nafion stock solution with 2-propanol. Then PPy/GR nanocomposites were mixed with of 0.5 wt.% Nafion-isopropyl-alcohol solution (1mg/mL) by ultrasonication for 30 mins. Prior to the surface modification, the bare glassy carbon electrode (GCE) was polished with 0.3 and 0.05 μm alumina slurries and washed with deionized (DI) water several times. Then the PPy/GR/Nafion paste was drop cast on the GCE with a surface area of 1.5 cm^2. The solvent was allowed to evaporate at room temperature (25 °C).

133

4.1.2.3 Preparation of Glucose Biosensor

Glucose biosensor was fabricated by the following route: GOD was dissolved in 50 mM phosphate buffer (PBS) solution (pH 7.4) to a final concentration of 20-60 mg/mL. Then, the casting solution was prepared by adding the PPy/GR/Nafion–isopropyl-alcohol suspension to the enzyme solution to meet the desired enzyme concentration. The suspension was ultrasonicated for 5 mins. Then this dispersion was drop cast onto the GCE with an area of 1.5 cm^2. The coating was dried at room temperature for 1 h. Then, the modified electrodes were soaked in 50 mM PBS (pH 7.4) for 30 mins, washed thoroughly with DI water and dried before use.

4.1.2.4 Instrumentation

Cyclic voltammetric and amperometic measurements were performed on an electrochemical analyzer (CHI Instruments, Inc., Austin, TX). Measurements were performed with a standard one compartment three electrode configuration cell with a modified GCE as the working electrode, platinum as the counter electrode and an Ag/AgCl as the reference electrode. The cyclic voltammograms (CVs) of the PPy/GR/Nafion composite film were obtained in 5 mM $K_4Fe(CN)_6$ and 0.1 M KCl solution. An amperometric response of the GOD/PPy/GR/Nafion/GCE to the sequential addition of a desired amount of glucose was measured at 900 mV with continuous gentle stirring in a 50 mM PBS (pH 7.4). All TEM measurements were carried out on a JEOL JEM-2100 transmission electron microscope at an accelerating voltage of 200 kV. The TEM samples were prepared by dispersing a small amount of powder sample in ethanol by ultrasonication. Then a single drop of the suspension was dropped on 300 mesh copper TEM grids covered with thin amorphous carbon films for analysis.

4.1.3 Results and discussion

PPy/GR composites were prepared by interfacial polymerization where pyrrole is dissolved in an organic solvent which acts as an organic phase and GR as well as

oxidant ferric chloride is dissolved in water which acts as an aqueous phase. Polymerization of pyrrole occurs at the surface of GR sheets. As a result a black film appears at the interface slowly. The reaction is controllable, slow and completed in 24 h. The prepared composite was then dispersed in a 0.5 wt.% Nafion–isopropyl-alcohol solution and cast on a GCE. Then GOD was immobilized on PPy/GR/Nafion/GCE, forming a bionanocomposite film. GOD catalyzes the oxidation of glucose to gluconolactone.

$$\text{Glucose} + O_2 \longrightarrow \text{gluconolactone} + H_2O_2$$
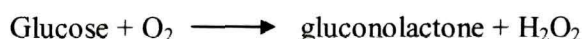
The quantification of glucose can be achieved via electrochemical detection of H_2O_2. Fig.4.1.1 represents the orientation of PPy/GR/GOD on the surface of GCE.
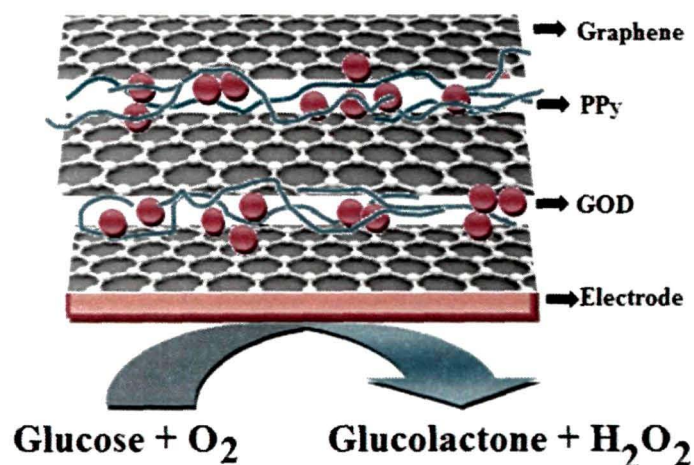
Fig. 4.1.1 Schematic diagram of PPy/GR/GOD on a GCE surface.

4.1.3.1 Morphology of the composite

TEM images for GR and PPy/GR composite are shown in Fig. 4.1.2. TEM image of GR (Fig. 4.1(a) and (b)) shows a crumpled and agglomerated sheet like structure with hundreds of nanometers. The wrinkled structure observed in the TEM image of GR sheets is due to the rapid removal of intercalated functional groups in GO during the reduction process.[21] TEM images of PPy/GR composite (Fig. 4.1.2 (c) and (d)) shows that the exfoliated GR sheets are decorated by PPy nanoparticles, leading to

the formation of well-dispersed composite sheets.[22] These changes in morphology of the composite from the individual components may introduce superior electrochemical properties. The morphology of the PPy/GR composites obtained by liquid/liquid interfacial polymerization is quite different from the earlier reported methods.[23,24]
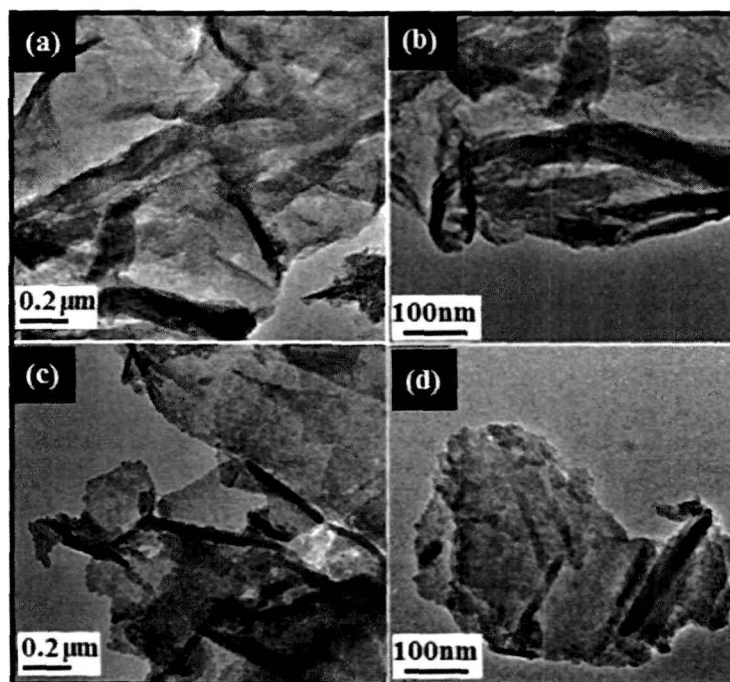
Fig. 4.1.2 TEM images (a) GR at lower magnification, (b) GR at higher magnification, (c) PPy/GR composite at lower magnification and (d) PPy/GR composite at higher magnification.

4.1.3.2 Raman Spectroscopy

Raman spectroscopy is an effective technique used to study the carbon products. The Raman spectra of PPy/GR composite and pure GR are shown in Fig. 4.1.3. The Raman spectra of GR (Fig. 4.1.3(a)) exhibits two distinctive peaks for the D and G bands at about 1340 and 1585 cm^{-1} respectively. The D band is due to the K-point phonons of A_{1g} symmetry, arises from the breathing vibration of aromatic rings and the G band arises from the zone center E_{2g} mode, corresponding to ordered sp^2-bonded carbon atoms.[25] The intensity ratio of D and G band (I_D/I_G) is found to be 1.17 which indicates the presence of unrepaired defects due to the removal of large amounts of

oxygen-containing functional groups.[26] In the Raman spectra of PPy/GR composite, characteristic peaks for PPy appeared in 1050, 930 and 980 cm^{-1}. Both D and G band in the composite shifted to 1332 and 1560 cm^{-1} which reveals the π-π interaction between the PPy and the GR sheets. Also the intensity ratio, I_D/I_G of the composites was found to be 1.15, indicating the presence of localized sp^3 defects within the sp^2 carbon network.
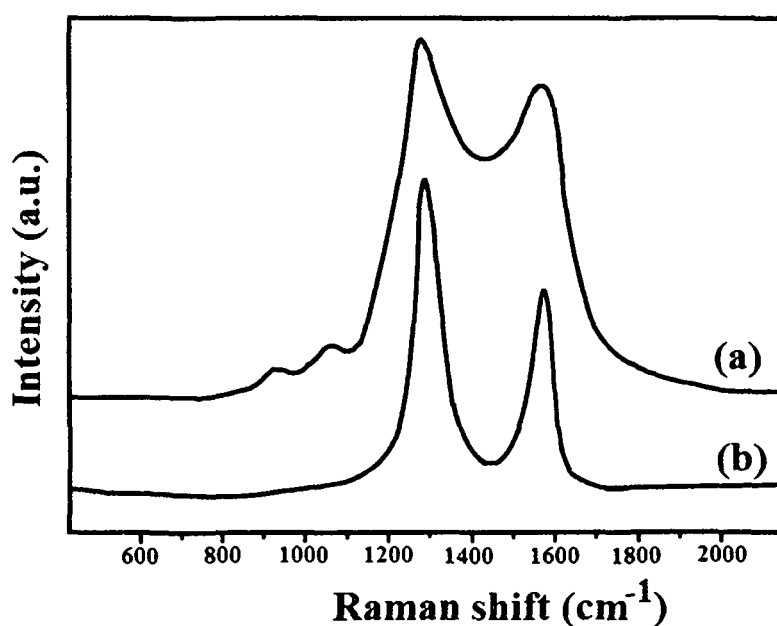

Fig. 4.1.3 Raman spectra of (a) PPy/GR composite and (b) GR.

4.1.3.3 Conductivity Measurements.

The conductivity of the composite is measured using a four-point probe method. The PPy/GR composite exhibited a conductivity of 19.2 S cm^{-1}, which is much higher than that of pure PPy (0.210 S cm^{-1}). This improvement of conductivity of the composite is due to the incorporation of highly conducting GR sheets with a high surface area which provide conducting bridges in the composite system.

4.1.3.4 Electrochemical study of the biosensor electrode

Cyclic voltammetry (CV) is a useful technique to evaluate electrochemical performance of PPy/GR/Nafion/GCE. Fig. 4.1.4 shows the CV curves of PPy/GR

composite at the different GR loading recorded in 5 mM ferrocyanide in 0.1 M KCl. The electrochemical responses obtained at the PPy/GR/Nafion/GCE are much larger than that obtained at the Nafion/GCE. The Nafion/GCE shows no redox peaks as Nafion film behaves as a barrier to the electron transport process. Incorporation of PPy/GR composite into Nafion increases the electrochemical performance and a well defined oxidation and reduction peak with increase in the peak current are obtained. CV curves of PPy/GR/Nafion/GCE have large rectangular areas, indicating higher double-layer capacitances and better charge generation within the electrode. Also it is observed that the peak separation increases with increasing GR loading in the composite. At the higher GR loading, the redox waves became wider and shifted to lower potentials which are possibly due to the increased conductivity and surface area of the composite on introduction of GR thereby decreasing the overpotential of the electrode.
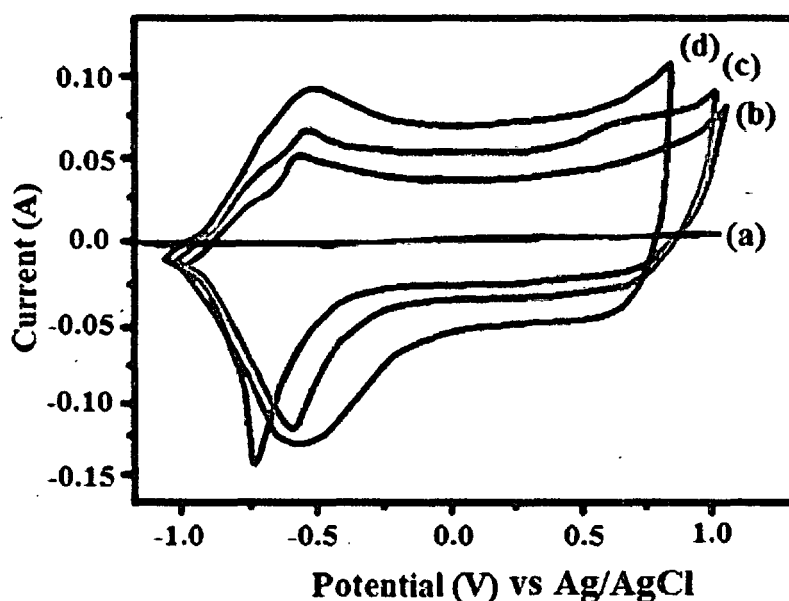
Fig. 4.1.4 Cyclic voltammetric response of 5 mM Fe(CN)$_6^{4-}$ in 0.1 M KCl for (a) Nafion and PPy/GR/Nafion composite with (b) 1 wt.%, (c) 2 wt.%, (d) 3 wt.% of GR loading at scan rate, 100 mV/s.

To study the electrocatalytic effect of the films to H$_2$O$_2$, CV was used. Fig. 4.1.5 shows the CV curves of PPy/GR/Nafion/GCE in a 50 mM phosphate buffer solution containing 2 mM H$_2$O$_2$ in comparison to nafion modified GCE. Nafion

modified electrode shows very weak electrochemical response and the oxidation of H_2O_2 at the Nafion modified GCE starts at 0.7 V. The electrochemical response obtained at the PPy/GR/Nafion/GCE is much larger than Nafion modified electrode. PPy/GR/Nafion modified electrode showed significant oxidation and reduction currents. It is observed that the oxidation and reduction of H_2O_2 started at around 0.3 V and -0.1 V respectively. The higher electrochemical response in case of PPy/GR/Nafion modified electrode indicates that PPy/GR composites catalyze the oxidation-reduction of H_2O_2. Also it is seen that the oxidation current increases with increase in potential and reduction current increases with a decrease in the potential at these modified electrodes. The decrease of the overpotential of H_2O_2 can be attributed to the increase in surface area as well as electrical conductivity of the composite system. Thus it can be concluded that the nanocomposite film with both GR and PPy showed a synergetic effect on the electrocatalytic activity to H_2O_2.
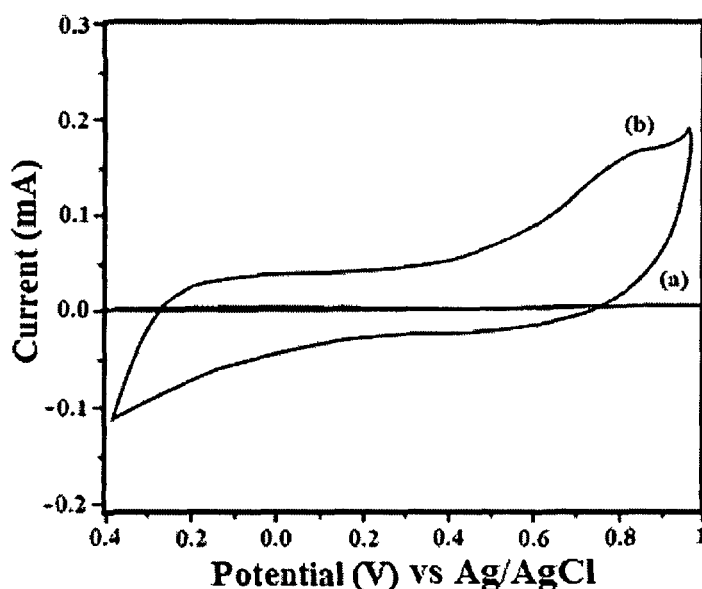

Fig. 4.1.5 CV curves obtained at (a) bare GCE; (b) PPy/GR/Nafion/GCE; in 50 mM PBS solution containing 2 mM H_2O_2.

4.1.3.5 Amperometric Measurement.

Amperometric technique was used for quantification of glucose by the use of the as prepared GR-based biosensor. The amperometric responses of

PPy/GR/GOD/Nafion biosensor at successive additions of various amounts of glucose at an applied potential of +0.9 V are shown in Fig. 4.1.6. The electrochemical response increased in proportion with the increase in the glucose concentration. It can be seen that the sensor is responsive to a low concentration of glucose, such as 0.1 μM (S/N = 3) glucose with a response time less than 6 s. This limit of detection value is much lower than the previously reported values of 0.02 mM for GOD/GR/chitosan modified electrode[15] and 5×10^{-6} M (S/N = 3) for GR/Au/Nafion biocomposite.[27]
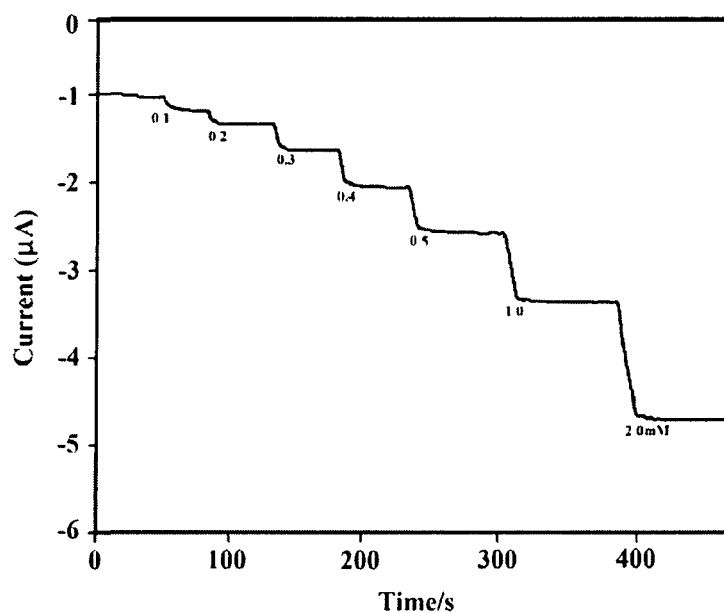
Fig. 4.1.6 Amperometric response of PPy/GR/GOD/Nafion glucose biosensor (GOD, 3 mg/mL) at an applied potential of +0.9 V to successive addition of varied amount of glucose in a stirred 50mM, PH 7.4, PBS solution.

Fig. 4.1.7 shows the calibration curves of GOD/Nafion and PPy/GR/GOD/Nafion biosensor. The linear detection range of PPy/GR/GOD/Nafion biosensor is 0.001-4.8 mM. Similar detection range was obtained for polydopamine/GR composite film modified enzyme electrode.[28] The sensitivity of PPy/GR based glucose biosensor is calculated and it was found to be 29.6 μA/(mM.cm^2) at a GOD concentration of 3 mg/mL. The sensitivity value obtained for this PPy/GR based glucose biosensor is superior to that of the glucose biosensors based on GR/cobalt oxide composite (13.52 μA/(mM.cm^2))[29] polydopamine/GR composite (28.4

$\mu A/(mM.cm^2))^{28}$ and CNTs.[30] Such improvement in sensitivity of the biosensor might be ascribed to a large surface area, a fast electron transfer activity of GR and high electrocatalytic activity from both PPy and GR.
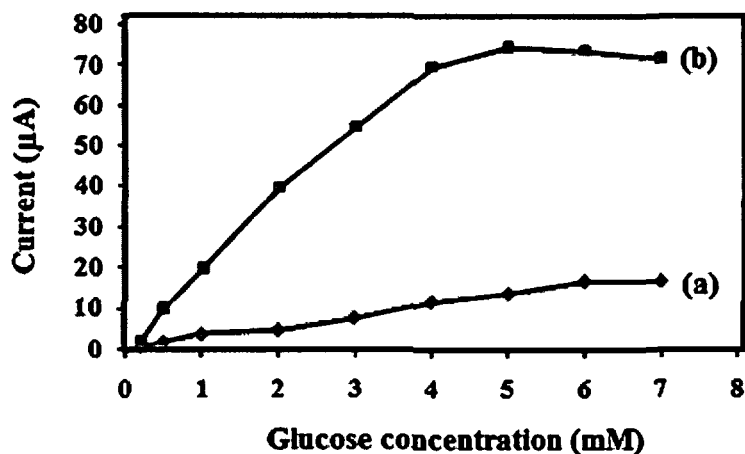

Fig. 4.1.7 Calibration curves and linear range of (a) GOD/Nafion and (b) PPy/GR/GOD/Nafion glucose biosensors at an applied potential of +0.9 V versus Ag/AgCl in 50 mM PBS solution.

4.1.3.6 Biosensor Interference and Storage Stability

The storage stability of the biosensor was studied by storing it at 4 °C. The biosensor showed a quite stable response to 0.5 mM glucose upto first week and it showed 13% loss in the sensitivity value after 1 month. This decrease in sensitivity is may be due to the enzyme degradation with time. The results showed that the prepared biosensor has a high sensitivity as well as a good stability for detection of glucose.

The selectivity of the biosensor for glucose was studied towards uric acid and ascorbic acid as they can interfere with glucose detection. The interfering effect of 0.1 mM ascorbic acid and 0.2 mM uric acid are evaluated with reference to 4 mM glucose, which is the concentration of glucose human blood. At the potential of +0.7 V both the components showed significant interference. However, when the operating potential was reduced to -0.5 V, the interference became negligible with a little decrease in the

sensitivity (96%) of the enzyme electrode. Thus, by changing the potential, the interference of uric acid and ascorbic acid can be avoided for the biosensor.

4.1.4 Conclusion

In this work, we have demonstrated the fabrication of a glucose biosensor based on PPy/GR nanocomposites prepared by interfacial polymerization. The TEM results showed good dispersion of GR within the polymer matrix. PPy/GR composite greatly enhanced the redox peak current of ferrocyanide solution and oxidation of H_2O_2 and also lowered the overpotential for monitoring enzymatically produced H_2O_2. The PPy/GR/Nafion/GOD film modified GCE is found to be active for the electrooxidation of H_2O_2. This PPy/GR based biosensor showed a high value of sensitivity (29.6 $\mu M/cm^2.mM$) and lower limit of detection (0.1 μM) compared to other GR and CNT based biosensor. The biosensor is able to detect glucose with high sensitivity and fast response. The biosensor also showed reasonable stability which is crucial for practical application of biosensors. This simple, controllable method may be used for the fabrication of other biosensors.

REFERENCES

1. Qiu, J.D., et al. Nanocomposite film based on graphene oxide for high performance flexible glucose biosensor, *Sens. Actuators B: Chem.* **160**, 287-294, 2011.

2. Adhikari, B. & Majumdar S. Polymers in sensor applications, *Prog. Polym. Sci.* **29**, 699-766, 2004.

3. Raitman, O.A., et al. Integration of polyaniline/poly(acrylic acid) films and redox enzymes on electrode supports: an in situ electrochemical/ surface plasmon resonance study of the bioelectrocatalyzed oxidation of glucose or lactate in the integrated bioelectrocatalytic systems, *J. Am. Chem. Soc.* **124**, 6487-6496, 2002.

4. Sung, W.J. & Bae, Y.H. A glucose oxidase electrode based on polypyrrole with polyanion/PEG/enzyme conjugate dopant, *Biosens. Bioelectron.* **18**, 1231-1239, 2003.

5. Garreau, S., et al. In-situ spectroelectrochemical Raman studies of poly(3,4-ethylenedioxythiophene) (PEDT), *Macromolecules* **32**, 6807-6812, 1999.

6. Chen, J., et al. Solution properties of single-walled carbon nanotubes, *Science* **282**, 95-98, 1998.

7. Liu, Y., et al. Biological and chemical sensors based on graphene materials, *Chem. Soc. Rev.* **41**, 2283-2307, 2012.

8. Pumera, M., et al. Graphene for electrochemical sensing and biosensing, *Trends Anal. Chem.* **29**, 954-965, 2010.

9. Baby, T.T., et al. Metal decorated graphene nanosheets as immobilization matrix for amperometric glucose biosensor, *Sens. Actuators B: Chem.* **145**, 71-77, 2010.

10. Mohanty, N. & Berry, V. Graphene-based single-bacterium resolution biodevice and DNA transistor: interfacing graphene derivatives with nanoscale and microscale biocomponents, *Nano Lett.* **8**, 4469-4476, 2008.

11. Wang, Z.J., et al. Direct electrochemical reduction of single-layer graphene oxide and subsequent functionalization with glucose oxidase, *J. Phys. Chem. C* **113**, 14071-14075, 2009.
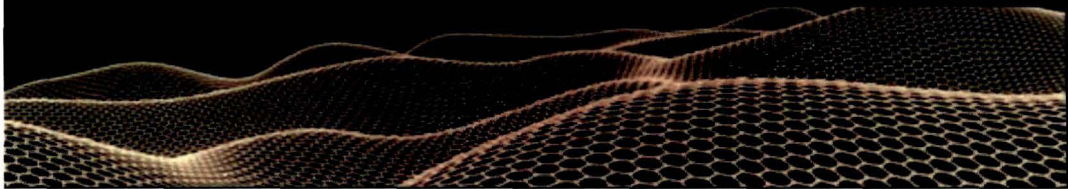
12. Wu, H., et al. Glucose biosensor based on immobilization of glucose oxidase in platinum nanoparticles/graphene/chitosan nanocomposite film, *Talanta* **80**, 403-406, 2009.

13. Zhou, M., et al. Electrochemical sensing and biosensing platform based on chemically reduced graphene oxide, *Anal. Chem.* **81**, 5603-5613, 2009.

14. Shan, C.S., et al. Direct electrochemistry of glucose oxidase and biosensing for glucose based on graphene, *Anal. Chem.* **81**, 2378-2382, 2009.

15. Kang, X.H., et al. Glucose oxidase-graphene-chitosan modified electrode for direct electrochemistry and glucose sensing, *Biosens. Bioelectron.* **25**, 901-905, 2009.

16. Wang, Y., et al. Nitrogen-doped graphene and its application in electrochemical biosensing, *ACS Nano* **4**, 1790-1798, 2010.

17. Chen, G.Z., et al. Carbon nanotube and polypyrrole composites: coating and doping, *Adv. Mater.* **12**, 522-526, 2000.

18. Wang, J., et al. Carbon nanotube-conducting-polymer composite nanowires, *Langmuir* **21**, 9-12, 2005.

19. Ham, H.T., et al. Single wall carbon nanotubes covered with polypyrrole nanoparticles by the miniemulsion polymerization, *Polymer* **46**, 6308-6315, 2005.

20. Hummers, W.S. & Offeman, R.E. Preparation of graphitic oxide, *J. Am. Chem. Soc.* **80**, 1339, 1958.

21. Zhang, D., et al. Enhanced capacitance and rate capability of graphene/polypyrrole composite as electrode material for supercapacitors, *J. Power Sources* **196**, 5990-5996, 2011.

22. Hao, Q.H., et al. Morphology-controlled fabrication of sulfonated graphene/polyaniline nanocomposites by liquid/liquid interfacial polymerization and investigation of their electrochemical properties, *Nano Res.* **4**, 323-333, 2011.

23. Bose, S., et al. In-situ synthesis and characterization of electrically conductive polypyrrole/graphene nanocomposites, *Polymer* **51**, 5921-5928, 2010.

24. Liu, A., et al. Electrochemical deposition of polypyrrole/sulfonated graphene composite films, *J. Phys. Chem. C* **114**, 22783-22789, 2010.

25. Wang, H., et al. Effect of graphene oxide on the properties of its composite with polyaniline, *Appl. Mater. Interfaces* **2**, 821-828, 2010.

26. Bora, C. & Dolui, S.K. Fabrication of polypyrrole/graphene oxide nanocomposites by liquid/liquid interfacial polymerization and evaluation of their optical, electrical and electrochemical properties, *Polymer* **53**, 923-932, 2012.

27. Zhou, K., et al. Electrocatalytic oxidation of glucose by the glucose oxidase immobilized in graphene-Au-nafion biocomposite, *Electroanalysis* **22**, 259-264, 2010.

28. Ruan, C., et al. One-pot preparation of glucose biosensor based on polydopamine-graphene composite film modified enzyme electrode, *Sens. Actuators B: Chem.* **177**, 826-832, 2013.

29. Karuppiaha, C., et al. A novel enzymatic glucose biosensor and sensitive non-enzymatic hydrogen peroxide sensor based on graphene and cobalt oxide nanoparticles composite modified glassy carbon electrode, *Sens. Actuators B: Chem.* **196**, 450-456, 2014.

30. Tsai, Y.C., et al. Cast thin film biosensor design based on a nafion backbone, a multiwalled carbon nanotube conduit and glucose oxidase function, *Langmuir* **21**, 3653-3658, 2005.
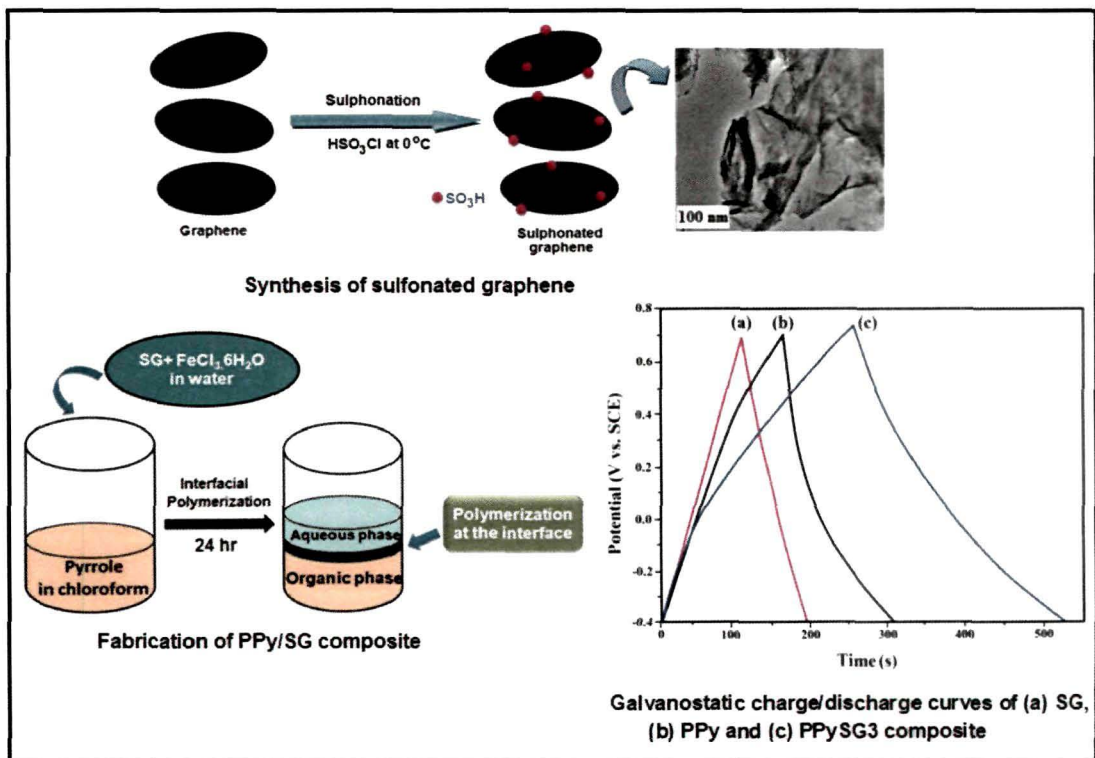
CHAPTER 4: Section B

Applications of graphene based polymer nanocomposites:

Polypyrrole (PPy)/sulfonated graphene (SG) composite as electrode material for supercapacitor

GRAPHICAL ABSTRACT

Synthesis of sulfonated graphene

Fabrication of PPy/SG composite

Galvanostatic charge/discharge curves of (a) SG, (b) PPy and (c) PPySG3 composite

4.2 Polypyrrole (PPy)/sulfonated graphene (SG) composite as electrode material for supercapacitor

4.2.1 Introduction

In the past few years, development of sustainable and renewable energy devices have gained great demand due to the growing global energy use along with the diminishing supply of fossil fuels and environmental problems. Among them, super capacitors, the energy storage devices, are of huge scientific interest recently for its high power density, cost effectiveness, long cycle life, safe operation and good eco-friendliness compared to traditional battery.[1-3] They have enormous utilization in satellites, computers, electronics, mobile communications, and electrical vehicles etc.[4,5] The traditional charge storage devices, such as batteries, cannot fulfill the increasing global power requirements. To overcome the drawbacks of conventional energy storage devices, now scientists and researchers have focused to develop solid state, lightweight and flexible supercapacitors, to meet the desired energy-storage needs for future. Based on the energy storage behavior, supercapacitors are divided into two categories: electrical double layer capacitor (EDLC) based on porous carbon materials and pesudocapacitor based on conducting polymers and metal oxides.[6]

Pseudocapacitive materials such as conducting polymers have higher charge storing capacity than carbon materials. However direct application of pseudocapacitors in supercapacitor applications are limited due to their lower cycle life in charging-discharging process compared to carbon based electrodes, Also they have poor stability and high resistance during cycling. Therefore combination of carbon materials and conducting polymers has advantages of both the components and are found to be effective for improving electrochemical performance of supercapacitors.

Recently, graphene (GR) is considered as the most attractive material electrochemical energy storage applications owing to its wonderful properties such as large surface area, magnificent electrical properties, good cycle stability, large double layer capacitance, good chemical stability and high mechanical strength.[7-9] This 2D sheet of closely packed carbon atoms has opened a new route for development of new functional materials for supercapacitor. Use of GR as a nanofiller in conducting polymer composites have shown great improvement in properties with a range of applications.[10] Polypyrrole (PPy) is the most widely used conducting polymer in supercapacitor electrodes due to its various advantages like good electrical conductivity, cost efficiency, simple fabrication, easy processing and good environmental stability. GR based PPy composites have exhibited synergetic properties such as vast improvements in electrical conductivity and electrochemical behavior with diverse technological applications. Bose et al.[11] reported synthesis of GR based PPy composites using in-situ polymerization method. A good enhancement in electrical conductivity and thermal stability was observed for the composites. Zhang et al.[12] prepared GR/PPy composite via in-situ polymerization which showed higher capacitance value (482 F g^{-1}) and better cycling stability compared to pure PPy.

Although GR has many advantages it has some demerits like easy agglomeration and stacking of GR sheets, which reduces its surface area significantly. Therefore, to overcome these drawbacks chemically modified graphene (CMG) has been introduced. Sulfonated graphene (SG) is a typical CMG which is often used as a dopant in conducting polymers.[13,14] The electrical conductivity and electrochemical performance of SG is found to be superior compared to pure graphene. However few works have been reported based on sulfonated graphene based conducting polymer composite. Hao et al.[15] reported a SG based polyaniline (SGEP) composites using interfacial polymerization. By varying the amount of SGE, the morphology of SGEP can be changed. The composite exhibited a high value of specific capacitance and capacity retention than that of pure polymer. Liu et al.[16] synthesized PPy/SG composite films by electrochemical deposition technique. The composite showed high conductivity and electrochemical stability.

In this report, a novel method has been employed to fabricate PPy/SG composites by interfacial polymerization technique, where SG served both as a substrate and acid dopant. Interfacial polymerization is an easy and simple way for preparation of polymers compared to other conventional polymerization methods.[17] The preparation methods greatly influences the properties of composite materials. So far, no report has been found on preparation of PPy/SG composite by this method. The synthesized composites were analyzed by FTIR, XRD, Raman spectroscopy, SEM, TEM techniques, cyclic voltammetry, impedance and charging-discharging respectively. The charge capacitive behavior of the resulting composite was investigated in1M H_2SO_4 aqueous electrolyte.

4.2.2 Experimental

4.2.2.1 Materials and methods

All the chemicals such as graphite, pyrrole, sulfuric acid, potassium permanganate sodium nitrate, ferric chloride, hydrogen peroxide, hydrazine monohydrate and chlorosulfonic acid were purchased from Sigma Aldrich and was used as received. GR was prepared from natural graphite using modified Hummers method as described in Chapter 2. To prepare SG, first 76 mg of GR was suspended in 30 ml of dichloromethane. The slurry was then dispersed by ultrasonication for 20 min, and to this 10 ml of chlorosulfonic acid was added dropwise at 0 °C. Then the reaction mixture was stirred at room temperature (25 °C) for 1 h and held overnight. The reaction was stopped by neutralisation with 20 wt.% NaOH. The obtained precipitate was filtered and purified by washing with 1M HCl solution followed by DI water and then dried at 80 °C.

PPy/SG composites were synthesized using interfacial polymerization as follows: At first, required amount of SG was dispersed in 15 mL of H_2O and then $FeCl_3 \cdot 6H_2O$ (300 mg) was mixed with it. In another reaction vessel, pyrrole monomer (0.8 mL) is dissolved in 15 mL chloroform which formed the organic phase. Then to this organic mixture, aqueous dispersion was added dropwise. A black colored composite film developed gradually at the interface of these immiscible phases. The

reaction was allowed to proceed for 24 h. The final product was filtered and washed with DI water followed by alcohol and then dried at room temperature (25 °C). Different compositions of the composites were prepared with 1, 2 and 3 wt.% of SG loading and termed as PPySG1, PPySG2 and PPySG3, respectively.

4.2.2.2 Preparation of supercapacitor electrodes

About 5 mg of the PPy/SG composite was mixed with 5 wt.% Nafion solution and coated over a stainless steel net with 1 cm^2 area. Then this coated electrode was dried at 100 °C for 10 h and was used as a working electrode. The supercapacitor setup was designed by placing a separator immersed in 1 M H_2SO_4 electrolyte solution in between two electrodes and then pressed tightly. Stainless steel wires were used as current collectors.

4.2.2.3 Characterization Techniques

Fourier transform infrared (FTIR) spectra were analysed with a Nicolet Impact spectrometer, in a frequency range of 4000-500 cm^{-1}. The X-ray diffraction (XRD) analysis was performed on Rigaku X-ray diffractometer at room temperature with Cu Kα radiation at 30 kV at the scan rate of 0.05θ/s. Raman analysis was done on a Nanofinder 30 confocal Raman employing He-Ne laser beam (λ=532 nm). Scanning electron microscope (SEM) analysis was taken out using a JEOL JSM-6390LV. For Transmission electron microscope (TEM) analysis, PHILIPS CM 200 microscope was used at an accelerating voltage of 200 kV. The electrical conductivity of the samples was measured with a four probe method (300K≤ T ≤413 K) using the following equations[11]

$$\text{Resistivity } (\rho, \text{ ohm-cm}) = (V/I) \, 2\pi d \qquad (1)$$

$$\text{Conductivity } (\sigma, \text{ S/cm}) = 1/\rho \qquad (2)$$

where V is the applied voltage, I is the measured current and d is the distance between the probes. Brunauer-Emmett-Teller (BET) surface area was measured with a Micrometrics (ASAP2020) surface area analyzer under inert atmosphere.

4.2.2.4 Electrochemical Analysis

Cyclic voltammetry (CV) of the electrode was studied with a Sycopel AEW2-10 cyclic voltammeter at the scan rates between 10 to 100 mV s^{-1}. The analysis was performed in a three electrode cell where the composite, platinum and Ag/AgCl electrodes were used as a working, counter and reference electrode, respectively. The galvanostatic charge–discharge test was performed on an Autolab PGSTAT302N in a two electrode system with the current density range between 0.5 to 5 A g^{-1}. For both the tests, 1 M H_2SO_4 solution was used as an electrolyte. Specific capacitance (C_s) was measured from the charge-discharge method by the following equation[16]

$$C_s = (I \times \Delta t)/ (m \times \Delta V) \qquad (3)$$

where I is the discharge current, Δt is the discharge time, ΔV is the voltage drop and m is the weight of active material (5 mg) per electrode. Electrochemical impedance spectroscopy (EIS) was performed on a Gamry EIS300 analyzer in a three electrode system in frequency range of 10^{-1} to 10^{5} Hz (AC voltage, 5 mV).

4.2.3 Results and Discussion:

4.2.3.1. FTIR Analysis

Fig.4.2.1 represents the FTIR spectra of GO, GR, SG, PPy and PPy/SG composite. GO shows peaks at 3409 cm^{-1}, 1409 cm^{-1}, 1719 cm^{-1} and 1234 cm^{-1} in the FTIR spectrum for O-H stretching, O-H deformation, carbonyl (C=O) stretching vibration and C-OH stretching vibration, respectively.[19] The appearance of the peak at around 1065 cm^{-1} confirms presence of epoxy group in GO. In the FTIR spectrum of GR (Fig.4.2.1 (a)), the peaks at 1630 cm^{-1} and 3426 cm^{-1} represent benzene ring stretching vibration and O-H stretching vibration, respectively. Disappearance of the peak for carbonyl group at 1719 cm^{-1} in the spectra of GR (Fig.4.2.1 (b)) indicates that GO is reduced to GR.

The FTIR spectrum of SG shows the reduction in the peak intensity at 1065 cm^{-1}, 1629 cm^{-1} and 1719 cm^{-1} indicating the sulfonation of GR (Fig.4.2.1 (c)). The

peaks at 1030 cm^{-1} (vs-phenyl), 1112 cm^{-1} and 1196 cm^{-1} (two vS-O) indicates that sulfonic acid group is present in SG. PPy shows peaks at 3460, 1549 and 1465 cm^{-1} due to the N-H, C-C and C-N stretching vibration of pyrrole (Fig.4.2.1 (e)). The peaks for asymmetric stretching and symmetric vibrations of CH$_2$ appear at 2920 and 2831 cm^{-1}.[20] FTIR spectrum of the composite, shows peaks associated with both PPy and SG (Fig.4.2.1d). The shifting of the peaks towards lower wavelength and also lowering in the peak intensity for the composite compared to pure PPy signifies successful inclusion of SG in PPy matrix.
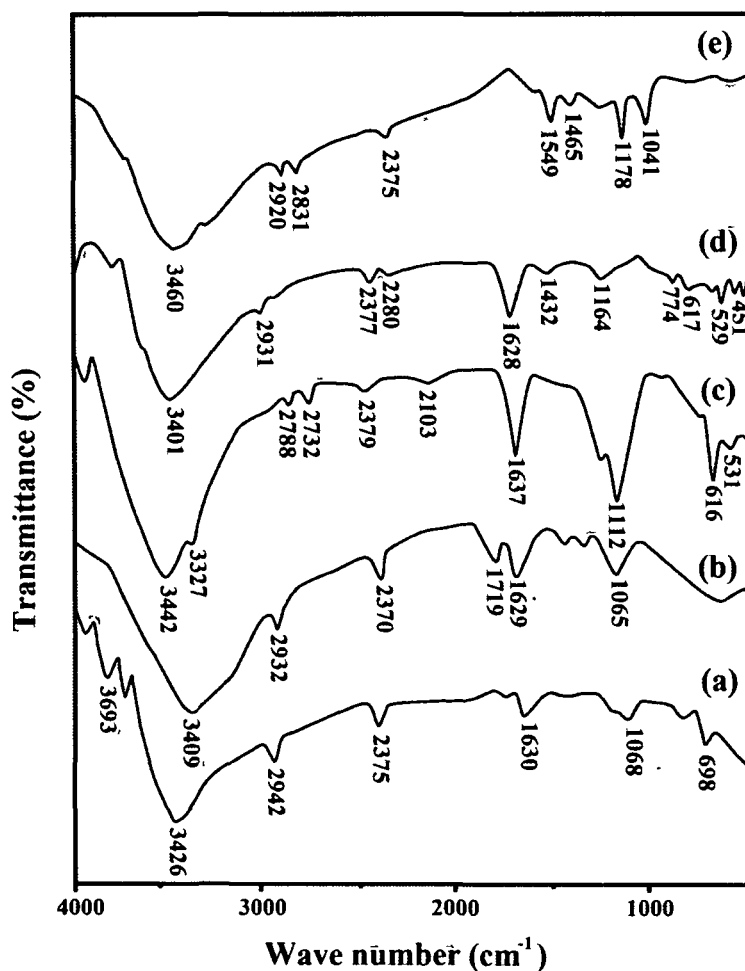
Fig. 4.2.1 FTIR spectra for (a) GO, (b) GR, (c) SG, (d) PPySG3 composite and (e) PPy.

4.2.3.2 XRD Analysis

In the XRD spectrum of GO, (Fig.4.2.2 (a)) a characteristic peak for GO appears at $2\theta= 11.45°$ ((001) diffraction peak).[11] A peak centered at $2\theta=25.6°$ is noticed in the XRD spectrum of SG. In PPy, a broad peak appears at $2\theta=24.6°$ that is in agreement with previous report.[16] This peak for PPy has been shifted to 24.8° in the PPySG3 composites, which reveals that PPy is present inside the composite. Thus the results indicate the homogeneously dispersion of SG sheets in PPy matrix and the possible π-π interaction between the two components.
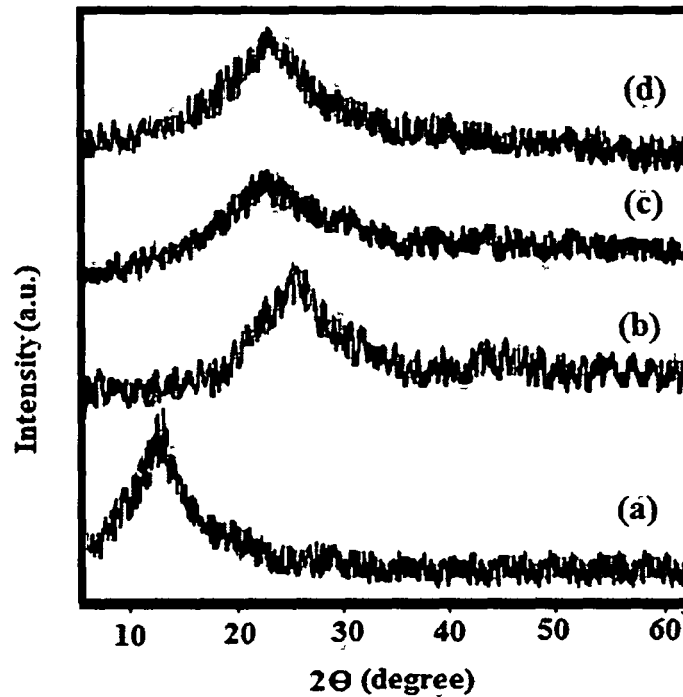
Fig. 4.2.2 XRD patterns of (a) GO, (b) SG, (c) PPy and (d) PPySG3 composite.

4.2.3.3 Raman Analysis

Fig.4.2.3 demonstrates the Raman spectra of PPy/SG and SG sheets. In the Raman spectra of SG, peak for D band appear at 1330 cm^{-1} and G band appear at and 1600 cm^{-1}.[16,21] D band arises from defect structures and G band is related to the vibration of sp^2-carbon. The peak intensity ratio between these two bands (I_D:I_G) is found to be 1.17 for SG which indicates the existence of defect structures which retained after reduction process due to the removal of functional groups. PPySG3

composite shows the distinctive peaks for PPy at 980 cm^{-1}, 930 cm^{-1} (for polaron and bipolaron structure of PPy) and 1050 cm^{-1} which confirms that PPy is present in the composite. Moreover, shifting of the D and G band to 1334 and 1590 cm^{-1} in the composite indicates π-π interaction among the two components. The intensity ratio, I_D/I_G of the composites was calculated to be 1.12, which implies the existence of localized sp^3 defects in the sp^2 carbon network structure. The results are in good consistent with FTIR results.
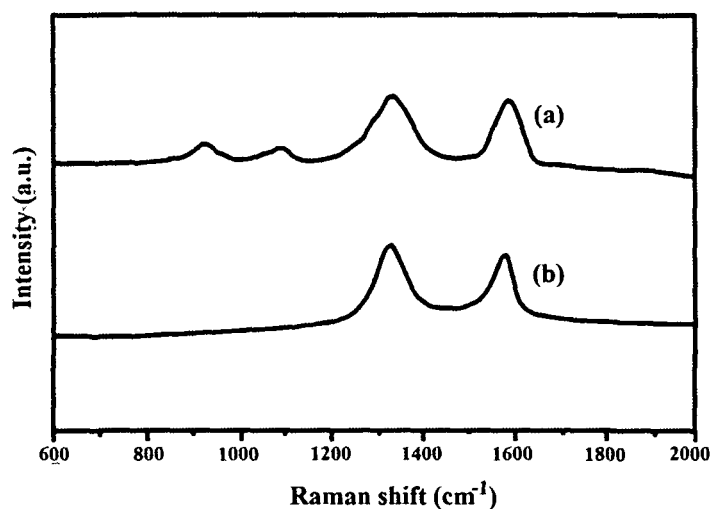

Fig. 4.2.3 Raman spectra of (a) PPySG3 composite and (b) SG.

4.2.3.4 Morphological Studies

The surface characteristic of SG, PPy/SG composite and PPy were investigated using scanning electron microscope. A flaky, sheet like morphology is noticed in the SEM and TEM images of SG (Fig.4.2.4 (a) and (b)). Pure PPy displays a regular, sphere-like structure (Fig.4.2.4 (c)). This spherical morphology vanishes and a rough, flaky structure appears in the PPySG3 composites (Fig.4.2.4 (d)). This morphological change in the composites results from the polymerization of PPy on the SG surface.
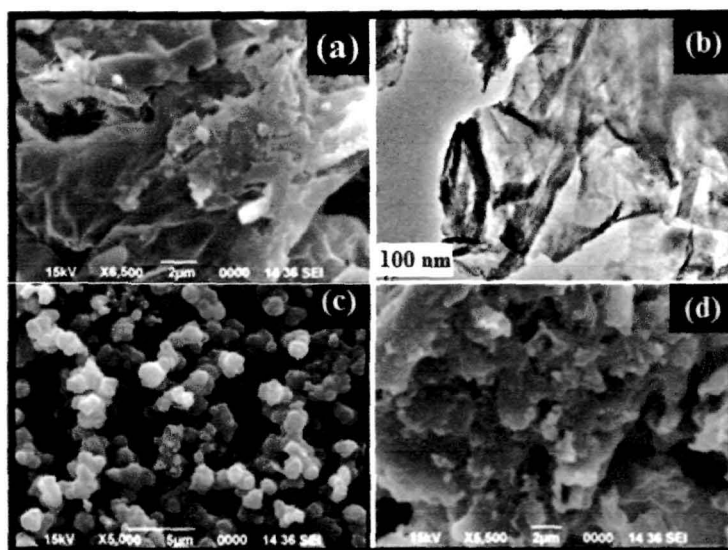
Fig. 4.2.4 SEM images of (a) SG, (c) PPy and (d) PPYSG3 composite; (b) TEM image of SG.

4.2.3.5 Electrical Conductivity

Electrical conductivity of the prepared samples is measured with a fourpoint probe system. PPy exhibited a conductivity value of 0.215 S cm^{-1}, which is lower than electrochemically prepared PPy $(10\text{-}50$ S cm$^{-1})$[16] but greater than the chemically prepared PPy $(0.07$ S cm$^{-1})$.[22] For PPySG1, PPySG2 and PPySG3, the conductivity values are obtained as 5.4, 10.6 and 15.2 S cm^{-1}, respectively at room temperature (25 ^{o}C). This improvement in electrical property can be ascribed to the incorporation of highly conducting SG sheets into PPy matrix with large specific surface area which works as conducting bridges between PPy chains.

4.2.3.6 Electrochemical Properties

4.2.3.6.1 Cyclic Voltammetry Study(CV)

To study the electrochemical properties of the samples CV test was conducted in a three-electrode system using 1M H_2SO_4 as an electrolyte. Fig.4.2.5 illustrates the CV of SG, PPy and PPy/SG composite electrode with a voltage range from -0.4 to 0.8 V (scan rate, 50 mV s^{-1}). SG shows a rectangular CV curve indicating ideal EDL capacitive behaviour. But area of the CV curve is much smaller, perhaps due to the compact structure of SG (Fig.4.2.5 (a)). CV curve of PPy exhibits peaks for reduction and oxidation at around -0.35 V and +4.6 V respectively, indicating the

pseudocapacitive nature of the polymer (Fig.4.2.5 (b)). The CV curve of PPySG3 composite shows nearly rectangular shape with a larger area, indicating ideal capacitive nature and superior charge transport than that of PPy (Fig.4.2.5 (c)). Also the redox peaks have been moved to more positive potentials in the composite, which is attributed to the presence of SG that increases conductivity of the composites, thereby facilitating the charge transfer mechanism. This improves the redox behaviour of the composite. Fig.4.2.6 illustrates CV of PPySG3 composite electrode at varied scan rates from 10 to 100 mV s^{-1}. The rectangular shape of CV curve remains unchanged upto 100 mV s^{-1} revealing great capacitance and good ion response of the composite.
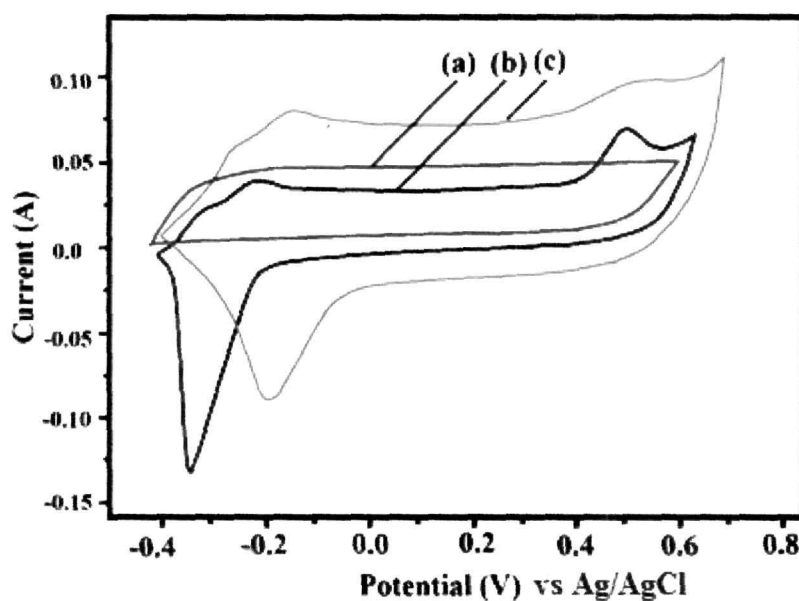

Fig. 4.2.5 Cyclic voltammograms of (a) SG, (b) PPy, (c) PPySG3 composite films potential from −0.4 to 0.8 V.
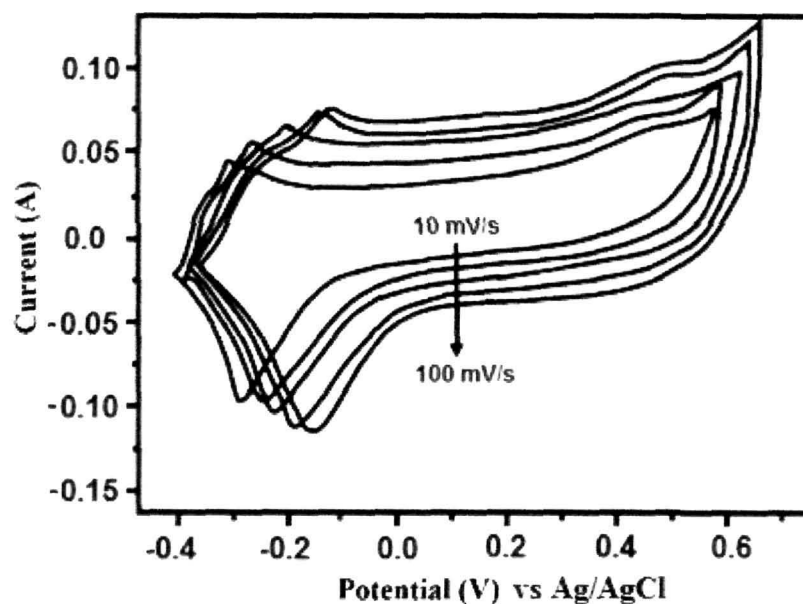
Fig. 4.2.6 Cyclic voltammograms of PPySG3 composite at various scan rates (10 to 100 mV s^{-1}).

4.2.3.6.2 Galvanostatic Charge-Discharge Study

To investigate charge capacity of the samples charge-discharge study was also conducted. Galvanostatic charge/discharge curves of PPy, SG and PPy/SG composite (at a current density of 1 A g^{-1}) are demonstrated in Fig.4.2.7 with a potential range between -0.4 to 0.8 V. SG shows a triangular shape in the curve, indicating pure EDL capacitance.[15,16] The PPySG3 composites exhibits a nearly triangular shape in the charge-discharge curve, implying the combined EDL and the pseudocapacitances of SG and PPy, respectively. Also, a longer discharge time was observed in the composite compared to pure PPy at the same current density. Table 4.2.1 summarizes the specific capacitances (C$_s$) of the samples that are calculated from the charge-discharge curves.
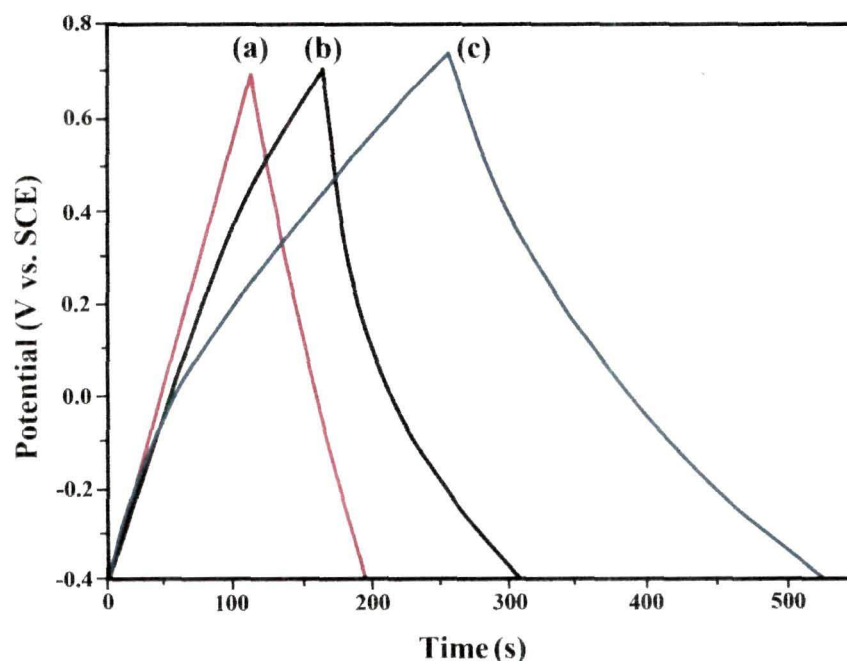
Fig. 4.2.7 Galvanostatic charge/discharge curves of (a) SG, (b) PPy and (c) PPySG3 composite (current density 1 A g^{-1}).

Table 4.2.1. Specific capacitance and Impedance parameters of PPy, SG and PPy/SG composite

Sample	specific capacitance (F/g) (galvanostatic)	R_s (ohm)	R_{ct} (ohm)
PPy	155	0.802	8
SG	142	0.805	6
PPySG3	360	0.795	2

A higher value of specific capacitance of 360 F g^{-1} is observed for PPy/SG (3 wt.%) composite compared to PPy and SG under the same current density (Table 4.2.1). This is due to the fact that highly conductive SG sheets promote the oxidation–reduction reaction of PPy and thus increases its capacitance. Secondly, SG sheets with high surface area increases the EDL capacitance of the PPy/SG composite. As reported in the previous literatures, the composites synthesized by interfacial polymerization have high surface area and show strong interaction between the polymer and filler components which enhances the capacitance.[23] The surface area of

the samples were analysed using the BET method which reveals a higher surface area of 54.5 m^2 g^{-1} for the 3 wt.% composite, compared to the 41.5 m^2 g^{-1} of pure PPy. The BET area of SG was obtained as 94 m^2 g^{-1}.

To examine the effect of current density on capacitance values of the resulting composite charging/discharging test was carried out at various current densities (Fig.4.2.8). On increasing current density from 1 to 5 A g^{-1}, PPySG3 composite showed 79% capacitance retention (360 to 285 F g^{-1}), whereas PPy exhibited about 52% loss (155 to 67 F g^{-1}) in its capacitance at the same range of current density. The improvement in capacitance may be due to the fact that highly conducting PPy/SG composite increases the charge-transport mechanism and favors ionic movements during discharging.[16]
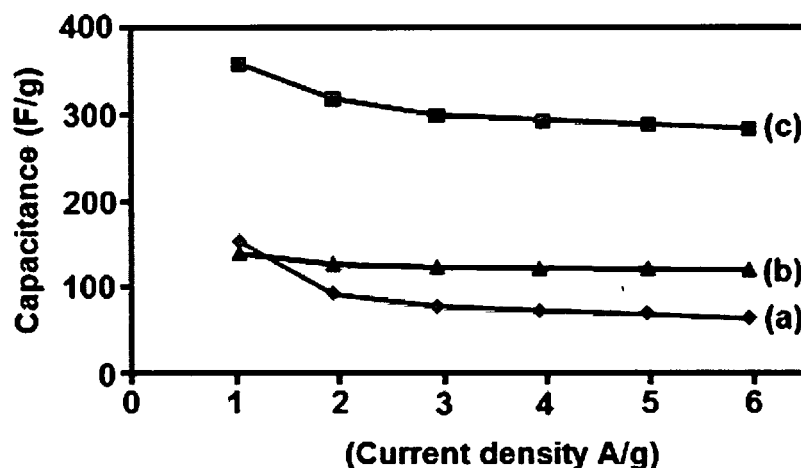

Fig. 4.2.8 The specific capacitances of (a) PPy, (b) SG and (c)PPySG3 composite electrodes at different discharging current densities.

One of the major problems with the conducting polymer based capacitor is its lack of stability during long-term charging/discharging cycle. The cycling stability of the PPYSG3 composite and PPy electrodes is represented in Fig.4.2.9 (scan rate, 50 mV s^{-1}). PPy losses 28% of its capacitance (from 155 to 112 F g^{-1}) during 500 charge/discharge cycles at 1 A g^{-1} current density. However, only 10% loss in the capacitance (from 360 to 323 F g^{-1}) was noticed in case of the composite at the same conditions. The superior electrochemical stability of the PPy/SG composite may be attributed to the fact that SG sheets restrict the shrinking and swelling of PPy during

charge/discharge cycling. Thus it decreases the change in structural and electrochemical properties of PPy during charge/discharge cycling.
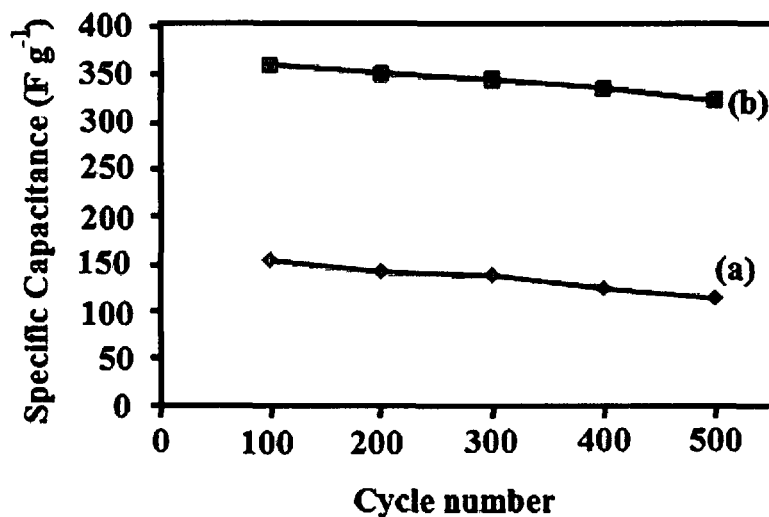

Fig. 4.2.9 Cycling stability test of the (a) PPy and (b) PPySG3 composite upto 500 charge/discharge cycles at a current density of 1 A g^{-1}.

4.2.3.6.3. Electrochemical Impedance Spectroscopy Study (EIS)

Fig.4.2.10 shows the complex plane impedance spectra of PPySG3, PPy and SG electrode. The equivalent electrical circuit is displayed in the inset of Fig.4.2.10 and fitting data are represented in Table 4.2.1. The intercept of the curves with real axis Z' in the high frequency region of Nyquist plot, represents the equivalent series resistances (R$_s$) which is the summation of solution resistance, resistance of the active material as well as the contact resistances.[23] All samples exhibited low R$_s$ value of around 0.8 ohm. The semicircle at the high frequency region of the plot refers to the interfacial charge-transfer resistance (R$_{ct}$), which are obtained as 8, 6 and 2 ohm for PPy, SG and PPySG3 composite, respectively. The 45° slope of the nearly vertical line in the low-frequency region indicates the Warburg resistance (W$_d$) which arises from diffusion of ions in the electrolyte. It is observed that the slope of the straight line in PPySG3 composite is much greater indicating good capacitance and low diffusion resistance of the composite.[24] The low resistance of the composites is due to the fact that the highly conducting SG helps in the adequate ingress of ions to its

surface and thereby minimizes the ion diffusion length. Thus EIS results indicate that PPy/SG composite possesses better capacitive nature and efficient transfer of charges than that of PPy or SG. These results are in consistent with the CV results.
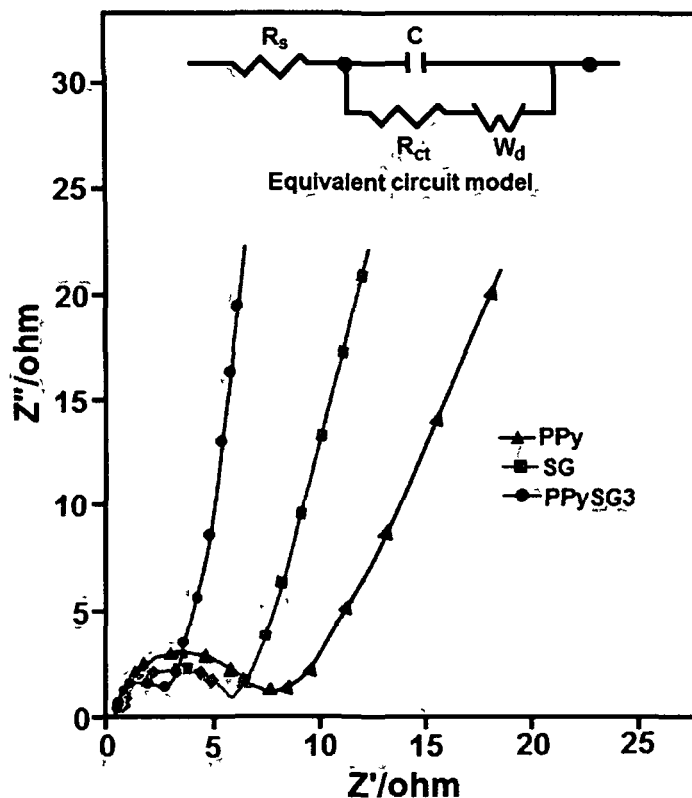

Fig. 4.2.10 Nyquist impedance plots of the PPy, SG and PPySG3 electrodes.

4.2.3.7 Comparative Study

Oliveira *et al.*[23] reported capacitance of 277.8 F g^{-1} for PPy/GR nanocomposites prepared by in-situ polymerization. Davies *et al.*[24] reported fabrication of supercapacitor electrodes based on GR/PPy composite synthesized using pulsed electropolymerization method. They achieved a capacitance of 237 F g^{-1} at a deposition time of 120 s. Bose *et al.*[25] reported capacitance of 267 F g^{-1} for PPy/GR composite synthesized by in-situ polymerization with a scan rate of 100 mV s^{-1}. Si *et al.*[26] developed PPy/GR nanoplatelets synthesized by an electrochemical method for supercapacitor application. The composite showed a maximum value of capacitance

of 285 F g^{-1} at a 0.5 A g^{-1} discharge rate. Biswas *et al.*[27] showed the capacitance of 165 F g^{-1} for GR nanosheets and PPy nanoarchitecture at 1 A g^{-1} current density. In the present work, SG based PPy composite exhibits a capacitance of 360 F g^{-1} at the current density of 1 A g^{-1} which is higher than that of the above reports. This may be attributed to the good adhesion between SG and PPy in the composite prepared by interfacial polymerization as well as increased conductivity of the composite on incorporation of SG sheet with high surface area.

4.2.4 Conclusions

In summary, PPy/SG composite was synthesized via interfacial polymerization and was found to be a promising candidate for supercapacitor electrode. Both structural and morphological analyses showed uniform distribution of SG in the polymer matrix. The composite showed higher electrical conductivity and superior electrochemical reversibility compared to PPy. These improvements can be ascribed to the large surface area and high aspect ratio of SG sheets that exist within the PPy matrix. Charging-discharging study revealed a high specific capacitance value (360 F g^{-1}) of PPySG3 composite at a current density of 1 A g^{-1}. Moreover, the composite exhibited a good electrochemical stability, around 90% capacitance retained after 500 charging/discharging cycles. This simple method opens a new way to fabricate other SG based nanocomposites for energy storage applications.

REFERENCES

1. Winter, M. & Brodd, R.J. What are batteries, fuel cells and supercapacitors, *Chem. Rev.* **104**, 4245-4268, 2004.

2. Du, C. & Pan, N. High power density supercapacitor electrodes of carbon nanotube films by electrophoretic deposition, *Nanotechnology* **17**, 5314-5318, 2006.

3. Nakamura, M., et al. Influence of physical properties of activated carbons on characteristics of electric double-layer capacitors, *J. Power Sources* **60**, 225-231, 1996.

4. Kotz, R. & Carlen, M. Principles and applications of electrochemical capacitors, *Electrochim. Acta* **45**, 2483-2498, 2000.

5. Nakanishi, H. & Grzybowski, B.A. Supercapacitors based on metal electrodes prepared from nanoparticle mixtures at room temperature, *J. Phys. Chem. Lett.* **1**, 1428-1431, 2010.

6. Conway, B.E. & Pell, W.G. Double-layer and pseudocapacitance types of electrochemical capacitors and their applications to the development of hybrid device, *J. Solid State Electrochem.* **7**, 637-644, 2003.

7. Zhou, X.F., et al. Graphene modified LiFePO$_4$ cathode materials for high power lithium ion batteries, *J. Mater. Chem.*, **21**, 3353-3358, 2011.

8. Wang, H.L., et al. Mn$_3$O$_4$-graphene hybrid as a high-capacity anode material for lithium ion batteries, *J. Am. Chem. Soc.* **132**, 13978-13980, 2010.

9. Wang, X., et al. Transparent, conductive graphene electrodes for dye-sensitized solar cells, *Nano Lett.* **8**, 323-327, 2008.

10. Potts, J.R., et al. Graphene-based polymer nanocomposites, *Polymer* **52**, 5-25, 2011.

11. Bose, S., et al. In-situ synthesis and characterization of electrically conductive polypyrrole/graphene nanocomposites, *Polymer* **51**, 5921-5928, 2010.

12. Zhang, D., et al. Enhanced capacitance and rate capability of graphene/polypyrrole composite as electrode material for supercapacitors, *J. Power Sources* **196**, 5990-5996, 2011.
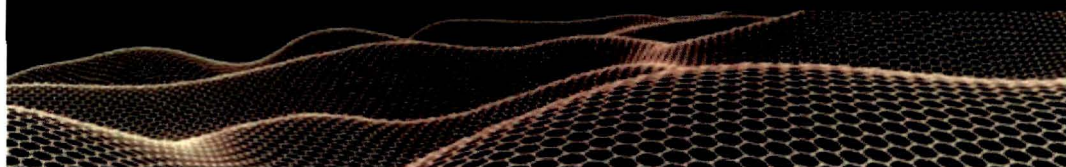
13. Wei, Z., et al. Polyaniline nanotubes doped with sulfonated carbon nanotubes made via a self-assembly process, *Adv. Mater.* **15**, 136-139, 2003.

14. Qiu, H., et al. Conducting polyaniline nanotubes by template-free polymerization, *Macromolecules* **34**, 675-677, 2001.

15. Hao, Q., et al, Morphology-controlled fabrication of sulfonated graphene/polyaniline nanocomposites by liquid/liquid interfacial polymerization and investigation of their electrochemical properties, *Nano Res.* **4**, 323-333, 2011.

16. Liu, A., et al. Electrochemical deposition of polypyrrole/sulfonated graphene composite films, *J. Phys. Chem. C* **114**, 22783-22789, 2010.

17. Dallas, P., et al. Interfacial polymerization of pyrrole and in-situ synthesis of polypyrrole/silver nanocomposites, *Polymer* **48**, 2007-2013, 2007.

18. Hummers, W.S. & Offeman, R.E. Preparation of graphitic oxide, *J. Am. Chem. Soc.* **80**, 1339-1339, 1958.

19. Patole, A.S:, et al. A facile approach to the fabrication of graphene/polystyrene nanocomposite by in-situ microemulsion polymerization, *J. Colloid Interface Sci.* **350**, 530-537, 2010.

20. Zhang, L.L., et al. Layered graphene oxide nanostructures with sandwiched conducting polymers as supercapacitor electrodes, *Langmuir* **26**, 17624-17628, 2010.

21. Coskun, E., et al. Synthesis of sulfonated graphene/polyaniline composites with improved electroactivity, *Carbon* **50**, 2235-2243, 2012.

22. Tsang, S.C., et al. A simple chemical method of opening and filling carbon nanotubes, *Nature* **372**, 159-162, 1994.

23. Oliveira, H.P., et al. Supercapacitors from free-standing polypyrrole/graphene nanocomposites, *J. Phys. Chem. C* **117**, 10270-10276, 2013.

24. Davies, A., et al. Graphene based flexible supercapacitors: pulse-electropolymerization of polypyrrole on free-standing graphene films, *J. Phys. Chem. C* **115**, 17612-17620, 2011.

25. Bose, S., et al. Electrochemical performance of a graphene-polypyrrole nanocomposite as a supercapacitor electrode, *Nanotechnology* **22**, 295202-295211, 2011.

26. Si, P., et al. An electrochemically formed three-dimensional structure of polypyrrole/graphene nanoplatelets for high-performance supercapacitors, *RSC Adv.* **1**, 1271-1278, 2011.

27. Biswas, S. & Drzal, L.T. Multilayered nanoarchitecture of graphene nanosheets and polypyrrole nanowires for high performance supercapacitor electrodes, *Chem. Mater.* **22**, 5667-5671, 2010.
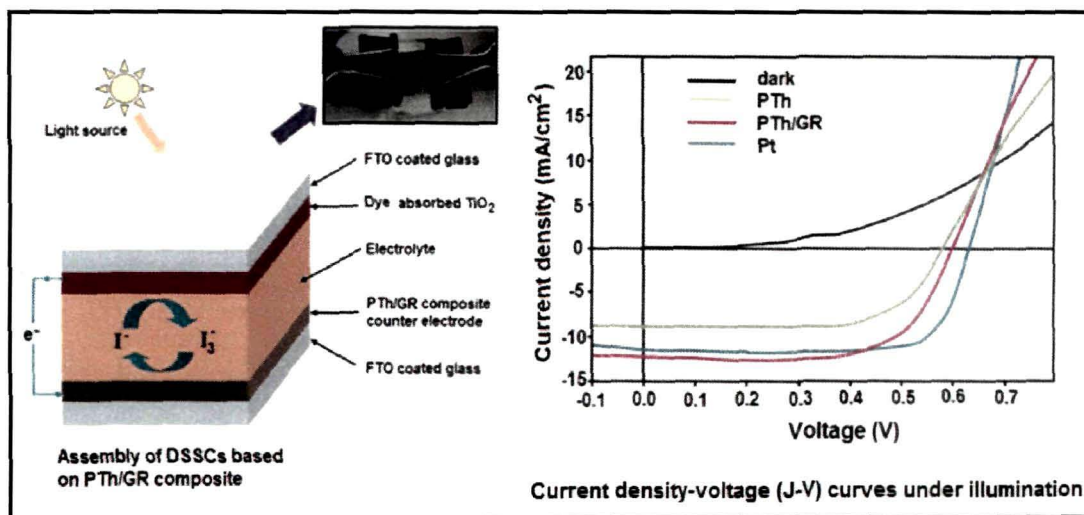
CHAPTER 4: Section C

Applications of graphene based polymer nanocomposites:

Polythiophene (PTh)/graphene (GR) composite as a highly efficient platinum-free counter electrode in dye-sensitized solar cells

GRAPHICAL ABSTRACT

Assembly of DSSCs based on PTh/GR composite

Current density-voltage (J-V) curves under illumination

4.3 Polythiophene (PTh)/graphene (GR) composite as a highly efficient platinum free counter electrode in dye-sensitized solar cells (DSSCs)

4.3.1 Introduction

Dye-sensitized solar cells (DSSCs) are considered as one of the most attractive low cost photovoltaic (PV) devices since their discovery by O'Regan and Gratzelz in 1991.[1-3] DSSCs are widely investigated recently for their low cost, easy fabrication and high energy conversion efficiency which makes it a promising alternative to conventional silicon solar cells. Usually, a DSSC consists of a dye-sensitized TiO_2 as a photoanode, a iodide/triiodide redox electrolyte and a counter electrode.[4] The counter electrode (CE) plays a crucial role in DSSCs which is mainly responsible for the fill factor characteristics of the PV device.[5] CE is used to carry electron from the external circuit to the electrolyte and catalyzes the cathodic reduction of I_3^- ions in electrolyte.[6] In general, a platinum (Pt) coated conductive substrate is used as a CE in typical DSSCs due to its high conductivity, high catalytic activity and stability.[7,8] However, Pt is a costly and less abundant metal which causes difficulties in commercialization of DSSCs. Another drawback of Pt is that it dissolves in the electrolyte solution creating by-products like PtI_4 and H_2PtI_6.[9] Therefore replacement of this expensive material by other cost effective materials is necessary to reduce production cost of DSSCs.

Several researchers have focused on developing new substitutes to replace platinum as CE by using various carbon based materials.[10-14] Among them, graphene (GR) has attracted huge attention as a promising alternative to Pt in solar cell applications due to its low cost, excellent electrical conductivity, high specific surface area and high mechanical strength.[15-18] However, GR has few numbers of active sites for I_3^-/I^- catalysis reaction which limits its application as a counter electrode in DSSCs.[19] To overcome this problem, conducting polymers, such as polypyrrole (PPy), polyaniline (PANI), poly(3,4-ethylenedioxythiophene) (PEDOT) have been introduced into GR as counter electrodes for their unique features, such as inexpensiveness, good electrochemical stability and high catalytic activity for I_3^- reduction.[20-25] Wang et al.[26] synthesized a nanocomposite material with PANI and GR sheets by an in situ polymerization and studied its application as CE in DSSCs. The

cell gave an efficiency of 6.09%, which was near to that of Pt CE. Wang et al.[27] reported the preparation of PANI/GR hybrids by in-situ polymerization. The resulting hybrid material was used as a CE in DSSCs which showed a conversion efficiency of 6.09%. The value was comparable to that of Pt CE. Gong et al.[28] reported fabrication of GR/PPy composite and used it as a CE for DSSCs. The incorporation of GR sheets improved short-circuit current density from 14.27 to 15.81 mA cm^{-2} and conversion efficiency from 7.11% to 8.14%. Lee et al.[29] developed a CE based on PEDOT/GR composite material which showed an efficiency of 6.26%, due to the high electronic charge transfer and electrochemical activity of the composite. PEDOT: PSS/GR composite was used as a CE in DSSCs by Hong et al.[30] which exhibited an efficiency of 4.5%. Among the conducting polymers, PTh and its derivatives have gained special appeal because of their easy synthesis, good environmental stability and good redox behaviors.[31-33] The incorporation of GR in PTh may enhance the conductivity in the polymer and thereby improving the PV performance. To the best of our knowledge, no works have been reported based on PTh/GR as a CE for DSSCs till now.

In this report we have demonstrated the preparation of PTh/GR composite by liquid/liquid interfacial polymerization and its application as CE in DSSC. Interfacial polymerization is a easy and controllable way for preparation of bulk quantities of polymers compared to other conventional polymerization system. The PTh/GR composite holds good potential for application as a CE material with advantages of both the component. The properties of composite and its PV performances were investigated by using various spectroscopic and analytical techniques. DSSCs based on PTh/GR composite shows energy conversion efficiency up to 4.8%, which is comparable to that of Pt electrode.

4.3.2 Experimental section

4.3.2.1 Materials and method

All chemicals such as graphite flakes, sodium nitrate, sulfuric acid, potassium permanganate, hydrogen peroxide, hydrazine monohydrate, ferric chloride, thiophene monomer and Cis88 bis (isothiocyanato) bis (2,2'-bipyridyl-4,4'-dicarboxylato)

ruthenium (II) bis89 tetrabutylammonium (N-719) were purchased from Sigma Aldrich and used directly without further purification. First, graphene oxide (GO) was prepared from natural graphite by modified Hummers method[34] using $KMnO_4$ and H_2SO_4 as oxidizing agents. The as synthesized GO dispersion is then reduced to GR by adding hydrazine monohydrate as described in the previous chapters. PTh/GR composite was prepared by interfacial polymerization as mentioned in Chapter 2.[35] 0.02 g GR was dispersed in 20 mL of CH_3NO_2 by ultrasonication for 1 h. 2.44 g $FeCl_3$ was added to the dispersion and stirred for 1 h. Then this mixture was added dropwise into 0.4 mL thiophene solution in 10 mL of n-hexane and was constantly stirred for 24 h at room temperature (298 K). For purification, the composite was washed with ethanol and then dried at 60 °C for 24 h.

4.3.2.2 Fabrication of PTh/GR CEs

Firstly the FTO glass substrates (Sigma-Aldrich, sheet resistance: 15Ω/sq) were cleaned with DI water followed by anhydrous ethanol and then dried under N_2 atmosphere. The PTh/GR composite paste was prepared by adding 0.20 g the powdered composite to 4 mL of 0.5 wt.% nafion–isopropylalcohol solution and stirred for 12 h. The paste was deposited on FTO-glass by the doctor-blade method. After that the electrode was dried at 80 °C for 1 h. For comparison, Pt electrode was prepared by coating a thin layer of Pt on FTO by vacuum coating.

4.3.2.3 Assembly of DSSCs

Nanocrystalline TiO_2 paste was deposited on FTO glass plate by doctor blade technique. The resulted electrode is sintered at 500 °C for 30 min and gradually cooled to room temperature (298 K). Then the TiO_2 electrode was immersed into 0.3 mM N719 dye in a mixture of acetonitrile-ethanol (1:1 volume ratio) and kept overnight at room temperature. After that the electrode was rinsed with ethanol and dried in air. The electrolyte was prepared by mixing 0.1 M lithium iodide (LiI), 0.6 M I_2, 0.5 M tertbutylpyridine (TBP) and 0.05 M 1-propyl-3-methyl-imidazolium iodide (MPI) in a mixed solvent of N-methyl-2-pyrrolidone (NMP) and acetonitrile (ratio 1:4). The electrolyte is dropped on the dye-adsorbed TiO_2 film and then the PTh/GR

based CE is clipped on the TiO_2 photoanode tightly using two clamps. Thus a sandwich-type DSSC was assembled with an active area of 1 cm^2 as shown in the Fig. 4.3.1.
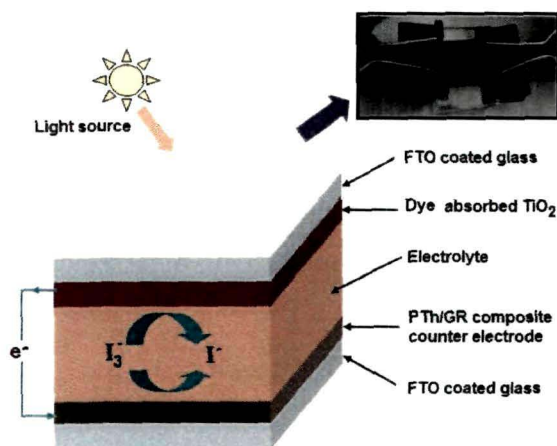
Fig. 4.3.1 Schematic diagram for assembly of DSSCs based on PTh/GR composite.

4.3.3 Characterization and measurements

FTIR spectra of the samples were recorded using a Nicolet Impact-410 IR spectrometer on KBr pellet in the frequency range of range of 500-4000 cm^{-1} at room temperature (298K). X-ray diffraction (XRD) study was done using a Rigaku X-ray diffractometer with Cu-Kα radiation at 30 kV and 15 mA with a scan rate of 0.05 θ/s in the 2θ range of 5-70°. Scanning electron microscopy (SEM) analysis of the prepared samples was performed with a JSM-6390LV instrument (JEOL, Japan). The surface of samples was coated with platinum for SEM analysis. Transmission electron microscopy (TEM) analysis was done with a Philips CM 200 TEM microscope. A small amount of sample was dispersed in ethanol and then the suspension was dropped on 300 mesh copper TEM grids covered with thin carbon films. Cyclic voltammetry (CV) study was performed on a Bio-Logic SP-150 potentiostat with a three electrode system where Pt, Ag/AgCl and PTh/GR/FTO electrode were used as auxiliary, reference and working electrodes respectively, at a scan rate of 100 mV s^{-1}. Acetonitrile solution containing 10 mM LiI, 1 mM I_2, and 0.1 M $LiClO_4$ was used as the supporting electrolyte. Electrochemical impedance spectroscopy (EIS)

measurements were also performed on Bio-Logic SP-150 potentiostat in the frequency range from 10^5 Hz to 0.1 Hz under illumination of a simulated Xenon arc lamp with a power density of 100 mW cm^{-2} at the open-circuit voltage.

Photovoltaic (PV) test:

The photocurrent voltage (J-V) characteristic curves of the DSSC (active area, 1 cm^2) were measured applying an external potential bias to a Keithley 2400 device under illumination with a Xenon lamp (100 mW cm^{-2}) in ambient atmosphere. The fill factor (FF) and photon-to-current conversion efficiency (η) were calculated from the J-V curve using the following equations: [36]

$$FF = \frac{J_{max} \times V_{max}}{J_{sc} \times V_{oc}} \tag{1}$$

$$\eta\,(\%) = \frac{V_{max} \times J_{max}}{P_{in}} \times 100 \tag{2}$$

where J_{max} is the current density (mA cm^{-2}), V_{max} is the voltage in the J-V curves, J_{sc} is the short-circuit current density (mA cm^{-2}), V_{oc} is the open-circuit voltage and P_{in} is the incident light power (100 mW cm^{-2}).

4.3.4 Results and discussion:

PTh/GR composite is prepared by interfacial polymerization as shown in Fig. 4.3.2. Thiophene monomer dissolved in n-Hexane formed the organic phase, while GR and the oxidant ferric chloride dispersed in CH_3NO_2 was used as an aqueous phase in the interfacial polymerization method. The reaction occurs at the interface between these two phases and is kept for 24 h at constant stirring. Black colored PTh/GR composite was collected from the reaction mixture which was further washed and dried. In our previous chapter (chapter 2) also, we have described preparation of PTh/GO composite by interfacial polymerization which showed good yield of the product as well as good enhancement in properties.[35] The prepared PTh/GR composite was then mixed with 0.5 wt.% Nafion–isopropylalcohol and deposited on FTO-glass by the doctor-blade method to prepare the CE for DSSC. The cell was assembled with

dye adsorbed TiO_2 as a photoanode, a iodide/triiodide redox electrolyte and the PTh/GR based CE. Ru complex dye absorbs the incident photon and is excited from the ground state to the excited state. The excited electrons are injected into the conduction band of the TiO_2 electrode which results in the oxidation of the photosensitive dye. The electrons in the conduction band of TiO_2 are diffused to the back FTO electrode and finally reach the CE through the circuit. The oxidized dye accepts electrons from the I^- ion in electrolyte and goes to the ground state with the simultaneous oxidation of I^- to I_3^-. The oxidized I_3^- ion moves to the CE and then reduced to I^- ions.
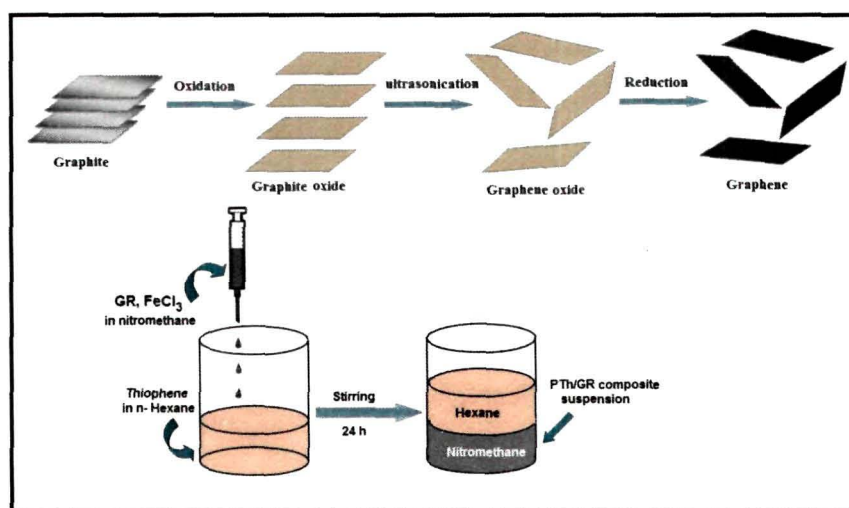

Fig. 4.3.2 Fabrication process of PTh/GR composite

4.3.4.1 FTIR analysis

For structural analysis of the PTh/GR composite, FTIR analysis was done. Fig.4.3.3 shows the FTIR spectra of PTh, GO, GR and PTh/GR composite. In PTh, a broad band appears at around 3423 cm^{-1} which is due to the O-H stretching vibration (Fig. 4.3.3(a)). The bands at 2923, 1640 and 1426 cm^{-1} is ascribed to C-H stretching vibration, C=C asymmetric and symmetric stretching vibrations of thiophene units respectively.[35] The band at 1167 cm^{-1} is assigned to C-H (in-plane) bending vibration of thiophene. A band at 790 cm^{-1} appears due to C-H (out-of-plane) bending vibration of thiophene unit indicating the α-position linkage

170

between the thiophene rings. Moreover, the bands at 830 and 692 cm^{-1} may be assigned to C-S stretching and C-S-C bending vibrations indicating the presence of thiophene rings. The FTIR spectrum of GO (Fig. 4.3.3(b)) shows a the broad peak at 3409 cm^{-1} for O-H stretching and a peak at 1719 cm^{-1} which can be assigned to the carbonyl (C=O) stretching vibration. The peak at 1066 cm^{-1} for C-O stretching vibrations appears due to the presence of the epoxide group in the GO layers. The peaks at 1236 and 1411 cm^{-1} can be ascribed to the C-OH stretching vibration and O-H deformation respectively.[37] In the spectrum of GR, the peaks at 3426 cm^{-1} and 1630 cm^{-1} represent the O-H stretching vibration and benzene ring stretching vibration respectively (Fig. 4.3.3(c)). The characteristic peak at 1719 cm^{-1} for carbonyl group in the FTIR spectrum of GO disappears in the spectrum of GR. This indicates successful reduction of GO into GR. The peak at 2912 cm^{-1} represents the C-H stretching vibration. In the FTIR spectrum of PTh/GR composite we have observed peaks for both PTh and GR (Fig. 3d). Comparing to the spectrum of pure PTh, we have seen that a little shifting of peaks occurs. Also peak intensity decreases in the composite. This indicates that GR was successfully incorporated in the polymer matrix in the composite.
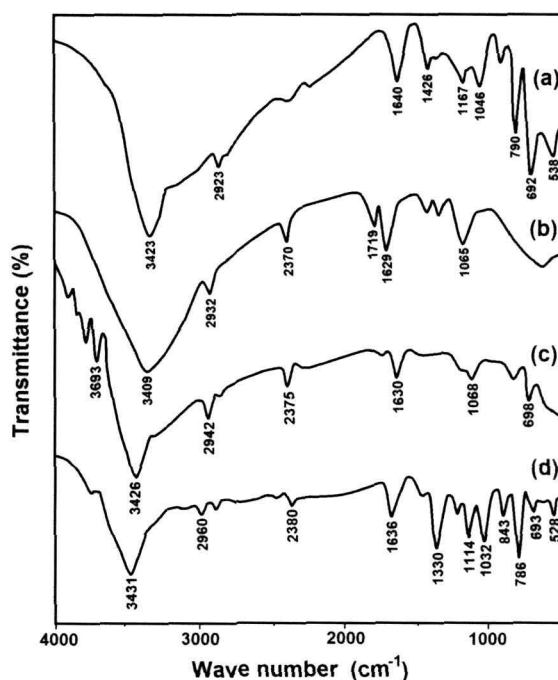
Fig. 4.3.3 FTIR spectra of (a) PTh, (b) GO, (c) GR and (d) PTh/GR composite.

4.3.4.2 XRD analysis

The XRD patterns of GO, GR, PTh/GR composite and pure PTh are presented in Fig. 4.3.4. Pure PTh exhibit a broad diffraction peak in the XRD spectrum at $2\theta= 22°$ indicating the amorphous nature of the polymer (Fig. 4.3.4 (a)).[35] The X-ray pattern of GO (Fig. 4.3.4 (b)) shows a strong peak at $2\theta= 11.46°$ corresponding to (001) reflection peak.[38] After reduction of GO into GR, one broad reflection peak centered at $2\theta= 24°$ was observed in the XRD pattern of GR (Fig. 4.3.4 (c)). In the PTh/GR composite (Fig. 4.3.4 (d)), the broad peak of the PTh and the characteristic peak of GR is observed indicating presence of GR in the PTh matrix. However, the peak for GR has been shifted to $2\theta= 24.5°$. Thus from the results we can say that GR is well exfoliated in the PTh matrix.
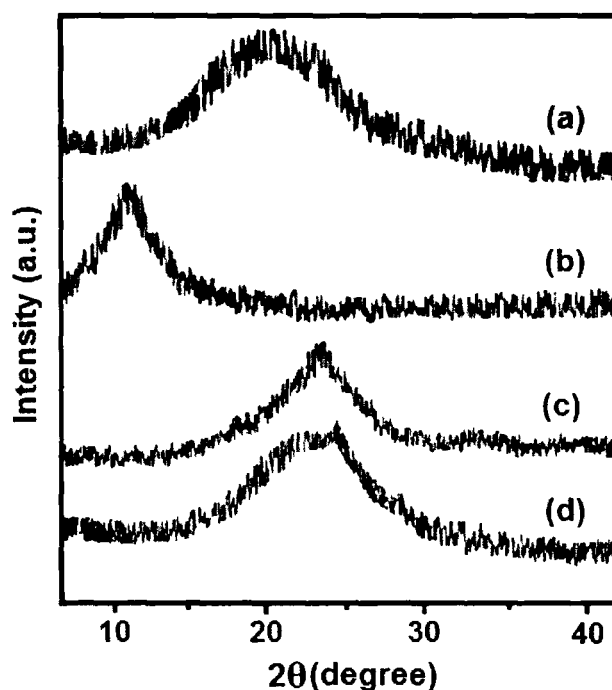

Fig. 4.3.4 XRD spectra of (a) PTh, (b) GO, (c) GR and (d) PTh/GR composite.

4.3.4.3 Morphological analysis

The surface morphology of PTh, GR and PTh/GR composite was investigated using SEM and TEM. In the SEM image of GR, a wrinkle-like layered structure was observed (Fig. 4.3.5 (a)). The pure PTh shows an granular structure of a few

micrometers (Fig. 4.3.5 (b)). This granular morphology vanished and an uneven, flaky morphology is observed in case of PTh/GR composites (Fig. 4.3.5 (c)). In the TEM image of the PTh/GR composite (Fig. 4.3.5 (d)), some spherical structures of PTh decorated at the surface of the GR sheets are observed which indicated the formation of the PTh chain on the surface of the GR sheets. The changes in morphology of the composites from the individual components can be attributed to the successful polymerization of PTh on the surface GR sheets.
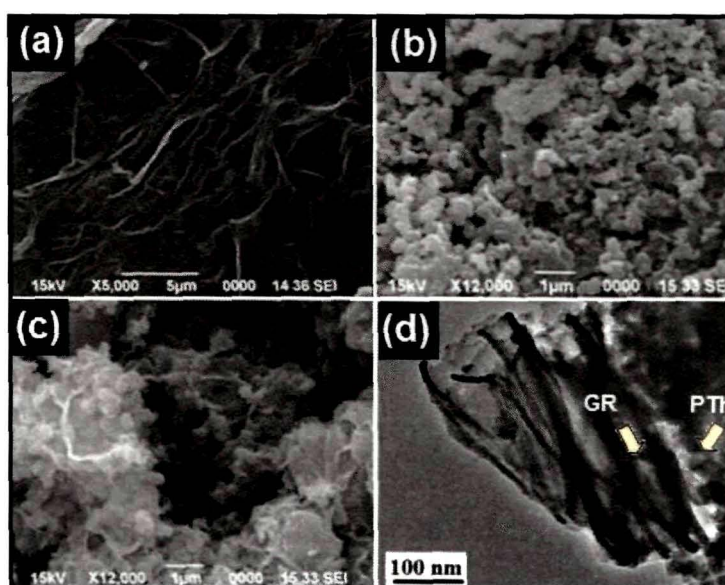
Fig. 4.3.5 SEM images of (a) GR, (b) PTh, (c) PTh/GR composite and (d) TEM image of PTh/GR composite.

4.3.4.4 Cyclic Voltammetr (CV)

CV was used to compare the electrocatalytic activity of Pt and PTh/GR composite electrode for I_3^-/I^- and I_2/I_3^- in a three electrode at a scan rate of 100 mV s^{-1}. A Pt wire and Ag/AgCl electrodes were used as auxiliary and reference electrode respectively, along with an electrolyte containing 0.01 M LiI, 1.0 mM I_2, and 0.1 M LiClO$_4$. Both the Pt and PTh/GR composite electrode exhibited similar redox peaks as shown in Fig. 4.3.6. Two pairs of redox peaks were observed in the CV curves of the PTh/GR electrode. The extreme left pair is associated with the redox reaction of I_3^-/I^-, wheres the extreme right pair is related to the redox reaction of I_2/I_3^-.[28]

173

$$I_3^- + 2e^- \leftrightarrow 3I^- \qquad\qquad (3)$$

$$3I_2 + 2e^- \leftrightarrow 2I_3^- \qquad\qquad (4)$$
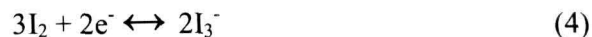
The left redox pair in the CV curves determines the ability of the CE towards the catalytic reduction of I_3^- to I^- in DSSC.[25,28] It is observed that the current density at this peak is higher for PTh/GR electrode compared to that of Pt CE indicating the superior catalytic activity of PTh/GR composite electrode in DSSCs. This may be attributed to the larger electrochemically active surface area and higher active sites of the PTh/GR based electrode for faster redox reaction that results in an increase of photoelectric performance of the PTh/GR composite electrode.
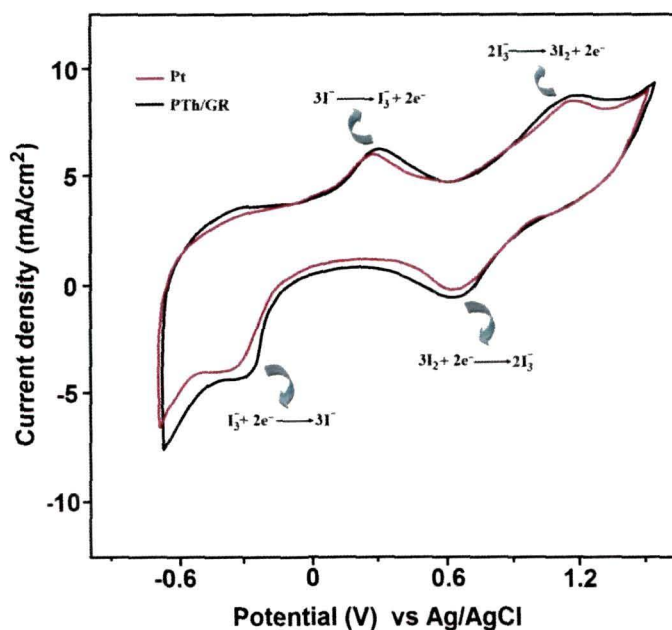
Fig. 4.3.6 Cyclic voltammetry of Pt and PTh/GR composite counter electrodes at a scan rate of 50 mV s^{-1} in 10 mM LiI, 1 mM I_2 and 0.1 M LiClO$_4$ in acetonitrile solution.

To study the electrochemical stability of the PTh/GR CE, CV was performed for 30 repeated cycles as shown in Fig. 4.3.7. It shows stable cathodic peak currents and no change in the CV curves during the cycles, indicating that the electrode possesses very good electrochemical stability.

174
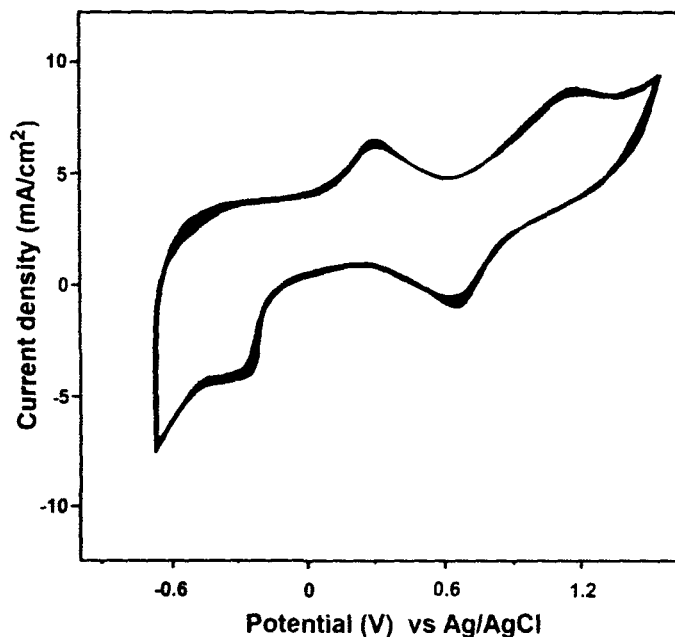
Fig. 4.3.7 Successive electrochemical cycles of the PPy/GR composite electrode up to 30 cycles.

4.3.4.5 Photovoltaic performances of DSSCs.

Photocurrent density-voltage (J-V) characteristic curves of the DSSCs under illumination with different counter electrodes are shown in the Fig. 4.3.8 and the corresponding data are summarized in Table 4.3.1. The conversion efficiency (η) of the DSSCs based on the PTh/GR CE is calculated from the J-V curve and is obtained as 4.8%. This value is comparable to the η of Pt electrode (5.5%) and much higher than that of PTh electrode (3.3%). The DSSCs based on PTh/GR composite CE exhibits higher values of short-circuit current density (J_{sc}, 12.65 mA cm^{-2}), open-circuit voltage (V_{oc}, 0.60 V), and Fill factor (FF, 63.2%) than those of pure PTh. Although the Pt based electrode showed higher V_{oc} (0.63 V) and FF (74.6%) values, its J_{sc} value (11.7 mA cm^{-2}) is slightly lower than that of the composite electrode. Such improvements can be attributed to the large surface area and higher electro-catalytic ability of the PTh/GR composite resulting from the incorporation of highly conducting GR sheets, which favors the reduction reaction of I_3^- ions.[25,27] The higher value of V_{oc} and FF for Pt compared to the PTh/GR electrode is due to the fact that due to its high electronic conductivity, Pt metal has lower charge transfer resistance

which facilitates faster reduction of I_3^- ions. Also surface morphology of the composite is less dense compared to the compact surface of Pt, which prevents the charge transfer at the composite electrode resulting in a lower value of V_{oc} and FF.[25] However, due to the high value of J_{sc} of the PTh/GR electrode, the overall efficiency value is obtained as close to that of Pt electrode.
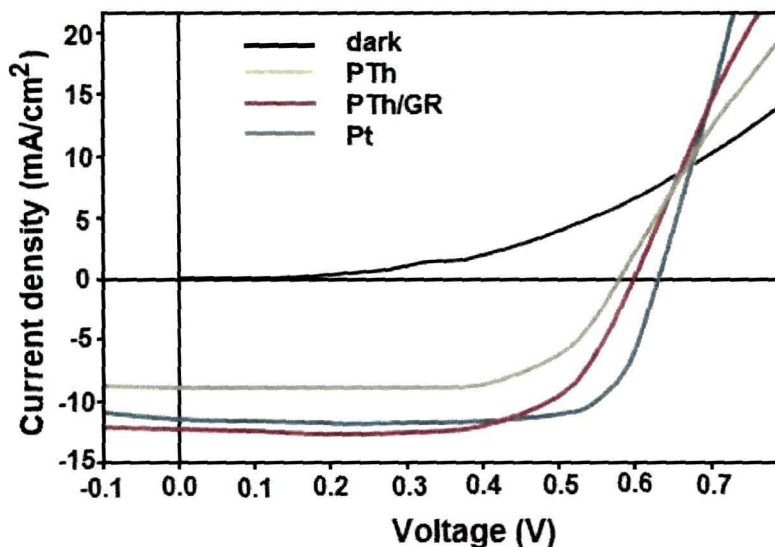
Fig. 4.3.8 Current density-Voltage (J-V) curves of Dark current, PTh, PTh/GR composite and Pt electrode.

Table 4.3.1 Photovoltaic performance of DSSCs based on Pt and PTh/GR CEs

Electrode	V_{oc} (V)	J_{sc} (mA cm^{-2})	Fill Factor (FF) (%)	Efficiency (η) (%)	R_s (Ω)	R_{ct} (Ω)
PTh	0.58	8.8	61.2	3.3	29.2	2.30
PTh/GR	0.60	12.65	63.2	4.8	27.1	1.25
Pt	0.63	11.7	74.6	5.5	21.5	0.85

4.3.4.6 Impedance spectra of DSSCs with different CEs

Electrochemical impedance spectroscopy (EIS) analysis was carried out to further investigate the electrocatalytic properties of the CE. The Nyquist plots of the DSSC under illumination in the measured frequency range 10^{-1} to 10^{5} Hz is shown in Fig. 4.3.9 and the corresponding parameters are presented in Table 4.3.1. The semicircle in the high frequency region of the spectra refers to the charge transfer resistance (R_{ct}) at the interface of the CE which determines catalytic properties of the CE towards I_3^- reduction.[28,39] The CE based on PTh composite showed a higher R_{ct} value of 2.30 Ω which is reduced to 1.25 Ω on incorporation of GR in the composite under the same conditions. The internal series resistance (R_s) of DSSCs, which is the combination of electrolyte resistance and the sheet resistance of the electrode can be obtained from the high-frequency intercept on the real axis of the EIS spectra.[28] The R_s value of the PTh/GR composite (27.1 Ω) was also lower compared to that of PTh (29.2 Ω) based composite. The lower values of R_{ct} and R_s of the composite electrode indicate its superior electrocatalytic property compared to the PTh based electrode. This is due to the high electrochemical active surface area of the composite electrode which promotes the charge transfer process at PTh/GR CE/electrolyte interface and catalyzes the reduction reaction.[39,40] Pt electrode showed much lower R_{ct} (0.85 Ω) and R_s (21.5 Ω) values compared to the PTh/GR based electrode. As FF value strongly depends upon the R_s and R_{ct} of DSSCs, therefore, Pt shows a higher value of FF than that of the composite electrode as obtained in the PV performance test (Table 4.3.1).
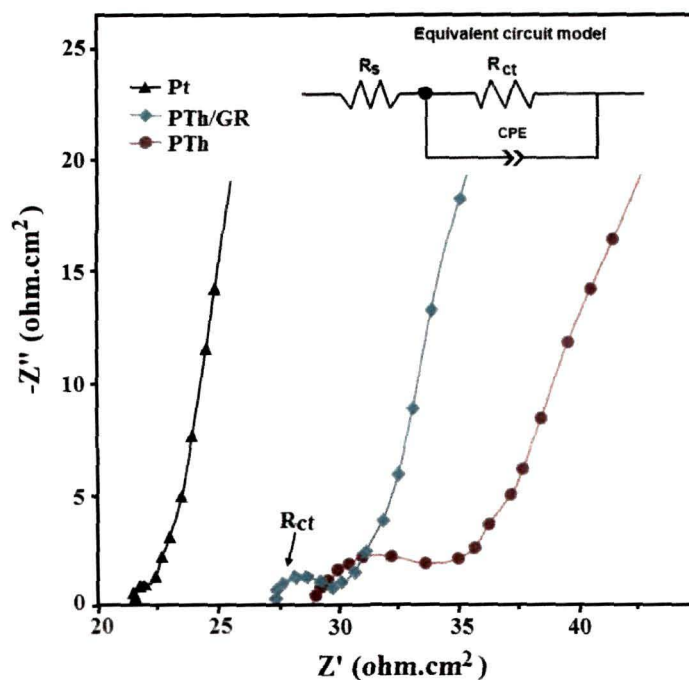
Fig. 4.3.9 Nyquist plots of DSSCs based on Pt, PTh and PTh/GR composite based counter electrodes obtained at open circuit conditions under 100 mW cm^{-2}.

4.3.5 Conclusion

PTh/GR composite has been successfully synthesized by simple liquid/liquid interfacial polymerization. The resulting composite was used as a CE in DSSC to replace the conventional Pt electrode. FTIR, Raman and XRD analysis revealed successful incorporation of GR in the PTh matrix. Morphological analysis indicated uniform distribution of GR throughout the polymer matrix. The composite electrode showed higher electrocatalytic activity compared to pristine PTh electrode towards of I_3^-/I^- reduction reaction due to its large active surface area and better charge transport. Higher J_{sc} and lower FF value was observed in case of the PTh/GR based DSSCs than that of PTh based device. This may due to the incorporation of GR sheets that significantly increases the electron transport process within the PTh by reducing the resistance. The PV performance of DSSCs was investigated which revealed a higher value of conversion efficiency 4.8% which was comparable to that of the device based on the Pt counter electrode. Thus the PTh/GR composite material has proven to be an effective alternative to the expensive Pt electrode for utilization as next generation

counter electrode in DSSCs. This simple method may provide a noted contribution in fabrication of other GR based composite materials for application in the cost-effective and efficient photoelectronic devices near future.

REFERENCES

1. O'Regan, B. & Grätzel, M. A low-cost, high-efficiency solar cell based on dye-sensitized colloidal TiO_2 films, *Nature* **353**, 737-740, 1991.

2. Wang, P.S., et al. Gelation of ionic liquid-based electrolytes with silica nanoparticles for quasi-solid-state dye-sensitized solar cells, *J. Am. Chem. Soc.* **125**, 1166-1167, 2003.

3. Grätzel, M. Photoelectrochemical cells, *Nature* **414**, 338-344, 2001.

4. Grätzel, M. Solar energy conversion by dye-sensitized photovoltaic cells, *Inorg. Chem.* **44**, 6841-6851, 2005.

5. Agarwala, S., et al. Mesophase ordering of TiO_2 film with high surface area and strong light harvesting for dye-sensitized solar cell, *ACS Appl. Mater. Interfaces* **2**, 1844-1850, 2010.

6. Sun, W., et al. A low cost mesoporous carbon/SnO_2/TiO_2 nanocomposite counter electrode for dye-sensitized solar cells, *J. Power Sources* **201**, 402-407, 2012.

7. Xia, J., et al. The influence of doping ions on poly(3,4-ethylenedioxythiophene) as a counter electrode of a dye-sensitized solar cell, *J. Mater. Chem.* **17**, 2845-2850, 2007.

8. Papageorgiou, N., et al. An iodine/triiodide reduction electrocatalyst for aqueous and organic media, *J. Electrochem. Soc.* **144**, 876-884, 1997.

9. Kay, A. & Grätzel, M. Low cost photovoltaic modules based on dye sensitized nanocrystalline titanium dioxide and carbon powder. *Sol. Energy Mater. Sol. Cells* **44**, 99-117, 1996.

10. Wang, G.Q., et al. Application of mesoporous carbon to counter electrode for dye-sensitized solar cells, *J. Power Sources* **194**, 568-573, 2009.

11. Chen, J.K., et al. A flexible carbon counter electrode for dye-sensitized solar cells, *Carbon* **47**, 2704-2708, 2009.

12. Choi, H., et al. Graphene counter electrodes for dye-sensitized solar cells prepared by electrophoretic deposition, *J. Mater. Chem.* **21**, 7548-7551, 2011.

13. Han, J., et al. Water-soluble polyelectrolyte-grafted multiwalled carbon nanotube thin films for efficient counter electrode of dye-sensitized solar cells, *ACS Nano* **4**, 3503-3509, 2010.

14. Geim, A.K. Graphene: status and prospects, *Science* **324**, 1530-1534, 2009.

15. Pang, S. Graphene as transparent electrode material for organic electronics, *Adv. Mater.* **23**, 2779-2795, 2011.

16. Novoselov, K.S., et al. Two-dimensional gas of massless Dirac fermions in graphene, *Nature* **438**, 197-200, 2005.

17. Zhang, Y., et al. Experimental observation of the quantum Hall effect and Berry's phase in graphene, *Nature* **438**, 201-204, 2005.

18. Zhang, D., et al. Graphene-based counter electrode for dye-sensitized solar cells, *Carbon* **49**, 5382-5388, 2011.

19. Kavan, L., et al. Optically transparent cathode for dye-sensitized solar cells based on graphene nanoplatelets, *ACS Nano* **5**, 165-172, 2011.

20. Li, Q.H., et al. Application of microporous polyaniline counter electrode for dye-sensitized solar cells, *Electrochem. Commun.* **10**, 1299-1302, 2008.

21. Zhang, J., et al. Nanostructured polyaniline counter electrode for dye-sensitised solar cells: Fabrication and investigation of its electrochemical formation mechanism, *Electrochim. Acta* **55**, 3664-3668, 2010.

22. Ahmad, S., et al. Dye-sensitized solar cells based on poly (3,4-ethylenedioxythiophene) counter electrode derived from ionic liquids, *J. Mater. Chem.* **20**, 1654-1658, 2010.

23. Yue, G., et al. Low cost poly(3,4-ethylenedioxythiophene): polystyrenesulfonate /carbon black counter electrode for dye-sensitized solar cells, *Electrochim. Acta* **67**, 113-118, 2012.

24. Yue, G., et al. Application of poly (3,4-ethylenedioxythiophene): polystyrenesulfonate/polypyrrole counter electrode for dye-sensitized solar cells, *J. Phys. Chem. C* **116**, 18057-18063, 2012.

25. Sun, W., et al. Hierarchically porous hybrids of polyaniline nanoparticles anchored on reduced graphene oxide sheets as counter electrodes for dye-sensitized solar cells, *J. Mater. Chem. A* **1**, 2762-2768, 2013.

26. Wang, G., et al. Graphene/polyaniline nanocomposite as counter electrode of dye-sensitized solar cells, *Mater. Lett.* **69**, 27-29, 2012.

27. Wang, G., et al. The production of polyaniline/graphene hybrids for use as a counter electrode in dye-sensitized solar cells, *Electrochim. Acta* **66**, 151-157, 2012.

28. Gong, F., et al. Enhanced charge transportation in a polypyrrole counter electrode via incorporation of reduced graphene oxide sheets for dye-sensitized solar cells, *Phys. Chem. Chem. Phys.* **15**, 546-552, 2013.

29. Lee, K.S., et al. Flexible and platinum-free dye-sensitized solar cells with conducting-polymer-coated graphene counter electrode, *Chem. Sus. Chem.* **5**, 379-382, 2012.

30. Hong, W., et al. Transparent graphene/PEDOT–PSS composite films as counter electrodes of dye-sensitized solar cells, *Electrochem. Commun.* **10**, 1555-1558, 2008.

31. Lee, K.M., et al. A high-performance counter electrode based on poly(3,4-alkylenedioxythiophene) for dye-sensitized solar cells, *J. Power Sources* **188**, 313-318, 2009.

32. Papageorgiou, N. Counter-electrode function in nanocrystalline photo electrochemical cell configurations, *Coord. Chem. Rev.* **248**, 1421-1446, 2004.

33. Chen, J.G., et al. Using modified poly(3,4-ethylene dioxythiophene): Poly(styrene sulfonate) film as a counter electrode in dye-sensitized solar cells, *Sol. Energy Mater. Sol. Cells* **91**, 1472-1477, 2007.

34. Hummers, W.S. & Offeman, R.E. Preparation of graphitic oxide, *J. Am. Chem. Soc.* **80**, 1339, 1958.

35. Bora, C., et al. Synthesis of polythiophene/graphene oxide composites by interfacial polymerization and evaluation of their electrical and electrochemical properties, *Polym. Int.* DOI 10.1002/pi.4739.

36. Nath, B.C., et al. High performance polyvinyl alcohol/multi walled carbon nanotube/polyaniline hydrogel (PVA/MWCNT/PANI) based dye sensitized solar cells. *Electrochim. Acta.* **146**, 106-111, 2014.

37. Bora, C. & Dolui, S.K. Fabrication of polypyrrole/graphene oxide nanocomposites by liquid/liquid interfacial polymerization and evaluation of their optical, electrical and electrochemical properties, *Polymer* **53**, 923-932, 2012.

38. Bose, S., et al. In-situ synthesis and characterization of electrically conductive polypyrrole/graphene nanocomposites, *Polymer* **51**, 5921-5928, 2010.

39. Liu, C.Y., et al. Graphene-modified polyaniline as the catalyst material for the counter electrode of a dye-sensitized solar cell, *J. Power Sources* **217**, 152-157, 2012.

40. Nagarajan, S., et al. PEDOT-reinforced exfoliated graphite composite as a Pt- and TCO-free flexible counter electrode for polymer electrolyte dye-sensitized solar cells, *J. Mater. Chem. A* **1**, 1048-1054, 2013.

CHAPTER 5

Conclusion and Future Scopes
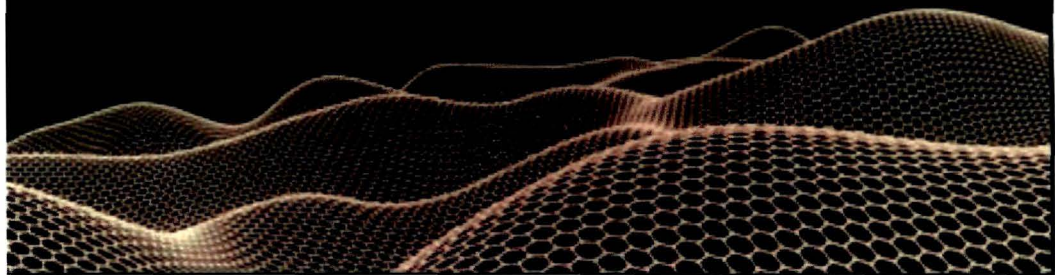
5.1 Conclusion

Graphene (GR)/graphene oxide (GO) based polymer nanocomposites are an exciting field of research today. These wonderful materials have shown diverse range of applications in areas such as energy storage, optoelectronics, sensors, solar cells, biomedical and many others. This thesis demonstrates the successful synthesis of a series of GR/GO based nanocomposites with polymers such as polypyrrole (PPy), polythiophene (PTh) and polyester (PE) resin. We have provided an insight to the characterization of the prepared composites and studied their electrical, electrochemical, thermal and mechanical properties. All the composites showed superior properties compared to the pure polymer at low filler loading. This property enhancement is due to the synergetic effects between the nanofiller and the polymer. The thesis also provided the study of applications of the composites in sensor, supercapacitor and solar cells. The results presented in this thesis may be useful for development of new high performance GR based polymer nanocomposites for applications in near future.

The major findings of the thesis are summarized below:

I.   *Synthesis of graphene (GR)/graphene oxide (GO) based polypyrrole (PPy) and polythiophene (PTh) nanocomposites by liquid/liquid interfacial polymerization and their optical, electrical and electrochemical properties.*

* GR and GO based PPy and PTh composites have been successfully prepared by liquid/liquid interfacial polymerization. Both Raman spectroscopy and XRD results indicate the incorporation of GO and GR in the polymer matrix. TEM and SEM study showed uniform distribution of the nanofillers throughout the polymer matrix.

* The composites exhibited an improved thermal stability compared to pure polymer. Both optical and electrochemical band gaps of the composites were calculated and found to be decreased dramatically on incorporation of GO and GR into the polymer matrix.

- The PPy/GR composites exhibited a higher value of conductivity (2.51-8.45 S cm^{-1}) compared to PPy (0.210 S cm^{-1}) and PPy/GO composites (0.360-0.507 S cm^{-1}), which may be attributed to the high aspect ratio and large specific surface area of GR nanosheets present within the polymer matrix. Electrical conductivity of the PTh/GR composites was found to be higher (7.4×10^{-3} Scm^{-1} for PTGR3 composite) than that of PPy/GO composite (2.7×10^{-4} S cm^{-1} for PTGO3) and pure PTh (5.8×10^{-5} S cm^{-1}).

- Both the composites showed reversible electrochemical response and a good cycling stability even up to 100th cycles. A charging-discharging study also reveals a consistent high capacitance value (260 F g^{-1}) for the PPy/GR composite (3 wt.% of GR loading) at 100mAg^{-1}. This value is much higher than that of PPy/GO composites which showed maximum capacitance value of only 92.2 F g^{-1} (for 3 wt.% GO loading). The specific capacitance of PTh/GR (3 wt. % of GR) composite electrode was evaluated as 210 F/g, where the specific capacitances of PTh/GO composite (3 wt.% of GO) and pure PTh were only 99 F/g and 71 F/g respectively.

- Also this work suggests that the GR based composites have superior thermal stability, electrical and electrochemical properties than that of GO based composites.

II. *Graphene oxide (GO) and graphene (GR) based polyester (PE) resin composites with improved mechanical strength*

- This work demonstrates the successful preparation of GO and GR based PE resin composite with high thermal stability and mechanical strength. The FTIR and XRD results indicate successful incorporation of GO and GR in the polymer matrix. Morphological analysis shows good dispersion of GO and GR within the resin matrix.

184

- The PE/GO composites show improved thermal stability compared to the pure PE. A significant improvement in major degradation temperature (260-285 °C) and weight retention value (15-25%) is obtained on incorporation of GO in the resin matrix. A much enhancement in thermal stability of the PE/GR composites was obtained compared to PE/GO composites. The major degradation temperature of the composite started at relatively higher temperature (260-285 °C) than that of PE/GO composites. Also, the PE/GR composites showed a higher weight retention value (25-30%) compared to PE/GO composites.

- The PE/GO composite films exhibited a significant improvement in the mechanical properties. A 76% increase of tensile strength and 41% increase in Young's modulus are obtained with 3 wt.% of GO loading, which reveals the efficient load transfer between GO and the polymer matrix. The PE/GR composite demonstrated superior mechanical properties compared to PE/GO composites at very low GR loading. Around 123% increase of tensile strength and 87% increase in Young's modulus are obtained with 3 wt.% of GR loading.

- The PE/GR composite film (with 3 wt.% GR loading) was found to possess a higher value of conductivity (3.7×10^{-4} S cm^{-1}) compared to pure resin due to the incorporation of highly conducting GR sheets which forms a conducting network in the insulating resin matrix.

- The PE/GR composites imply proficient antibacterial activity towards the five different kinds of bacterial strains and the antibacterial activity was found to be increased with increasing GR content. Among all the bacterial strains, *Pseudomonas aeruginosa* was much more sensitive toward the PE/GR composites.

- These mechanically strong and ductile PE/GO and PE/GR composite films exhibit good potential in industrial applications. The GR based PE resin composites with improved antibacterial activity could offer new opportunities for the development of a new range of environmental friendly and high strength structural material.

III. Applications of GR based polymer nanocomposites

(A) Highly sensitive glucose biosensor based on polypyrrole (PPy)/graphene (GR) composite synthesized by interfacial polymerization

- We have demonstrated the fabrication of a glucose biosensor based on PPy/GR nanocomposites prepared by interfacial polymerization.

- The PPy/GR/Nafion/GOD film modified GCE is found to be active for the electro-oxidation of hydrogen peroxide.

- This PPy/GR based biosensor showed a high value of sensitivity (29.6 $\mu M/cm^2.mM$) and lower limit of detection (0.1 μM) compared to other GR and CNT based biosensor.

- The biosensor is able to detect glucose as substrate with high sensitivity and fast response. The biosensor also showed reasonable stability which is crucial for practical application of biosensors.

(B) Polypyrrole (PPy)/sulfonated graphene (SG) composite as electrode material for supercapacitor

- PPy/SG composite was synthesized via interfacial polymerization and was found to be a promising candidate for supercapacitor electrode.

186

- , The composite showed higher electrical conductivity and excellent electrochemical reversibility compared to pure polypyrrole.

- Charging-discharging study revealed a high specific capacitance value (360 F g^{-1}) of PPySG3 composite at a current density of 1 A g^{-1}. Furthermore, the composite exhibited a good electrochemical stability, around 90% capacitance retained after 500 charging/discharging cycles at a current density of 1 A g^{-1}.

- This simple method provides a new route to fabricate other sulfonated graphene based nanocomposites for application in energy storage devices.

(C) Polythiophene(PTh)/graphene (GR) composite as a highly efficient platinum-free counter electrode in dye-sensitized solar cells (DSSCs)

- PTh/GR composite has been used as a counter electrode in DSSC to replace the conventional Pt counter electrode.

- The composite electrode showed higher electrocatalytic activity compared to pristine PTh electrode towards of I_3^-/I^- reduction reaction mainly due to its large active surface area and better charge transport.

- Higher short-circuit current density and lower fill factor value was observed in case of the PTh/GR based DSSCs than that of PTh based device. The photovoltaic performance of DSSCs was investigated which revealed a higher value of conversion efficiency 4.8% which was comparable to that of the device based on the Pt counter electrode.

- Thus the PTh/GR composite material has proven to be an effective alternative to the expensive Pt electrode for utilization as next generation counter electrode in DSSCs.

5.2 Challenges and Future Scopes

The discovery of GR has opened many opportunities for creating high performance polymer composites. A lot of emphasis has been given to the applications of these composites in diverse fields. However, researchers are still facing some challenges associated with the production of GR based materials. For example, it is difficult to get a uniform dispersion of GR in polymer matrix as it tends to form agglomeration. Use of some new advanced dispersion methods may solve this problem. Another problem is the lack of large scale production methods to synthesize GR with desirable thickness. It is still highly challenging to prepare single layer GR. Therefore some effective, low cost methods to produce high quality GR in large scale are yet to come. Although works on developments of GR based materials are growing fast, there is still room for broad fundamental research for basic understanding of the subject and their future commercial utilization.

Some future scopes of study of the present investigation are:

❖ Synthesis of GR/GO based composites with new host polymers.

❖ Applications of the composites in other optoelectronic devices e.g. LED, transistor etc.

❖ Study of biomedical applications of GR based composites.

Appendix: List of publications

Publications in International journals:

1. **Chandramika Bora**, Swapan K. Dolui. Synthesis of polypyrrole/graphene oxide nanocomposites and evaluation of their optical, electrical and electrochemical properties. _Polymer_ 2012, 50, 324-325.

2. **Chandramika Bora**, Amarjyoti Kalita, Dhaneswar Das, Swapan K. Dolui*. Preparation of polyaniline/nickel oxide nanocomposites by liquid/liquid interfacial polymerization and evaluation of their electrical, electrochemical and magnetic Properties. _Polymer International_ 2014, 63, 445-452.

3. **Chandramika Bora**, Pronob Gogoi, Silpi Baglari, Swapan K. Dolui. Preparation of polyester resin/graphene oxide nanocomposite with improved mechanical strength. _Journal of Applied Polymer Science_ 2013, 129, 3432-3438.

4. **Chandramika Bora**, P Bharali, Silpi Baglari, Swapan K. Dolui. Strong and conductive reduced graphene oxide/polyester resin composite films with improved mechanical strength and thermal stability. _Composites Science and Technology_ 2013, 87, 1-7.

5. **Chandramika Bora**, Swapan K. Dolui. Interfacial synthesis of polypyrrole/graphene nanocomposites by liquid/liquid interfacial polymerization and their optical, electrical and electrochemical properties. _Polymer International_ 2013, 63, 1439-1446.

6. **Chandramika Bora**, Swapan K. Dolui. Synthesis of polythiophene/graphene oxide composite by interfacial polymerization and evaluation of their electrical and electrochemical properties. _Polymer International_ 2014, _DOI 10.1002/pi.4739._

Appendix: List of publications

7. **Chandramika Bora**, Jahnabi Sharma, Swapan Kr. Dolui. Polypyrrole/Sulfonated Graphene Composite as Electrode Material for Supercapacitor. *Journal of Physical Chemistry C* , 2014 *(Just Accepted)*.

8. **Chandramika Bora**, Swapan K. Dolui. Polypyrrole/graphene composite as glucose biosensor. *Biosensor and Bioelectronics (Communicated)*.

9. **Chandramika Bora**, Swapan K. Dolui. A green approach for reduction of graphene oxide in aqueous extract of Piper betel leaf. *Nano Research. (Communicated)*.

10. **Chandramika Bora**, Chandrama Sarkar, Kiron J Mohan, Swapan Kr. Dolui. Polythiophene/graphene composite as a highly efficient platinum-free counter electrode in dye-sensitized solar cells. *Journal of Physical Chemistry C (Communicated)*.

11. Amarjyoti Kalita, **Chandramika Bora**, Swapan K. Dolui. Melamine-Formaldehyde Supported Titanium-Based Heterogeneous Ziegler-Natta Catalyst for Ethylene Polymerization in Slurry Process. *International Journal of Polymeric Materials* 2013, *DOI:10.1080/00914037.2012.664212.*

12. Pronob Gogoi, Monalisha Boruah, **Chandramika Bora**, Swapan K. Dolui. Jatropha curcas oil based alkyd/epoxy resin/expanded graphite (EG) reinforced bio-composite: Evaluation of the thermal, mechanical and flame retardancy properties. *Progress in Organic Coatings*. 2014, 77, 87-93.

13. Chandrama Sarkar, **Chandramika Bora**, and Swapan K. Dolui. Selective Dye Adsorption by pH Modulation on Amine-Functionalized Reduced Graphene Oxide-Carbon Nanotube Hybrid. *Industrial Engineering and Chemistry Research* 2014, *DOI: 10.1021/ie502653t.*

Appendix: List of publications

Presentation in conferences:

1. **Chandramika Bora**, S.K. Dolui. *Synthesis of polypyrrole/graphene oxide nanocomposites: their optical, electrical and electrochemical behavior.* Poster presented in 99th Indian Science Congress, KIIT University, Bhubaneswar, India, January 3-7, 2012.

2. **Chandramika Bora**, S.K. Dolui. *Synthesis of graphene oxide filled polyester nanocomposite with improved mechanical strength.* Poster presented at National Conference on Chemistry, Chemical Technology and Society, Department of Chemical Sciences, Tezpur University, Assam, India, November 12, 2011.

3. **Chandramika Bora**, S.K. Dolui. Preparation of polyester resin/graphene oxide nanocomposite with improved mechanical strength. International Seminar on Frontiers in Polymer Science and Technology (POLY-2012), North Bengal University & Siliguri Institute of Technology. Darjeeling, West Bengal. November 1-3, 2012 *(Awarded as best oral presentation).*

4. **Chandramika Bora**, S.K. Dolui. *Polypyrrole/graphene composite as glucose biosensor.* Oral presentation at *Young Scientists Award Programme* in 100th Indian Science Congress, Calcutta University, Kolkata, India, January 4, 2013.

5. **Chandramika Bora**, S K Dolui, *Polypyrrole/ sulphonated graphene composites as supercapacitor.* 8th Mid-Year National Symposium in Chemistry, Chemical Research Society of India **(CRSI)**, July 10-12, 2014, CSIR NEIST, Jorhat, Assam *(Awarded as best poster presentation).*

Patent filed:

Chandramika Bora and S.K. Dolui, 'Polypyrrole/sulphonated graphene composite as supercapacitor electrode' (Patent application no. E-2/749/2014 KOL).